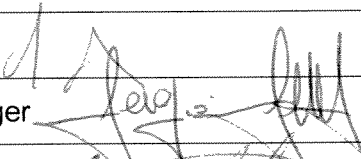
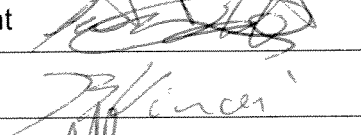
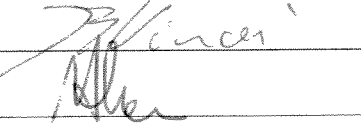
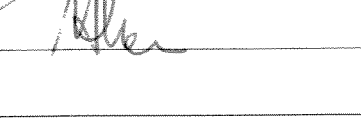
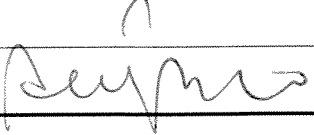




**PERFORMANCE REQUIREMENTS AND BUDGETS  
FOR THE GRADIOMETRIC MISSION**

DCG No.:

| <b>Written by</b>            | <b>Responsibility</b><br>+ handwritten signature if no informatic workflow tool                                |
|------------------------------|----------------------------------------------------------------------------------------------------------------|
| S. Cesare                    | Author                     |
| <b>Verified by</b>           |                                                                                                                |
| S. Cesare                    | Checker                    |
| <b>Approved by</b>           |                                                                                                                |
| C. Gennaro                   | Gradiometer Manager        |
| S. Silvestri                 | Product Assurance Manager  |
| L. Candela                   | Configuration Management   |
| B. Vinai                     | System Manager             |
| A. Allasio                   | Program Manager            |
| N/A                          | Customer Approval                                                                                              |
| <b>Documentation Manager</b> | A. Berto                   |

The validations evidence are kept through the documentation management system.

DOCUMENT CHANGE RECORD

| ISSUE    | DATE         | REASON FOR CHANGE                                                                                                                                                                                                                                                                                                                                                                                                                                                             | AFFECTED PARAGRAPHS                     |
|----------|--------------|-------------------------------------------------------------------------------------------------------------------------------------------------------------------------------------------------------------------------------------------------------------------------------------------------------------------------------------------------------------------------------------------------------------------------------------------------------------------------------|-----------------------------------------|
| DRAFT 1  | 8 MARCH 2001 | First issue                                                                                                                                                                                                                                                                                                                                                                                                                                                                   |                                         |
| DRAFT 2  | JUNE 2001    | Derivation of the gradiometric error in the OAGRF. Implementation of ONERA comments and suggestions.<br>Re-apportionment of the requirements among the Instrument-Satellite Coupling Errors.                                                                                                                                                                                                                                                                                  | All                                     |
| ISSUE 01 | 14 FEB. 2002 | Reference frames update.<br>Magnetic field requirement derivation.<br>Addition of the angular acceleration measurement error analysis and of the derived requirements.<br>Addition of the first error budget.                                                                                                                                                                                                                                                                 | All                                     |
| ISSUE 02 | 8 JULY 2002  | Implementation of the instructions of the RID 3796.<br>Modification of the OAGRF definition and of the formulation of some of the error terms accordingly.<br>Updating of the breakdown of the errors related to the GRF pointing in the LORF.<br>Introduction of the inverse Calibration Matrix in the gradiometric error analysis.<br>Updating of the gradiometric error break-down and budget.<br>Addition of the error budget for the off diagonal components of the GGT. | All                                     |
| ISSUE 03 | 4 MAY 2005   | Re-formulation and re-computation of the error budget according to the new System Requirements Document and the new system configuration, following the cancellation of the micro-propulsion for the drag and attitude control.                                                                                                                                                                                                                                               | All                                     |
| ISSUE 04 | 22 FEB. 2008 | New maximum values of common and differential K2 by construction.<br><br>New GGT trace error apportionment.<br><br>New requirements on the differential scale factors and quadratic factors.<br><br>Update of the in-flight performance prediction accprding to the as-built satellite and payload.                                                                                                                                                                           | 4.1.2.2<br><br>5.3<br>6.1, 6.3<br><br>7 |

**TABLE OF CONTENTS**

|           |                                                                                              |           |
|-----------|----------------------------------------------------------------------------------------------|-----------|
| <b>1.</b> | <b>SCOPE.....</b>                                                                            | <b>8</b>  |
| 1.1       | PURPOSE.....                                                                                 | 8         |
| 1.2       | APPLICABILITY.....                                                                           | 8         |
| <b>2.</b> | <b>APPLICABLE AND REFERENCE DOCUMENTS .....</b>                                              | <b>9</b>  |
| 2.1       | APPLICABLE DOCUMENTS.....                                                                    | 9         |
| 2.2       | REFERENCE DOCUMENTS.....                                                                     | 9         |
| <b>3.</b> | <b>GRAVIMETRIC REFERENCE MISSION AND PERFORMANCE REQUIREMENTS.....</b>                       | <b>10</b> |
| 3.1       | SCIENTIFIC OBJECTIVES.....                                                                   | 10        |
| 3.2       | REFERENCE MISSION AND MISSION REFERENCE FRAMES.....                                          | 11        |
| 3.3       | THE GRAVITY GRADIOMETER .....                                                                | 13        |
| 3.3.1     | Gradiometer Composition.....                                                                 | 13        |
| 3.3.2     | Gradiometer Relevant Reference Frames.....                                                   | 14        |
| 3.4       | THE GRAVITY GRADIENT TENSOR.....                                                             | 26        |
| 3.4.1     | GGT Components in the LORF.....                                                              | 26        |
| 3.4.2     | GGT Components in the GRF.....                                                               | 27        |
| 3.5       | SATELLITE GRAVITY GRADIOMETRY PERFORMANCE REQUIREMENTS.....                                  | 31        |
| <b>4.</b> | <b>GRAVITY GRADIENT TENSOR MEASUREMENT PROCESS.....</b>                                      | <b>32</b> |
| 4.1       | GRAVITY GRADIENT TENSOR MEASUREMENT IN THE GRADIOMETER REFERENCE FRAME.....                  | 32        |
| 4.1.1     | Measurement with an Ideal Gradiometer.....                                                   | 32        |
| 4.1.2     | Measurement with a Real Gradiometer.....                                                     | 36        |
| 4.1.2.1   | Accelerometer Misplacement and Position Variation in Time.....                               | 37        |
| 4.1.2.2   | Accelerometer Mispointing, Coupling, Scale Factor, Quadratic Factor, Noise and Bias.....     | 38        |
| 4.1.2.3   | The Calibration Matrix and its Inverse.....                                                  | 43        |
| 4.1.2.4   | Tasks of the Gradiometer In-Flight Calibration.....                                          | 45        |
| 4.1.2.5   | From Level 0 to Level 1A/1B Gradiometric Products.....                                       | 47        |
| 4.1.2.6   | Gravity Gradient Tensor Measurement Errors in the OAGRF.....                                 | 49        |
| 4.1.2.7   | Gravity Gradient Tensor Measurement Errors in the GRF.....                                   | 56        |
| 4.2       | GGT MEASUREMENTS SPATIAL LOCATION.....                                                       | 58        |
| 4.3       | ANGULAR ACCELERATION MEASUREMENT ERRORS IN THE GRF.....                                      | 59        |
| <b>5.</b> | <b>ERROR TERMS CLASSIFICATION AND ERROR ALLOCATION .....</b>                                 | <b>61</b> |
| 5.1       | GRADIOMETRIC ERRORS CLASSIFICATION.....                                                      | 61        |
| 5.1.1     | Instrument Errors.....                                                                       | 62        |
| 5.1.2     | Instrument-Satellite Coupling Errors.....                                                    | 64        |
| 5.1.3     | Satellite Errors.....                                                                        | 68        |
| 5.1.4     | Processing Errors.....                                                                       | 68        |
| 5.2       | ANGULAR ACCELERATION MEASUREMENT ERRORS.....                                                 | 69        |
| 5.3       | ERROR TREE.....                                                                              | 73        |
| <b>6.</b> | <b>SPACECRAFT PERFORMANCE REQUIREMENTS.....</b>                                              | <b>78</b> |
| 6.1       | REQUIREMENTS RELATED TO THE INSTRUMENT-SATELLITE COUPLING ERRORS.....                        | 78        |
| 6.1.1     | C.1.1: Coupling with Non-Gravitational Linear Acceleration of the Satellite COM.....         | 78        |
| 6.1.1.1   | Differential Scale Factors, Misalignments and Couplings Knowledge and Stability Requirements | 78        |
| 6.1.1.2   | Non-Gravitational Linear Acceleration Control Requirements.....                              | 81        |
| 6.1.2     | C.2.1: Coupling with the Angular Acceleration of the Satellite About its COM.....            | 82        |
| 6.1.2.1   | Common, Misalignments and Couplings Knowledge and Stability Requirements.....                | 82        |
| 6.1.2.2   | Angular Acceleration Control Requirements.....                                               | 84        |
| 6.1.3     | C.2.2: Coupling with the centrifugal accelerations and the GGT.....                          | 85        |
| 6.1.3.1   | Common Scale Factors Knowledge and Stability Requirements.....                               | 85        |

|           |                                                                                                                                     |            |
|-----------|-------------------------------------------------------------------------------------------------------------------------------------|------------|
| 6.1.3.2   | Angular Rates Control Requirements .....                                                                                            | 87         |
| 6.1.4     | C.1.2: Couplings with COM Location and Stability in the OAGRF .....                                                                 | 89         |
| 6.1.5     | C.3: Quadratic Couplings .....                                                                                                      | 89         |
| 6.1.6     | C.4: Coupling with Accelerometer Misplacement from their Nominal Position in the OAGRF .....                                        | 90         |
| 6.1.7     | C.5: Coupling with the Platform Magnetic Field .....                                                                                | 90         |
| 6.1.8     | C.7: Coupling with the High Frequency Noise .....                                                                                   | 91         |
| 6.1.9     | C.8: Coupling with the Transfer Function Difference .....                                                                           | 91         |
| 6.1.10    | C.9: Angular-Linear Acceleration Coupling at Accelerometer Level .....                                                              | 92         |
| 6.2       | REQUIREMENTS RELATED TO THE SATELLITE ERRORS .....                                                                                  | 93         |
| 6.2.1     | S.1: Platform Self Gravity .....                                                                                                    | 93         |
| 6.3       | REQUIREMENTS RELATED TO PROCESSING ERRORS .....                                                                                     | 93         |
| 6.3.1     | P.1: Centrifugal Accelerations Recovery Error .....                                                                                 | 93         |
| 6.3.2     | Derived Requirements: Angular Acceleration Recovery Error .....                                                                     | 94         |
| <b>7.</b> | <b>IN-FLIGHT PERFORMANCE PREDICTION FOR THE GRADIOMETRIC MISSION .....</b>                                                          | <b>100</b> |
| 7.1       | PROCEDURE AND REFERENCE DATA FOR THE PERFORMANCE PREDICTION COMPUTATION .....                                                       | 100        |
| 7.1.1     | Instrument Errors Contributors .....                                                                                                | 100        |
| 7.1.1.1   | Accelerometer Noise (I.1) .....                                                                                                     | 100        |
| 7.1.1.2   | Accelerometer Position Stability (I.2) .....                                                                                        | 102        |
| 7.1.1.3   | OAGRFs alignment errors in the GRF and alignment stability in the GRF (I.3) .....                                                   | 102        |
| 7.1.1.4   | Gradiometer Self Gravity (I.4) .....                                                                                                | 102        |
| 7.1.1.5   | Coupling with Gradiometer Magnetic Field (I.5) .....                                                                                | 103        |
| 7.1.1.6   | Accelerometer Noise Coupling with Common/Differential Misalignments and Scale Factors (I.6)                                         | 103        |
| 7.1.2     | Instrument-Satellite Coupling Errors .....                                                                                          | 103        |
| 7.1.2.1   | Coupling with Common-Mode Accelerations (C.1) .....                                                                                 | 103        |
| 7.1.2.1.1 | Coupling with Non-Gravitational Linear Accelerations of the Satellite COM (C.1.1) .....                                             | 103        |
| 7.1.2.1.2 | Coupling with Satellite COM Location and Stability in the GRF (C.1.2) .....                                                         | 105        |
| 7.1.2.2   | Coupling with Differential-Mode Accelerations (C.2) .....                                                                           | 105        |
| 7.1.2.2.1 | Coupling with the Angular Acceleration of the Satellite about its COM (C.2.1) .....                                                 | 105        |
| 7.1.2.2.2 | Coupling with the Centrifugal Accelerations and the Gravity Gradient Tensor (C.2.2) .....                                           | 106        |
| 7.1.2.3   | Quadratic Coupling (C.3) .....                                                                                                      | 106        |
| 7.1.3     | Coupling with Accelerometer Misplacement from their Nominal Position (C.4) .....                                                    | 107        |
| 7.1.3.1   | Coupling with Platform Magnetic Field (C.5) .....                                                                                   | 107        |
| 7.1.3.2   | Coupling of Accelerometer Noise with Common and Differential-Mode Misalignments and Scale Factors Knowledge Uncertainty (C.6) ..... | 109        |
| 7.1.3.3   | Coupling with High Frequency Noise (C.7) .....                                                                                      | 109        |
| 7.1.3.4   | Coupling with the Transfer Function Difference (C.8) .....                                                                          | 110        |
| 7.1.3.5   | Coupling Between Angular and Linear Acceleration at Accelerometer Level (C.9) .....                                                 | 110        |
| 7.1.4     | Satellite Errors .....                                                                                                              | 111        |
| 7.1.4.1   | Platform Self Gravity (S.1) .....                                                                                                   | 111        |
| 7.1.5     | Processing Errors .....                                                                                                             | 111        |
| 7.1.5.1   | Centrifugal Accelerations Recovery Error (P.1) .....                                                                                | 111        |
| 7.2       | PERFORMANCE BUDGET FOR THE GGT DIAGONAL COMPONENTS AND FOR THE GGT TRACE                                                            | 112        |
| 7.3       | PERFORMANCE BUDGET FOR THE OFF-DIAGONAL COMPONENTS OF THE GGT .....                                                                 | 115        |
| 7.4       | PERFORMANCE BUDGET TREE .....                                                                                                       | 118        |
| 7.4.1     | Payloads Performance Prediction vs Specified Requirements .....                                                                     | 121        |
| 7.4.2     | Comparison of the analytical error budget with the numerical simulation results .....                                               | 124        |
| <b>8.</b> | <b>ACRONYMS AND ABBREVIATIONS .....</b>                                                                                             | <b>127</b> |

Figure 3.1-1: Example of definition of geoid height and gravity anomaly .....10

Figure 3.2-1: The GOCE orbit ( $i$  = inclination,  $\Omega$  = longitude of the ascending node,  $u$  = argument of latitude), the JERF ( $\equiv$  IRF) and the LORF. Note: the orbit size is not to scale with the Earth size .....12

Figure 3.3-1: Exploded view of the accelerometer core .....19

Figure 3.3-2: Accelerometer Electrode System Reference Frame and location/nomenclature of the 8 electrode pairs .....19

Figure 3.3-3: Accelerometer Reference Frames orientation corresponding to the accelerometers installation in the Three-Axis Gradiometer .....20

Figure 3.3-4: Accelerometer Alignment Reference Frame and Accelerometer External Reference Frame ( $U_E, V_E, W_E$ )  $\equiv$  ( $Y_E, Z_E, X_E$ ) .....20

Figure 3.3-5: One-Axis Gradiometer Reference Frame definition for the accelerometer pair  $A_1, A_4$  (top left) and nominal orientation of the ARF<sub>1</sub>, ARF<sub>4</sub> in the OAGRF<sub>1</sub> (top right), of the ARF<sub>2</sub>, ARF<sub>5</sub> in the OAGRF<sub>2</sub> (bottom left) and of the ARF<sub>3</sub>, ARF<sub>6</sub> in the OAGRF<sub>3</sub> (bottom right) .....21

Figure 3.3-6: Gradiometer Reference Frame (top) and its nominal orientation in the Satellite Physical Coordinate Reference Frame (Bottom). Thick arrow = accelerometer ultra sensitive axis; dashed arrow = less sensitive axis .....22

Figure 3.3-7: Orientation of the GRF (and of the Satellite Physical Coordinate Reference Frame) along the orbit during the measurement phase for a dusk-dawn orbit (summer launch) and dawn-dusk orbit (winter launch). .....23

Figure 3.3-8: Gradiometer Reference Frame ( $X_{GR}, Y_{GR}, Z_{GR}$ ), Gradiometer Assembly Reference Frame ( $X_{GR-ASSY}, Y_{GR-ASSY}, Z_{GR-ASSY}$ ) and Gradiometer Alignment Reference Frames ( $X_{GALI,2}, Y_{GALI,2}, Z_{GALI,2}$ ) .....24

Figure 3.3-9: Star Sensor Reference Frame of each Star Sensor installed on GOCE. The illustrated position of the Star Sensors on the satellite and the orientation of their SSRF with respect to the GRF refer to the case of a dawn- dusk sun-synchronous orbit. ....25

Figure 3.4-1: Components of the GGT in the LORF along ten orbits of GOCE .....28

Figure 3.4-2: Spectral density of the GGT components in the LORF .....29

Figure 3.4-3: Reference spectral density in the MBW of the GGT components in the GRF (smoothed) .....30

Figure 3.5-1: Upper limit of the total measurement error spectral density of the GGT trace built from the GGT diagonal components measured in the GRF (the blu line is the requirement in the MBW) .....31

Figure 4.1-1: Acceleration detected by each accelerometer .....32

Figure 4.1-2: Definition of the vectors  $\underline{R}_i, \underline{A}_i, \underline{C}$ , for the OAG<sub>1</sub> and the accelerometers  $A_1, A_4$  .....34

Figure 4.1-3: Definition of the vectors  $\underline{R}_i, \underline{A}_i, \underline{C}_k, \delta \underline{A}_i$  for the OAG<sub>1</sub> and the accelerometers  $A_1, A_4$  .....37

Figure 4.1-4: Relationship between the lateral misalignment  $\underline{\delta}$  of the accelerometer  $A_1$  in the ARF of the accelerometer  $A_4$  and the rotation angles  $\theta_1, \psi_1$  of the ARF<sub>1</sub> in the OAGRF<sub>1</sub> .....39

Figure 5.3-1: Gradiometric error tree .....74

Figure 5.3-2: Apportionment of the GGT trace error spectral density in the MBW among the four top-level contributors .....75

Figure 5.3-3: Instrument contributor to the GGT trace error, as per requirement defined in [AD 1] .....75

Figure 5.3-4: Apportionments of the requirement on the Gravity Gradient Tensor trace error among the various contributors at 5 mHz .....76

Figure 5.3-5: Apportionments of the requirement on the Gravity Gradient Tensor trace error among the various contributors at 100 mHz .....77

Figure 6.1-1: Contributions to the maximum value achieved by the elements of  $\delta \underline{M}_{ij}$  throughout a scientific measurement phase .....79

Figure 6.1-2: Spectral density upper limits for  $\delta \tilde{K}_{d,14,X}^W(\nu), \delta \tilde{K}_{d,25,Y}^W(\nu), \delta \tilde{K}_{d,36,Z}^W(\nu)$  .....81

Figure 6.1-3: Spectral density upper limits for  $\tilde{D}_X^W(\nu), \tilde{D}_Y^W(\nu), \tilde{D}_Z^W(\nu)$  .....82

Figure 6.1-4: Spectral density upper limits for  $\tilde{\omega}_X^W(\nu), \tilde{\omega}_Y^W(\nu), \tilde{\omega}_Z^W(\nu)$  .....85

Figure 6.1-5: Spectral density upper limits for  $\delta \tilde{K}_{c,14,X}^W(\nu), \delta \tilde{K}_{c,25,Y}^W(\nu), \delta \tilde{K}_{c,36,Z}^W(\nu)$  .....87

Figure 6.1-6: Spectral density upper limits for  $\tilde{\omega}_X^W(\nu), \tilde{\omega}_Y^W(\nu), \tilde{\omega}_Z^W(\nu)$  .....88

Figure 6.3-1: Spectral density upper limits for  $\delta \hat{\omega}_X^W(\nu), \delta \hat{\omega}_Y^W(\nu), \delta \hat{\omega}_Z^W(\nu)$  .....94

Figure 6.3-2: Spectral density upper limits for  $\delta \hat{\omega}_X^W(\nu), \delta \hat{\omega}_Y^W(\nu), \delta \hat{\omega}_Z^W(\nu)$  .....95

Figure 6.3-3: Spectral density upper limits for the accelerometer noise along the less sensitive axis .....96

Figure 7.1-1: Predicted spectral density of the accelerometer noise along the ultra sensitive axes .....101

Figure 7.1-2: Predicted spectral density of the accelerometer noise along the less sensitive axes .....101

Figure 7.1-3: Predicted spectral density of the accelerometer noise along the ultra sensitive axes after the compensation of a quadratic factor of  $1206 \text{ s}^2/\text{m}$  by displacement of the proof mass. ....102

Figure 7.1-4: Differential scale factor spectral densities for ultra sensitive ( $\delta\text{MI}_{14,41}$ ,  $\delta\text{MI}_{14,63}$ ,  $\delta\text{MI}_{25,41}$ ,  $\delta\text{MI}_{25,52}$ ,  $\delta\text{MI}_{36,41}$ ,  $\delta\text{MI}_{36,63}$ ) and less sensitive axes ( $\delta\text{MI}_{14,52}$ ,  $\delta\text{MI}_{25,63}$ ,  $\delta\text{MI}_{36,52}$ ) ..... 104

Figure 7.1-5: Common scale factor spectral densities for ultra sensitive ( $\delta\text{MI}_{14,44}$ ,  $\delta\text{MI}_{14,66}$ ,  $\delta\text{MI}_{25,44}$ ,  $\delta\text{MI}_{25,55}$ ,  $\delta\text{MI}_{36,44}$ ,  $\delta\text{MI}_{36,66}$ ) and less sensitive axes ( $\delta\text{MI}_{14,55}$ ,  $\delta\text{MI}_{25,66}$ ,  $\delta\text{MI}_{36,56}$ ) ..... 106

Figure 7.1-6: Spectral density of the platform magnetic field at the accelerometer location ( $B_{i,P}^W$ ) considered for the gradiometric error budget computation ..... 108

Figure 7.1-7: Spectral density of the high-frequency common-mode acceleration assumed for the computation of the aliasing by coupling with the accelerometer quadratic factor..... 109

Figure 7.2-1: Gradiometric error budget for the MOP-1 mission scenario (no effect on the noise from K2 compensation) ..... 113

Figure 7.2-2: Gradiometric error budget for the MOP-1 mission scenario (maximum effect on the noise from K2 compensation) ..... 114

Figure 7.3-1: Error budget for the off-diagonal GGT components for the MOP-1 mission scenario (no effect on the noise from K2 compensation) ..... 117

Figure 7.3-2: Error budget for the off-diagonal GGT components for the MOP-1 mission scenario (maximum effect on the noise from K2 compensation) ..... 117

Figure 7.4-1: Performance budget for Gravity Gradient Tensor trace at 5 mHz, ..... 119

Figure 7.4-2: Performance budget for Gravity Gradient Tensor trace at 100 mHz, ..... 120

Figure 7.4-3: Accelerometer noise error budget vs requirements (no effect on the noise from the in-flight compensation of the quadratic factor) ..... 121

Figure 7.4-4: Accelerometer noise error budget vs requirements (maximum effect on the noise from the in-flight compensation of the quadratic factor) ..... 121

Figure 7.4-5: Satellite linear acceleration control performance vs requirements ..... 122

Figure 7.4-6: Satellite angular acceleration control performance vs requirements ..... 123

Figure 7.4-7: Satellite angular rate control performance vs requirements ..... 123

Figure 7.4-8: Status of the implementation of the error tree within the E2E simulator ..... 124

Figure 7.4-9: PSD of the diagonal GGT components [ $\text{mE}/\text{Hz}^{1/2}$ ] and trace from the E2E L1B Product ..... 125

Figure 7.4-10: PSD of the off-diagonal GGT components from the E2E L1B Product ..... 126

|                                                                                                                                                                                                                                                                                                                                                                           |     |
|---------------------------------------------------------------------------------------------------------------------------------------------------------------------------------------------------------------------------------------------------------------------------------------------------------------------------------------------------------------------------|-----|
| Table 3.3-1: Correspondence between the axes of the AESRF and the axes of the ARF                                                                                                                                                                                                                                                                                         | 15  |
| Table 3.4-1: Gravity gradient tensor characteristics in the LORF for the GOCE 250-km orbit                                                                                                                                                                                                                                                                                | 26  |
| Table 3.4-2: Reference GGT characteristics in the GRF for requirements derivation, and error budget                                                                                                                                                                                                                                                                       | 27  |
| Table 4.1-1: Predicted maximum values of the common and differential quadratic factors of the three accelerometer pairs throughout the mission lifetime (in case of non adjustment on orbit).                                                                                                                                                                             | 42  |
| Table 4.1-2: Predicted maximum values of the common and differential scale factors, misalignment and coupling of the three accelerometer pairs throughout the mission lifetime.                                                                                                                                                                                           | 43  |
| Table 4.1-3: Expected upper limits for the values of the elements of $\mathbf{MI}_{ij}$ , all along the on-orbit mission lifetime                                                                                                                                                                                                                                         | 46  |
| Table 6.1-1: Knowledge accuracy requirements of the in-line elements of $[\mathbf{MI}]_{d,14}$ , $[\mathbf{MI}]_{d,25}$ , $[\mathbf{MI}]_{d,36}$ ( $\cong$ in-line differential scale factors, misalignments and couplings) during the measurement phases, and apportionement between measurement errors at calibration and stability between calibration phases.         | 80  |
| Table 6.1-2: Specification for the maximum value in the MBW of the spectral density of the in-line, elements of $[\delta\mathbf{MI}]_{d,14}$ , $[\delta\mathbf{MI}]_{d,25}$ , $[\delta\mathbf{MI}]_{d,36}$ during the measurement phases.                                                                                                                                 | 80  |
| Table 6.1-3: Control requirements of the non-gravitational accelerations of the spacecraft COM                                                                                                                                                                                                                                                                            | 81  |
| Table 6.1-4: Knowledge accuracy requirements of the in-line elements of $[\mathbf{MI}]_{c,14}$ , $[\mathbf{MI}]_{c,25}$ , $[\mathbf{MI}]_{c,36}$ ( $\cong$ in-line common misalignments and couplings) during the measurement phases, and apportionement between measurement errors at calibration and stability between calibration phases.                              | 83  |
| Table 6.1-5: Specification for the maximum value in the MBW of the spectral density of the in-line elements of $[\delta\mathbf{MI}]_{c,14}$ , $[\delta\mathbf{MI}]_{c,25}$ , $[\delta\mathbf{MI}]_{c,36}$ ( $\cong$ in-line common misalignments and couplings) during the measurement phases.                                                                            | 84  |
| Table 6.1-6: Control requirements of the angular accelerations of the spacecraft about its COM                                                                                                                                                                                                                                                                            | 84  |
| Table 6.1-7: Knowledge accuracy requirements of the in-line common scale factor element of $[\mathbf{MI}]_{c,14}$ , $[\mathbf{MI}]_{c,25}$ , $[\mathbf{MI}]_{c,36}$ during the measurement phases, and apportionement between measurement errors at calibration and stability between calibration phases.                                                                 | 86  |
| Table 6.1-8: Specification for the maximum value in the MBW of the spectral density of the in-line common scale factor element of $[\delta\mathbf{MI}]_{c,14}$ , $[\delta\mathbf{MI}]_{c,25}$ , $[\delta\mathbf{MI}]_{c,36}$ during the measurement phases.                                                                                                               | 87  |
| Table 6.1-9: Control requirements of the angular rates of the spacecraft about its COM                                                                                                                                                                                                                                                                                    | 88  |
| Table 6.1-10: Requirements on spacecraft COM location and stability in the OAGRF                                                                                                                                                                                                                                                                                          | 89  |
| Table 6.1-11: Requirements on the values of the in-line common and differential quadratic factors and their stability                                                                                                                                                                                                                                                     | 90  |
| Table 6.1-12: Requirements on displacements of the accelerometers in the OAGRF (= requirements on OAG baseline length knowledge accuracy and stability)                                                                                                                                                                                                                   | 90  |
| Table 6.2-1: Requirements on platform generated differential self-gravity acceleration on the proof masses                                                                                                                                                                                                                                                                | 93  |
| Table 6.3-1: Requirements on angular rates recovery accuracy                                                                                                                                                                                                                                                                                                              | 93  |
| Table 6.3-2: Requirements on angular acceleration recovery accuracy                                                                                                                                                                                                                                                                                                       | 94  |
| Table 6.3-3: Requirements on the common and differential noise of the accelerometer along the less sensitive axis                                                                                                                                                                                                                                                         | 95  |
| Table 6.3-4: Requirements on the on the variation rates of the accelerometer differential displacements in the OAGRF                                                                                                                                                                                                                                                      | 96  |
| Table 6.3-5: Requirements on the transversal components of the differential acceleration between the accelerometers belonging to the same OAG generated by the overall satellite self-gravity                                                                                                                                                                             | 96  |
| Table 6.3-6: Requirements on the transversal components of the differential acceleration between the accelerometers belonging to the same OAG generated by the coupling with spacecraft and Earth magnetic fields                                                                                                                                                         | 96  |
| Table 6.3-7: Knowledge accuracy requirements of the transversal elements of $[\mathbf{MI}]_{d,14}$ , $[\mathbf{MI}]_{d,25}$ , $[\mathbf{MI}]_{d,36}$ and $[\mathbf{MI}]_{c,14}$ , $[\mathbf{MI}]_{c,25}$ , $[\mathbf{MI}]_{c,36}$ , during the measurement phases, and apportionement between measurement errors at calibration and stability between calibration phases. | 97  |
| Table 6.3-8: Specification for the maximum value in the MBW of the spectral density of the transversal element of $[\mathbf{MI}]_{d,14}$ , $[\mathbf{MI}]_{d,25}$ , $[\mathbf{MI}]_{d,36}$ and $[\mathbf{MI}]_{c,14}$ , $[\mathbf{MI}]_{c,25}$ , $[\mathbf{MI}]_{c,36}$ , during the measurement phases.                                                                  | 98  |
| Table 6.3-9: Requirements on the values of the transversal common and differential quadratic factors and their stability                                                                                                                                                                                                                                                  | 98  |
| Table 6.3-10: Requirements on the mutual alignment of the three OAGRFs ( $\varphi$ , $\theta$ , $\psi$ = rotation angles defining the relative orientation between any pair of OAGRFs)                                                                                                                                                                                    | 98  |
| Table 6.3-11: Requirements on the contribution to CMRR along the OAG transversal axes of the accelerometer TF and of the Gradiometer structure TF                                                                                                                                                                                                                         | 99  |
| Table 6.3-12: Requirements on the angular-linear acceleration coupling factors at accelerometer level                                                                                                                                                                                                                                                                     | 99  |
| Table 7.1-1: Errors on the determination of the of $[\mathbf{MI}]_{d,14}$ , $[\mathbf{MI}]_{d,25}$ , $[\mathbf{MI}]_{d,36}$ and $[\mathbf{MI}]_{c,14}$ , $[\mathbf{MI}]_{c,25}$ , $[\mathbf{MI}]_{c,36}$ , resulting from the in-flight calibration                                                                                                                       | 104 |
| Table 7.1-2: Values of the quadratic factors considered for the gradiometric error budget computation                                                                                                                                                                                                                                                                     | 107 |

## 1. SCOPE

### 1.1 PURPOSE

The purpose of this document is:

- to provide a description of the GOCE gravimetric reference mission and of the reference gravity gradient tensor (GGT) model for the performance analysis
- to provide an end-to-end analysis of the GGT measurement process
- to provide the classification of the error sources of affecting the measurement of the GGT
- to allocate performance requirements to the identified error sources through the apportionment of the assigned top-level gradiometric performance requirement
- to define the procedure for the compilation of the error budget for the measurement of the GGT
- to provide the error budget for the measurement of the GGT (diagonal and off-diagonal components)

The error budget provided here represents the best current prediction of the in-flight mission performance, derived from the tests and analyses performed on the as-built GOCE payload and platform elements which concur to the determination of the Level 1b product of the GOCE gradiometric mission, so defined (ref. [AD 1]):

gravity gradients, in the Gradiometer Reference Frame and in the J2000 Reference Frame, together with the transformation matrices.

In particular, the top-level gradiometric performance requirement is specified only for the measurement of the GGT in the Gradiometer Reference Frame ([AD 1]). Thus this document is focused on this requirement either for the derivation of the lower level requirements derivation and for the error budget computation.

### 1.2 APPLICABILITY

This document represents:

- the reference document for the higher level performance requirements of the payload and platform subsystems/elements descending from the gradiometric mission implementation on GOCE
- the reference document for the prediction of the in-flight performances achievable in the measurement of the GGT (main Level 1b product of the GOCE gradiometric mission).

## 2. APPLICABLE AND REFERENCE DOCUMENTS

Unless explicitly indicated, all the documents in the following list are to be considered updated at their last issue.

### 2.1 APPLICABLE DOCUMENTS

[AD 1] GO-RS-ESA-SY-0002 GOCE System Requirements Document for Phase B/C/D/E1

### 2.2 REFERENCE DOCUMENTS

[RD 1] Accelerometer Model GO-TN-ONE-GR-0002

[RD 2] Gradiometer Performance Analysis and Budgets, GO-RP-ASC-0109

[RD 3] GA&E AC-CH Performance Analysis, GO-TN-ONE-0014

[RD 4] Gradiometer Ground Processing Algorithms Documentation

[RD 5] Gradiometer Transfer Function and Rejection of High Frequency, GO-TN-ONE-0004

[RD 6] Magnetic Field Interference with Gradiometer Measurement Analysis, GO-TN-AI-0050

[RD 7] Gradiometer on-orbit calibration procedure analysis, GO-TN-AI-0069

[RD 8] GOCE-DFAC Interface Control Document, GO-IC-ASG-0005, Issue5

[RD 9] GOCE System Thermo-Elastic Distortion Analysis, GO-TN-AI-0108

[RD 10] Assessment on the contribution of phase difference between accelerometers to the CMRR limitations, Fax GO-ONE-0079-2002, April 26 2002.

[RD 11] Computation of the transfer functions of the Gradiometer for stability purposes, GO-TN-ASC-0346

[RD 12] Annex 1 of GO-MI-AI-0355, 30-31/03/2004, and Annex 1 of GO-MI-AI-0381, 7/07/2004

[RD 13] Gradiometer Ground Processing Analysis, GO-TN-AI-0068

[RD 14] Gradiometer FM Performances In Flight, GO-RP-ASC-0919

[RD 15] OAG-X (OAG 1-4) Performance Verification, GO-TN-ONE-0074, Issue 3

### 3. GRAVIMETRIC REFERENCE MISSION AND PERFORMANCE REQUIREMENTS

#### 3.1 SCIENTIFIC OBJECTIVES

The aim of the GOCE mission is to provide global and regional models of the Earth's gravity field and of the geoid with high spatial resolution and high accuracy. The scientific requirements have been established as [AD 1]:

- after ground data processing, the accuracy of the geoid height calculated from the GOCE data shall be better than **0.1 cm** at degree and order  $\ell = 50$  (resolution on ground = **400 km**), and better than **1.0 cm** at degree and order  $L = 200$  (resolution on ground = **100 km**),
- after ground data processing, the accuracy of the gravity anomalies calculated from the GOCE data shall be better than **1 mgal** at degree and order  $\ell = 200$  (resolution on ground = **100 km**),

where an example of geoid height and the gravity anomaly definition is provided in Figure 3.1-1, and the degree and order refer to the expansion in spherical harmonics of the Earth gravity field.

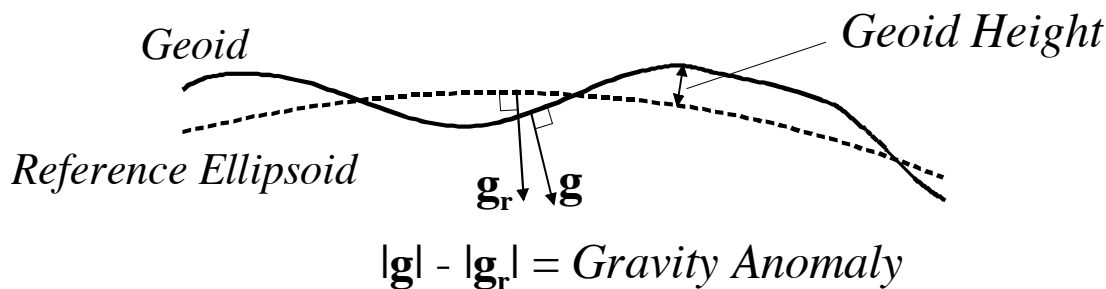


Figure 3.1-1: Example of definition of geoid height and gravity anomaly

GOCE will implement two measurement techniques for the recovery of the gravity field:

- Measurements of the components of the gravity gradient tensor by means of a gravity gradiometer (satellite gravity gradiometry – SGG – technique).
- Precise orbit determination (POD) by satellite-to-satellite tracking (SST) with the Global Positioning System (GPS), and by laser ranging.

The two techniques are complementary: by means of the POD it is possible to reconstruct with high accuracy the lower harmonics of the gravity field, while the SGG provides better performances at the medium and high degrees. The intersection is somewhere close to  $\ell = 15$ , according to the analyses performed so far. This complementarity aspect was investigated during the GOCE feasibility studies together with the critical issues related to the SGG instrument manufacturing, in order to define the optimal Measurement Bandwidth (MBW) for the SGG (i.e. the frequency region where the measurement accuracy of the gravity gradient tensor is maximised). As result of these analyses, an SGG MBW from 0.005 Hz to 0.1 Hz was established. In fact, numerical simulations of the gravity field recovery process have shown that the GOCE gradiometer data optimised in this frequency range may provide with a 70 km spatial resolution (= half wavelength of the highest harmonic degree and order solved for), in a global spherical harmonic analysis.

### 3.2 REFERENCE MISSION AND MISSION REFERENCE FRAMES

The GOCE satellite will fly on a circular, sun-synchronous dawn-dusk or dusk-dawn orbit (depending on the selected launch period along the year). The launch is planned to take place in May 2008 and the overall mission will last from 20 months (nominal lifetime) to 30 months (extended lifetime). The GOCE mission will take place during the ascending leg of the solar activity cycle, the minimum of which occurred in the year 2007. Within this mission, the gradiometric measurements are planned to be accomplished in two (nominal lifetime) or three (extended lifetime) phases of 6 months each. In the first measurement phase the mean altitude of the orbit will be around 268 km, while in the successive measurement phase(s), it will be raised to about 278 km.

The reference frames relevant for the GOCE gradiometric mission (all right-handed and orthogonal) are:

#### Inertial Reference Frame (IRF)

The fundamental inertial reference frame of the mission will be realised by the J2000 Equatorial Reference Frame (JERF), in accordance with [AD 1]. Thus it is defined as follows:

- Origin,  $O_{J2000}$ , located at the centre of the Earth.
- $X_{J2000}$  axis at the intersection of the mean ecliptic plane with the mean equatorial plane at the date of 01/01/2000 and pointing positively towards the vernal equinox.
- $Z_{J2000}$  axis orthogonal to the mean equatorial plane at the date 01/01/2000.
- $Y_{J2000}$  axis completing a right-handed reference frame.

#### Local Orbital Reference Frame (LORF)

- Origin,  $O_0$ , located at the actual satellite COM position
- $X_0$  (roll) axis parallel to the instantaneous direction of the orbital velocity vector ( $\underline{V}$ ), with the same sign of  $\underline{V}$ .
- $Y_0$  (pitch) axis parallel to instantaneous direction of the orbital angular momentum ( $\underline{N}$ ), with the same sign of  $\underline{N}$  ( $\underline{V}$  and  $\underline{N}$  are orthogonal by definition, since  $\underline{N} = \underline{R} \times \underline{V}$ , where  $\underline{R}$  is the vector from the Earth centre to  $O_0$ ).
- $Z_0$  (yaw) axis parallel to  $\underline{V} \times \underline{N}$ , with the same sign of  $\underline{V} \times \underline{N}$ .

Because of the unavoidable residual orbit eccentricity,  $Z_0$  will not be exactly parallel to the radial direction (from the Earth centre to the spacecraft). Along the GOCE mission, the orbit will evolve mainly under the gravitational perturbations, being the skin forces (atmospheric drag, solar radiation pressure) compensated by the drag-free control. In particular, under the effect of the gravitational perturbations, the mean orbit eccentricity is expected to reach a maximum value of about  $4.5 \cdot 10^{-3}$  along the mission, which originates in turn a deviation between  $Z_0$  and the radial direction up to  $0.26^\circ$ .

The LORF defines the reference attitude that must be (approximately) followed by the satellite during the gravimetric mission. This earth-pointing attitude allows in addition maintaining the minimum cross section of the satellite in the direction of motion, so minimising the atmospheric drag perturbation.

The GOCE orbit, the JERF ( $\equiv$  IRF) and the LORF are shown in Figure 3.2-1.

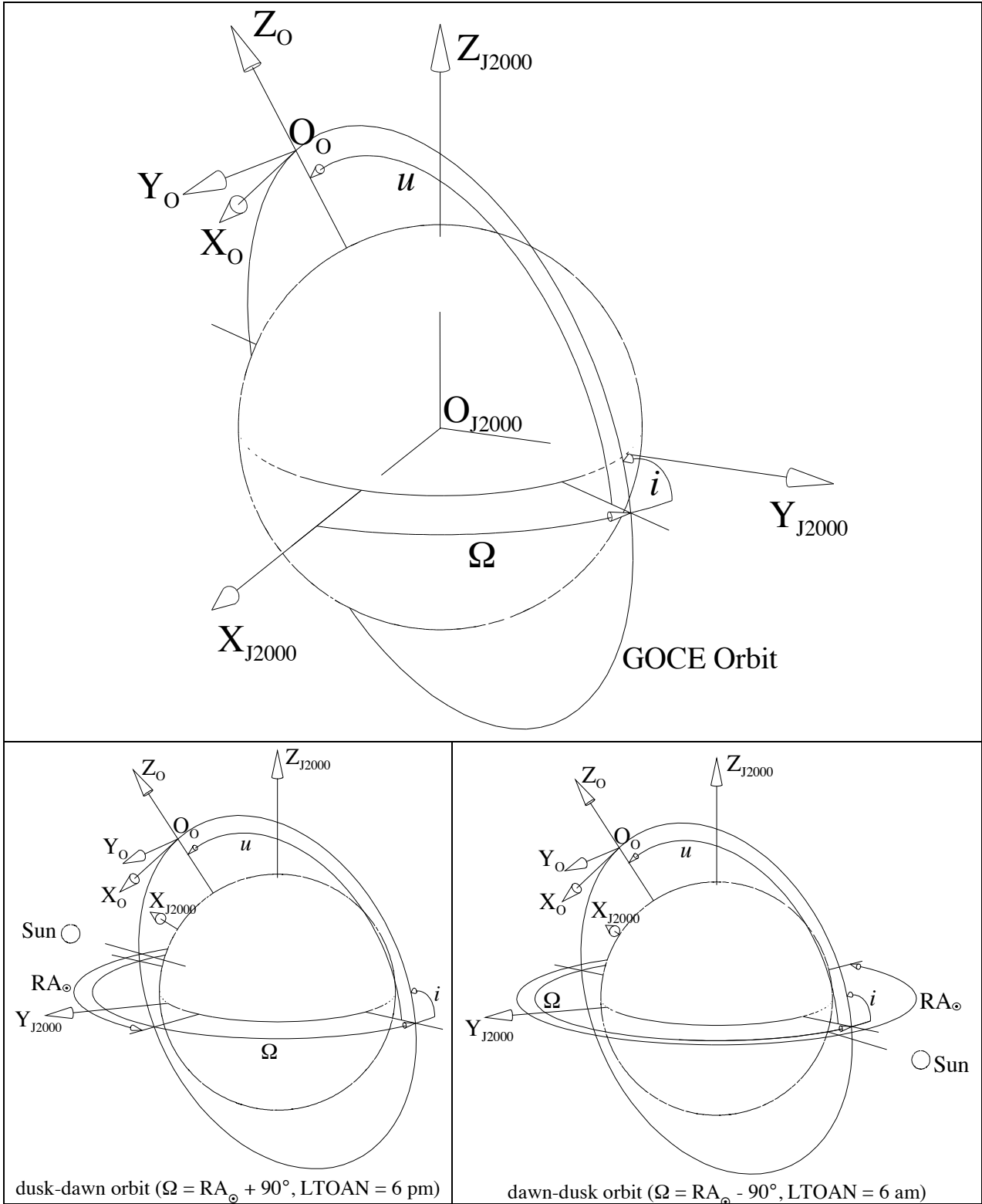


Figure 3.2-1: The GOCE orbit ( $i$  = inclination,  $\Omega$  = longitude of the ascending node,  $u$  = argument of latitude), the JERF (= IRF) and the LORF. Note: the orbit size is not to scale with the Earth size

### 3.3 THE GRAVITY GRADIOMETER

#### 3.3.1 Gradiometer Composition

The gravity gradient tensor along the GOCE orbit will be measured by an Electrostatic Gravity Gradiometer (EGG). The Gradiometer is composed by an ensemble of 6 three-axial accelerometers ( $A_1, \dots, A_6$ ). In each accelerometer a platinum-rhodium, 4x4x1 cm, 320 g proof mass is electrostatically suspended and actively controlled (in 6 DOFs) at the centre of a ULE™ cage by means of voltages applied to 16 electrodes (8 pairs) machined on the internal walls of the upper plate (4), the lower plate (4) and the ring plate (8) constituting the cage. A polarisation voltage is applied to the proof mass through a  $\varnothing = 5 \mu\text{m}$  gold wire glued on it (acting also as a charge control system to remove the charged particles in excess from the proof mass). The proof mass displacement relative to the electrodes is measured by capacitance sensors. The control voltages are representative of the accelerations of the proof mass relative to the cage. A picture of the GOCE accelerometer is shown in Figure 3.3-1.

The centre of the accelerometer is the point where the acceleration is measured. It is located at the geometric centre of the electrode ULE™ cage, where the COM of the proof mass (nominally coinciding with its geometric centre) is actively maintained by the accelerometer control loop.

Each accelerometer has two ultra sensitive axes and one less sensitive axis (perpendicular to the 4x4 wide side of the proof mass) designed to sustain 1g during ground tests. The accelerometers are designed to achieve the maximum sensitivity in the gradiometry measurement bandwidth (MBW), ranging from 5 mHz to 100 mHz. The upper limit of this band matches the resolution in the reconstruction of the gravity field. The lower limit of this band is defined by the crossover point at the low-degree harmonics between the gravity field reconstruction accuracy provided by the gravity gradiometry and that provided by the POD. The position control loops of the proof mass have cut-off frequencies well above the 100 mHz (for all axes), so that the sensor response to accelerations of the proof mass relative to the cage is substantially flat in the MBW.

The 6 accelerometers are mounted two by two on three support structures (spacers) having the function of keeping the sensors centres apart at a fixed distance. The mechanical interface between the accelerometer and the support structure is denoted as “sole plate”. A set of two accelerometers connected to their spacer forms a One-Axis Gradiometer (OAG), i.e. a device capable to measure the spatial gradient of the acceleration along the segment joining the centres of the two sensors (i.e. the centre of the ULE™ cages). This segment will be denoted as “baseline”.

The three OAGs are the fundamental gradiometric measurement units of the GOCE Gradiometer. The GGT components are in fact obtained from a combination of the measurements taken independently by the three OAGs.

By definition the accelerometers forming the three OAGs and their baseline lengths are denoted as:

- OAG<sub>1</sub>: accelerometers  $A_1$  and  $A_4$ ; baseline length =  $L_X$  (measured value = 513.0135 mm, reference for error budget)
- OAG<sub>2</sub>: accelerometers  $A_2$  and  $A_5$ ; baseline length =  $L_Y$  (measured value = 499.890 mm, reference for error budget)
- OAG<sub>3</sub>: accelerometers  $A_3$  and  $A_6$ ; baseline length =  $L_Z$  (measured value = 500.201 mm, reference for error budget)

One of the two ultra sensitive axes of each of the two accelerometers forming a OAG is nominally parallel to the OAG baseline. In the EGG, three OAGs are mounted nominally perpendicularly one to the other, so to have the mean points of the three baselines nominally coincident. This ensemble of three OAGs forms the Three-Axis Gradiometer (TAG), that will be also called Gradiometer for short (note: the name EGG will be used to denote the whole instrument comprising the TAG, the read-out electronics with its software, the structure and thermal control).

During the gravimetric measurements, the Gradiometer will be kept oriented such that its three baselines are nominally parallel to the axes of the LORF with:

- OAG<sub>1</sub> baseline along  $X_0$  with the accelerometer  $A_1$  towards the positive direction of  $X_0$ .
- OAG<sub>2</sub> baseline along  $Y_0$  with the accelerometer  $A_2$  towards the positive direction of  $Y_0$ .
- OAG<sub>3</sub> baseline along  $Z_0$  with the accelerometer  $A_3$  towards the positive direction of  $Z_0$ .

### 3.3.2 Gradiometer Relevant Reference Frames

The reference frames relevant to the GOCE Gradiometer (all right-handed and orthogonal), as far as the gravimetric measurement is concerned, are described hereafter.

#### Accelerometer Electrode System Reference Frame (AESRF)

This is the co-ordinate system with respect to which the locations of the control electrodes of the proof mass are referred (see Figure 3.3-2). For each accelerometer, it is defined as follows:

- Origin  $O_c$  located at the centre of the accelerometer.
- $X_c$ ,  $Y_c$  and  $Z_c$  axes parallel to the axes of the Accelerometer Reference Frame, with  $X_c$  along the less sensitive axis of the accelerometer and  $Y_c$ ,  $Z_c$  along the ultra sensitive axes of the accelerometer, so to form a right-handed co-ordinate system.

#### Accelerometer Reference Frame (ARF)

This is the reference frame in which the components of the acceleration of the proof mass relative to the cage are measured by the sensor. It is defined in a different way for three accelerometer pairs belonging to the three OAGs, so that the corresponding axes of all the ARFs are nominally aligned when the six accelerometers are installed in the Three-Axis Gradiometer (see Figure 3.3-3).

For all accelerometers  $A_i$

- Origin,  $O_i$ , located at the centre of the accelerometer  $A_i$ .

For the accelerometers  $A_1$ ,  $A_4$  belonging to OAG<sub>1</sub>

- $X_i$  axis parallel to the accelerometer ultra sensitive axis nominally aligned with the OAG<sub>1</sub> baseline, positive from the location of  $A_4$  to the location of  $A_1$ .
- $Z_i$  axis =  $\underline{X}_i \times \underline{L}$ , where  $\underline{X}_i$  is the unit vector of the axis  $X_i$  and  $\underline{L}$  is unit vector normal to the internal wall of the lower plate of the ULE<sup>TM</sup> cage (the lower plate is placed on the same side of the sole plate), positive in the opposite direction of the sole plate.  $Z_i$  is nominally parallel to the second ultra-sensitive axis of the accelerometer.
- $Y_i$  axis parallel to  $\underline{Z}_i \times \underline{X}_i$ , with the same sign of  $\underline{Z}_i \times \underline{X}_i$ .  $Y_i$  is nominally parallel to the less sensitive axis of the accelerometer.

For the accelerometers  $A_2$ ,  $A_5$  belonging to OAG<sub>2</sub>

- $Y_i$  axis parallel to the accelerometer ultra sensitive axis nominally aligned with the OAG<sub>2</sub> baseline, positive from the location of  $A_5$  to the location of  $A_2$ .
- $X_i$  axis =  $\underline{Y}_i \times \underline{L}$ , where  $\underline{Y}_i$  is the unit vector of the axis  $Y_i$  and  $\underline{L}$  is unit vector normal to the internal wall of the lower plate of the ULE<sup>TM</sup> cage, positive in the opposite direction of the sole plate.  $X_i$  is nominally parallel to the second ultra-sensitive axis of the accelerometer.
- $Z_i$  axis parallel to  $\underline{X}_i \times \underline{Y}_i$ , with the same sign of  $\underline{X}_i \times \underline{Y}_i$ .  $Z_i$  is nominally parallel to the less sensitive axis of the accelerometer.

For the accelerometers  $A_3$ ,  $A_6$  belonging to OAG<sub>3</sub>

- $Z_i$  axis parallel to the accelerometer ultra sensitive axis nominally aligned with the OAG<sub>3</sub> baseline, positive from the location of  $A_6$  to the location of  $A_3$ .
- $X_i$  axis =  $\underline{L} \times \underline{Z}_i$ , where  $\underline{Z}_i$  is the unit vector of the axis  $Z_i$  and  $\underline{L}$  is unit vector normal to the internal wall of the lower plate of the ULE<sup>TM</sup> cage, positive in the opposite direction of the sole plate.  $X_i$  is nominally parallel to the second ultra-sensitive axis of the accelerometer.
- $Y_i$  axis parallel to  $\underline{Z}_i \times \underline{X}_i$ , with the same sign of  $\underline{Z}_i \times \underline{X}_i$ .  $Y_i$  is nominally parallel to the less sensitive axis of the accelerometer.

The correspondence between the axes of the AESRFs and those of the ARFs for the 6 accelerometers is as in Table 3.3-1:

| Accelerometer                   | Axis of the AESRF | Corresponding axis of the ARF     |
|---------------------------------|-------------------|-----------------------------------|
| A <sub>1</sub> , A <sub>4</sub> | +X <sub>e</sub>   | +Y <sub>1</sub> , +Y <sub>4</sub> |
|                                 | +Y <sub>e</sub>   | -Z <sub>1</sub> , -Z <sub>4</sub> |
|                                 | +Z <sub>e</sub>   | -X <sub>1</sub> , -X <sub>4</sub> |
| A <sub>2</sub> , A <sub>5</sub> | +X <sub>e</sub>   | +Z <sub>2</sub> , +Z <sub>5</sub> |
|                                 | +Y <sub>e</sub>   | -X <sub>2</sub> , -X <sub>5</sub> |
|                                 | +Z <sub>e</sub>   | -Y <sub>2</sub> , -Y <sub>5</sub> |
| A <sub>3</sub> , A <sub>6</sub> | +X <sub>e</sub>   | +Y <sub>3</sub> , +Y <sub>6</sub> |
|                                 | +Y <sub>e</sub>   | -X <sub>3</sub> , -X <sub>6</sub> |
|                                 | +Z <sub>e</sub>   | +Z <sub>3</sub> , +Z <sub>6</sub> |

Table 3.3-1: Correspondence between the axes of the AESRF and the axes of the ARF

Accelerometer Alignment Reference Frame (AARF)

This frame is associated the six reference markers accessible from the outside of the accelerometer (they are on the sole plate) which are utilised for the positioning and alignment of the accelerometers within the OAGs (see Figure 3.3-4). For each accelerometer, it is defined as follows:

Let P1 be the plane including the markers 1, 2, 3. Let P2 be the plane orthogonal to P1 and including the markers 4, 5. Let P3 be the plane orthogonal to P1 and P2 and including the marker 6.

- The origin O<sub>A</sub> of the AARF is located at the intersection of the planes P1, P2, P3.
- The X<sub>A</sub> axis of the AARF is perpendicular to the plane P1, oriented from the sole plate to the proof mass.
- The Z<sub>A</sub> axis of the AARF is parallel to the intersection of the planes P1 and P2, oriented from the marker 5 to the marker 4.
- The axis Y<sub>A</sub> is parallel to  $\underline{Z}_A \times \underline{X}_A$ , with the same sign of  $\underline{Z}_A \times \underline{X}_A$ .

The axes X<sub>A</sub>, Y<sub>A</sub>, Z<sub>A</sub> of the AARF are nominally aligned to the axes X<sub>e</sub>, Y<sub>e</sub>, Z<sub>e</sub> of the AESRF, with the same versus.

Accelerometer External Reference Frame (AERF)

This frame is rigidly linked to the AARF (so it is accessible from the outside of the accelerometer as a consequence of the external accessibility of the AARF), but its origin is located at the center at the centre of the accelerometer, as for the ARF (see Figure 3.3-4). As for the ARF, the definition of the AERF is different for the three accelerometer pairs belonging to the three OAGs.

The AERF has the same definition for all accelerometers A<sub>i</sub>.

- Origin, O<sub>E</sub>, located in the point with co-ordinates X = +17.63 mm, Y = +80 mm, Z = +80 mm in the AARF (nominal location of the centre of the accelerometer in the AARF).
- Axes X<sub>E</sub>, Y<sub>E</sub>, Z<sub>E</sub> of the AERF nominally aligned to the axes X<sub>A</sub>, Y<sub>A</sub>, Z<sub>A</sub> of the AARF, with the same versus.

One-Axis Gradiometer Reference Frame (OAGRF)

This is the reference frame in which the components of the gravity gradient tensor are measured by the OAG, and is defined as follows (see Figure 3.3-5):

For OAG<sub>1</sub>

- Origin, O<sub>1OGR</sub>, located in the mid-point of the straight line joining the origin O<sub>4</sub> of ARF<sub>4</sub> to the origin O<sub>1</sub> of ARF<sub>1</sub>.
- X<sub>1OGR</sub> axis parallel to the line joining O<sub>4</sub> to O<sub>1</sub>, oriented from O<sub>4</sub> to O<sub>1</sub>.

- $Y1_{OGR}$  parallel to and with the same versus of the vector  $\bar{Y} = \frac{Y'_1}{|Y'_1|} + \frac{Y'_4}{|Y'_4|}$  where  $Y'_1, Y'_4$  are the projections of the vectors  $Y_1$  and  $Y_4$  on the plane perpendicular to  $X1_{OGR}$ .
- $Z1_{OGR}$  parallel to  $X1_{OGR} \times Y1_{OGR}$ , with the same sign of  $X1_{OGR} \times Y1_{OGR}$ .

For OAG<sub>2</sub>

- Origin,  $O2_{OGR}$ , located in the mid-point of the straight line joining the origin  $O_5$  of ARF<sub>5</sub> to the origin  $O_2$  of ARF<sub>2</sub>.
- $Y2_{OGR}$  axis parallel to the line joining  $O_5$  to  $O_2$ , oriented from  $O_5$  to  $O_2$ .
- $Z2_{OGR}$  parallel to and with the same versus of the vector  $\bar{Z} = \frac{Z'_2}{|Z'_2|} + \frac{Z'_5}{|Z'_5|}$  where  $Z'_2, Z'_5$  are the projections of the vectors  $Z_2$  and  $Z_5$  on the plane perpendicular to  $Y2_{OGR}$ .
- $X2_{OGR}$  parallel to  $Y2_{OGR} \times Z2_{OGR}$ , with the same sign of  $Y2_{OGR} \times Z2_{OGR}$ .

For OAG<sub>3</sub>

- Origin,  $O3_{OGR}$ , located in the mid-point of the straight line joining the origin  $O_6$  of ARF<sub>6</sub> to the origin  $O_3$  of ARF<sub>3</sub>.
- $Z3_{OGR}$  axis parallel to the line joining  $O_6$  to  $O_3$ , oriented from  $O_6$  to  $O_3$ .
- $Y3_{OGR}$  parallel to and with the same versus of the vector  $\bar{Y} = \frac{Y'_3}{|Y'_3|} + \frac{Y'_6}{|Y'_6|}$  where  $Y'_3, Y'_6$  are the projections of the vectors  $Y_3$  and  $Y_6$  on the plane perpendicular to  $Z3_{OGR}$ .
- $X3_{OGR}$  parallel to  $Y3_{OGR} \times Z3_{OGR}$ , with the same sign of  $Y3_{OGR} \times Z3_{OGR}$ .

The nominal positions of the origins of the 6 ARFs (coincident with the nominal position of the origins of the 6 AERFs) in each of the OAGRFs are defined by the following vectors:

$$\underline{A}_1 = \frac{L_X}{2} \begin{pmatrix} 1 \\ 0 \\ 0 \end{pmatrix}, \underline{A}_4 = \frac{L_X}{2} \begin{pmatrix} -1 \\ 0 \\ 0 \end{pmatrix} \text{ nominal position vectors of } O_1, O_4 (O_{E,1}, O_{E,4}) \text{ in the OAGRF}_1,$$

$$\underline{A}_2 = \frac{L_Y}{2} \begin{pmatrix} 0 \\ 1 \\ 0 \end{pmatrix}, \underline{A}_5 = \frac{L_Y}{2} \begin{pmatrix} 0 \\ -1 \\ 0 \end{pmatrix} \text{ nominal position vectors of } O_2, O_5 (O_{E,2}, O_{E,5}) \text{ in the OAGRF}_2,$$

$$\underline{A}_3 = \frac{L_Z}{2} \begin{pmatrix} 0 \\ 0 \\ 1 \end{pmatrix}, \underline{A}_6 = \frac{L_Z}{2} \begin{pmatrix} 0 \\ 0 \\ -1 \end{pmatrix} \text{ nominal position vectors of } O_3, O_6 (O_{E,3}, O_{E,6}) \text{ in the OAGRF}_3.$$

with

$L_X$  = nominal length of the OAG<sub>1</sub> baseline along the  $X1_{OGR}$  axis

$L_Y$  = nominal length of the OAG<sub>2</sub> baseline along the  $Y2_{OGR}$  axis

$L_Z$  = nominal length of the OAG<sub>3</sub> baseline along the  $Z3_{OGR}$  axis

### Gradiometer Reference Frame (GRF)

The GRF represents the Three-Axis Gradiometer common reference for the mutual positioning and alignment of the three OAGs, and for definition of the positioning and orientation of the whole instrument w.r.t. external reference frames. It can be thus identified as the reference frame in which the components of the gravity gradient tensor are measured by the Gradiometer. The GRF is defined to be coincident with the OAGRF<sub>3</sub>:

- Origin,  $O_{GR}$ , located in the position of  $O_{3OGR}$
- $X_{GR}, Y_{GR}, Z_{GR}$  parallel to  $X_{3OGR}, Y_{3OGR}, Z_{3OGR}$ , with the same sign.

The nominal configuration of the Gradiometer, is such that:

- $O_{1OGR}, O_{2OGR}, O_{3OGR}$ , are coincident (thus  $O_{GR}$  is located at the intersection of the three baselines)
- The corresponding axes of the three OAGRFs are parallel and pointing in the same directions.
- The corresponding axes of the 6 ARFs are parallel and pointing in the same directions.

The GRF is shown in Figure 3.3-6. In this picture the accelerometer ultra sensitive axes are indicated by solid arrows and the less sensitive axes are indicated by dashed arrows. In this document we will denote as "in-line axis" the accelerometer sensitive axis aligned to the baseline of the OAG to which it belongs and as "transversal axes" the other two axes.

The Gradiometer is mounted on the satellite with the GRF axes nominally aligned to the Satellite Physical Coordinate Reference Frame, which is defined as follows:

- Origin,  $O-SL$ , located on the Satellite/Launcher separation plane at the centre of the SL to Launcher interface circle.
- $X-SL$  axis perpendicular to the Satellite/Launcher separation plane, pointing positively from the separation plane towards the Satellite.
- $Y-SL$  axis orthogonal to the Solar Arrays plane, pointing positively towards the direction opposite to the surface where solar cells are mounted.
- $Z-SL$  axis completing a right-handed coordinate system.

The accommodation of the Gradiometer on the satellite and the orientation of the GRF relatively to the Satellite Physical Coordinate Reference Frame are shown in Figure 3.3-6.

During the measurement phase the GRF is kept approximately aligned to the LORF as shown in Figure 3.4-6:  $X_{GR}, Y_{GR}, Z_{GR}$  parallel to  $X_O, Y_O, Z_O$ , with the same sign. The arrangement of the accelerometer ultra sensitive axes ensures the maximum sensitivity for the measurement of the diagonal components of the GGT in the GRF ( $U_{XX}, U_{YY}, U_{ZZ}$ , which represent the main input for the determination of the Earth's gravity field), of the off-diagonal component  $U_{XZ}$ , and of the angular acceleration about the Y axis of the GRF.

As said in section 3.2, the sun-synchronous orbit of GOCE can be of two types: dusk-dawn or dawn-dusk (the choice depends on the launch date). Depending on the chosen orbit, the GRF will have different orientations in the LORF (this orientation is constrained by the presence of the solar cells on the negative Y-SL axis):

- dusk-dawn :  $X_{GR} \rightarrow +X_O, Y_{GR} \rightarrow -Y_O, Z_{GR} \rightarrow -Z_O$
- dawn-dusk :  $X_{GR} \rightarrow +X_O, Y_{GR} \rightarrow +Y_O, Z_{GR} \rightarrow +Z_O$

Therefore, for instance, the radial component of the GGT in the GRF, computed as described in this document, will be positive when the satellite will fly a dawn-dusk orbit and negative for a dusk-dawn orbit.

The orientation of the satellite and of the GTF along the orbit for a dusk-dawn and a dawn-dusk is shown in Figure 3.3-8.

#### Gradiometer Assembly Reference Frame (GASRF)

This frame is associated to the interface (separation) plane between the Gradiometer and the satellite and is defined as follows (see Figure 3.3-8):

- Origin,  $O_{GR-ASSY}$ , located at the centre of the Intermediate Tray (platform which supports the Gradiometer core with the 6 accelerometers, and is connected to the structure of the satellite), on the mechanical interface plane between the Gradiometer core and the spacecraft
- $X_{GR-ASSY}$  axis aligned to the  $X_{GR}$  axis of the GRF

- $Y_{GR-ASSY}$  axis aligned to the  $Y_{GR}$  axis of the GRF
- $Z_{GR-ASSY}$  axis aligned to the  $Z_{GR}$  axis of the GRF

#### Gradiometer Alignment Reference Frame (GARF)

This frame is associated to the two Gradiometer Reference Cubes installed on the EGG core and utilised for the measurement of the orientation of the Three-Axis Gradiometer relative to the satellite. For each Gradiometer Reference Cube it is defined as follows:

- Origin,  $O_{GAL}$ , located at the centre of the Gradiometer Reference Cube(s)
- $X_{GAL}$ ,  $Y_{GAL}$ ,  $Z_{GAL}$  axes perpendicular to the faces of the Gradiometer Reference Cube(s).

The nominal orientation of the GARF w.r.t. the GRF (the axes of the two frames are not aligned) depends on the Gradiometer Reference Cubes to which the frame definition is referred. For the Gradiometer Reference Cube 1, the  $(X_{GAL1}, Y_{GAL1}, Z_{GAL1})$  frame has the  $X_{GAL1}$  parallel to  $X_{GR}$  and is rotated through an angle of  $5^\circ$  about the  $X_{GAL1}$  in the clockwise direction. For the Gradiometer Reference Cube 2, the  $(X_{GAL2}, Y_{GAL2}, Z_{GAL2})$  frame has the  $X_{GAL2}$  parallel to  $X_{GR}$  and is rotated through an angle of  $5^\circ$  about the  $X_{GAL2}$  in the counter clockwise direction (see Figure 3.3-8).

#### Star Sensor Reference Frame (SSRF)

This is the reference frame whose inertial orientation is provided by the measurements of the Star Sensor itself. It is defined as follows:

- $Z_s$  axis along the boresight of the star sensor.
- $X_s$ ,  $Y_s$  axes lying on the star sensor focal plane, perpendicular with the  $Z_s$  axis and forming with it a right-handed coordinate system.

There are three Star Sensors on GOCE. The position of the Star Sensors on the satellite and the orientation of their SSRF with respect to the GRF depend on the type of sun-synchronous orbit in which GOCE will be launched: dusk-dawn or dawn-dusk. Figure 3.3-9 shows the case relative to the dawn-dusk orbit.

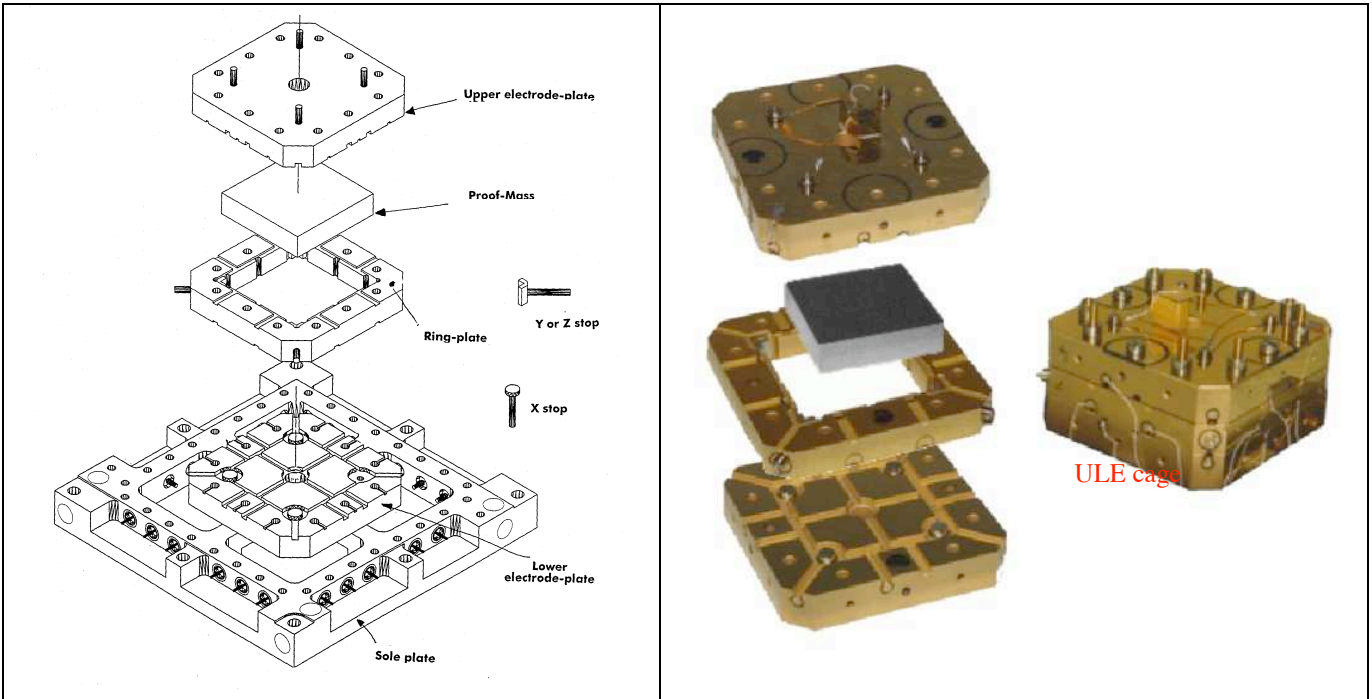


Figure 3.3-1: Exploded view of the accelerometer core

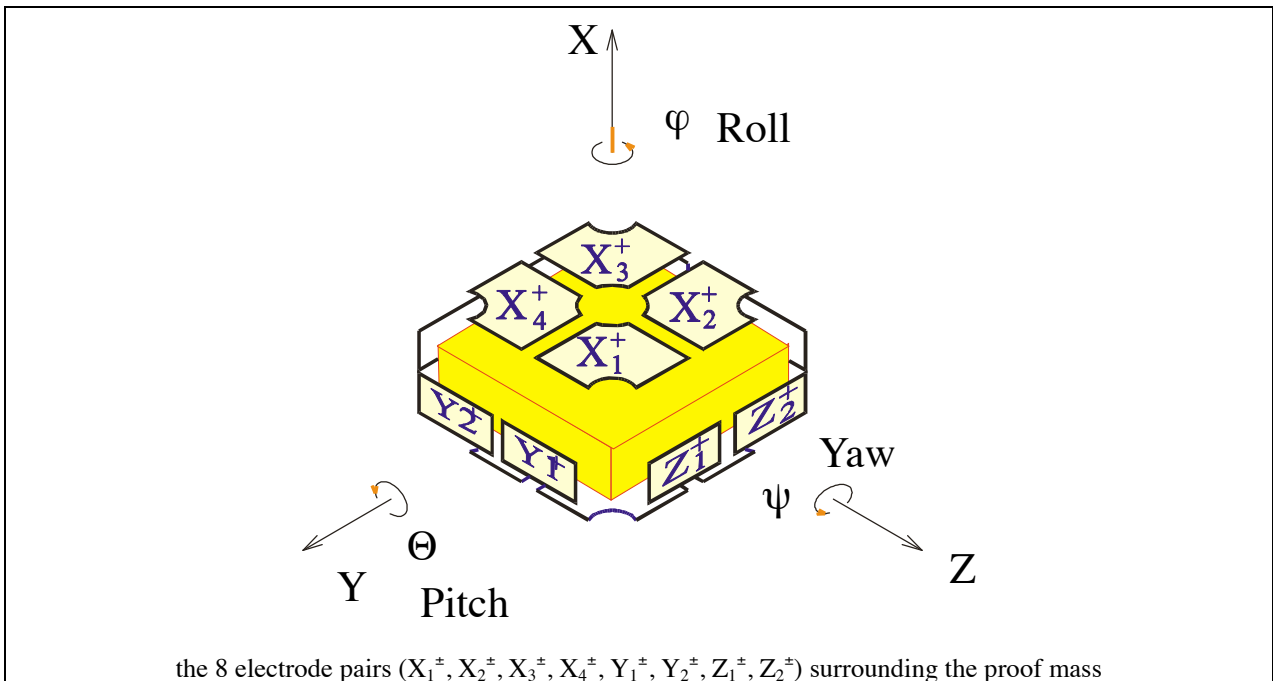


Figure 3.3-2: Accelerometer Electrode System Reference Frame and location/nomenclature of the 8 electrode pairs

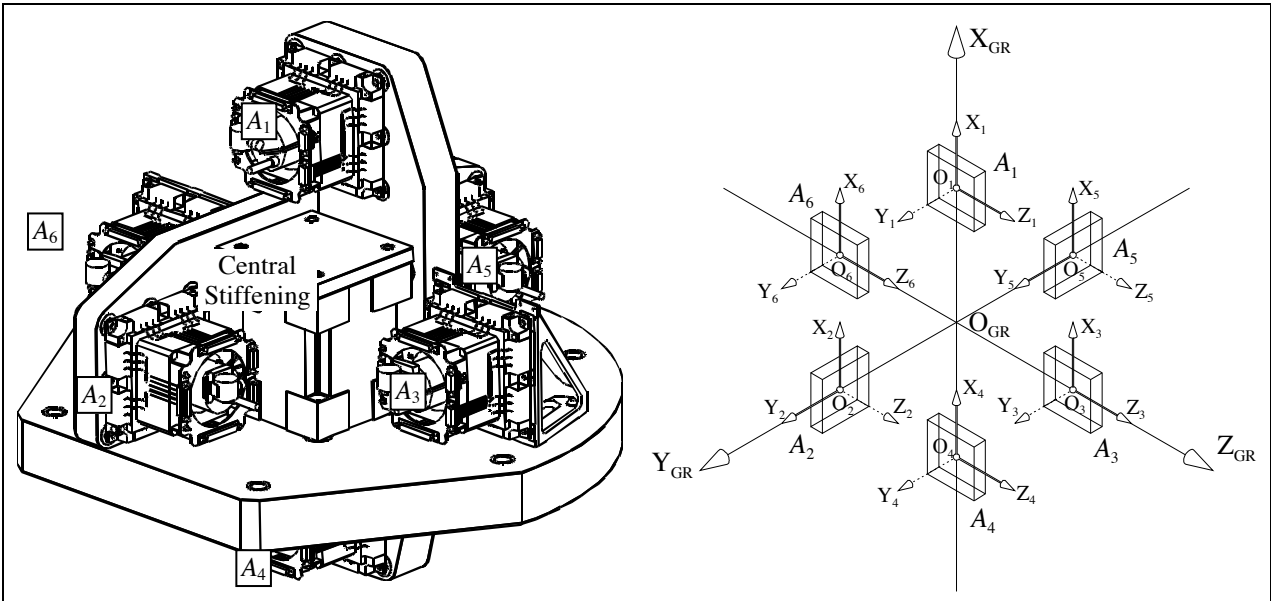


Figure 3.3-3: Accelerometer Reference Frames orientation corresponding to the accelerometers installation in the Three-Axis Gradiometer

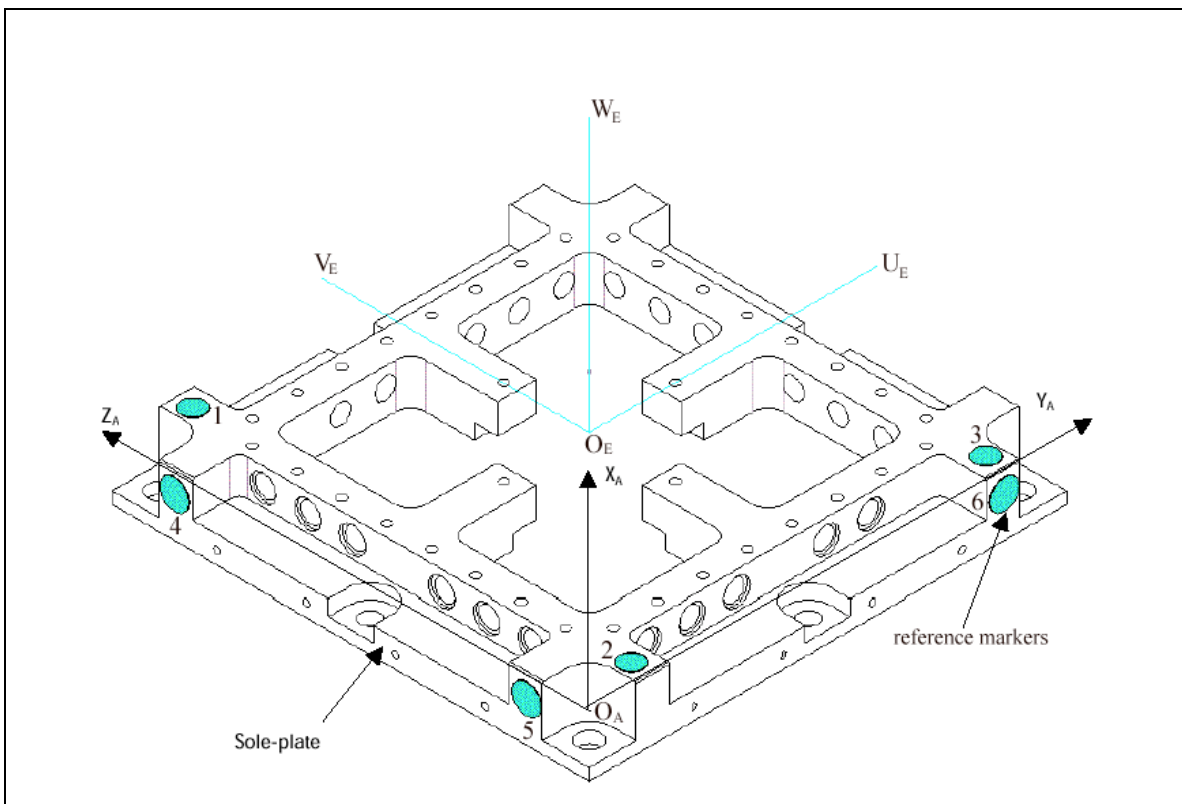


Figure 3.3-4: Accelerometer Alignment Reference Frame and Accelerometer External Reference Frame  $(U_E, V_E, W_E) \equiv (Y_E, Z_E, X_E)$

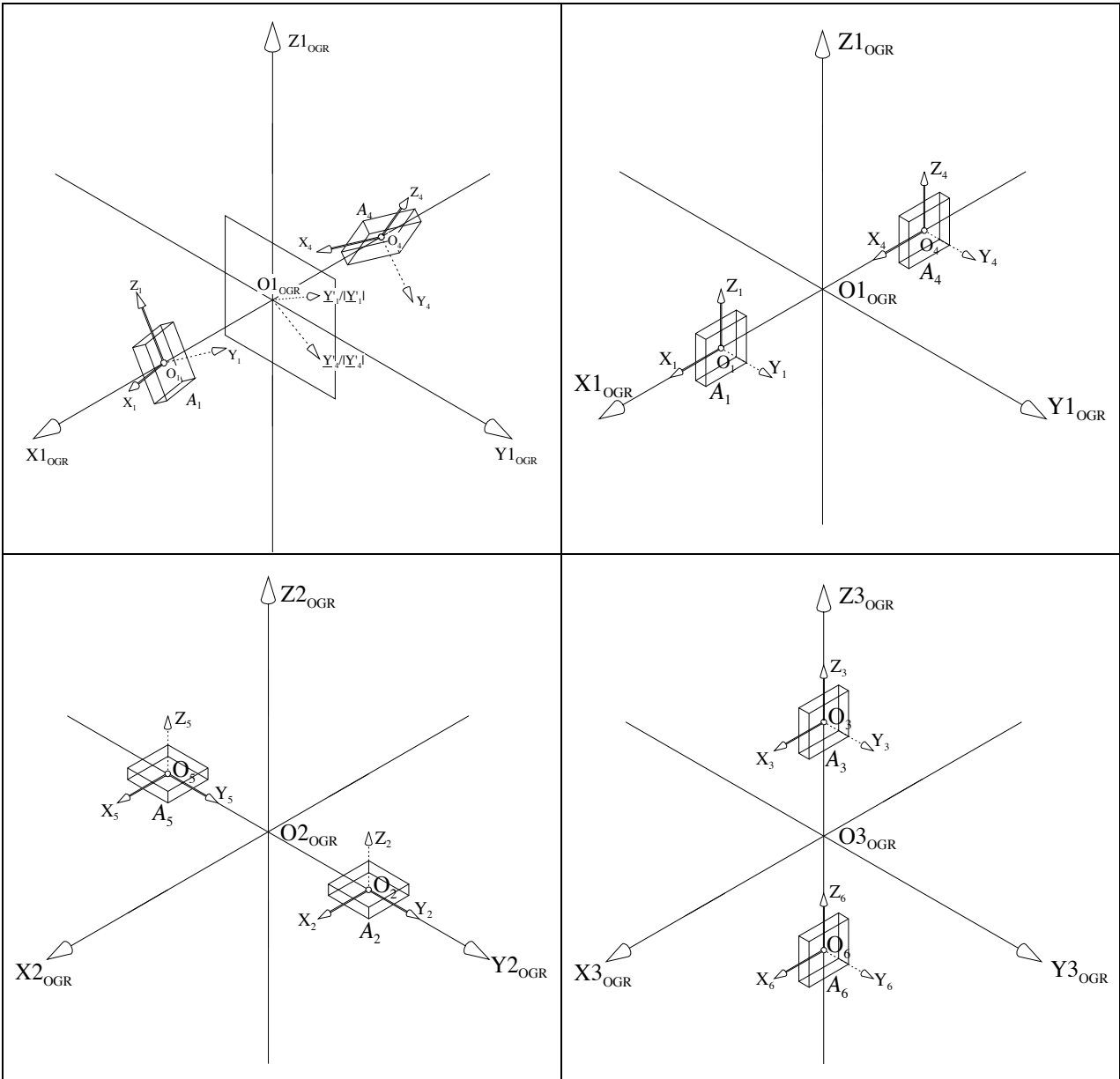


Figure 3.3-5: One-Axis Gradiometer Reference Frame definition for the accelerometer pair  $A_1, A_4$  (top left) and nominal orientation of the  $ARF_1, ARF_4$  in the  $OAGRF_1$  (top right), of the  $ARF_2, ARF_5$  in the  $OAGRF_2$  (bottom left) and of the  $ARF_3, ARF_6$  in the  $OAGRF_3$  (bottom right)

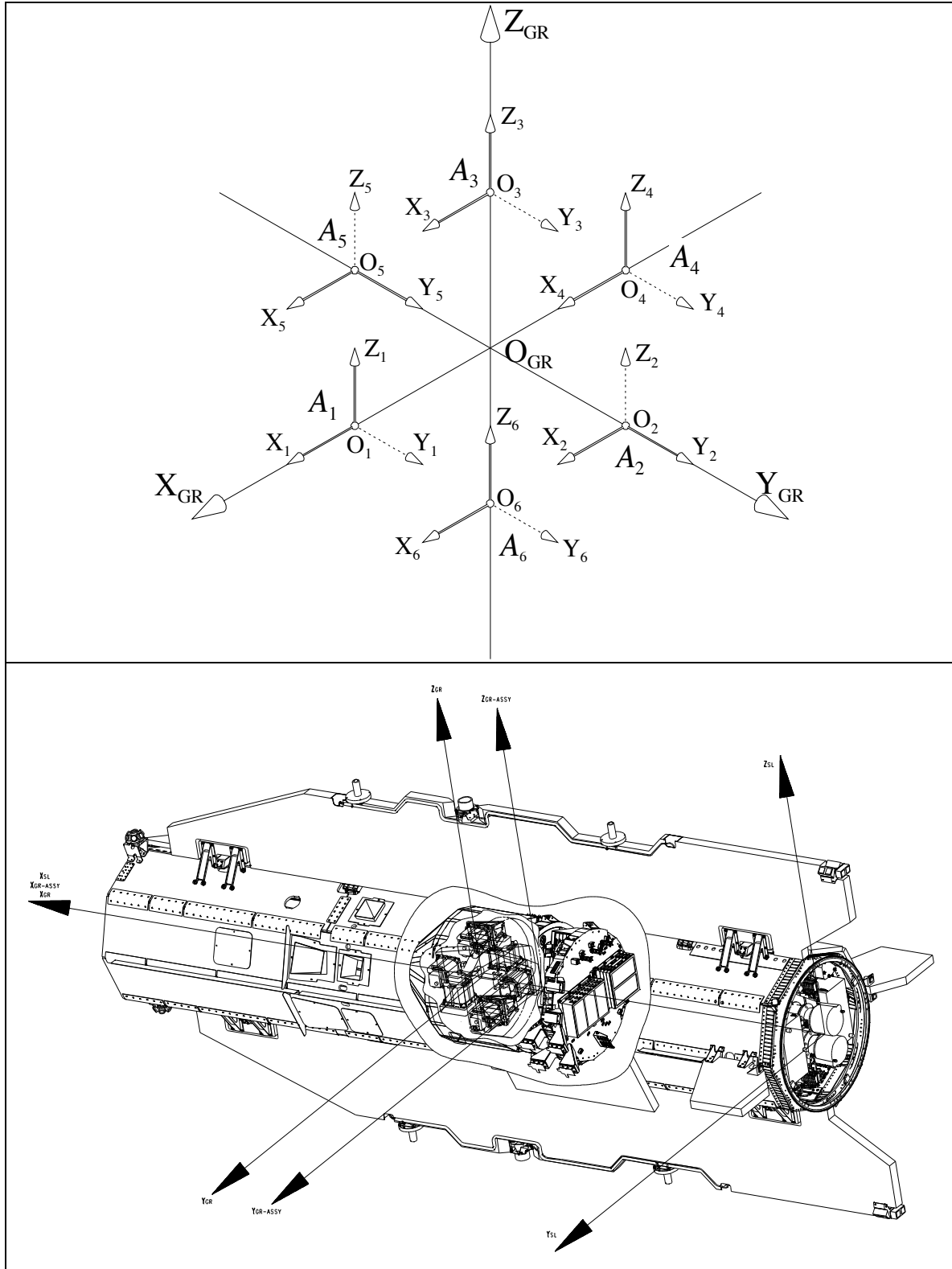


Figure 3.3-6: Gradiometer Reference Frame (top) and its nominal orientation in the Satellite Physical Coordinate Reference Frame (Bottom). Thick arrow = accelerometer ultra sensitive axis; dashed arrow = less sensitive axis.

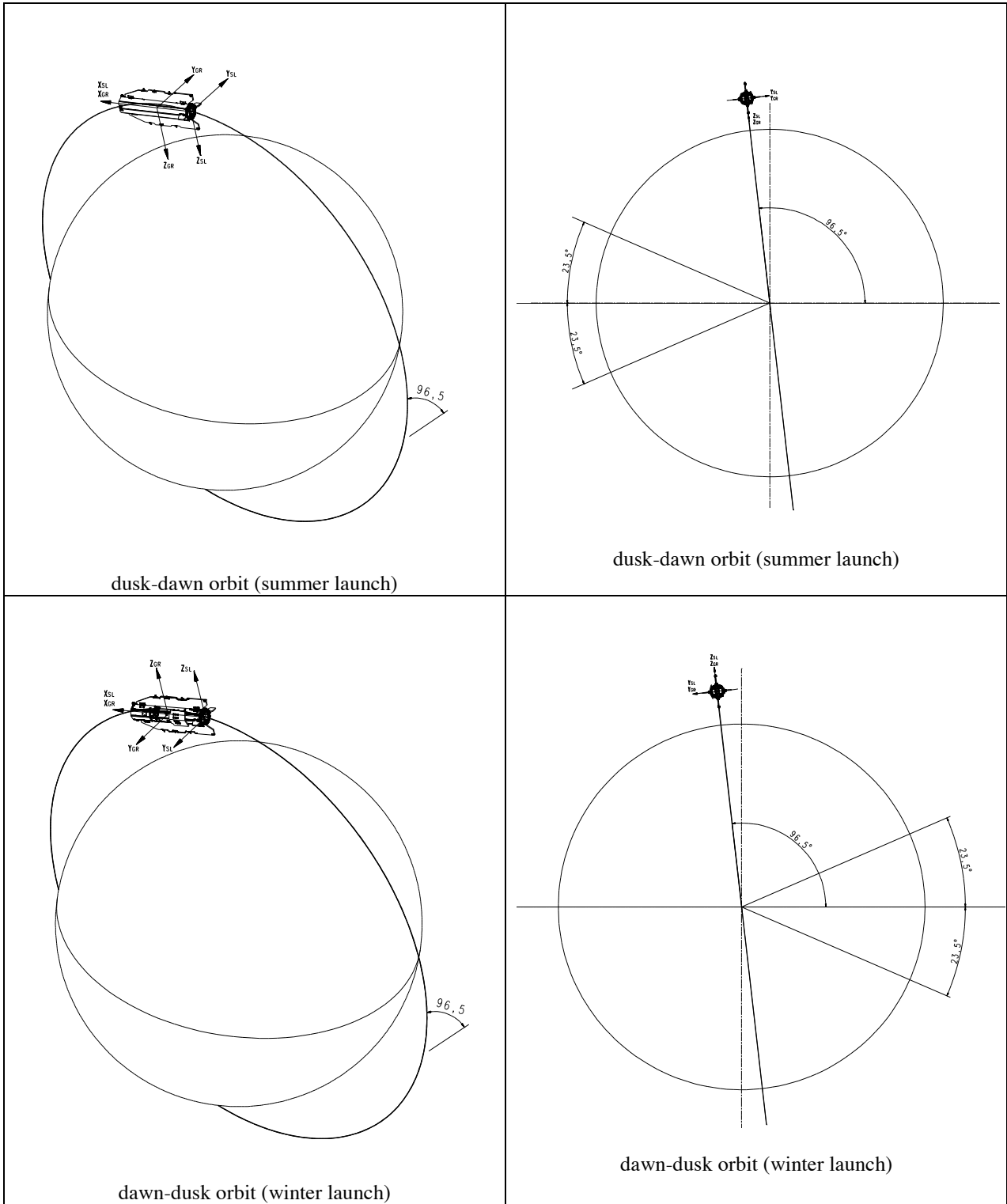


Figure 3.3-7: Orientation of the GRF (and of the Satellite Physical Coordinate Reference Frame) along the orbit during the measurement phase for a dusk-dawn orbit (summer launch) and dawn-dusk orbit (winter launch).

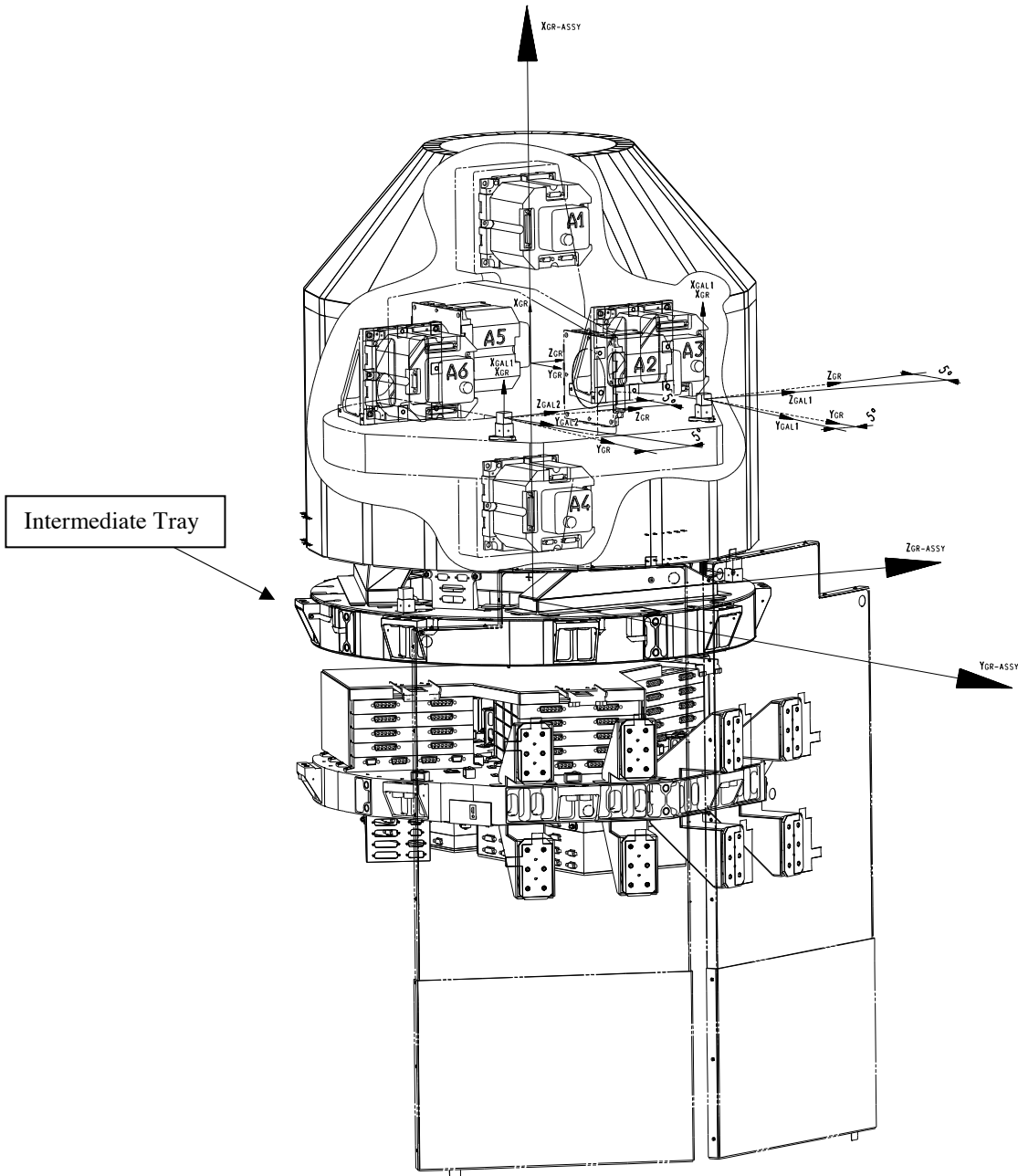


Figure 3.3-8: Gradiometer Reference Frame ( $X_{GR}$ ,  $Y_{GR}$ ,  $Z_{GR}$ ), Gradiometer Assembly Reference Frame ( $X_{GR-ASSY}$ ,  $Y_{GR-ASSY}$ ,  $Z_{GR-ASSY}$ ) and Gradiometer Alignment Reference Frames ( $X_{GAL1,2}$ ,  $Y_{GAL1,2}$ ,  $Z_{GAL1,2}$ )

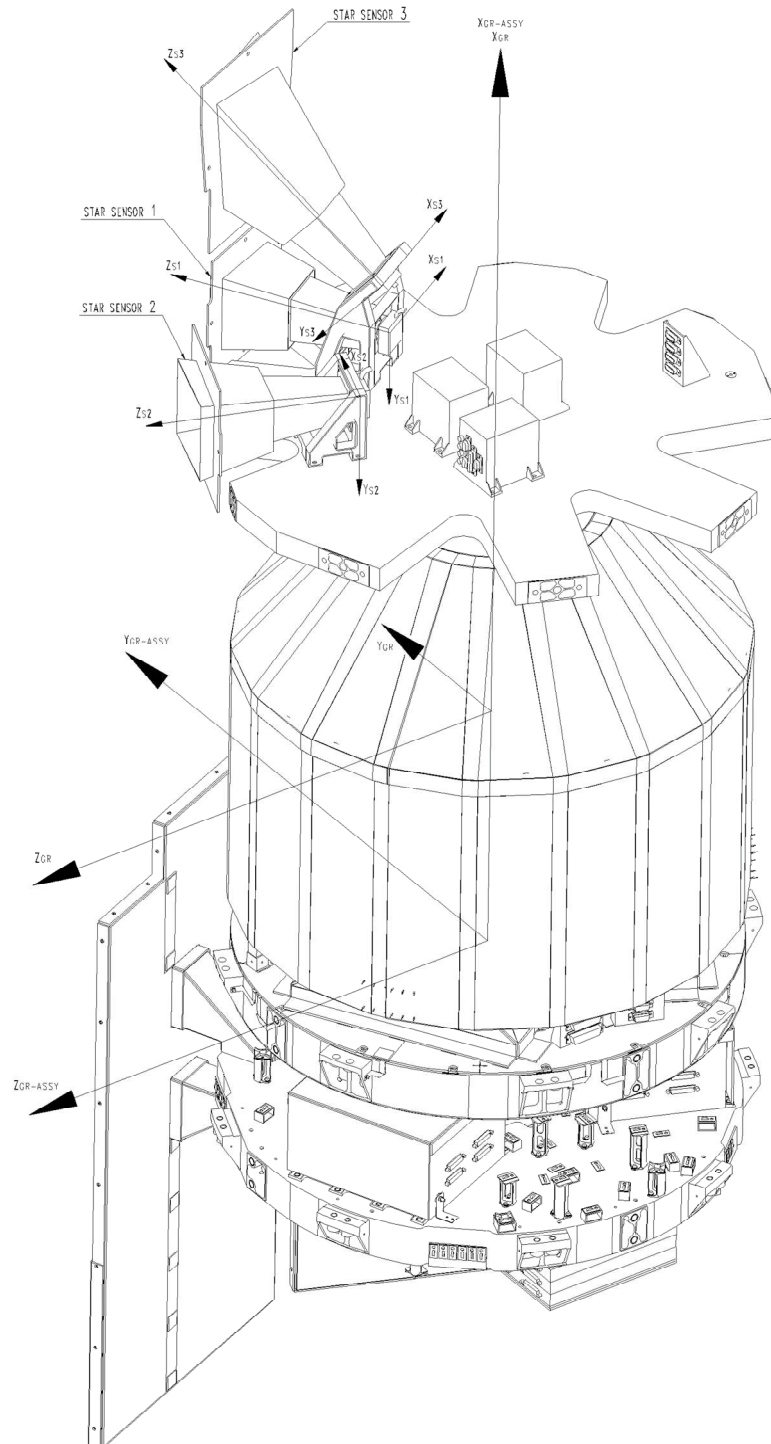


Figure 3.3-9: Star Sensor Reference Frame of each Star Sensor installed on GOCE. The illustrated position of the Star Sensors on the satellite and the orientation of their SSRF with respect to the GRF refer to the case of a dawn- dusk sun-synchronous orbit.

### 3.4 THE GRAVITY GRADIENT TENSOR

The gravity gradient tensor (GGT) consists of the nine second spatial derivatives of the gravitational potential U:

$$[U] = \begin{pmatrix} U_{XX} & U_{XY} & U_{XZ} \\ U_{XY} & U_{YY} & U_{YZ} \\ U_{XZ} & U_{YZ} & U_{ZZ} \end{pmatrix}, \quad U_{ij} = \frac{\partial^2 U}{\partial r_i \partial r_j} \quad i, j = X, Y, Z.$$

The GGT is symmetric ( $U_{ij} = U_{ji}$ ) and traceless in space ( $\sum_i U_{ii} = 0$ ), so only five components are independent.

#### 3.4.1 GGT Components in the LORF

The values of the GGT components in the LORF have been computed over 6 months of the GOCE mission at 250 km of mean altitude. The GGT time series, with a time step = 5 s, are obtained from the gravity field model EGM96 complete up to the degree and order 360. The time histories of the  $U_{XX}$ ,  $U_{YY}$ ,  $U_{ZZ}$ ,  $U_{XY}$ ,  $U_{XZ}$ ,  $U_{YZ}$ , components in the LORF, spanning the full period of 6 months, are plotted in Figure 3.4-1, while their discrete spectral densities (computed from the FFT of the complete 29-day time vectors) are plotted in Figure 3.4-2.

In Table 3.4-1 there are the GGT characteristics in the LORF, derived from the 6-month mission simulation. The maximum values of the spectral densities in the MBW refer to smoothed spectra. The smoothing is achieved by averaging several spectral densities computed over a shorter time duration, and by computing the rms value of the spectrum so obtained over 23 small sub-bands in which the 5 ÷ 100 mHz MBW has been divided.

|                                               | $U_{XX}$ | $U_{YY}$ | $U_{ZZ}$ | $U_{XY}$              | $U_{XZ}$              | $U_{YZ}$              |
|-----------------------------------------------|----------|----------|----------|-----------------------|-----------------------|-----------------------|
| Mean value [E]                                | -1374.69 | -1372.71 | 2747.40  | $1.035 \cdot 10^{-5}$ | $2.463 \cdot 10^{-4}$ | $4.171 \cdot 10^{-3}$ |
| $U_{ij}^0$ [E] <sup>(1)</sup>                 | 1388.42  | 1384.52  | 2772.80  | 0.879                 | 16.81                 | 2.39                  |
| $\tilde{U}_{ij}^W$ [mE/√Hz] <sup>(2)</sup>    | 1228.97  | 896.49   | 1858.76  | 673.57                | 1423.30               | 1129.02               |
| $\tilde{U}_{ij}^{HW}$ [mE/√Hz] <sup>(3)</sup> | < 1      | < 1      | < 1      | < 1                   | < 1                   | < 1                   |

<sup>(1)</sup> maximum value (in modulus) of  $U_{ij}$  in the low frequency region outside the measurement bandwidth (from DC to 5 mHz)

<sup>(2)</sup> maximum value of the SD of  $U_{ij}$  in the MBW (5 to 100 mHz).

<sup>(3)</sup> maximum value of the SD of  $U_{ij}$  in the upper part of the MBW (50 to 100 mHz).

Table 3.4-1: Gravity gradient tensor characteristics in the LORF for the GOCE 250-km orbit

### 3.4.2 GGT Components in the GRF

The relationship between the GGT expressed in the LORF ( $[U]_O$ ) and the GGT expressed in the GRF ( $[U]_G$ ) is given by:

$$[U]_G = [R]_{G/O} [U]_O ([R]_{G/O})^T = [U]_O + [dR]_{G/O} [U]_O + [U]_O ([dR]_{G/O})^T + [dR]_{G/O} [U]_O ([dR]_{G/O})^T$$

where  $[R]_{G/O}$  is the rotation matrix defining the orientation of the GRF in the LORF (from LORF to GRF), which for small rotation angles  $\varphi, \theta, \psi$  about the X, Y, Z axes can be expressed as follow

$$[R]_{G/O} \cong [1]_3 + \begin{pmatrix} 0 & \psi & -\theta \\ -\psi & 0 & \varphi \\ \theta & -\varphi & 0 \end{pmatrix} \cong [1]_3 + [dR]_{G/O}, \quad [1]_3 = 3 \times 3 \text{ identity matrix.}$$

The GGT components in the GRF have been computed from the GGT components in the LORF (Table 3.4-1), considering the following mispointing angles and angle stability of the GRF in the LORF:

$$\varphi_{\max} = 4^\circ \text{ (roll)}, \quad \theta_{\max} = 1^\circ \text{ (roll)}, \quad \psi_{\max} = 4^\circ \text{ (roll)}$$

$$\varphi^w = 1 \cdot 10^{-5} \text{ rad/Hz}^{1/2}, \quad \theta^w = 1 \cdot 10^{-5} \text{ rad/Hz}^{1/2}, \quad \psi^w = 1 \cdot 10^{-5} \text{ rad/Hz}^{1/2}.$$

In addition, for the purpose of the gradiometric error analysis and requirements derivation, and for the gradiometric error budget:

- 1) a 30% margin has been applied to the maximum spectral density value in the MBW of the GGT components in the GRF;
- 2) a value of 10 mE/√Hz has been assumed for the spectral density in the upper part of the MBW (above 50 mHz) of the GGT components in the GRF (very large margin w.r.t. the computed value).

The reference values of the GGT in the GRF utilised in this document for the requirements derivation and the gradiometric error budget are reported in **Error! Reference source not found.** The reference smoothed spectral densities in the MBW (5 to 100 mHz) are provided in Figure 3.4-3.

|                                               | $U_{XX}$ | $U_{YY}$ | $U_{ZZ}$ | $U_{XY}$ | $U_{XZ}$ | $U_{YZ}$ |
|-----------------------------------------------|----------|----------|----------|----------|----------|----------|
| $U_{ij}^0$ [E] <sup>(1)</sup>                 | 1400     | 1400     | 2800     | 200      | 110      | 410      |
| $\tilde{U}_{ij}^w$ [mE/√Hz] <sup>(2)</sup>    | 1600     | 1200     | 2400     | 900      | 1900     | 1650     |
| $\tilde{U}_{ij}^{HW}$ [mE/√Hz] <sup>(3)</sup> | 10       | 10       | 10       | 10       | 10       | 10       |

- <sup>(1)</sup> maximum value (in modulus) of  $U_{ij}$  in the low frequency region outside the measurement bandwidth (from DC to 5 mHz)
- <sup>(2)</sup> maximum value of the SD of  $U_{ij}$  in the MBW (5 to 100 mHz) – a 30% margin w.r.t. the computed values has been applied here.
- <sup>(3)</sup> maximum value of the SD of  $U_{ij}$  in the upper part of the MBW (50 to 100 mHz) – a large margin w.r.t. to the computed values has been applied here.

Table 3.4-2: Reference GGT characteristics in the GRF for requirements derivation, and error budget

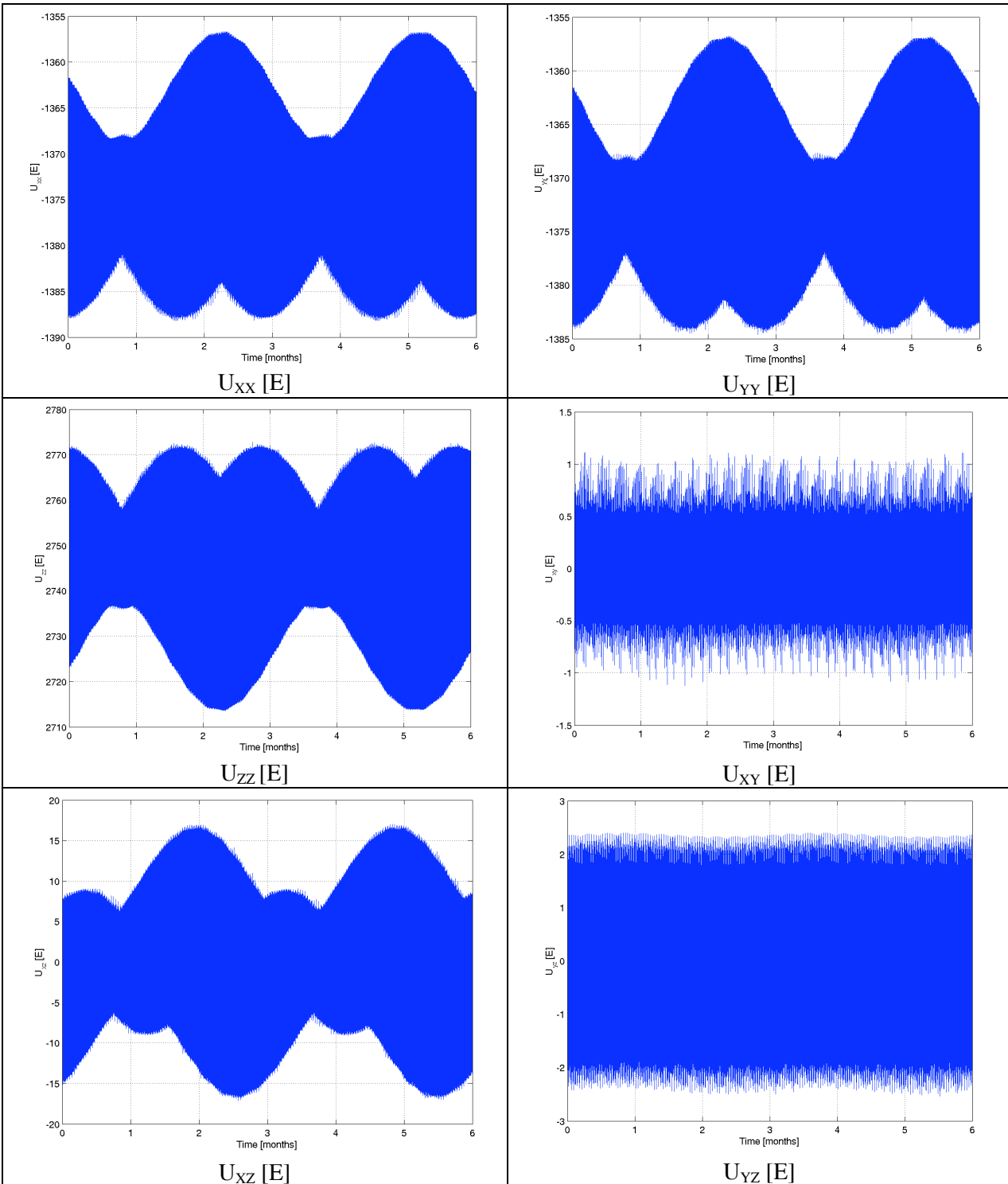


Figure 3.4-1: Components of the GGT in the LORF along ten orbits of GOCE

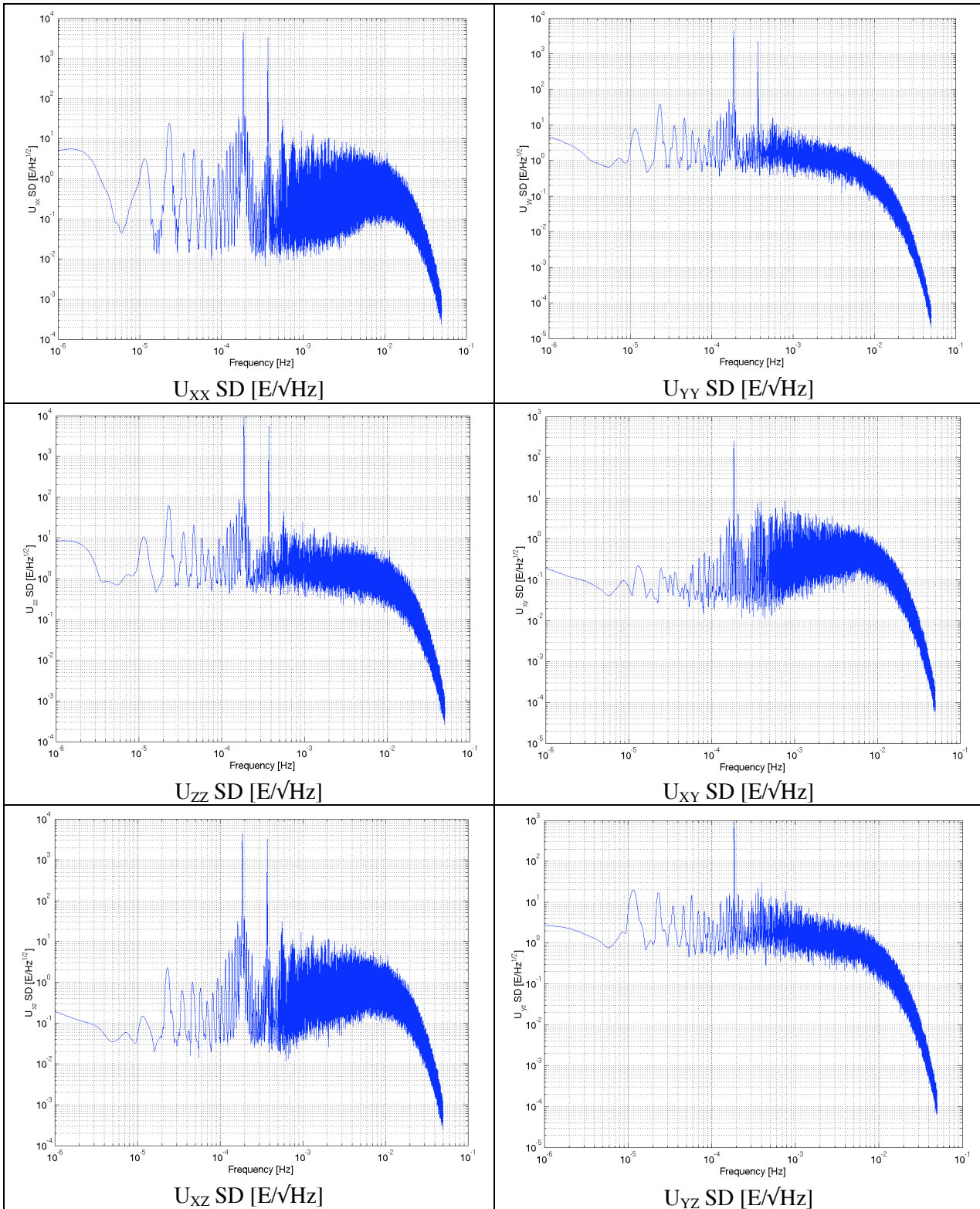


Figure 3.4-2: Spectral density of the GGT components in the LORF

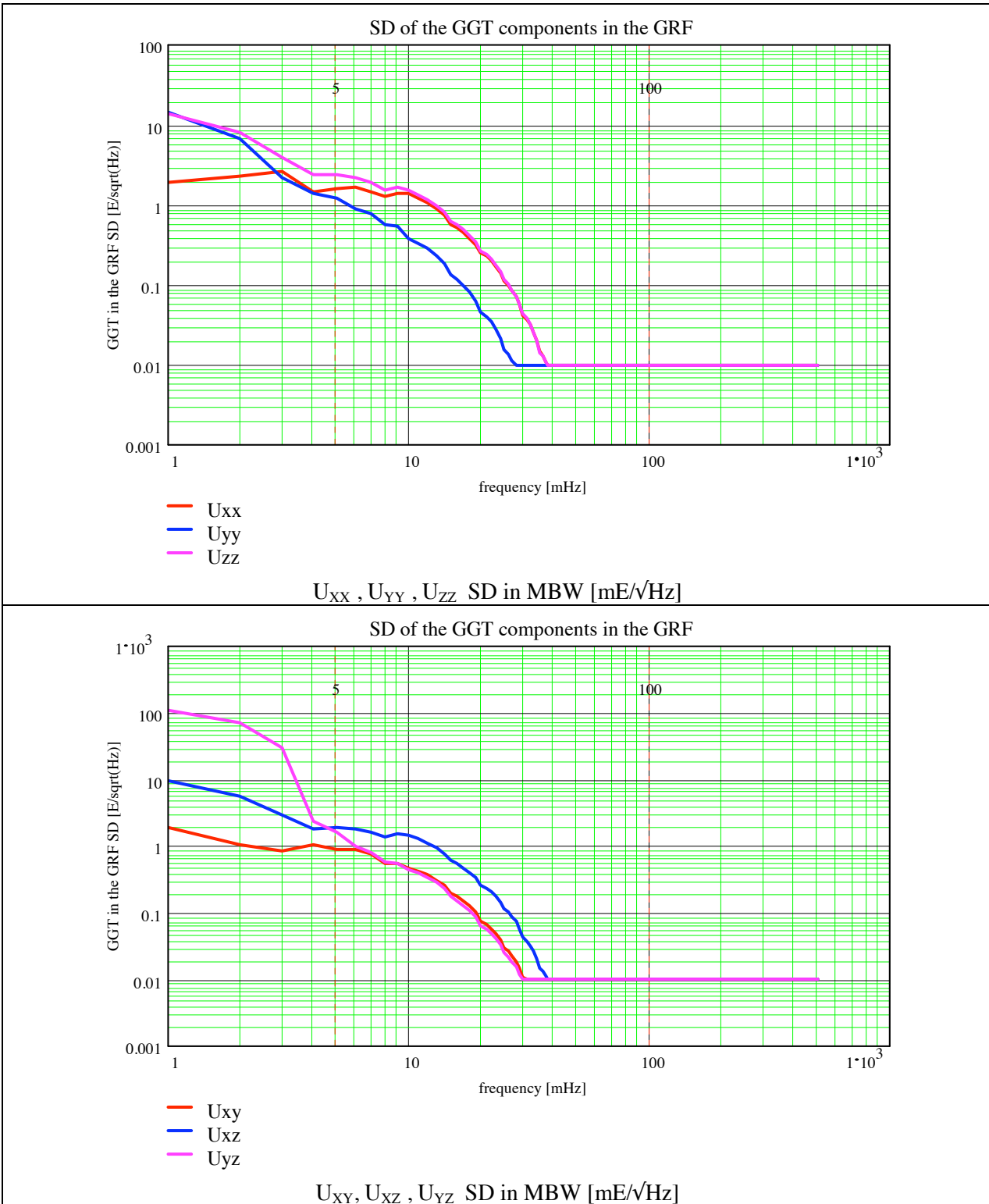


Figure 3.4-3: Reference spectral density in the MBW of the GGT components in the GRF (smoothed)

3.5 SATELLITE GRAVITY GRADIOMETRY PERFORMANCE REQUIREMENTS

The design of the Gravity Gradiometer and, more in general, the overall GOCE satellite and mission is driven by the following fundamental gravimetric performance requirement ([AD 1]):

**“after Level 0 to Level 1a/1b ground processing, the trace of the gravity gradient tensor diagonal components shall not exceed the spectral density limits defined in Figure 3.5-1 in the measurement bandwidth 0.005 to 0.1 Hz in the gradiometer reference frame”**

where the following definitions apply (as far as the gradiometric products are concerned):

GOCE Level 0 products: time-ordered raw data downlinked from the satellite

GOCE Level 1a products: time series of payload data with calibration data attached including satellite ancillary data

GOCE Level 1b products: time series along the orbit consisting of calibrated, corrected and geolocated data, sorted in files, including:

- gravity gradients in gradiometer reference frame and in J2000 reference frame together with the transformation matrices;
- linear accelerations and angular rates and accelerations.

Outside the measurement bandwidth, the following requirements apply to the total measurement error spectral density ( $\tilde{T}_{GGT}(\nu)$ ) of the GGT trace in the GRF, after Level 0 to Level1 1a/1b ground processing:

- above 0.1 Hz:  $\tilde{T}_{GGT}(\nu) \leq 11 \left( \frac{\nu}{0.1 \text{ Hz}} \right)^2 \text{ mE/Hz}^{1/2};$
- below 0.001 Hz:  $\tilde{T}_{GGT}(\nu) \leq \tilde{T}_{GGT}(0.001) \frac{0.001 \text{ Hz}}{\nu} \text{ mE/Hz}^{1/2}.$

The upper limit of  $\tilde{T}_{GGT}(\nu)$  versus frequency (in MBW and above MBW, as prescribed by the above requirements) is shown in Figure 3.5-1.

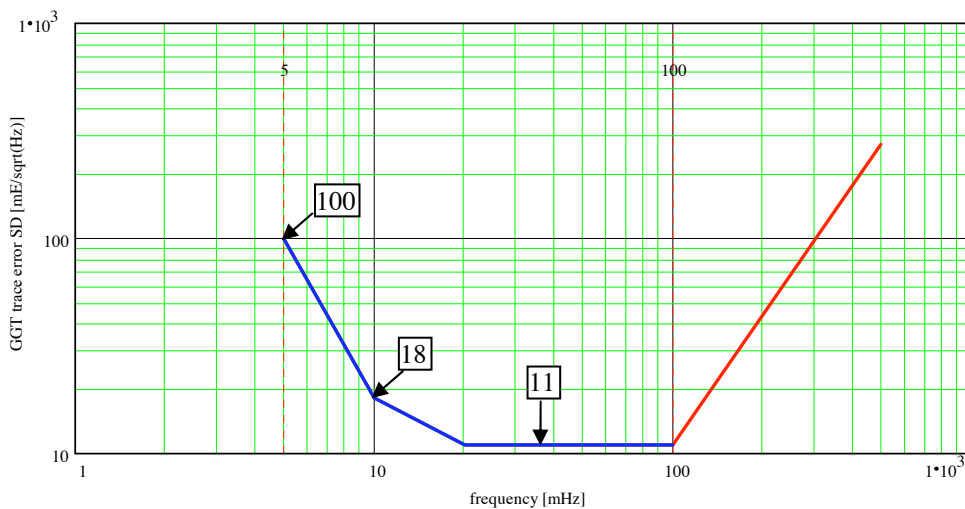


Figure 3.5-1: Upper limit of the total measurement error spectral density of the GGT trace built from the GGT diagonal components measured in the GRF (the blu line is the requirement in the MBW)

**4. GRAVITY GRADIENT TENSOR MEASUREMENT PROCESS**

**4.1 GRAVITY GRADIENT TENSOR MEASUREMENT IN THE GRADIOMETER REFERENCE FRAME**

**4.1.1 Measurement with an Ideal Gradiometer**

To describe the principle of the GGT measurement, let's start by considering an ideal Gradiometer in which:

- the internal dynamics and the read-out process of each accelerometer do not alter the input acceleration;
- the accelerometer sensitive axes are perfectly aligned to the axes of the corresponding ARFs (i.e. they are mutually perpendicular);
- all the 6 accelerometers occupy their nominal positions in the respective OAGRFs, and the axes of their ARFs are perfectly aligned to the corresponding axes of the respective OAGRFs;
- the origins of the 3 OAGRFs are coincident and their corresponding axes are perfectly aligned (i.e. the OAGRFs coincide with the GRF);
- the position/alignment of the 6 accelerometers in the respective OAGRFs and the position/alignment of the OAGRFs in the GRF do not change in time.

In this ideal situation, we will obtain in this section the expressions relating the GGT components in the GRF to the accelerations measured by the 6 accelerometers.

Each accelerometer is designed to detect the difference between the acceleration of the cage and that of the proof mass (whatever the cause that has produced this relative acceleration), as shown in Figure 4.1-1.

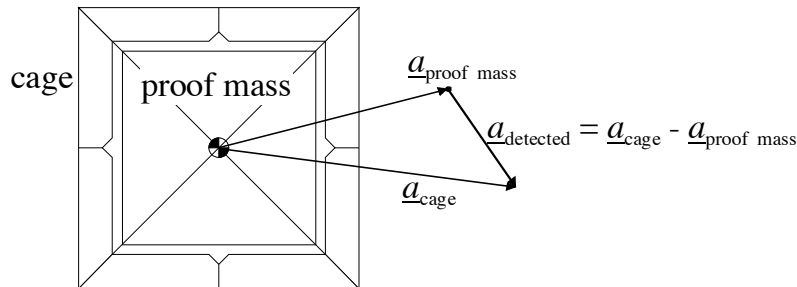


Figure 4.1-1: Acceleration detected by each accelerometer

On orbit, the relative acceleration between the cage and the proof mass of the accelerometer  $A_i$  ( $\underline{a}_i = \underline{a}_{\text{cage},i} - \underline{a}_{\text{proof mass},i}$ ) is the sum of the contributors included in the following vectorial expression:

$$\underline{a}_i = -([\mathbf{U}] - [\mathbf{\Omega}^2] - [\dot{\mathbf{\Omega}}]) \underline{R}_i + 2[\mathbf{\Omega}] \dot{\underline{R}}_i + \ddot{\underline{R}}_i + \underline{D} - \underline{S}_i - \underline{M}_i \quad (4.1)$$

This equation holds in any reference frame rigidly connected with the spacecraft (i.e. any frame experiencing the same dynamics of the spacecraft), and in particular in the OAGRF $_k$  of the accelerometer  $A_i$ . The components of the various elements appearing in the (4.1), wherever they will be made explicit in this section, must be considered expressed in this reference frame.

The vector  $\underline{R}_i$  defines the position of the centre of the accelerometer  $A_i$  (i.e. the position of the COM of its proof mass) relative to the satellite COM:  $\underline{R}_i$  points from the satellite COM to  $O_i$ .

The matrix  $[\mathbf{U}]$  contains the components of the GGT expressed in the reference frame where the ( $\underline{a}_i$ ) components are projected (the OAGRF $_k$  in this case):

$$[U] = \begin{pmatrix} U_{XX} & U_{XY} & U_{XZ} \\ U_{XY} & U_{YY} & U_{YZ} \\ U_{XZ} & U_{YZ} & U_{ZZ} \end{pmatrix}$$

Under the effect of the gravity gradient, the proof mass experiences an acceleration  $[U] \cdot \underline{R}_i$  relatively to the satellite COM. The accelerometer cage, instead, doesn't move relatively to the satellite under the gravity gradient, being the cage rigidly connected to the satellite structure. Thus the detected gravity gradient acceleration is  $-[U] \cdot \underline{R}_i$ .

The matrices  $[\Omega]$ ,  $[\Omega^2]$ ,  $[\dot{\Omega}]$  are defined as:

$$[\Omega] = \begin{pmatrix} 0 & -\omega_Z & \omega_Y \\ \omega_Z & 0 & -\omega_X \\ -\omega_Y & \omega_X & 0 \end{pmatrix}, [\Omega^2] = \begin{pmatrix} -\omega_Z^2 - \omega_Y^2 & \omega_X \omega_Y & \omega_X \omega_Z \\ \omega_X \omega_Y & -\omega_Z^2 - \omega_X^2 & \omega_Y \omega_Z \\ \omega_X \omega_Z & \omega_Y \omega_Z & -\omega_X^2 - \omega_Y^2 \end{pmatrix},$$

$$[\dot{\Omega}] = \begin{pmatrix} 0 & -\dot{\omega}_Z & \dot{\omega}_Y \\ \dot{\omega}_Z & 0 & -\dot{\omega}_X \\ -\dot{\omega}_Y & \dot{\omega}_X & 0 \end{pmatrix}$$

where  $\omega_X$ ,  $\omega_Y$ ,  $\omega_Z$  are the components of the satellite angular velocities about its COM relatively to an inertial system, expressed in the reference frame where the  $(\underline{a}_i)$  components are projected (the OAGRF<sub>k</sub> in this case), and  $\dot{\omega}_X$ ,  $\dot{\omega}_Y$ ,  $\dot{\omega}_Z$  are their time derivatives (angular accelerations).

The vector  $-[\Omega^2] \underline{R}_i$  (equivalent to  $-\underline{\Omega} \times (\underline{\Omega} \times \underline{R}_i)$ , where  $\underline{\Omega}$  is the angular velocity vector) is the centrifugal acceleration of the accelerometer  $A_i$  proof mass in the satellite rotating frame, induced by the satellite angular rotation about its COM.

The vector  $-[\dot{\Omega}] \underline{R}_i$  (equivalent to  $-\dot{\underline{\Omega}} \times \underline{R}_i$ , where  $\dot{\underline{\Omega}}$  is the angular acceleration vector) is the linear acceleration of the accelerometer  $A_i$  proof mass in the satellite rotating frame, induced by the satellite angular acceleration about its COM.

The vector  $-2[\Omega] \dot{\underline{R}}_i$  (equivalent to  $-2\underline{\Omega} \times \dot{\underline{R}}_i$ , where  $\dot{\underline{R}}_i$  is the time derivative of the position vector  $\underline{R}_i$ ) is the Coriolis acceleration of the accelerometer  $A_i$  proof mass in the satellite rotating frame, induced by the coupling of the rate of change of the proof mass position w.r.t. the satellite COM with the satellite angular rotation about its COM.

Again, the angular rotation and acceleration of the satellite do not change the position of the accelerometer cage relatively to the satellite, being the cage rigidly connected to the satellite structure. Thus the detected centrifugal, angular and Coriolis acceleration are  $+[\Omega^2] \underline{R}_i + [\dot{\Omega}] \underline{R}_i + 2[\Omega] \dot{\underline{R}}_i$ .

The vector  $\ddot{\underline{R}}_i$  is the acceleration of the accelerometer  $A_i$  cage relative to the satellite, due to causes internal to the satellite itself (thermo-elastic deformations of the structure to which the cage is connected, vibrations originated inside the satellite and propagating to through the structure up to the cage, etc..).

The vector  $\underline{D}$  is the linear acceleration of the satellite COM resulting from all the non-gravitational forces acting on it (atmospheric drag, radiation pressure, action of the thrusters, etc..). It is therefore also the linear acceleration of the cages of each accelerometer, being the cages rigidly connected to the satellite.

The vector  $\underline{S}_i$  is the linear acceleration of the accelerometer  $A_i$  proof mass produced by the gravitational attraction of the other satellite masses (satellite self-gravity). No motion of the cage relative to the satellite is produced by the self-gravity, thus this acceleration is detected as  $-\underline{S}_i$ .

The vector  $\underline{M}_i$  is the linear acceleration of the accelerometer  $A_i$  proof mass produced by its coupling with the external magnetic field. No motion of the cage relative to the satellite is produced by the coupling with the external magnetic field, thus this acceleration is detected as  $-\underline{M}_i$ . The accelerometer proof mass couples with an external magnetic field of strength  $\underline{B}$  at its location (not including shielding factors) through its magnetic susceptibility  $\chi_m (= 3 \cdot 10^{-4})$ . The expression of the resulting acceleration can be approximated as:

$$\underline{M} = \frac{1}{2} \frac{\chi_m}{\mu_0} \frac{V}{m} \alpha_b \nabla(\underline{B} \cdot \underline{B})$$

( $\mu_0 =$  vacuum magnetic permeability  $= 4\pi \cdot 10^{-7}$  henry/m;  $V, m =$  volume, mass of the proof mass,  $\alpha_b =$  magnetic field attenuation factor due to the accelerometer housing and to the shield placed around the accelerometer).

Let's introduce the vector  $\underline{C}_k$  defining the position of the satellite COM relative to the origin of the OAGRF $_k$  of the OAG $_k$  to which the accelerometer  $A_i$  belongs:  $\underline{C}_k$  points from  $O_{k_{OGR}}$  ( $k = 1,2,3$ ) to the satellite COM. Being in this ideal case the three OAGRFs coincident, we have:

$$\underline{C}_1 = \underline{C}_2 = \underline{C}_3 \equiv \underline{C}$$

The vectors  $\underline{R}_i$  and its derivatives can thus be expressed as

$$\underline{R}_i = \underline{A}_i - \underline{C}, \quad \dot{\underline{R}}_i = -\dot{\underline{C}}, \quad \ddot{\underline{R}}_i = -\ddot{\underline{C}}$$

where  $\underline{A}_i$  defines the position of the COM of the proof mass of the accelerometer  $A_i$  relative to  $O_{k_{OGR}}$ :  $\underline{A}_i$  points from  $O_{k_{OGR}}$  to  $O_i$  (see Figure 4.1-2). So we can rewrite the (4.1) as:

$$\underline{a}_i = -([\underline{U}] - [\underline{\Omega}^2] - [\dot{\underline{\Omega}}]) \underline{A}_i + ([\underline{U}] - [\underline{\Omega}^2] - [\dot{\underline{\Omega}}]) \underline{C} - 2[\underline{\Omega}] \dot{\underline{C}} - \ddot{\underline{C}} + \underline{D} - \underline{S}_i - \underline{M}_i \quad (4.2)$$

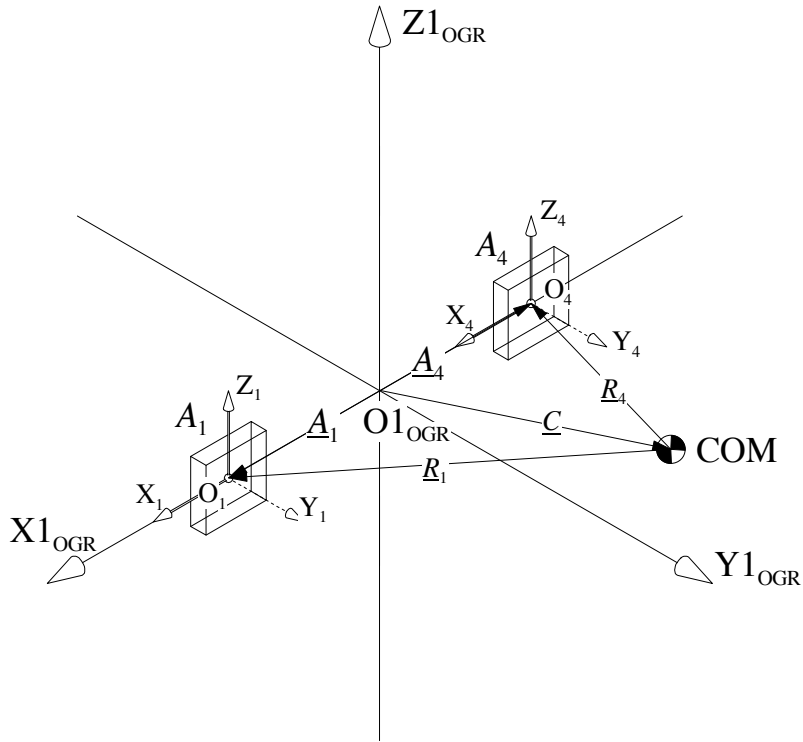


Figure 4.1-2: Definition of the vectors  $\underline{R}_i, \underline{A}_i, \underline{C}$ , for the OAG $_1$  and the accelerometers  $A_1, A_4$

Let's form the following quantities:

- $\underline{a}_{c,ij} = \frac{1}{2} (\underline{a}_i + \underline{a}_j)$  : common-mode acceleration measured by the accelerometers  $A_i, A_j$
- $\underline{a}_{d,ij} = \frac{1}{2} (\underline{a}_i - \underline{a}_j)$  : differential-mode acceleration measured by the accelerometers  $A_i, A_j$

Making use of the (4.2), the common and differential-mode accelerations assume the expression:

$$\underline{a}_{c,ij} = -([U] - [\Omega^2] - [\dot{\Omega}]) \underline{A}_{c,ij} + ([U] - [\Omega^2] - [\dot{\Omega}]) \underline{C} - 2 [\Omega] \dot{\underline{C}} - \ddot{\underline{C}} + \underline{D} - \underline{S}_{c,ij} - \underline{M}_{c,ij} \quad (4.3)$$

$$\underline{a}_{d,ij} = -([U] - [\Omega^2] - [\dot{\Omega}]) \underline{A}_{d,ij} - \underline{S}_{d,ij} - \underline{M}_{d,ij}$$

where  $\underline{A}_{c,ij} = \frac{1}{2} (\underline{A}_i + \underline{A}_j)$ ,  $\underline{A}_{d,ij} = \frac{1}{2} (\underline{A}_i - \underline{A}_j)$ ,  $\underline{S}_{c,ij} = \frac{1}{2} (\underline{S}_i + \underline{S}_j)$ ,  $\underline{S}_{d,ij} = \frac{1}{2} (\underline{S}_i - \underline{S}_j)$ ,  $\underline{M}_{c,ij} = \frac{1}{2} (\underline{M}_i + \underline{M}_j)$ ,  $\underline{M}_{d,ij} = \frac{1}{2} (\underline{M}_i - \underline{M}_j)$ .

If the accelerometers  $A_i, A_j$  belong to the same OAG ( $ij = 14, 25, 36$ ), then  $\underline{A}_{c,ij} = 0$  and  $\underline{A}_{d,ij} = \underline{A}_i$ . Thus:

$$\underline{a}_{c,ij} = ([U] - [\Omega^2] - [\dot{\Omega}]) \underline{C} - 2 [\Omega] \dot{\underline{C}} - \ddot{\underline{C}} + \underline{D} - \underline{S}_{c,ij} - \underline{M}_{c,ij} =$$

$$= \begin{pmatrix} U_{XX} + \omega_Y^2 + \omega_Z^2 & U_{XY} - \omega_X \omega_Y + \dot{\omega}_Z & U_{XZ} - \omega_X \omega_Z - \dot{\omega}_Y \\ U_{XY} - \omega_X \omega_Y - \dot{\omega}_Z & U_{YY} + \omega_X^2 + \omega_Z^2 & U_{YZ} - \omega_Y \omega_Z + \dot{\omega}_X \\ U_{XZ} - \omega_X \omega_Z + \dot{\omega}_Y & U_{YZ} - \omega_Y \omega_Z - \dot{\omega}_X & U_{ZZ} + \omega_X^2 + \omega_Y^2 \end{pmatrix} \begin{pmatrix} C_X \\ C_Y \\ C_Z \end{pmatrix} - 2 [\Omega] \dot{\underline{C}} - \ddot{\underline{C}} + \underline{D} - \underline{S}_{c,ij} - \underline{M}_{c,ij} \quad (4.4)$$

$$\underline{a}_{d,ij} = -([U] - [\Omega^2] - [\dot{\Omega}]) \underline{A}_i - \underline{S}_{d,ij} - \underline{M}_{d,ij} =$$

$$= - \begin{pmatrix} U_{XX} + \omega_Y^2 + \omega_Z^2 & U_{XY} - \omega_X \omega_Y + \dot{\omega}_Z & U_{XZ} - \omega_X \omega_Z - \dot{\omega}_Y \\ U_{XY} - \omega_X \omega_Y - \dot{\omega}_Z & U_{YY} + \omega_X^2 + \omega_Z^2 & U_{YZ} - \omega_Y \omega_Z + \dot{\omega}_X \\ U_{XZ} - \omega_X \omega_Z + \dot{\omega}_Y & U_{YZ} - \omega_Y \omega_Z - \dot{\omega}_X & U_{ZZ} + \omega_X^2 + \omega_Y^2 \end{pmatrix} \underline{A}_i - \underline{S}_{d,ij} - \underline{M}_{d,ij} \quad (4.5)$$

Provided that the contribution of the quantities  $([U] - [\Omega^2] - [\dot{\Omega}])\underline{C}$ ,  $2[\Omega]\dot{\underline{C}}$ ,  $\ddot{\underline{C}}$ ,  $\underline{S}_{c,ij}$ ,  $\underline{M}_{c,ij}$ ,  $\underline{S}_{d,ij}$ ,  $\underline{M}_{d,ij}$  to the expressions of  $\underline{a}_{c,ij}$  and  $\underline{a}_{d,ij}$  is negligible, the common-mode accelerations  $\underline{a}_{c,ij}$  provide the information about the non-gravitational acceleration of the satellite COM ( $\underline{D}$ ), and the differential-mode accelerations  $\underline{a}_{d,ij}$  provide the information about the components of the GGT mixed to the centrifugal accelerations, and about the angular accelerations of the satellite about its COM:

$$a_{c,14,X} = a_{c,25,X} = a_{c,36,X} = D_X, a_{c,14,Y} = a_{c,25,Y} = a_{c,36,Y} = D_Y, a_{c,14,Z} = a_{c,25,Z} = a_{c,36,Z} = D_Z$$

$$-2 \frac{a_{d,14,X}}{L_X} = U_{XX} + \omega_Y^2 + \omega_Z^2, \quad -2 \frac{a_{d,25,Y}}{L_Y} = U_{YY} + \omega_X^2 + \omega_Z^2, \quad -2 \frac{a_{d,36,Z}}{L_Z} = U_{ZZ} + \omega_X^2 + \omega_Y^2 \quad (4.6)$$

$$-\frac{a_{d,25,X}}{L_Y} - \frac{a_{d,14,Y}}{L_X} = U_{XY} - \omega_X \omega_Y, \quad -\frac{a_{d,14,Z}}{L_X} - \frac{a_{d,36,X}}{L_Z} = U_{XZ} - \omega_X \omega_Z, \quad -\frac{a_{d,36,Y}}{L_Z} - \frac{a_{d,25,Z}}{L_Y} = U_{YZ} - \omega_Y \omega_Z$$

$$-\frac{a_{d,36,Y}}{L_Z} + \frac{a_{d,25,Z}}{L_Y} = \dot{\omega}_X, \quad -\frac{a_{d,14,Z}}{L_X} + \frac{a_{d,36,X}}{L_Z} = \dot{\omega}_Y, \quad -\frac{a_{d,25,X}}{L_Y} + \frac{a_{d,14,Y}}{L_X} = \dot{\omega}_Z$$

The GGT components can be then obtained from the differential accelerations as:

$$U_{XX} = -2 \frac{a_{d,14,X}}{L_X} - \omega_Y^2 - \omega_Z^2, U_{YY} = -2 \frac{a_{d,25,Y}}{L_Y} - \omega_X^2 - \omega_Z^2, U_{ZZ} = -2 \frac{a_{d,36,Z}}{L_Z} - \omega_X^2 - \omega_Y^2 \quad (4.7)$$

$$U_{XY} = -\frac{a_{d,25,X}}{L_Y} - \frac{a_{d,14,Y}}{L_X} + \omega_X \omega_Y, U_{XZ} = -\frac{a_{d,14,Z}}{L_X} - \frac{a_{d,36,X}}{L_Z} + \omega_X \omega_Z, U_{YZ} = -\frac{a_{d,36,Y}}{L_Z} - \frac{a_{d,25,Z}}{L_Y} + \omega_Y \omega_Z$$

The angular rates to be removed from the combination of the differential accelerations in the (4.7), can be obtained as output of an estimator which combines the angular accelerations provided by the (4.6) with the satellite attitude quaternion ( $\mathbf{q}$ ) measured by means of the star sensors:

$$\omega_X(t) = \mathcal{C}(\dot{\omega}_X, \mathbf{q}), \omega_Y(t) = \mathcal{C}(\dot{\omega}_Y, \mathbf{q}), \hat{\omega}_Z(t) = \mathcal{C}(\dot{\omega}_Z, \mathbf{q}) \quad (4.8)$$

where  $\mathcal{C}$  denotes formally the estimation algorithm.

In this ideal situation, in which the three OAGRFs are coincident, and coincide with the GRF, the components of the GGT so obtained are expressed equivalently in each of these frames. The combination of differential accelerations measured by accelerometers belonging to different OAGs (as necessary to obtain the angular accelerations and the off-diagonal GGT components) does not introduce any error.

However, even when measured by an ideal Gradiometer, the GGT components and the non-gravitational acceleration of the satellite COM are not immune from errors. They are due to:

- the terms 
$$\begin{pmatrix} U_{XX} + \omega_Y^2 + \omega_Z^2 & U_{XY} - \omega_X \omega_Y + \dot{\omega}_Z & U_{XZ} - \omega_X \omega_Z - \dot{\omega}_Y \\ U_{XY} - \omega_X \omega_Y - \dot{\omega}_Z & U_{YY} + \omega_X^2 + \omega_Z^2 & U_{YZ} - \omega_Y \omega_Z + \dot{\omega}_X \\ U_{XZ} - \omega_X \omega_Z + \dot{\omega}_Y & U_{YZ} - \omega_Y \omega_Z - \dot{\omega}_X & U_{ZZ} + \omega_X^2 + \omega_Y^2 \end{pmatrix} \begin{pmatrix} C_X \\ C_Y \\ C_Z \end{pmatrix} - 2 [\Omega] \dot{\underline{C}} - \ddot{\underline{C}} - \underline{S}_{c,ij} - \underline{M}_{c,ij} \quad (4.9)$$

for what concerns the measurement of  $\underline{D}$ ,

- the differential accelerations produces by the satellite self gravity and the coupling with the magnetic field 
$$- \underline{S}_{d,ij} - \underline{M}_{d,ij} \quad (4.10)$$

for what concerns the measurement of  $\dot{\omega}_X, \dot{\omega}_Y, \dot{\omega}_Z$  and for the measurement of the GGT components.

The latter ones are, in addition, affected by the estimation errors of  $\omega_X, \omega_Y, \omega_Z$ .

#### 4.1.2 Measurement with a Real Gradiometer

Let's now examine here and in the following sections the situation described in the previous section changes for a real Gradiometer in which:

- the 6 accelerometers do not occupy their nominal positions in the respective OAGRFs;
- the accelerometer sensitive axes are not mutually perpendicular;
- the axes of their ARFs are not perfectly aligned to the corresponding axes of the respective OAGRFs;
- the internal dynamics and the read-out process of each accelerometer alter the input acceleration;
- the origins of the 3 OAGRFs are not coincident and their corresponding axes are not perfectly aligned;
- the position/alignment of the 6 accelerometers in the respective OAGRFs and the position/alignment of the OAGRFs in the GRF are not constant in time.

4.1.2.1 Accelerometer Misplacement and Position Variation in Time

The mispositioning of the centre of the accelerometer  $A_i$  in the OAGRF is defined by the vector  $\delta\mathbf{A}_i$ , joining the nominal position of  $O_i$  to the actual position occupied by  $O_i$ , being  $O_i$  the origin of the ARF of the accelerometer  $A_i$ . According to the way the OAGRF is defined (origin in the mid-point of the segment  $O_i-O_j$ , in-line axis parallel to the segment  $O_i-O_j$ ), the vectors  $\delta\mathbf{A}_i, \delta\mathbf{A}_j$  of two accelerometers belonging to the same OAG are equal and opposite ( $\delta\mathbf{A}_i = -\delta\mathbf{A}_j$ ) and have a non-null component only along the in-line axis of the OAGRF (see Figure 4.1-3):

$$\delta\mathbf{A}_1 = \begin{pmatrix} \delta A_{1,X} \\ 0 \\ 0 \end{pmatrix}, \delta\mathbf{A}_2 = \begin{pmatrix} 0 \\ \delta A_{2,Y} \\ 0 \end{pmatrix}, \delta\mathbf{A}_3 = \begin{pmatrix} 0 \\ 0 \\ \delta A_{3,Z} \end{pmatrix}, \delta\mathbf{A}_4 = \begin{pmatrix} -\delta A_{1,X} \\ 0 \\ 0 \end{pmatrix}, \delta\mathbf{A}_5 = \begin{pmatrix} 0 \\ -\delta A_{2,Y} \\ 0 \end{pmatrix}, \delta\mathbf{A}_6 = \begin{pmatrix} 0 \\ 0 \\ -\delta A_{3,Z} \end{pmatrix}$$

The quantity  $\delta A_{1,X} (\delta A_{2,Y}, \delta A_{3,Z})$  represents half of the difference  $\delta L_X (\delta L_Y, \delta L_Z)$  between the actual value of the baseline length and its nominal value  $L_X (L_Y, L_Z)$ :  $\delta L_X = 2\delta A_{1,X}, \delta L_Y = 2\delta A_{2,Y}, \delta L_Z = 2\delta A_{3,Z}$ .

The expression of  $\mathbf{R}_i$  and of its time derivatives, considering that the nominal position vector of  $A_i$  in the OAGRF is constant by definition, becomes:

$$\mathbf{R}_i = \mathbf{A}_i + \delta\mathbf{A}_i - \mathbf{C}_k, \quad \dot{\mathbf{R}}_i = \dot{\delta\mathbf{A}}_i - \dot{\mathbf{C}}_k, \quad \ddot{\mathbf{R}}_i = \ddot{\delta\mathbf{A}}_i - \ddot{\mathbf{C}}_k \quad (k = 1 \text{ for } OAG_1, \dots) \quad (4.11)$$

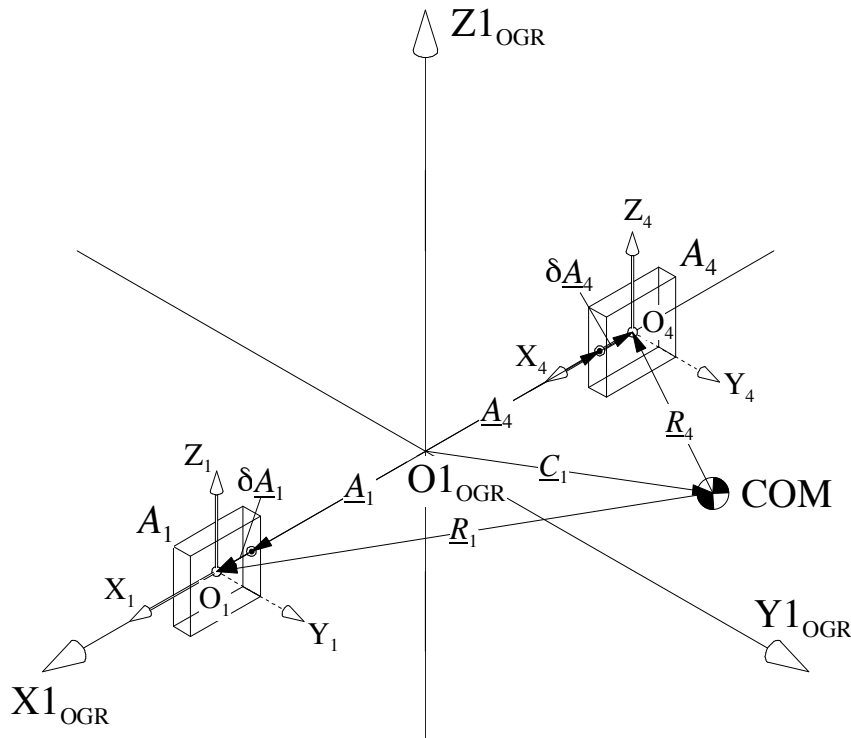


Figure 4.1-3: Definition of the vectors  $\mathbf{R}_i, \mathbf{A}_i, \mathbf{C}_k, \delta\mathbf{A}_i$  for the  $OAG_i$  and the accelerometers  $A_1, A_4$

By plugging the (4.11) in the (4.1) we get

$$\begin{aligned} \mathbf{a}_i &= -([\mathbf{U}] - [\mathbf{\Omega}^2] - [\dot{\mathbf{\Omega}}]) \cdot (\mathbf{A}_i + \delta\mathbf{A}_i - \mathbf{C}_k) + 2[\mathbf{\Omega}] \cdot (\delta\dot{\mathbf{A}}_i - \dot{\mathbf{C}}_k) + \delta\ddot{\mathbf{A}}_i - \ddot{\mathbf{C}}_k + \mathbf{D} - \mathbf{S}_i - \mathbf{M}_i \\ &= -([\mathbf{U}] - [\mathbf{\Omega}^2] - [\dot{\mathbf{\Omega}}]) \cdot \mathbf{A}_i - ([\mathbf{U}] - [\mathbf{\Omega}^2] - [\dot{\mathbf{\Omega}}]) \cdot \delta\mathbf{A}_i + ([\mathbf{U}] - [\mathbf{\Omega}^2] - [\dot{\mathbf{\Omega}}]) \cdot \mathbf{C}_k + 2[\mathbf{\Omega}] \cdot \delta\dot{\mathbf{A}}_i - 2[\mathbf{\Omega}] \cdot \dot{\mathbf{C}}_k + \delta\ddot{\mathbf{A}}_i - \ddot{\mathbf{C}}_k \\ &\quad + \mathbf{D} - \mathbf{S}_i - \mathbf{M}_i, \end{aligned} \quad (4.12)$$

and the expressions of the common and differential-mode accelerations for two accelerometers  $A_i, A_j$  belonging to the same OAG ( $ij = 14, 25, 36$ ), for which

$$\underline{A}_{c,ij} = 0, \underline{A}_{d,ij} = \underline{A}_i, \delta \underline{A}_{c,ij} = \frac{1}{2}(\delta \underline{A}_i + \delta \underline{A}_j) = \frac{1}{2}(\delta \underline{A}_i - \delta \underline{A}_j) = 0, \delta \underline{A}_{d,ij} = \frac{1}{2}(\delta \underline{A}_i - \delta \underline{A}_j) = \frac{1}{2}(\delta \underline{A}_i + \delta \underline{A}_j) = \delta \underline{A}_i,$$

become:

$$\begin{aligned} \underline{a}_{c,ij} &= -([\mathbf{U}] - [\mathbf{\Omega}^2] - [\dot{\mathbf{\Omega}}]) \delta \underline{A}_{c,ij} + ([\mathbf{U}] - [\mathbf{\Omega}^2] - [\dot{\mathbf{\Omega}}]) \underline{C}_k + 2[\mathbf{\Omega}] \cdot \delta \dot{\underline{A}}_{c,ij} - 2[\mathbf{\Omega}] \cdot \dot{\underline{C}}_k + \delta \ddot{\underline{A}}_{c,ij} - \ddot{\underline{C}}_k + \underline{D} - \underline{S}_{c,ij} - \underline{M}_{c,ij} \\ &= ([\mathbf{U}] - [\mathbf{\Omega}^2] - [\dot{\mathbf{\Omega}}]) \underline{C}_k + 2[\mathbf{\Omega}] \cdot \delta \dot{\underline{A}}_{c,ij} - 2[\mathbf{\Omega}] \cdot \dot{\underline{C}}_k + \delta \ddot{\underline{A}}_{c,ij} - \ddot{\underline{C}}_k + \underline{D} - \underline{S}_{c,ij} - \underline{M}_{c,ij}, \end{aligned} \quad (4.13)$$

$$\begin{aligned} \underline{a}_{d,ij} &= -([\mathbf{U}] - [\mathbf{\Omega}^2] - [\dot{\mathbf{\Omega}}]) \underline{A}_i - ([\mathbf{U}] - [\mathbf{\Omega}^2] - [\dot{\mathbf{\Omega}}]) \delta \underline{A}_{d,ij} + 2[\mathbf{\Omega}] \cdot \delta \dot{\underline{A}}_{d,ij} + \delta \ddot{\underline{A}}_{d,ij} - \underline{S}_{d,ij} - \underline{M}_{d,ij} \\ &= -([\mathbf{U}] - [\mathbf{\Omega}^2] - [\dot{\mathbf{\Omega}}]) \underline{A}_i - ([\mathbf{U}] - [\mathbf{\Omega}^2] - [\dot{\mathbf{\Omega}}]) \delta \underline{A}_i + 2[\mathbf{\Omega}] \cdot \delta \dot{\underline{A}}_{d,ij} + \delta \ddot{\underline{A}}_{d,ij} - \underline{S}_{d,ij} - \underline{M}_{d,ij}. \end{aligned} \quad (4.14)$$

#### 4.1.2.2 Accelerometer Mispointing, Coupling, Scale Factor, Quadratic Factor, Noise and Bias

The mispointing of the ARF of the accelerometer  $A_i$  in the OAGRF is defined by the rotation matrix  $[\mathbf{R}]_i$  which, for small angles, can be approximated with the following expression:

$$[\mathbf{R}]_i = \begin{pmatrix} 1 & \psi_i & -\theta_i \\ -\psi_i & 1 & \varphi_i \\ \theta_i & -\varphi_i & 1 \end{pmatrix} = [1]_3 + \begin{pmatrix} 0 & \psi_i & -\theta_i \\ -\psi_i & 0 & \varphi_i \\ \theta_i & -\varphi_i & 0 \end{pmatrix} \equiv [1]_3 + [d\mathbf{R}]_i \quad (4.15)$$

where  $[1]_3 = 3 \times 3$  identity matrix,  $\varphi_i, \theta_i, \psi_i =$  (small) rotation angles of the ARF in the OAGRF about the  $X_i, Y_i, Z_i$  axes (the matrix  $[\mathbf{R}]_i$  transforms the components of a vector from the OAGRF to the ARF of the accelerometer  $A_i$ ).

Note that, for the given definition of the OAGRF, rotations of the ARF<sub>1</sub> about the Y and Z axes of the OAGRF<sub>1</sub> arise also in presence of a lateral misplacement, along Y and Z, of the accelerometer  $A_1$  relatively to the ARF of the accelerometer  $A_4$  and viceversa (see Figure 4.1-4). Similarly, lateral misplacements, along X and Z of the accelerometer  $A_2, A_5$  relatively to their ARFs give rise to rotations of ARF<sub>2</sub>, ARF<sub>5</sub> about the X and Z axes of the OAGRF<sub>2</sub>, and lateral misplacements, along X and Y of the accelerometer  $A_3, A_6$  relatively to their ARFs give rise to rotations of ARF<sub>3</sub>, ARF<sub>6</sub> about the X and Y axes of the OAGRF<sub>3</sub>.

Such lateral misplacements, which formally do not appear in the equations of the gradiometric measurements, are in reality contained in the rotation angles of the ARFs relatively to the OAGRFs.

Moreover, again for the given definition of the OAGRF, we have that:

- $\varphi_4 = -\varphi_1 \rightarrow \varphi_4 + \varphi_1 = 0, \quad 0.5(\varphi_4 - \varphi_1) = \varphi_1$
- $\theta_5 = -\theta_2 \rightarrow \theta_5 + \theta_2 = 0, \quad 0.5(\theta_5 - \theta_2) = \theta_2$
- $\psi_6 = -\psi_3 \rightarrow \psi_6 + \psi_3 = 0, \quad 0.5(\psi_6 - \psi_3) = \psi_3$

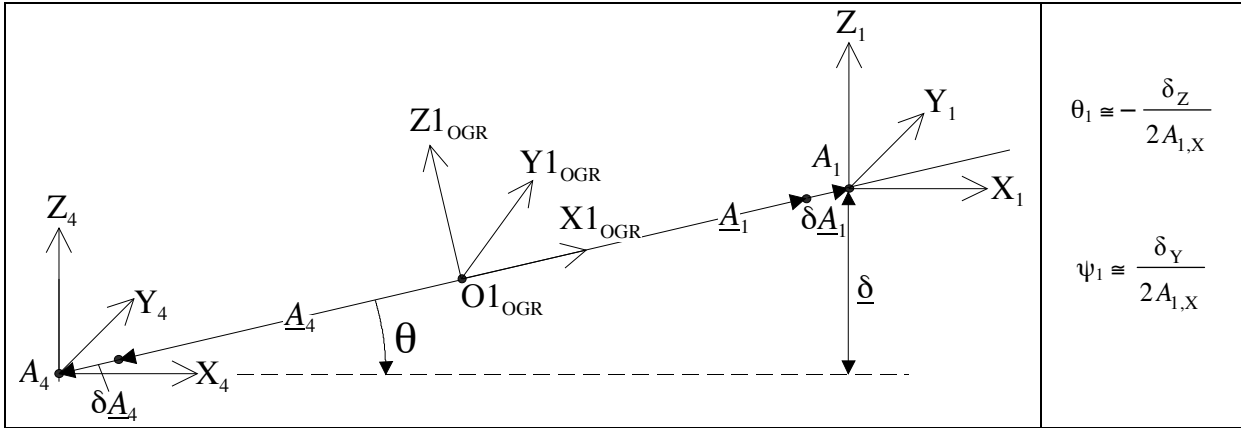


Figure 4.1-4: Relationship between the lateral misalignment  $\underline{\delta}$  of the accelerometer  $A_1$  in the ARF of the accelerometer  $A_4$  and the rotation angles  $\theta_1, \psi_1$  of the ARF $_1$  in the OAGRF $_1$

In addition, there are in general cross couplings between the accelerometer sensitive axes due their non-perfect orthogonality, etc... The cross couplings of the sensitive axes of the accelerometer  $A_i$ , can be approximated, for small coupling factors, by the symmetric matrix:

$$[S]_i = \begin{pmatrix} 1 & \varepsilon_i & \eta_i \\ \varepsilon_i & 1 & \zeta_i \\ \eta_i & \zeta_i & 1 \end{pmatrix} = [1]_3 + \begin{pmatrix} 0 & \varepsilon_i & \eta_i \\ \varepsilon_i & 0 & \zeta_i \\ \eta_i & \zeta_i & 0 \end{pmatrix} \equiv [1]_3 + [dS]_i \quad (4.16)$$

where  $\varepsilon_i = X_i \leftrightarrow Y_i$  (small) coupling factor,  $\eta_i = X_i \leftrightarrow Z_i$  coupling factor,  $\zeta_i = Y_i \leftrightarrow Z_i$  coupling factor.

Under an acceleration  $\underline{a}_i$  of the proof mass relative to its cage, the accelerometer applies to the electrodes control voltages (along each axis) that maintain the mass at the centre of the cage. When the proof mass is controlled in a motionless condition, the acceleration  $a_{i,k}$  of the accelerometer  $A_i$  proof mass along its sensitive axis  $k$  is, at first order, proportional to the control voltage  $V_{i,k}$  (see [RD 1] for more details). The following relationships hold between the proof accelerations and control voltages (in the AESRF):

$$\begin{aligned} a_{i,Xe} &= \frac{1}{4 \cdot G_{read}} (G_{el\_X1} V_{i,X1} + G_{el\_X2} V_{i,X2} + G_{el\_X3} V_{i,X3} + G_{el\_X4} V_{i,X4}) \\ a_{i,Ye} &= \frac{1}{2 \cdot G_{read}} (G_{el\_Y1} V_{i,Y1} + G_{el\_Y2} V_{i,Y2}) \\ a_{i,Ze} &= \frac{1}{2 \cdot G_{read}} (G_{el\_Z1} V_{i,Z1} + G_{el\_Z2} V_{i,Z2}) \end{aligned} \quad (4.17)$$

where  $G_{el\_X1}, G_{el\_X2}, G_{el\_X3}, G_{el\_X4}, G_{el\_Y1}, G_{el\_Y2}, G_{el\_Z1}, G_{el\_Z2}$  are the electrostatic gains of the accelerometer (which are function of the electrode surface, the gap between the proof mass and the electrodes, the weight of the proof mass and the polarization voltage of the mass), and  $G_{read}$  is the read-out gain.

The measurement  $a'_{i,k}$  of the acceleration  $a_{i,k}$  is then obtained from  $V_{i,k}$  and from the knowledge of the electrostatic gains and of the read-out gain. Being these quantities known with a certain uncertainty, the measured accelerations are slightly different from the actual ones. This difference can be expressed as:

$$a'_{i,k} = (1 + K_{i,k}) \cdot a_{i,k} \quad (4.18)$$

where  $K_{i,k}$  is the accelerometer "scale factor" (it is the result of the uncertainty in the knowledge of  $G_{el\_X1}, \dots, G_{read}$ ).

Actually, the relationship between  $a_{i,k}$  and  $V_{i,k}$  is linear only at first order. In a real accelerometer, the differences between the surface of the electrodes and between the drive voltage amplifier gains, and the offsets in the position sensor detectors give rise to a non linearity in the relationship between the input acceleration and the measured acceleration (see [RD 2] more details). This non-linearity can be expressed as an additional term in the (4.18) proportional to the square of the input acceleration through a “quadratic factor”  $K2_{i,k}$ .

In addition, the electronics readout chain of the sensor introduces in the measured acceleration a bias ( $b_{i,k}$ ), again due to imperfections of the accelerometer, and a noise ( $n_{i,k}$ ).

Therefore, including all the effects described above, a linear acceleration  $\underline{a}_i$  of the accelerometer proof mass having the expression (4.1) in the OAGRF, is measured by the accelerometer  $A_i$  as:

$$\begin{aligned} \underline{a}'_i &= ([1]_3 + [dK]_i) \cdot ([1]_3 + [dR]_i) \cdot ([1]_3 + [dS]_i) \cdot \underline{a}_i + [K2]_i \cdot \underline{a}_i^2 + \underline{b}_i + \underline{n}_i \\ &\approx ([1]_3 + [dK]_i + [dR]_i + [dS]_i) \cdot \underline{a}_i + [K2]_i \cdot \underline{a}_i^2 + \underline{b}_i + \underline{n}_i \quad (1) \\ \underline{a}'_i &= ([K]_i + [dR]_i + [dS]_i) \cdot \underline{a}_i + [K2]_i \cdot \underline{a}_i^2 + \underline{b}_i + \underline{n}_i \quad (4.19) \end{aligned}$$

where

$$\begin{aligned} [K]_i = \text{scale factor matrix} &= \begin{pmatrix} 1 + K_{i,X} & 0 & 0 \\ 0 & 1 + K_{i,Y} & 0 \\ 0 & 0 & 1 + K_{i,Z} \end{pmatrix} = [1]_3 + \begin{pmatrix} K_{i,X} & 0 & 0 \\ 0 & K_{i,Y} & 0 \\ 0 & 0 & K_{i,Z} \end{pmatrix} = [1]_3 + [dK]_i \\ [K2]_i = \text{quadratic factor matrix} &= \begin{pmatrix} K2_{i,X} & 0 & 0 \\ 0 & K2_{i,Y} & 0 \\ 0 & 0 & K2_{i,Z} \end{pmatrix} \\ \underline{b}_i = \text{accelerometer bias vector} &= \begin{pmatrix} b_{i,X} \\ b_{i,Y} \\ b_{i,Z} \end{pmatrix}, \quad \underline{n}_i = \text{accelerometer noise vector} = \begin{pmatrix} n_{i,X} \\ n_{i,Y} \\ n_{i,Z} \end{pmatrix} \end{aligned}$$

Lets' form from the (4.19) the measured common and differential mode accelerations  $\underline{a}'_{c,ij} = \frac{1}{2}(\underline{a}'_i + \underline{a}'_j)$ ,  $\underline{a}'_{d,ij} = \frac{1}{2}(\underline{a}'_i - \underline{a}'_j)$  measured by the three OAGs ( $ij = 14, 25, 36$ ). Their relationship with common and differential mode accelerations ( $\underline{a}_{c,ij}$ ,  $\underline{a}_{d,ij}$ ) experienced by the accelerometer proof masses is

$$\begin{pmatrix} \underline{a}'_{c,ij} \\ \underline{a}'_{d,ij} \end{pmatrix} = \mathbf{M}_{ij} \begin{pmatrix} \underline{a}_{c,ij} \\ \underline{a}_{d,ij} \end{pmatrix} + \frac{1}{2} \mathbf{K}2_{ij} \begin{pmatrix} (\underline{a}_{c,ij} + \underline{a}_{d,ij})^2 \\ (\underline{a}_{c,ij} - \underline{a}_{d,ij})^2 \end{pmatrix} + \begin{pmatrix} \underline{b}_{c,ij} \\ \underline{b}_{d,ij} \end{pmatrix} + \begin{pmatrix} \underline{n}_{c,ij} \\ \underline{n}_{d,ij} \end{pmatrix} \quad (4.20)$$

with the following definitions:

$$\mathbf{M}_{ij} = \begin{pmatrix} 1 + K_{c,ij,X} & \Psi_{c,ij} + \varepsilon_{c,ij} & -\theta_{c,ij} + \eta_{c,ij} & K_{d,ij,X} & \Psi_{d,ij} + \varepsilon_{d,ij} & -\theta_{d,ij} + \eta_{d,ij} \\ -\Psi_{c,ij} + \varepsilon_{c,ij} & 1 + K_{c,ij,Y} & \varphi_{c,ij} + \varsigma_{c,ij} & -\Psi_{d,ij} + \varepsilon_{d,ij} & K_{d,ij,Y} & \varphi_{d,ij} + \varsigma_{d,ij} \\ \theta_{c,ij} + \eta_{c,ij} & -\varphi_{c,ij} + \varsigma_{c,ij} & 1 + K_{c,ij,Z} & \theta_{d,ij} + \eta_{d,ij} & -\varphi_{d,ij} + \varsigma_{d,ij} & K_{d,ij,Z} \\ K_{d,ij,X} & \Psi_{d,ij} + \varepsilon_{d,ij} & -\theta_{d,ij} + \eta_{d,ij} & 1 + K_{c,ij,X} & \Psi_{c,ij} + \varepsilon_{c,ij} & -\theta_{c,ij} + \eta_{c,ij} \\ -\Psi_{d,ij} + \varepsilon_{d,ij} & K_{d,ij,Y} & \varphi_{d,ij} + \varsigma_{d,ij} & -\Psi_{c,ij} + \varepsilon_{c,ij} & 1 + K_{c,ij,Y} & \varphi_{c,ij} + \varsigma_{c,ij} \\ \theta_{d,ij} + \eta_{d,ij} & -\varphi_{d,ij} + \varsigma_{d,ij} & K_{d,ij,Z} & \theta_{c,ij} + \eta_{c,ij} & -\varphi_{c,ij} + \varsigma_{c,ij} & 1 + K_{c,ij,Z} \end{pmatrix}$$

<sup>1</sup> This simplification is allowed by the knowledge of the size of the terms of  $[dK]_i + [dR]_i + [dS]_i$  (Table 4.1-2)

$$\mathbf{K2}_{ij} = \begin{pmatrix} K2_{c,ij,X} + K2_{d,ij,X} & 0 & 0 & K2_{c,ij,X} - K2_{d,ij,X} & 0 & 0 \\ 0 & K2_{c,ij,Y} + K2_{d,ij,Y} & 0 & 0 & K2_{c,ij,Y} - K2_{d,ij,Y} & 0 \\ 0 & 0 & K2_{c,ij,Z} + K2_{d,ij,Z} & 0 & 0 & K2_{c,ij,Z} - K2_{d,ij,Z} \\ K2_{c,ij,X} + K2_{d,ij,X} & 0 & 0 & K2_{d,ij,X} - K2_{c,ij,X} & 0 & 0 \\ 0 & K2_{c,ij,Y} + K2_{d,ij,Y} & 0 & 0 & K2_{d,ij,Y} - K2_{c,ij,Y} & 0 \\ 0 & 0 & K2_{c,ij,Z} + K2_{d,ij,Z} & 0 & 0 & K2_{d,ij,Z} - K2_{c,ij,Z} \end{pmatrix} = \begin{pmatrix} \left[ \mathbf{K2} \right]_{+,ij} & \left[ \mathbf{K2} \right]_{-,ij} \\ \left[ \mathbf{K2} \right]_{+,ij} & -\left[ \mathbf{K2} \right]_{-,ij} \end{pmatrix}$$

$$\begin{pmatrix} (a_{c,ij} + a_{d,ij})^2 \\ (a_{c,ij} - a_{d,ij})^2 \end{pmatrix} = \begin{pmatrix} (a_{c,ij,X} + a_{d,ij,X})^2 \\ (a_{c,ij,Y} + a_{d,ij,Y})^2 \\ (a_{c,ij,Z} + a_{d,ij,Z})^2 \\ (a_{c,ij,X} - a_{d,ij,X})^2 \\ (a_{c,ij,Y} - a_{d,ij,Y})^2 \\ (a_{c,ij,Z} - a_{d,ij,Z})^2 \end{pmatrix}, \frac{1}{2} \mathbf{K2}_{ij} \begin{pmatrix} (a_{c,ij} + a_{d,ij})^2 \\ (a_{c,ij} - a_{d,ij})^2 \end{pmatrix} = \begin{pmatrix} (a_{c,ij,X}^2 + a_{d,ij,X}^2) K2_{c,ij,X} + 2 \cdot K2_{d,ij,X} a_{c,ij,X} a_{d,ij,X} \\ (a_{c,ij,Y}^2 + a_{d,ij,Y}^2) K2_{c,ij,Y} + 2 \cdot K2_{d,ij,Y} a_{c,ij,Y} a_{d,ij,Y} \\ (a_{c,ij,Z}^2 + a_{d,ij,Z}^2) K2_{c,ij,Z} + 2 \cdot K2_{d,ij,Z} a_{c,ij,Z} a_{d,ij,Z} \\ (a_{c,ij,X}^2 + a_{d,ij,X}^2) K2_{d,ij,X} + 2 \cdot K2_{c,ij,X} a_{c,ij,X} a_{d,ij,X} \\ (a_{c,ij,Y}^2 + a_{d,ij,Y}^2) K2_{d,ij,Y} + 2 \cdot K2_{c,ij,Y} a_{c,ij,Y} a_{d,ij,Y} \\ (a_{c,ij,Z}^2 + a_{d,ij,Z}^2) K2_{d,ij,Z} + 2 \cdot K2_{c,ij,Z} a_{c,ij,Z} a_{d,ij,Z} \end{pmatrix} \quad (4.21)$$

$1 + K_{c,ij,X} (K_{d,ij,X})$  = common (differential) scale factor of the accelerometer pair  $A_i, A_j$  along the X axis of the

$$\text{OAGRF: } 1 + K_{c,ij,X} = 1 + \frac{1}{2} (K_{i,X} + K_{j,X}), K_{d,ij,X} = \frac{1}{2} (K_{i,X} - K_{j,X}), \dots$$

$\varphi_{c,ij} (\varphi_{d,ij})$  = common (differential) misalignment of the accelerometer pair  $A_i, A_j$  about the X axis of the OAGRF:

$$\varphi_{c,ij} = \frac{1}{2} (\varphi_i + \varphi_j), \varphi_{d,ij} = \frac{1}{2} (\varphi_i - \varphi_j), \dots$$

$\zeta_{c,ij} (\zeta_{d,ij})$  = component along the X axis of the OAGRF of the common (differential) coupling among the axes of the

$$\text{accelerometer pair } A_i, A_j: \zeta_{c,ij} = \frac{1}{2} (\zeta_i + \zeta_j), \zeta_{d,ij} = \frac{1}{2} (\zeta_i - \zeta_j) \dots$$

$K2_{c,ij,X} (K2_{d,ij,X})$ : common (differential) quadratic factor of the accelerometer pair  $A_i, A_j$  along the X axis of the OAGRF:

$$K2_{c,ij,X} = \frac{1}{2} (K2_{i,X} + K2_{j,X}), K2_{d,ij,X} = \frac{1}{2} (K2_{i,X} - K2_{j,X}), \dots$$

$b_{c,ij,X} (b_{d,ij,X})$ : common (differential) biases of the accelerometer pair  $A_i, A_j$  along the X of the OAGRF, ...

$n_{c,ij,X} (n_{d,ij,X})$ : common (differential) noises of the accelerometer pair  $A_i, A_j$  along the X of the OAGRF, ...

The accelerometer scale factor, misalignment, coupling, quadratic factor, bias and noise bring additional errors to the GGT components and the non-gravitational accelerations obtained from the Gradiometer measurements.

The accelerometer bias is constant by definition and does not contribute, alone, to the measurement error in the Gradiometer MBW. Its value is established at the accelerometer manufacturing and integration, and cannot be modified afterwards.

The accelerometer noise is one of the main the measurement errors in the MBW. Its value is also established at the accelerometer manufacturing and integration, and cannot be modified afterwards.

The quadratic factor contributes to the measurement error in the MBW through its coupling with the square of the input acceleration. It is the main source of the aliasing in the MBW of the high-frequency noise (i.e. the noise with frequency

contents > 0.1 Hz) of the input acceleration. The accelerometer quadratic factors can be physically adjusted in flight (reduced) once their value is known. The upper limits of the quadratic factors during the measurement phases are therefore the result of their adjustment during the in-flight calibration and of their successive drifts. In case no adjustment operation is performed, the maximum values that the common and differential quadratic factors can achieve all along the mission lifetime are determined by the manufacturing/integration of the accelerometers and their electronics and by the further modifications that they can suffer during the ground testing and handling, during launch, and during all the time spent on orbit. The predicted maximum values of the quadratic factors throughout the mission lifetime are provided in Table 4.1-1 (ref. [RD 14]).

| Sensor Pair                     | OAGRF axis |   |   | Common Quadratic Factors                  | Differential Quadratic Factors            |
|---------------------------------|------------|---|---|-------------------------------------------|-------------------------------------------|
| A <sub>1</sub> , A <sub>4</sub> | X          | ↑ | U | $K2_{c,14,X} < 1206 \text{ s}^2/\text{m}$ | $K2_{d,14,X} < 1206 \text{ s}^2/\text{m}$ |
|                                 | Y          | → | L | $K2_{c,14,Y} < 1 \text{ s}^2/\text{m}$    | $K2_{d,14,Y} < 1 \text{ s}^2/\text{m}$    |
|                                 | Z          | → | U | $K2_{c,14,Z} < 1206 \text{ s}^2/\text{m}$ | $K2_{d,14,Z} < 1206 \text{ s}^2/\text{m}$ |
| A <sub>2</sub> , A <sub>5</sub> | X          | → | U | $K2_{c,25,X} < 1206 \text{ s}^2/\text{m}$ | $K2_{d,25,X} < 1206 \text{ s}^2/\text{m}$ |
|                                 | Y          | ↑ | U | $K2_{c,25,Y} < 1206 \text{ s}^2/\text{m}$ | $K2_{d,25,Y} < 1206 \text{ s}^2/\text{m}$ |
|                                 | Z          | → | L | $K2_{c,25,Z} < 1 \text{ s}^2/\text{m}$    | $K2_{d,25,Z} < 1 \text{ s}^2/\text{m}$    |
| A <sub>3</sub> , A <sub>6</sub> | X          | → | U | $K2_{c,36,X} < 1206 \text{ s}^2/\text{m}$ | $K2_{d,36,X} < 1206 \text{ s}^2/\text{m}$ |
|                                 | Y          | → | L | $K2_{c,36,Y} < 1 \text{ s}^2/\text{m}$    | $K2_{d,36,Y} < 1 \text{ s}^2/\text{m}$    |
|                                 | Z          | ↑ | U | $K2_{c,36,Z} < 1206 \text{ s}^2/\text{m}$ | $K2_{d,36,Z} < 1206 \text{ s}^2/\text{m}$ |

- ↑ : in-line axis, aligned to the baseline of the OAG to which the accelerometer belongs
- : transversal axis, perpendicular to the baseline of the OAG to which the accelerometer belongs
- U : accelerometer ultra sensitive axis, L : accelerometer less sensitive axis

Table 4.1-1: Predicted maximum values of the common and differential quadratic factors of the three accelerometer pairs throughout the mission lifetime (in case of non adjustment on orbit).

The accelerometer scale factor, the misalignment of its ARF in the OAGRF, and the coupling among its sensitive axes contribute to the measurement error in the MBW through their coupling with the input acceleration along the OAGRF axis aligned to the accelerometer measurement axis (scale factor) and with input acceleration along the other (transversal) OAGRF axes (misalignment and coupling). The values of these parameters are established by the manufacturing and integration of the single accelerometers (scale factor, coupling among the sensitive axes), and by the integration of the accelerometers in the respective OAGs (misalignment of the ARF in the OAGRF), and cannot be physically modified afterwards. The values that these parameters will have along the GOCE mission are therefore determined by the result of the manufacturing/integration and by the further modifications that they can suffer during the ground testing and handling, during launch, and during all the time spent on orbit. The design and implementation of the accelerometers and of the Gradiometer shall guarantee that, as consequence of all these processes (manufacturing/integration, ground activities, launch, on orbit lifetime effects), the values of the common and differential scale factors, misalignment and coupling among the axes of the three accelerometer pair A<sub>i</sub>, A<sub>j</sub> (ij = 14, 25, 36) do not exceed the limits provided in Table 4.1-2 (confirmed by the measurements performed on the flight Gradiometer; ref. [RD 14]).

Although not modifiable, the values of these elements can be measured in flight and their knowledge can be utilised to reduce their contribution to the Gradiometer measurement error.

| Sensor Pair | OAG Axis  | Common, Differential Scale Factor             | Common, Differential Misalignment + Coupling [rad]                                                                                                     |
|-------------|-----------|-----------------------------------------------|--------------------------------------------------------------------------------------------------------------------------------------------------------|
|             | X   ↑   U | $K_{c,14,X}, K_{d,14,X} < 4.05 \cdot 10^{-3}$ | $(\psi_{c,14} + \epsilon_{c,14}), (-\theta_{c,14} + \eta_{c,14}), (\psi_{d,14} + \epsilon_{d,14}), (-\theta_{d,14} + \eta_{d,14}) < 1.3 \cdot 10^{-4}$ |

|                                 |                |   |   |                                               |                                                                                                                                                                                                                                              |
|---------------------------------|----------------|---|---|-----------------------------------------------|----------------------------------------------------------------------------------------------------------------------------------------------------------------------------------------------------------------------------------------------|
| A <sub>1</sub> , A <sub>4</sub> | Y              | → | L | $K_{c,14,Y}, K_{d,14,Y} < 5.18 \cdot 10^{-2}$ | $(-\psi_{c,14+\varepsilon_{c,14}}, (-\psi_{d,14+\varepsilon_{d,14}}), (\varphi_{d,14+\zeta_{d,14}}) < 1.3 \cdot 10^{-4}$<br>$(\varphi_{c,14+\zeta_{c,14}}) = \zeta_{c,14} < 1.0 \cdot 10^{-5}$ (for the OAGRF <sub>1</sub> definition)       |
|                                 | Z              | → | U | $K_{c,14,Z}, K_{d,14,Z} < 4.05 \cdot 10^{-3}$ | $(\theta_{c,14+\eta_{c,14}}, (\theta_{d,14+\eta_{d,14}}), (-\phi_{d,14+\zeta_{d,14}}) < 1.3 \cdot 10^{-4}$<br>$(-\varphi_{c,14+\zeta_{c,14}}) = \zeta_{c,14} < 1.0 \cdot 10^{-5}$ (for the OAGRF <sub>1</sub> definition)                    |
| A <sub>2</sub> , A <sub>5</sub> | X <sub>i</sub> | → | U | $K_{c,25,X}, K_{d,25,X} < 4.05 \cdot 10^{-3}$ | $(\psi_{c,25+\varepsilon_{c,25}}, (\psi_{d,25+\varepsilon_{d,25}}), (-\theta_{d,25+\eta_{d,25}}) < 1.3 \cdot 10^{-4}$<br>$(-\theta_{c,25+\eta_{c,25}}) = \eta_{c,25} < 1.0 \cdot 10^{-5}$ (for the OAGRF <sub>2</sub> definition)            |
|                                 | Y <sub>i</sub> | ↑ | U | $K_{c,25,Y}, K_{d,25,Y} < 4.05 \cdot 10^{-3}$ | $(-\psi_{c,25+\varepsilon_{c,25}}, (\varphi_{c,25+\zeta_{c,25}}), (-\psi_{d,25+\varepsilon_{d,25}}), (\varphi_{d,25+\zeta_{d,25}}) < 1.3 \cdot 10^{-4}$                                                                                      |
|                                 | Z <sub>i</sub> | → | L | $K_{c,25,Z}, K_{d,25,Z} < 5.18 \cdot 10^{-2}$ | $(-\varphi_{c,25+\zeta_{c,25}}, (\theta_{d,25+\eta_{d,25}}), (-\varphi_{d,25+\zeta_{d,25}}) < 1.3 \cdot 10^{-4}$<br>$(\theta_{c,25+\eta_{c,25}}) = \eta_{c,25} < 1.0 \cdot 10^{-5}$ (for the OAGRF <sub>2</sub> definition)                  |
| A <sub>3</sub> , A <sub>6</sub> | X <sub>i</sub> | → | U | $K_{c,36,X}, K_{d,36,X} < 4.05 \cdot 10^{-3}$ | $(-\theta_{c,36+\eta_{c,36}}, (\psi_{d,36+\varepsilon_{d,36}}), (-\theta_{d,36+\eta_{d,36}}) < 1.3 \cdot 10^{-4}$<br>$(\psi_{c,36+\varepsilon_{c,36}}) = \varepsilon_{c,36} < 1.0 \cdot 10^{-5}$ (for the OAGRF <sub>3</sub> definition)     |
|                                 | Y <sub>i</sub> | → | L | $K_{c,36,Y}, K_{d,36,Y} < 5.18 \cdot 10^{-2}$ | $(\varphi_{c,36+\zeta_{c,36}}, (-\psi_{d,36+\varepsilon_{d,36}}), (\varphi_{d,36+\zeta_{d,36}}) < 1.3 \cdot 10^{-4}$<br>$(-\psi_{c,36+\varepsilon_{c,36}}) = \varepsilon_{c,36} < 1.0 \cdot 10^{-5}$ (for the OAGRF <sub>3</sub> definition) |
|                                 | Z <sub>i</sub> | ↑ | U | $K_{c,36,Z}, K_{d,36,Z} < 4.05 \cdot 10^{-3}$ | $(\theta_{c,36+\eta_{c,36}}, (-\varphi_{c,36+\zeta_{c,36}}), (\theta_{d,36+\eta_{d,36}}), (-\varphi_{d,36+\zeta_{d,36}}) < 1.3 \cdot 10^{-4}$                                                                                                |

- ↑ : in-line axis, aligned to the baseline of the OAG to which the accelerometer belongs  
 → : transversal axis, perpendicular to the baseline of the OAG to which the accelerometer belongs  
 U : accelerometer ultra sensitive axis, L : accelerometer less sensitive axis

Table 4.1-2: Predicted maximum values of the common and differential scale factors, misalignment and coupling of the three accelerometer pairs throughout the mission lifetime.

#### 4.1.2.3 The Calibration Matrix and its Inverse

The 6x6 matrix  $M_{ij}$ , introduced in the previous section and hereafter named “Calibration Matrix”, is defined for each OAG and contains the common and differential scale factors, misalignment and coupling among the axes of the accelerometer pair  $A_i, A_j$  ( $ij = 14, 25, 36$ ). It is also useful to express the Calibration Matrix in a form in which the unit matrix is separated from the other elements of  $M_{ij}$  and which highlights the common-mode elements and the differential-mode elements:

$$M_{ij} = \begin{pmatrix} 1 & 0 & 0 & 0 & 0 & 0 \\ 0 & 1 & 0 & 0 & 0 & 0 \\ 0 & 0 & 1 & 0 & 0 & 0 \\ 0 & 0 & 0 & 1 & 0 & 0 \\ 0 & 0 & 0 & 0 & 1 & 0 \\ 0 & 0 & 0 & 0 & 0 & 1 \end{pmatrix} + \begin{pmatrix} K_{c,ij,X} & \psi_{c,ij} + \varepsilon_{c,ij} & -\theta_{c,ij} + \eta_{c,ij} & K_{d,ij,X} & \psi_{d,ij} + \varepsilon_{d,ij} & -\theta_{d,ij} + \eta_{d,ij} \\ -\psi_{c,ij} + \varepsilon_{c,ij} & K_{c,ij,Y} & \phi_{c,ij} + \zeta_{c,ij} & -\psi_{d,ij} + \varepsilon_{d,ij} & K_{d,ij,Y} & \phi_{d,ij} + \zeta_{d,ij} \\ \theta_{c,ij} + \eta_{c,ij} & -\phi_{c,ij} + \zeta_{c,ij} & K_{c,ij,Z} & \theta_{d,ij} + \eta_{d,ij} & -\phi_{d,ij} + \zeta_{d,ij} & K_{d,ij,Z} \\ K_{d,ij,X} & \psi_{d,ij} + \varepsilon_{d,ij} & -\theta_{d,ij} + \eta_{d,ij} & K_{c,ij,X} & \psi_{c,ij} + \varepsilon_{c,ij} & -\theta_{c,ij} + \eta_{c,ij} \\ -\psi_{d,ij} + \varepsilon_{d,ij} & K_{d,ij,Y} & \phi_{d,ij} + \zeta_{d,ij} & -\psi_{c,ij} + \varepsilon_{c,ij} & K_{c,ij,Y} & \phi_{c,ij} + \zeta_{c,ij} \\ \theta_{d,ij} + \eta_{d,ij} & -\phi_{d,ij} + \zeta_{d,ij} & K_{d,ij,Z} & \theta_{c,ij} + \eta_{c,ij} & -\phi_{c,ij} + \zeta_{c,ij} & K_{c,ij,Z} \end{pmatrix}$$

$$= \begin{pmatrix} 1 & 0 & 0 & 0 & 0 & 0 \\ 0 & 1 & 0 & 0 & 0 & 0 \\ 0 & 0 & 1 & 0 & 0 & 0 \\ 0 & 0 & 0 & 1 & 0 & 0 \\ 0 & 0 & 0 & 0 & 1 & 0 \\ 0 & 0 & 0 & 0 & 0 & 1 \end{pmatrix} + \begin{pmatrix} dM_{c,ij,11} & dM_{c,ij,12} & dM_{c,ij,13} & dM_{d,ij,11} & dM_{d,ij,12} & dM_{d,ij,13} \\ dM_{c,ij,21} & dM_{c,ij,22} & dM_{c,ij,23} & dM_{d,ij,21} & dM_{d,ij,22} & dM_{d,ij,23} \\ dM_{c,ij,31} & dM_{c,ij,32} & dM_{c,ij,33} & dM_{d,ij,31} & dM_{d,ij,32} & dM_{d,ij,33} \\ dM_{d,ij,11} & dM_{d,ij,12} & dM_{d,ij,13} & dM_{c,ij,11} & dM_{c,ij,12} & dM_{c,ij,13} \\ dM_{d,ij,21} & dM_{d,ij,22} & dM_{d,ij,23} & dM_{c,ij,21} & dM_{c,ij,22} & dM_{c,ij,23} \\ dM_{d,ij,31} & dM_{d,ij,32} & dM_{d,ij,33} & dM_{c,ij,31} & dM_{c,ij,32} & dM_{c,ij,33} \end{pmatrix} = [1]_6 + \begin{pmatrix} [dM]_{c,ij} & [dM]_{d,ij} \\ [dM]_{d,ij} & [dM]_{c,ij} \end{pmatrix}$$

(4.22)

$$= [1]_6 + dM_{ij} \text{ (with } [1]_6 = 6 \times 6 \text{ identity matrix)}$$

Let's denote as  $MI_{ij}$  the inverse of the Calibration Matrix  $M_{ij}^{-1}$ .

$$\mathbf{MI}_{ij} = \begin{pmatrix} MI_{ij,11} & MI_{ij,12} & MI_{ij,13} & MI_{ij,14} & MI_{ij,15} & MI_{ij,16} \\ MI_{ij,21} & MI_{ij,22} & MI_{ij,23} & MI_{ij,24} & MI_{ij,25} & MI_{ij,26} \\ MI_{ij,31} & MI_{ij,32} & MI_{ij,33} & MI_{ij,34} & MI_{ij,35} & MI_{ij,36} \\ MI_{ij,41} & MI_{ij,42} & MI_{ij,43} & MI_{ij,44} & MI_{ij,45} & MI_{ij,46} \\ MI_{ij,51} & MI_{ij,52} & MI_{ij,53} & MI_{ij,54} & MI_{ij,55} & MI_{ij,56} \\ MI_{ij,61} & MI_{ij,62} & MI_{ij,63} & MI_{ij,64} & MI_{ij,65} & MI_{ij,66} \end{pmatrix} = \mathbf{M}_{ij}^{-1} = ([1]_6 + d\mathbf{M}_{ij})^{-1} \cong [1]_6 - d\mathbf{M}_{ij} \quad (4.23)$$

By introducing this approximation, the first terms neglected in the expansion of  $([1]_6 + d\mathbf{M}_{ij})^{-1}$  are  $d\mathbf{M}_{ij} \cdot d\mathbf{M}_{ij}$  and  $d\mathbf{M}_{ij} \cdot d\mathbf{M}_{ij} \cdot d\mathbf{M}_{ij}$ . Their contribution to the various elements of  $\mathbf{MI}_{ij}$  is (considering the limits of the Calibration Matrix elements provided in Table 4.1-2):

**MI<sub>14</sub>**

$$\Delta MI_{14,11}, \Delta MI_{14,33}, \Delta MI_{14,44}, \Delta MI_{14,66}, \Delta MI_{14,14}, \Delta MI_{14,36}, \Delta MI_{14,41}, \Delta MI_{14,63} < 3.3 \cdot 10^{-5}$$

$$\Delta MI_{14,22}, \Delta MI_{14,55}, \Delta MI_{14,25}, \Delta MI_{14,52} < 5.9 \cdot 10^{-3}$$

$$\Delta MI_{14,13}, \Delta MI_{14,16}, \Delta MI_{14,31}, \Delta MI_{14,34}, \Delta MI_{14,43}, \Delta MI_{14,46}, \Delta MI_{14,61}, \Delta MI_{14,64} < 2.2 \cdot 10^{-6}$$

$$\Delta MI_{14,12}, \Delta MI_{14,15}, \Delta MI_{14,21}, \Delta MI_{14,24}, \Delta MI_{14,42}, \Delta MI_{14,45}, \Delta MI_{14,51}, \Delta MI_{14,54} < 1.6 \cdot 10^{-5}$$

$$\Delta MI_{14,23}, \Delta MI_{14,26}, \Delta MI_{14,32}, \Delta MI_{14,35}, \Delta MI_{14,53}, \Delta MI_{14,56}, \Delta MI_{14,62}, \Delta MI_{14,65} < 8.7 \cdot 10^{-6}$$

**MI<sub>25</sub>**

$$\Delta MI_{25,11}, \Delta MI_{25,22}, \Delta MI_{25,44}, \Delta MI_{25,55}, \Delta MI_{25,14}, \Delta MI_{25,25}, \Delta MI_{25,41}, \Delta MI_{25,52} < 3.3 \cdot 10^{-5}$$

$$\Delta MI_{25,33}, \Delta MI_{25,66}, \Delta MI_{25,36}, \Delta MI_{25,63} < 5.9 \cdot 10^{-3}$$

$$\Delta MI_{25,12}, \Delta MI_{25,15}, \Delta MI_{25,21}, \Delta MI_{25,24}, \Delta MI_{25,42}, \Delta MI_{25,45}, \Delta MI_{25,51}, \Delta MI_{25,54} < 2.2 \cdot 10^{-6}$$

$$\Delta MI_{25,23}, \Delta MI_{25,26}, \Delta MI_{25,32}, \Delta MI_{25,35}, \Delta MI_{25,53}, \Delta MI_{25,56}, \Delta MI_{25,62}, \Delta MI_{25,65} < 1.6 \cdot 10^{-5}$$

$$\Delta MI_{25,13}, \Delta MI_{25,16}, \Delta MI_{25,31}, \Delta MI_{25,34}, \Delta MI_{25,43}, \Delta MI_{25,46}, \Delta MI_{25,61}, \Delta MI_{25,64} < 8.7 \cdot 10^{-6}$$

**MI<sub>36</sub>**

$$\Delta MI_{36,11}, \Delta MI_{36,33}, \Delta MI_{36,44}, \Delta MI_{36,66}, \Delta MI_{36,14}, \Delta MI_{36,36}, \Delta MI_{36,41}, \Delta MI_{36,63} < 3.3 \cdot 10^{-5}$$

$$\Delta MI_{36,22}, \Delta MI_{36,55}, \Delta MI_{36,25}, \Delta MI_{36,52} < 5.9 \cdot 10^{-3}$$

$$\Delta MI_{36,13}, \Delta MI_{36,16}, \Delta MI_{36,31}, \Delta MI_{36,34}, \Delta MI_{36,43}, \Delta MI_{36,46}, \Delta MI_{36,61}, \Delta MI_{36,64} < 2.2 \cdot 10^{-6}$$

$$\Delta MI_{36,23}, \Delta MI_{36,26}, \Delta MI_{36,32}, \Delta MI_{36,35}, \Delta MI_{36,53}, \Delta MI_{36,56}, \Delta MI_{36,62}, \Delta MI_{36,65} < 1.6 \cdot 10^{-5}$$

$$\Delta MI_{36,12}, \Delta MI_{36,15}, \Delta MI_{36,21}, \Delta MI_{36,24}, \Delta MI_{36,42}, \Delta MI_{36,45}, \Delta MI_{36,51}, \Delta MI_{36,54} < 8.7 \cdot 10^{-6}$$

Within the errors introduced by the approximation  $\mathbf{MI}_{ij} \cong [1]_6 - d\mathbf{M}_{ij}$ , the following equalities holds between the elements of  $\mathbf{MI}_{ij}$ :

$$MI_{ij,11} \cong MI_{ij,44} \cong 1 - dM_{c,ij,11} = 1 - K_{c,ij,X}; MI_{ij,14} \cong MI_{ij,41} \cong -dM_{d,ij,11} = -K_{d,ij,X}$$

$$MI_{ij,12} \cong MI_{ij,45} \cong -dM_{c,ij,12} = -\psi_{c,ij} - \epsilon_{c,ij}; MI_{ij,15} \cong MI_{ij,42} \cong -dM_{d,ij,12} = -\psi_{d,ij} - \epsilon_{d,ij}$$

$$\begin{aligned}
 MI_{ij,13} &\equiv MI_{ij,46} \equiv -dM_{c,ij,13} = \theta_{c,ij} - \eta_{c,ij} ; MI_{ij,16} \equiv MI_{ij,43} \equiv -dM_{d,ij,13} = \theta_{d,ij} - \eta_{d,ij} \\
 MI_{ij,21} &\equiv MI_{ij,54} \equiv -dM_{c,ij,21} = \psi_{c,ij} - \epsilon_{c,ij} ; MI_{ij,24} \equiv MI_{ij,51} \equiv -dM_{d,ij,21} = \psi_{d,ij} - \epsilon_{d,ij} \\
 MI_{ij,22} &\equiv MI_{ij,55} \equiv 1 - dM_{c,ij,22} = 1 - K_{c,ij,Y} ; MI_{ij,25} \equiv MI_{ij,52} \equiv -dM_{d,ij,22} = -K_{d,ij,Y} \\
 MI_{ij,23} &\equiv MI_{ij,56} \equiv -dM_{c,ij,23} = -\varphi_{c,ij} - \zeta_{c,ij} ; MI_{ij,26} \equiv MI_{ij,53} \equiv -dM_{d,ij,23} = -\varphi_{d,ij} - \zeta_{d,ij} \\
 MI_{ij,31} &\equiv MI_{ij,64} \equiv -dM_{c,ij,31} = -\theta_{c,ij} - \eta_{c,ij} ; MI_{ij,34} \equiv MI_{ij,61} \equiv -dM_{d,ij,31} = -\theta_{d,ij} - \eta_{d,ij} \\
 MI_{ij,32} &\equiv MI_{ij,65} \equiv -dM_{c,ij,32} = \varphi_{c,ij} - \zeta_{c,ij} ; MI_{ij,35} \equiv MI_{ij,62} \equiv -dM_{d,ij,32} = \varphi_{d,ij} - \zeta_{d,ij} \\
 MI_{ij,33} &\equiv MI_{ij,66} \equiv 1 - dM_{c,ij,33} = 1 - K_{c,ij,Z} ; MI_{ij,36} \equiv MI_{ij,63} \equiv -dM_{d,ij,33} = -K_{d,ij,Z}
 \end{aligned}$$

Let's introduce for  $MI_{ij}$  a block form similar to that of  $M_{ij}$ :

$$MI_{ij} = \left( \begin{array}{ccc|ccc}
 MI_{ij,11} & MI_{ij,12} & MI_{ij,13} & MI_{ij,14} & MI_{ij,15} & MI_{ij,16} \\
 MI_{ij,21} & MI_{ij,22} & MI_{ij,23} & MI_{ij,24} & MI_{ij,25} & MI_{ij,26} \\
 MI_{ij,31} & MI_{ij,32} & MI_{ij,33} & MI_{ij,34} & MI_{ij,35} & MI_{ij,36} \\
 \hline
 MI_{ij,41} & MI_{ij,42} & MI_{ij,43} & MI_{ij,44} & MI_{ij,45} & MI_{ij,46} \\
 MI_{ij,51} & MI_{ij,52} & MI_{ij,53} & MI_{ij,54} & MI_{ij,55} & MI_{ij,56} \\
 MI_{ij,61} & MI_{ij,62} & MI_{ij,63} & MI_{ij,64} & MI_{ij,65} & MI_{ij,66}
 \end{array} \right) \equiv \left( \begin{array}{cc}
 [MI']_{c,ij} & [MI']_{d,ij} \\
 [MI]_{d,ij} & [MI]_{c,ij}
 \end{array} \right) \quad (4.24)$$

where  $[MI']_{c,ij} \equiv [MI]_{c,ij}$ ,  $[MI']_{d,ij} \equiv [MI]_{d,ij}$  within the errors introduced by the approximation  $MI_{ij} \equiv [1]_6 - dM_{ij}$ .

The inverse Calibration Matrix plays a fundamental role in the GGT measurement process because, starting from the measured common and differential accelerations ( $\underline{a}'_{c,ij}$ ,  $\underline{a}'_{d,ij}$ ), it allows to recover the original differential accelerations  $\underline{a}_{d,ij}$  experienced by the proof masses of the accelerometer pair  $A_i, A_j$ , from which the GGT components are obtained:

$$\begin{pmatrix} \underline{a}_{c,ij} \\ \underline{a}_{d,ij} \end{pmatrix} = MI_{ij} \begin{pmatrix} \underline{a}'_{c,ij} \\ \underline{a}'_{d,ij} \end{pmatrix}, \quad \underline{a}_{d,ij} = [MI]_{d,ij} \underline{a}'_{c,ij} + [MI]_{c,ij} \underline{a}'_{d,ij} \quad (4.25)$$

The measurement of the elements of the inverse Calibration Matrix to the accuracy required to meet the GOCE Gradiometric performance requirements is one of the tasks of the in-flight calibration of the Gradiometer.

#### 4.1.2.4 Tasks of the Gradiometer In-Flight Calibration

The tasks of the in flight calibration of the Gradiometer are:

- Measure the common and differential quadratic factors of the three accelerometer pairs ( $K2_{c,ij,k}$ ,  $K2_{d,ij,k}$ ,  $ij = 14, 25, 36$ ,  $k = X, Y, Z$ ) and, if necessary, physically reduce them below the specified limits (see section 6.1 and 6.3) by proof mass position adjustment.
- Measure the elements of the inverse Calibration Matrices  $MI_{ij}$  ( $ij = 14, 25, 36$ ) involved in the recovery of the differential accelerations (i.e. the elements of  $[MI]_{d,ij}$ ,  $[MI]_{c,ij}$ ) with the specified accuracy (see section 6.1 and 6.3).

The Gradiometer on-orbit calibration will be performed before starting each Measurement Operational Phase. Intermediate calibrations, to be performed during the Measurement Operational Phase, cannot be planned in advance, depending on the rate of change of the quadratic factors, scale factors, misalignments and couplings after the Payload Calibration Phase. They will be

activated on the basis of the gradiometric performance degradation observed in the Level 1b products (GGT components), checked by means of the traceless property of the GGT, and may involve the measurement/adjustment of some parameters only (this applies only to the quadratic factors, since the method defines for the measurement of  $MI_{ij}$  determines globally all the elements). In any case the Gradiometer shall not require the execution of the intermediate calibrations more often than once per month, and the re-calibration shall not take longer than 1 day (system specification, [AD 1]).

Concerning the value of the quadratic factors elements before the first in-flight calibration, they are expected not to exceed the upper limits provided in Table 4.1-1.

About the common/differential scale factors, misalignment and couplings, they are expected not to exceed the upper limits provided in Table 4.1-2 all along the mission lifetime. Thus, according to the relationship (4.23) between  $MI_{ij}$  and  $M_{ij}$ , and considering the maximum errors introduced by the approximation  $M_{ij}^{-1} \approx [1]_6 - dMI_{ij}$ , we can expect that the elements of  $MI_{ij}$  will not the upper limits provided in Table 4.1-3 all along the mission lifetime. They represent the maximum error on the knowledge of these elements before the in-flight calibration (if we assume for the scale factors a unitary value and for the misalignments and couplings a null value).

|                                   |                                   |                                   |                                   |                                   |                                   |
|-----------------------------------|-----------------------------------|-----------------------------------|-----------------------------------|-----------------------------------|-----------------------------------|
| $dMI_{14,11} < 4.1 \cdot 10^{-3}$ | $MI_{14,12} < 1.5 \cdot 10^{-4}$  | $MI_{14,13} < 1.3 \cdot 10^{-4}$  | $MI_{14,14} < 4.1 \cdot 10^{-3}$  | $MI_{14,15} < 1.5 \cdot 10^{-4}$  | $MI_{14,16} < 1.3 \cdot 10^{-4}$  |
| $MI_{14,21} < 1.5 \cdot 10^{-4}$  | $dMI_{14,22} < 5.8 \cdot 10^{-2}$ | $MI_{14,23} < 1.9 \cdot 10^{-5}$  | $MI_{14,24} < 1.5 \cdot 10^{-4}$  | $MI_{14,25} < 5.8 \cdot 10^{-2}$  | $MI_{14,26} < 1.4 \cdot 10^{-4}$  |
| $MI_{14,31} < 1.3 \cdot 10^{-4}$  | $MI_{14,32} < 1.9 \cdot 10^{-5}$  | $dMI_{14,33} < 4.1 \cdot 10^{-3}$ | $MI_{14,34} < 1.3 \cdot 10^{-4}$  | $MI_{14,35} < 1.4 \cdot 10^{-4}$  | $MI_{14,36} < 4.1 \cdot 10^{-3}$  |
| $MI_{14,41} < 4.1 \cdot 10^{-3}$  | $MI_{14,42} < 1.5 \cdot 10^{-4}$  | $MI_{14,43} < 1.3 \cdot 10^{-4}$  | $dMI_{14,44} < 4.1 \cdot 10^{-3}$ | $MI_{14,45} < 1.5 \cdot 10^{-4}$  | $MI_{14,46} < 1.3 \cdot 10^{-4}$  |
| $MI_{14,51} < 1.5 \cdot 10^{-4}$  | $MI_{14,52} < 5.8 \cdot 10^{-2}$  | $MI_{14,53} < 1.4 \cdot 10^{-4}$  | $MI_{14,54} < 1.5 \cdot 10^{-4}$  | $dMI_{14,55} < 5.8 \cdot 10^{-2}$ | $MI_{14,56} < 1.9 \cdot 10^{-5}$  |
| $MI_{14,61} < 1.3 \cdot 10^{-4}$  | $MI_{14,62} < 1.4 \cdot 10^{-4}$  | $MI_{14,63} < 4.1 \cdot 10^{-3}$  | $MI_{14,64} < 1.3 \cdot 10^{-4}$  | $MI_{14,65} < 1.9 \cdot 10^{-5}$  | $dMI_{14,66} < 4.1 \cdot 10^{-3}$ |

|                                   |                                   |                                   |                                   |                                   |                                   |
|-----------------------------------|-----------------------------------|-----------------------------------|-----------------------------------|-----------------------------------|-----------------------------------|
| $dMI_{25,11} < 4.1 \cdot 10^{-3}$ | $MI_{25,12} < 1.3 \cdot 10^{-4}$  | $MI_{25,13} < 1.9 \cdot 10^{-5}$  | $MI_{25,14} < 4.1 \cdot 10^{-3}$  | $MI_{25,15} < 1.3 \cdot 10^{-4}$  | $MI_{25,16} < 1.4 \cdot 10^{-4}$  |
| $MI_{25,21} < 1.3 \cdot 10^{-4}$  | $dMI_{25,22} < 4.1 \cdot 10^{-3}$ | $MI_{25,23} < 1.5 \cdot 10^{-4}$  | $MI_{25,24} < 1.3 \cdot 10^{-4}$  | $MI_{25,25} < 4.1 \cdot 10^{-3}$  | $MI_{25,26} < 1.5 \cdot 10^{-4}$  |
| $MI_{25,31} < 1.9 \cdot 10^{-5}$  | $MI_{25,32} < 1.5 \cdot 10^{-4}$  | $dMI_{25,33} < 5.8 \cdot 10^{-2}$ | $MI_{25,34} < 1.4 \cdot 10^{-4}$  | $MI_{25,35} < 1.5 \cdot 10^{-4}$  | $MI_{25,36} < 5.8 \cdot 10^{-2}$  |
| $MI_{25,41} < 4.1 \cdot 10^{-3}$  | $MI_{25,42} < 1.3 \cdot 10^{-4}$  | $MI_{25,43} < 1.4 \cdot 10^{-4}$  | $dMI_{25,44} < 4.1 \cdot 10^{-3}$ | $MI_{25,45} < 1.3 \cdot 10^{-4}$  | $MI_{25,46} < 1.9 \cdot 10^{-5}$  |
| $MI_{25,51} < 1.3 \cdot 10^{-4}$  | $MI_{25,52} < 4.1 \cdot 10^{-3}$  | $MI_{25,53} < 1.5 \cdot 10^{-4}$  | $MI_{25,54} < 1.3 \cdot 10^{-4}$  | $dMI_{25,55} < 4.1 \cdot 10^{-3}$ | $MI_{25,56} < 1.5 \cdot 10^{-4}$  |
| $MI_{25,61} < 1.4 \cdot 10^{-4}$  | $MI_{25,62} < 1.5 \cdot 10^{-4}$  | $MI_{25,63} < 5.8 \cdot 10^{-2}$  | $MI_{25,64} < 1.9 \cdot 10^{-5}$  | $MI_{25,65} < 1.5 \cdot 10^{-4}$  | $dMI_{25,66} < 5.8 \cdot 10^{-2}$ |

|                                   |                                   |                                   |                                   |                                   |                                   |
|-----------------------------------|-----------------------------------|-----------------------------------|-----------------------------------|-----------------------------------|-----------------------------------|
| $dMI_{36,11} < 4.1 \cdot 10^{-3}$ | $MI_{36,12} < 1.9 \cdot 10^{-5}$  | $MI_{36,13} < 1.3 \cdot 10^{-4}$  | $MI_{36,14} < 4.1 \cdot 10^{-3}$  | $MI_{36,15} < 1.4 \cdot 10^{-4}$  | $MI_{36,16} < 1.3 \cdot 10^{-4}$  |
| $MI_{36,21} < 1.9 \cdot 10^{-5}$  | $dMI_{36,22} < 5.8 \cdot 10^{-2}$ | $MI_{36,23} < 1.5 \cdot 10^{-4}$  | $MI_{36,24} < 1.4 \cdot 10^{-4}$  | $MI_{36,25} < 5.8 \cdot 10^{-2}$  | $MI_{36,26} < 1.5 \cdot 10^{-4}$  |
| $MI_{36,31} < 1.3 \cdot 10^{-4}$  | $MI_{36,32} < 1.5 \cdot 10^{-4}$  | $dMI_{36,33} < 4.1 \cdot 10^{-3}$ | $MI_{36,34} < 1.3 \cdot 10^{-4}$  | $MI_{36,35} < 1.5 \cdot 10^{-4}$  | $MI_{36,36} < 4.1 \cdot 10^{-3}$  |
| $MI_{36,41} < 4.1 \cdot 10^{-3}$  | $MI_{36,42} < 1.4 \cdot 10^{-4}$  | $MI_{36,43} < 1.3 \cdot 10^{-4}$  | $dMI_{36,44} < 4.1 \cdot 10^{-3}$ | $MI_{36,45} < 1.9 \cdot 10^{-5}$  | $MI_{36,46} < 1.3 \cdot 10^{-4}$  |
| $MI_{36,51} < 1.4 \cdot 10^{-4}$  | $MI_{36,52} < 5.8 \cdot 10^{-2}$  | $MI_{36,53} < 1.5 \cdot 10^{-4}$  | $MI_{36,54} < 1.9 \cdot 10^{-5}$  | $dMI_{36,55} < 5.8 \cdot 10^{-2}$ | $MI_{36,56} < 1.5 \cdot 10^{-4}$  |
| $MI_{36,61} < 1.3 \cdot 10^{-4}$  | $MI_{36,62} < 1.5 \cdot 10^{-4}$  | $MI_{36,63} < 4.1 \cdot 10^{-3}$  | $MI_{36,64} < 1.3 \cdot 10^{-4}$  | $MI_{36,65} < 1.5 \cdot 10^{-4}$  | $dMI_{36,66} < 4.1 \cdot 10^{-3}$ |

$$dMI_{ij,kk} = \text{difference from unity of } MI_{ij,kk} \text{ (} MI_{ij,kk} = 1 + dMI_{ij,kk}, ij=14, 25, 36, k = 1, 2, 3, 4, 5, 6)$$

Table 4.1-3: Expected upper limits for the values of the elements of  $MI_{ij}$ , all along the on-orbit mission lifetime

The in-flight calibration is planned to directly measure only the elements of the inverse Calibration Matrices involved in the recovery of the differential accelerations  $\underline{a}_{d,ij}$ , from which the GGT components are obtained. These are elements of the last three rows of  $MI_{ij}$ , contained in the  $3 \times 3$  sub-matrices  $[MI]_{d,ij}$ ,  $[MI]_{c,ij}$ . However, taking into account the relationship existing among the elements of  $MI_{ij}$ , the determination of the last three rows implies that also the first three ones will be determined, with an accuracy which is limited by the size ( $\Delta MI_{ij,kk}$ ) of the neglected terms in the expansion of  $([1]_6 + dMI_{ij})^{-1}$  (see previous section).

The results of the in-flight calibration of the Gradiometer will allow obtaining an estimation of the inverse Calibration Matrix, that will be denoted with the notation  $\hat{MI}_{ij}$  :

$$\hat{MI}_{ij} = MI_{ij} + \delta MI_{ij} \quad (ij = 14, 25, 36), \quad (4.26)$$

where  $\delta MI_{ij}$  = difference between  $\hat{MI}_{ij}$  and  $MI_{ij}$  due to the measurement errors and the variations of the accelerometer scale factors, misalignments, couplings between the calibration phases:

$$\delta MI_{ij} = \begin{pmatrix} \delta MI_{ij,11} & \delta MI_{ij,12} & \delta MI_{ij,13} & \delta MI_{ij,14} & \delta MI_{ij,15} & \delta MI_{ij,16} \\ \delta MI_{ij,21} & \delta MI_{ij,22} & \delta MI_{ij,23} & \delta MI_{ij,24} & \delta MI_{ij,25} & \delta MI_{ij,26} \\ \delta MI_{ij,31} & \delta MI_{ij,32} & \delta MI_{ij,33} & \delta MI_{ij,34} & \delta MI_{ij,35} & \delta MI_{ij,36} \\ \delta MI_{ij,41} & \delta MI_{ij,42} & \delta MI_{ij,43} & \delta MI_{ij,44} & \delta MI_{ij,45} & \delta MI_{ij,46} \\ \delta MI_{ij,51} & \delta MI_{ij,52} & \delta MI_{ij,53} & \delta MI_{ij,54} & \delta MI_{ij,55} & \delta MI_{ij,56} \\ \delta MI_{ij,61} & \delta MI_{ij,62} & \delta MI_{ij,63} & \delta MI_{ij,64} & \delta MI_{ij,65} & \delta MI_{ij,66} \end{pmatrix} \equiv \begin{pmatrix} [\delta MI']_{c,ij} & [\delta MI']_{d,ij} \\ [\delta MI]_{d,ij} & [\delta MI]_{c,ij} \end{pmatrix} \quad (4.27)$$

The matrices  $\hat{MI}_{ij}$  are utilised in the Level 0 to Level 1a/1b processing of the Gradiometer products.

#### 4.1.2.5 From Level 0 to Level 1A/1B Gradiometric Products

The Level 0 scientific product of the Gradiometer is represented by the 8 control voltages applied to the 8 electrode pair surrounding the proof mass to keep it in a nearly motionless condition at the centre of its cage under the effect of the forces acting on the spacecraft and directly on the proof mass itself. These control voltages, provided by the instrument with a ~1 Hz output frequency (more precisely at 1/0.999360 Hz), together with the relevant instrument and satellite housekeeping and ancillary data, are contained in the Gradiometer telemetry packets downlinked by the satellite. The Level 0 to Level 1a process will extract the control voltages from the telemetry and will arrange them in an ordered time series (e.g. files with the time on the first column and the other parameters on the other columns), after their conversion in engineering units.

The Level 1a to Level 1b processing leading to the computation of the GGT components from the accelerometer control voltages is accomplished through the following steps (detailed in [RD 4]).

##### Step N. 1

From the proof mass control voltages, compute linear accelerations  $\underline{a}'_i$  measured by the accelerometers in their ARFs.

##### Step N. 2

From the  $\underline{a}'_i$  form the common-mode and differential-mode accelerations for the three OAGs:

$$\underline{a}'_{c,ij} = \frac{1}{2} (\underline{a}'_i + \underline{a}'_j) = \frac{1}{2} \begin{pmatrix} a'_{i,X} + a'_{j,X} \\ a'_{i,Y} + a'_{j,Y} \\ a'_{i,Z} + a'_{j,Z} \end{pmatrix} \text{ common-mode acceleration measured by the OAGs } (ij = 14, 25, 36)$$

$$\underline{a}'_{d,ij} = \frac{1}{2} (\underline{a}'_i - \underline{a}'_j) = \frac{1}{2} \begin{pmatrix} a'_{i,X} - a'_{j,X} \\ a'_{i,Y} - a'_{j,Y} \\ a'_{i,Z} - a'_{j,Z} \end{pmatrix} \text{ differential-mode acceleration measured by the three OAGs}$$

and arrange of these quantities in three 6-component vectors (one for each OAG):

$$\begin{pmatrix} \underline{a}'_{c,ij} \\ \underline{a}'_{d,ij} \end{pmatrix} = \frac{1}{2} \begin{pmatrix} a'_{i,X} + a'_{j,X} \\ a'_{i,Y} + a'_{j,Y} \\ a'_{i,Z} + a'_{j,Z} \\ a'_{i,X} - a'_{j,X} \\ a'_{i,Y} - a'_{j,Y} \\ a'_{i,Z} - a'_{j,Z} \end{pmatrix} \quad (ij = 14, 25, 36)$$

**Step N.3**

Use the inverse of the Calibration Matrices ( $\hat{M}_{ij}$ ) obtained from the in-flight calibration of the gradiometer to recover the common and differential accelerations of the proof masses of the three OAGs from  $\underline{a}'_{c,ij}$ ,  $\underline{a}'_{d,ij}$ :

$$\begin{pmatrix} \hat{a}_{c,ij} \\ \hat{a}_{d,ij} \end{pmatrix} = \hat{M}_{ij} \begin{pmatrix} \underline{a}'_{c,ij} \\ \underline{a}'_{d,ij} \end{pmatrix} \quad (4.28)$$

where  $\hat{a}_{c,ij}$ ,  $\hat{a}_{d,ij}$  denotes the values of the common and differential-mode accelerations ( $\underline{a}_{c,ij}$ ,  $\underline{a}_{d,ij}$ ) recovered through this process.

**Step N.4**

From the  $\hat{a}_{d,ij}$  recover the angular accelerations about the three GRF axes:

$$\hat{\omega}_X = -\frac{\hat{a}_{d,36,Y}}{L_Z} + \frac{\hat{a}_{d,25,Z}}{L_Y}, \quad \hat{\omega}_Y = -\frac{\hat{a}_{d,14,Z}}{L_X} + \frac{\hat{a}_{d,36,X}}{L_Z}, \quad \hat{\omega}_Z = -\frac{\hat{a}_{d,25,X}}{L_Y} + \frac{\hat{a}_{d,14,Y}}{L_X} \quad (4.29)$$

$L_X$ ,  $L_Y$ ,  $L_Z$  are the nominal values of the baseline length of OAG<sub>1</sub> OAG<sub>2</sub>, OAG<sub>3</sub>. These values are the results of the ground measurement of the distance between the accelerometers belonging to the same pair. The actual (unknown) values of the baseline lengths differ from the nominal ones by the quantities (see section 4.1.2.1):

$$\delta L_X = 2 \cdot \delta A_{1,X}, \quad \delta L_Y = 2 \cdot \delta A_{2,Y}, \quad \delta L_Z = 2 \cdot \delta A_{3,Z}.$$

**Step N.5**

From  $\hat{\omega}_X$ ,  $\hat{\omega}_Y$ ,  $\hat{\omega}_Z$  and from the satellite attitude quaternion ( $\mathbf{q}$ ), measured by means of the star sensors, recover the angular rates about the three GRF:

$$\hat{\omega}_X(t) = \mathcal{E}(\hat{\omega}_X, \mathbf{q}), \quad \hat{\omega}_Y(t) = \mathcal{E}(\hat{\omega}_Y, \mathbf{q}), \quad \hat{\omega}_Z(t) = \mathcal{E}(\hat{\omega}_Z, \mathbf{q})$$

where  $\mathcal{E}$  denotes formally the estimation algorithm (see [RD 4] for a description of this algorithm).

**Step N.6**

From  $\hat{a}_{d,ij}$  and  $\hat{\omega}_X$ ,  $\hat{\omega}_Y$ ,  $\hat{\omega}_Z$  recover the gravity gradient tensor components in the Gradiometer Reference Frame

$$\begin{aligned} \hat{U}_{XX} &= -2 \frac{\hat{a}_{d,14,X}}{L_X} - \hat{\omega}_Y^2 - \hat{\omega}_Z^2, \quad \hat{U}_{YY} = -2 \frac{\hat{a}_{d,25,Y}}{L_Y} - \hat{\omega}_X^2 - \hat{\omega}_Z^2, \quad \hat{U}_{ZZ} = -2 \frac{\hat{a}_{d,36,Z}}{L_Z} - \hat{\omega}_X^2 - \hat{\omega}_Y^2 \\ \hat{U}_{XY} &= -\frac{\hat{a}_{d,25,X}}{L_Y} - \frac{\hat{a}_{d,14,Y}}{L_X} + \hat{\omega}_X \hat{\omega}_Y, \quad \hat{U}_{XZ} = -\frac{\hat{a}_{d,14,Z}}{L_X} - \frac{\hat{a}_{d,36,X}}{L_Z} + \hat{\omega}_X \hat{\omega}_Z, \quad \hat{U}_{YZ} = -\frac{\hat{a}_{d,36,Y}}{L_Z} - \frac{\hat{a}_{d,25,Z}}{L_Y} + \hat{\omega}_Y \hat{\omega}_Z \end{aligned} \quad (4.30)$$

The time series of  $\hat{U}_{XX}, \hat{U}_{YY}, \hat{U}_{ZZ}, \hat{U}_{XY}, \hat{U}_{XZ}, \hat{U}_{YZ}$ , of the recovered common-mode, differential-mode and angular accelerations ( $\hat{a}_{c,ij}, \hat{a}_{d,ij}, \hat{\omega}_X, \hat{\omega}_Y, \hat{\omega}_Z$ ), together with the relevant instrument and satellite housekeeping and ancillary data, form the Level 1b scientific product of the Gradiometer. In particular, the time series of  $\hat{U}_{XX}, \hat{U}_{YY}, \hat{U}_{ZZ}$  will constitute the main input for the reconstruction of the Earth gravity field at the higher degrees and orders.

#### 4.1.2.6 Gravity Gradient Tensor Measurement Errors in the OAGRF

The relationship between the common-mode and differential-mode accelerations ( $\hat{a}_{c,ij}, \hat{a}_{d,ij}$ ) recovered in the Level 1b ground processing and the accelerations originally experienced by the proof masses ( $a_{c,ij}, a_{d,ij}$ ) can be obtained by plugging the (4.20) in the (4.28):

$$\begin{aligned} \begin{pmatrix} \hat{a}_{c,ij} \\ \hat{a}_{d,ij} \end{pmatrix} &= \hat{M}I_{ij} \begin{pmatrix} a'_{c,ij} \\ a'_{d,ij} \end{pmatrix} = \hat{M}I_{ij} \left[ M_{ij} \begin{pmatrix} a_{c,ij} \\ a_{d,ij} \end{pmatrix} + \frac{1}{2} K2_{ij} \begin{pmatrix} (a_{c,ij} + a_{d,ij})^2 \\ (a_{c,ij} - a_{d,ij})^2 \end{pmatrix} + \begin{pmatrix} b_{c,ij} \\ b_{d,ij} \end{pmatrix} + \begin{pmatrix} n_{c,ij} \\ n_{d,ij} \end{pmatrix} \right] \\ &= \hat{M}I_{ij} M_{ij} \begin{pmatrix} a_{c,ij} \\ a_{d,ij} \end{pmatrix} + \frac{1}{2} \hat{M}I_{ij} K2_{ij} \begin{pmatrix} (a_{c,ij} + a_{d,ij})^2 \\ (a_{c,ij} - a_{d,ij})^2 \end{pmatrix} + \hat{M}I_{ij} \left[ \begin{pmatrix} b_{c,ij} \\ b_{d,ij} \end{pmatrix} + \begin{pmatrix} n_{c,ij} \\ n_{d,ij} \end{pmatrix} \right] \\ &= (M I_{ij} + \delta M I_{ij}) M_{ij} \begin{pmatrix} a_{c,ij} \\ a_{d,ij} \end{pmatrix} + \frac{1}{2} (M I_{ij} + \delta M I_{ij}) K2_{ij} \begin{pmatrix} (a_{c,ij} + a_{d,ij})^2 \\ (a_{c,ij} - a_{d,ij})^2 \end{pmatrix} + (M I_{ij} + \delta M I_{ij}) \left[ \begin{pmatrix} b_{c,ij} \\ b_{d,ij} \end{pmatrix} + \begin{pmatrix} n_{c,ij} \\ n_{d,ij} \end{pmatrix} \right] \end{aligned} \quad (4.31)$$

Making use of the approximated expressions (4.22), (4.23) for  $M_{ij}, M I_{ij}$ , and expanding the products  $(M I_{ij} + \delta M I_{ij}) M_{ij}, (M I_{ij} + \delta M I_{ij}) K2_{ij}$  to the first-order terms only:

$$\begin{aligned} (M I_{ij} + \delta M I_{ij}) M_{ij} &= M I_{ij} M_{ij} + \delta M I_{ij} M_{ij} = [1]_6 + \delta M I_{ij} M_{ij} \cong [1]_6 + \delta M I_{ij} ([1]_6 + dM_{ij}) \cong [1]_6 + \delta M I_{ij} \\ (M I_{ij} + \delta M I_{ij}) K2_{ij} &\cong ([1]_6 - dM_{ij} + \delta M I_{ij}) K2_{ij} \cong K2_{ij} \quad (3) \end{aligned} \quad (4.32)$$

the (4.31) becomes

$$\begin{pmatrix} \hat{a}_{c,ij} \\ \hat{a}_{d,ij} \end{pmatrix} \cong \begin{pmatrix} a_{c,ij} \\ a_{d,ij} \end{pmatrix} + \begin{pmatrix} b_{c,ij} \\ b_{d,ij} \end{pmatrix} + \begin{pmatrix} n_{c,ij} \\ n_{d,ij} \end{pmatrix} + \delta M I_{ij} \begin{pmatrix} a_{c,ij} \\ a_{d,ij} \end{pmatrix} + \frac{1}{2} K2_{ij} \begin{pmatrix} (a_{c,ij} + a_{d,ij})^2 \\ (a_{c,ij} - a_{d,ij})^2 \end{pmatrix} - (dM_{ij} - \delta M I_{ij}) \left[ \begin{pmatrix} b_{c,ij} \\ b_{d,ij} \end{pmatrix} + \begin{pmatrix} n_{c,ij} \\ n_{d,ij} \end{pmatrix} \right] \quad (4.33)$$

Thus:

$$\begin{aligned} \hat{a}_{c,ij} &\cong a_{c,ij} + b_{c,ij} + n_{c,ij} + [\delta M I']_{c,ij} a_{c,ij} + [\delta M I']_{d,ij} a_{d,ij} + 0.5[K2]_{+,ij} (a_{c,ij} + a_{d,ij})^2 + 0.5[K2]_{-,ij} (a_{c,ij} - a_{d,ij})^2 \\ &\quad - ([dM]_{c,ij} - [\delta M I']_{c,ij}) \cdot (b_{c,ij} + n_{c,ij}) - ([dM]_{d,ij} - [\delta M I']_{d,ij}) \cdot (b_{d,ij} + n_{d,ij}) \end{aligned} \quad (4.34)$$

<sup>3</sup> By itself,  $K2_{ij}$  is a "zero-order" term. But in the equation (4.31),  $K2_{ij} \begin{pmatrix} (a_{c,ij} + a_{d,ij})^2 \\ (a_{c,ij} - a_{d,ij})^2 \end{pmatrix}$  is a "first-order" term. For this reason, the terms  $dM_{ij} K2_{ij}, \delta M I_{ij} K2_{ij}$  have been neglected.

$$\hat{a}_{d,ij} \cong \underline{a}_{d,ij} + \underline{b}_{d,ij} + \underline{n}_{d,ij} + [\delta\mathbf{M}\mathbf{I}]_{d,ij} \cdot \underline{a}_{c,ij} + [\delta\mathbf{M}\mathbf{I}]_{c,ij} \cdot \underline{a}_{d,ij} + 0.5[\mathbf{K}\mathbf{2}]_{+,ij} \cdot (\underline{a}_{c,ij} + \underline{a}_{d,ij})^2 - 0.5[\mathbf{K}\mathbf{2}]_{-,ij} \cdot (\underline{a}_{c,ij} - \underline{a}_{d,ij})^2 \quad (4.35)$$

$$-([\mathbf{d}\mathbf{M}]_{d,ij} - [\delta\mathbf{M}\mathbf{I}]_{d,ij}) \cdot (\underline{b}_{c,ij} + \underline{n}_{c,ij}) - ([\mathbf{d}\mathbf{M}]_{c,ij} - [\delta\mathbf{M}\mathbf{I}]_{c,ij}) \cdot (\underline{b}_{d,ij} + \underline{n}_{d,ij})$$

By plugging the (4.35) in the (4.30) we get

$$\begin{aligned} \hat{U}_{XX} &= -2 \frac{\hat{a}_{d,14,X}}{L_X} - \hat{\omega}_Y^2 - \hat{\omega}_Z^2 \quad (4.36) \\ &\cong -2 \frac{a_{d,14,X}}{L_X} - \omega_Y^2 - \omega_Z^2 - \delta\omega_Y^2 - \delta\omega_Z^2 - \frac{2}{L_X} \left( b_{d,14,X} + n_{d,14,X} + ([\delta\mathbf{M}\mathbf{I}]_{d,14} \underline{a}_{c,14})_X + ([\delta\mathbf{M}\mathbf{I}]_{c,14} \underline{a}_{d,14})_X \right) \\ &\quad - \frac{1}{L_X} \left( [\mathbf{K}\mathbf{2}]_{+,14} (\underline{a}_{c,14} + \underline{a}_{d,14})^2 \right)_X + \frac{1}{L_X} \left( [\mathbf{K}\mathbf{2}]_{-,14} (\underline{a}_{c,14} - \underline{a}_{d,14})^2 \right)_X \\ &\quad + \frac{2}{L_X} \left( ([\mathbf{d}\mathbf{M}]_{d,14} - [\delta\mathbf{M}\mathbf{I}]_{d,14}) (\underline{b}_{c,14} + \underline{n}_{c,14}) \right)_X + \frac{2}{L_X} \left( ([\mathbf{d}\mathbf{M}]_{c,14} - [\delta\mathbf{M}\mathbf{I}]_{c,14}) (\underline{b}_{d,14} + \underline{n}_{d,14}) \right)_X \end{aligned}$$

where the notation  $\delta\omega_Y^2$  has been used to denote the difference  $\hat{\omega}_Y^2 - \omega_Y^2$  etc..

Analogous expressions can be obtained for the other GGT components.

The differential acceleration for in-line axis of the OAG<sub>1</sub> is (from (4.14)):

$$a_{d,14,X} = -\frac{L_X}{2} (U_{XX} + \omega_Y^2 + \omega_Z^2) - ([\mathbf{U}] - [\Omega^2] - [\dot{\Omega}]) \delta \underline{A}_1)_X + 2 ([\Omega] \cdot \delta \dot{\underline{A}}_{d,14})_X + \delta \ddot{\underline{A}}_{d,14,X} - S_{d,14,X} - M_{d,14,X} \quad (4.31)$$

and the (4.36) becomes:

$$\hat{U}_{XX} = -2 \frac{\hat{a}_{d,14,X}}{L_X} - \hat{\omega}_Y^2 - \hat{\omega}_Z^2 = U_{XX} + \delta U_{XX} \quad (4.37)$$

with

$$\begin{aligned} \delta U_{XX} &= \frac{2}{L_X} \left( ([\mathbf{U}] - [\Omega^2] - [\dot{\Omega}]) \delta \underline{A}_1)_X + 2 ([\Omega] \cdot \delta \dot{\underline{A}}_{d,14})_X - \delta \ddot{\underline{A}}_{d,14,X} + S_{d,14,X} + M_{d,14,X} \right) \quad (4.38) \\ &\quad - \delta\omega_Y^2 - \delta\omega_Z^2 - \frac{2}{L_X} \left( b_{d,14,X} + n_{d,14,X} + ([\delta\mathbf{M}\mathbf{I}]_{d,14} \underline{a}_{c,14})_X + ([\delta\mathbf{M}\mathbf{I}]_{c,14} \underline{a}_{d,14})_X \right) \\ &\quad - \frac{1}{L_X} \left( [\mathbf{K}\mathbf{2}]_{+,14} (\underline{a}_{c,14} + \underline{a}_{d,14})^2 \right)_X + \frac{1}{L_X} \left( [\mathbf{K}\mathbf{2}]_{-,14} (\underline{a}_{c,14} - \underline{a}_{d,14})^2 \right)_X \\ &\quad + \frac{2}{L_X} \left( ([\mathbf{d}\mathbf{M}]_{d,14} - [\delta\mathbf{M}\mathbf{I}]_{d,14}) (\underline{b}_{c,14} + \underline{n}_{c,14}) \right)_X + \frac{2}{L_X} \left( ([\mathbf{d}\mathbf{M}]_{c,14} - [\delta\mathbf{M}\mathbf{I}]_{c,14}) (\underline{b}_{d,14} + \underline{n}_{d,14}) \right)_X \end{aligned}$$

where, in turn  $\underline{a}_{c,14}$  and  $\underline{a}_{d,14}$  are given by the (4.13) and (4.14) respectively.

The expression of  $\delta U_{XX}$  must be completed with two additional terms.

The first additional error term is due to the different behavior of the transfer function (TF) of two accelerometers (including their readout electronics) belonging to the same OAG, and of the transfer function of the structure connecting each accelerometer to the center of the Gradiometer. So far we have implicitly assumed that this transfer functions (TFA<sub>i</sub>(v) =

$B_i(\nu)e^{j\phi_i(\nu)}$  of two accelerometer have the same modulus ( $B_i(\nu)$ ) and the same phase ( $\phi_i(\nu)$ ) up to the upper frequency of the MBW ( $\nu = 0.1$  Hz). In addition, we have assumed that the structure of the gradiometer is rigid. This is only approximately true. The difference in the accelerometer transfer functions ( $\delta TFA_{ij,k}$ ) implies that, under a common acceleration along the axis  $k$  ( $a_{c,ij,k}$ ), the outputs of the two accelerometers are slightly different, giving rise to a differential acceleration along the same axis:

$$a_{d,ij,k} = \delta TFA_{ij,k} \cdot a_{c,ij,k},$$

where (see ref. [RD 10] for the detailed derivation of the transfer function difference contribution to the “common-mode rejection ratio”):

- $\delta TFA_{ij,k}(\nu) \cong B_{c,ij,k}(\nu) \sin(\phi_{d,ij,k}(\nu))$  differential transfer function along the axis  $k$  of  $A_i, A_j$  at frequency  $\nu$
- $B_{c,ij,k}(\nu) = \frac{1}{2} (B_{i,k}(\nu) + B_{j,k}(\nu))$  common-mode modulus of the transfer functions of the accelerometers  $A_i, A_j$  along the  $k$  axis
- $\phi_{d,ij,k}(\nu) = \frac{1}{2} (\phi_{i,k}(\nu) - \phi_{j,k}(\nu))$  differential-mode phase of the transfer functions of the accelerometers  $A_i, A_j$  along the  $k$  axis

Concerning the Gradiometer structure, if there is a differential propagation of the disturbance acceleration from the Central Stiffening of the Gradiometer (the Central Stiffening is shown in Figure 3.3-3; it can be considered the zone where the linear accelerations experienced by the Gradiometer are still common to all the accelerometers) to the position of the various sensors (because the two “halves” of the gradiometer arms have slightly different resonance frequencies and damping factors) we have again the transformation of a common acceleration into a differential one at the accelerometer location:

$$a_{d,ij,k} = \delta TFS_{ij,k} \cdot a_{c,ij,k},$$

where  $\delta TFS_{ij,k}$  is the differential transfer function along the axis  $k$  of the structural elements connecting the accelerometers  $A_i, A_j$  to the Central Stiffening. In practice, the largest source of differential response to common-mode accelerations is the phase difference ( $\delta \Phi S_{ij,k}$ ) between the transfer functions, because the phase of the transfer function is more sensitive than its module to a variation the resonance frequency and of the damping factor:

$$\delta TFS_{ij,k} \cong \delta \Phi S_{ij,k}$$

By assuming a second-order model of the structure transfer function, we can write  $\delta \Phi S_{ij,k}$  as:

$$\delta \Phi S_{ij,k}(\nu) \cong 2 \frac{\zeta_0}{f_0} \left| \frac{\Delta f_{ij,k} - \Delta \zeta_{ij,k}}{1 + \Delta f_{ij,k}} \right| \nu \quad (\text{approximation valid for } \nu \ll f_0 \text{ and } \Delta f_{ij,k} \neq \Delta \zeta_{ij,k})$$

where

- $f_0$  and  $\zeta_0$  are the mean values of the resonant frequency and of the damping factor of the first vibration mode of the chain of structural elements connecting the accelerometers to the Central Stiffening;
- $\Delta f_{ij,k}, \Delta \zeta_{ij,k}$  is the percentual difference between the resonant frequencies and the damping factors of the structural elements connecting the accelerometers  $A_i, A_j$  to the Central Stiffening.

The largest contribution to the in-line “common-mode rejection ratio” (CMRR) are the longitudinal vibration modes of the structure (i.e., the traction-compression modes along the direction of the gradiometer arm). The vibration modes along the transversal axes (structure bending) have a much smaller effect on the in-line CMRR, but dominate the transversal CMRR.

The second, additional error term is due to the coupling between the angular and the linear acceleration at accelerometer level. The translations and rotations of the proof mass relative to its cage are controlled by the voltages applied to pairs of electrodes. A mismatch between the electrostatic gains of the electrodes implies that the control of a pure angular acceleration of the proof mass is performed through a combination of control voltages which is interpreted as the presence of an additional (spurious) linear acceleration on the proof mass. The correspondence between the angular accelerations of the proof mass of the

accelerometers  $A_1, \dots, A_6$  (which are equal to the angular accelerations of the satellite about its COM) and the linear acceleration resulting from this gain mismatch are provided in Table 4.1-4:

| Sensor      | Angular acceleration about ARF axes | Spurious linear acceleration about the ARF axes                                                                                                                   |
|-------------|-------------------------------------|-------------------------------------------------------------------------------------------------------------------------------------------------------------------|
| $A_1 (A_4)$ | $\dot{\omega}_X$                    | $a_{1cY} = C_{ZeXe} \cdot \dot{\omega}_X$ ( $a_{4cY} = C_{ZeXe} \cdot \dot{\omega}_X$ )                                                                           |
|             | $\dot{\omega}_Y$                    | $a_{1cX} = C_{Ze} \cdot \dot{\omega}_Y, a_{1cZ} = C_{Ye} \cdot \dot{\omega}_Y$ ( $a_{4cX} = C_{Ze} \cdot \dot{\omega}_Y, a_{4cZ} = C_{Ye} \cdot \dot{\omega}_Y$ ) |
|             | $\dot{\omega}_Z$                    | $a_{1cY} = C_{YeXe} \cdot \dot{\omega}_Z$ ( $a_{4cY} = C_{YeXe} \cdot \dot{\omega}_Z$ )                                                                           |
| $A_2 (A_5)$ | $\dot{\omega}_X$                    | $a_{2cZ} = C_{YeXe} \cdot \dot{\omega}_X$ ( $a_{5cZ} = C_{YeXe} \cdot \dot{\omega}_X$ )                                                                           |
|             | $\dot{\omega}_Y$                    | $a_{2cZ} = C_{ZeXe} \cdot \dot{\omega}_Y$ ( $a_{5cZ} = C_{ZeXe} \cdot \dot{\omega}_Y$ )                                                                           |
|             | $\dot{\omega}_Z$                    | $a_{2cX} = C_{Ye} \cdot \dot{\omega}_Z, a_{2cY} = C_{Ze} \cdot \dot{\omega}_Z$ ( $a_{5cX} = C_{Ye} \cdot \dot{\omega}_Z, a_{5cY} = C_{Ze} \cdot \dot{\omega}_Z$ ) |
| $A_3 (A_6)$ | $\dot{\omega}_X$                    | $a_{3cY} = C_{YeXe} \cdot \dot{\omega}_X$ ( $a_{6cY} = C_{YeXe} \cdot \dot{\omega}_X$ )                                                                           |
|             | $\dot{\omega}_Y$                    | $a_{3cX} = C_{Ye} \cdot \dot{\omega}_Y, a_{3cZ} = C_{Ze} \cdot \dot{\omega}_Y$ ( $a_{6cX} = C_{Ye} \cdot \dot{\omega}_Y, a_{6cZ} = C_{Ze} \cdot \dot{\omega}_Y$ ) |
|             | $\dot{\omega}_Z$                    | $a_{3cY} = C_{ZeXe} \cdot \dot{\omega}_Z$ ( $a_{6cY} = C_{ZeXe} \cdot \dot{\omega}_Z$ )                                                                           |

Table 4.1-4: Relationships between the proof mass angular accelerations and the spurious linear accelerations resulting from the coupling with the electrode drivers gain mismatch

The angular-linear acceleration coupling factors written in Table 4.1-4, have to following approximate expressions:

$$C_{YeXe} \cong 2 \frac{\delta e}{e_{Xi}^0} \frac{I_{\Theta}}{m \cdot d_X}, C_{ZeXe} \cong 2 \frac{\delta e}{e_{Xi}^0} \frac{I_{\Psi}}{m \cdot d_X}, C_{Ye} \cong \frac{\delta e}{e_{Yi}^0} \frac{I_{\Phi}}{m \cdot d_{YZ}}, C_{Ze} \cong \frac{\delta e}{e_{Zi}^0} \frac{I_{\Phi}}{m \cdot d_{YZ}}$$

where

- $m$  = weight of the proof mass
- $I_{\Phi}, I_{\Theta}, I_{\Psi}$  = moments of inertia of the proof mass about the  $X_e, Y_e, Z_e$  axes of the AESRF
- $d_X$  = nominal distance between the barycenter of any  $X_i^+, X_i^-$  electrode and the  $X_e Y_e$  (or  $X_e Z_e$ ) plane
- $d_{YZ}$  = nominal distance between the barycenter of any  $Y_i^+, Y_i^-$  electrode (or any  $Z_i^+, Z_i^-$  electrode) and the  $X_e Y_e$  plane (or  $X_e Z_e$  plane respectively)
- $e_{Xi}^0$  = nominal gap between the proof mass and the electrodes  $X_i^+, X_i^-$  ( $i = 1,2,3,4$ )
- $e_{Yi}^0$  = nominal gap between the proof mass and the electrodes  $Y_i^+, Y_i^-$  ( $i = 1,2$ )
- $e_{Zi}^0$  = nominal gap between the proof mass and the electrodes  $Z_i^+, Z_i^-$  ( $i = 1,2$ )
- $\delta e$  = differential gap error between two electrode pairs of the same axis

The resulting gradiometric errors due to these two additional terms are (for  $U_{XX}$ ):

$$\delta U_{XX,TF} = \frac{2}{L_X} (\delta TFA_{14,X} + \delta TFS_{14,X}) \cdot a_{c,14,X} \quad (4.39)$$

$$\delta U_{XX,alc} = \frac{2}{L_X} a_{d,14,cX}, \quad a_{d,14,cX} = \frac{1}{2} (a_{1cX} - a_{4cX}) = \frac{\sqrt{2}}{2} C_{Ze} \cdot \dot{\omega}_Y \text{ (adding RSS } a_{1cX} \text{ and } a_{4cX}\text{)}$$

Thus the complete expression of the the error affecting the component  $U_{XX}$  measured in the OAGR $_1$  is:

$$\delta U_{XX} = \frac{2}{L_X} ((U_{XX} + \omega_Y^2 + \omega_Z^2) \delta A_{1,X} - \delta \ddot{A}_{d,14,X} + S_{d,14,X} + M_{d,14,X}) \quad (4.40)$$

$$- \delta \omega_Y^2 - \delta \omega_Z^2 - \frac{2}{L_X} (b_{d,14,X} + n_{d,14,X} + ([\delta MI]_{d,14} a_{c,14})_X + ([\delta MI]_{f,14} a_{d,14})_X)$$

$$-\frac{1}{L_X} \left( [K2]_{+,14} (a_{c,14} + a_{d,14})^2 \right)_X + \frac{1}{L_X} \left( [K2]_{-,14} (a_{c,14} - a_{d,14})^2 \right)_X$$

$$+ \frac{2}{L_X} \left( ([dM]_{d,14} - [\delta MI]_{d,14}) (b_{c,14} + n_{c,14}) \right)_X + \frac{2}{L_X} \left( ([dM]_{c,14} - [\delta MI]_{c,14}) (b_{d,14} + n_{d,14}) \right)_X + \delta U_{XX,TF} + \delta U_{XX,alc}$$

where we have also expanded the term  $\frac{2}{L_X} \left( ([U] - [\Omega^2] - [\dot{\Omega}]) \delta \underline{A}_1 \right)_X + 2 \left( [\Omega] \cdot \delta \underline{\dot{A}}_{d,14} \right)_X$ , making use of the definition of  $\delta \underline{A}_1$ .

Analogous expressions can be obtained for  $\delta U_{YY}$ ,  $\delta U_{ZZ}$ :

$$\delta U_{YY} = \frac{2}{L_Y} \left( (U_{YY} + \omega_X^2 + \omega_Z^2) \delta A_{2,Y} - \delta \ddot{A}_{d,25,Y} + S_{d,25,Y} + M_{d,25,Y} \right) \quad (4.41)$$

$$- \delta \omega_X^2 - \delta \omega_Z^2 - \frac{2}{L_Y} \left( b_{d,25,Y} + n_{d,25,Y} + ([\delta MI]_{d,25} a_{c,25})_Y + ([\delta MI]_{c,25} a_{d,25})_Y \right)$$

$$- \frac{1}{L_Y} \left( [K2]_{+,25} (a_{c,25} + a_{d,25})^2 \right)_Y + \frac{1}{L_Y} \left( [K2]_{-,25} (a_{c,25} - a_{d,25})^2 \right)_Y$$

$$+ \frac{2}{L_Y} \left( ([dM]_{d,25} - [\delta MI]_{d,25}) (b_{c,25} + n_{c,25}) \right)_Y + \frac{2}{L_Y} \left( ([dM]_{c,25} - [\delta MI]_{c,25}) (b_{d,25} + n_{d,25}) \right)_Y + \delta U_{YY,TF} + \delta U_{YY,alc}$$

$$\text{with } \delta U_{YY,TF} = \frac{2}{L_Y} (\delta TFA_{25,Y} + \delta TFS_{25,Y}) \cdot a_{c,25,Y}, \quad \delta U_{YY,alc} = \frac{2}{L_Y} a_{d,25,cY}, \quad a_{d,25,cY} = \frac{1}{2} (a_{2cY} - a_{5cY}) = \frac{\sqrt{2}}{2} C_{Ze} \cdot \dot{\omega}_Z$$

$$\delta U_{ZZ} = \frac{2}{L_Z} \left( (U_{ZZ} + \omega_X^2 + \omega_Y^2) \delta A_{3,Z} - \delta \ddot{A}_{d,36,Z} + S_{d,36,Z} + M_{d,36,Z} \right) \quad (4.42)$$

$$- \delta \omega_X^2 - \delta \omega_Y^2 - \frac{2}{L_Z} \left( b_{d,36,Z} + n_{d,36,Z} + ([\delta MI]_{d,36} a_{c,36})_Z + ([\delta MI]_{c,36} a_{d,36})_Z \right)$$

$$- \frac{1}{L_Z} \left( [K2]_{+,36} (a_{c,36} + a_{d,36})^2 \right)_Z + \frac{1}{L_Z} \left( [K2]_{-,36} (a_{c,36} - a_{d,36})^2 \right)_Z$$

$$+ \frac{2}{L_Z} \left( ([dM]_{d,36} - [\delta MI]_{d,36}) (b_{c,36} + n_{c,36}) \right)_Z + \frac{2}{L_Z} \left( ([dM]_{c,36} - [\delta MI]_{c,36}) (b_{d,36} + n_{d,36}) \right)_Z + \delta U_{ZZ,TF} + \delta U_{ZZ,alc}$$

$$\text{with } \delta U_{ZZ,TF} = \frac{2}{L_Z} (\delta TFA_{36,Z} + \delta TFS_{36,Z}) \cdot a_{c,36,Z}, \quad \delta U_{ZZ,alc} = \frac{2}{L_Z} a_{d,36,cZ}, \quad a_{d,36,cZ} = \frac{1}{2} (a_{3cZ} - a_{6cZ}) = \frac{\sqrt{2}}{2} C_{Ze} \cdot \dot{\omega}_Y$$

The difference between the recovered off-diagonal component  $\hat{U}_{XY}$  and the actual one  $U_{XY}$  can be obtained by plugging in the (4.30) the expression of the  $\hat{a}_{d,25,X}$ ,  $\hat{a}_{d,14,Y}$  obtained from the (4.35):

$$-\frac{\hat{a}_{d,25,X}}{L_Y} \cong -\frac{a_{d,25,X}}{L_Y} - \frac{1}{L_Y} \left( b_{d,25,X} + n_{d,25,X} + ([\delta MI]_{d,25} a_{c,25})_X + ([\delta MI]_{c,25} a_{d,25})_X \right)$$

$$- \frac{1}{2L_Y} \left( [K2]_{+,25} (a_{c,25} + a_{d,25})^2 \right)_X + \frac{1}{2L_Y} \left( [K2]_{-,25} (a_{c,25} - a_{d,25})^2 \right)_X$$

$$\begin{aligned}
 & + \frac{1}{L_Y} \left( ([dM]_{d,25} - [\delta MI]_{d,25})(\underline{b}_{c,25} + \underline{n}_{c,25}) \right)_X + \frac{1}{L_Y} \left( ([dM]_{f,25} - [\delta MI]_{f,25})(\underline{b}_{d,25} + \underline{n}_{d,25}) \right)_X \\
 & - \frac{\hat{a}_{d,14,Y}}{L_X} \equiv - \frac{a_{d,14,Y}}{L_X} - \frac{1}{L_X} \left( b_{d,14,Y} + n_{d,14,Y} + ([\delta MI]_{d,14} \underline{a}_{c,14})_Y + ([\delta MI]_{f,14} \underline{a}_{d,14})_Y \right) \\
 & - \frac{1}{2L_X} \left( [K2]_{f,14} (\underline{a}_{c,14} + \underline{a}_{d,14})^2 \right)_Y + \frac{1}{2L_X} \left( [K2]_{f,14} (\underline{a}_{c,14} - \underline{a}_{d,14})^2 \right)_Y \\
 & + \frac{1}{L_X} \left( ([dM]_{d,14} - [\delta MI]_{d,14})(\underline{b}_{c,14} + \underline{n}_{c,14}) \right)_Y + \frac{1}{L_X} \left( ([dM]_{f,14} - [\delta MI]_{f,14})(\underline{b}_{d,14} + \underline{n}_{d,14}) \right)_Y
 \end{aligned}$$

with  $\underline{a}_{c,ij}$  and  $\underline{a}_{d,ij}$  given by the (4.13) and (4.14). In particular:

$$\begin{aligned}
 a_{d,25,X} &= - \frac{L_Y}{2} (U_{XY} - \omega_X \omega_Y + \dot{\omega}_Z) - (U_{XY} - \omega_X \omega_Y + \dot{\omega}_Z) \delta A_{2,Y} - 2 \omega_Z \delta \dot{A}_{d,25,Y} - S_{d,25,X} - M_{d,25,X} \\
 a_{d,14,Y} &= - \frac{L_X}{2} (U_{XY} - \omega_X \omega_Y - \dot{\omega}_Z) - (U_{XY} - \omega_X \omega_Y - \dot{\omega}_Z) \delta A_{1,X} + 2 \omega_Z \delta \dot{A}_{d,14,X} - S_{d,14,Y} - M_{d,14,Y}
 \end{aligned}$$

Thus we can write

$$\hat{U}_{XY} = - \frac{\hat{a}_{d,25,X}}{L_Y} - \frac{\hat{a}_{d,14,Y}}{L_X} + \hat{\omega}_X \hat{\omega}_Y = U_{XY} + \delta U_{XY}$$

with:

$$\begin{aligned}
 \delta U_{XY} &= \frac{1}{L_Y} \left( (U_{XY} - \omega_X \omega_Y + \dot{\omega}_Z) \delta A_{2,Y} + 2 \omega_Z \delta \dot{A}_{d,25,Y} + S_{d,25,X} + M_{d,25,X} \right) \quad (4.43) \\
 & - \frac{1}{L_Y} \left( b_{d,25,X} + n_{d,25,X} + ([\delta MI]_{d,25} \underline{a}_{c,25})_X + ([\delta MI]_{f,25} \underline{a}_{d,25})_X \right) \\
 & - \frac{1}{2L_Y} \left( [K2]_{f,25} (\underline{a}_{c,25} + \underline{a}_{d,25})^2 \right)_X + \frac{1}{2L_Y} \left( [K2]_{f,25} (\underline{a}_{c,25} - \underline{a}_{d,25})^2 \right)_X \\
 & + \frac{1}{L_Y} \left( ([dM]_{d,25} - [\delta MI]_{d,25})(\underline{b}_{c,25} + \underline{n}_{c,25}) \right)_X + \frac{1}{L_Y} \left( ([dM]_{f,25} - [\delta MI]_{f,25})(\underline{b}_{d,25} + \underline{n}_{d,25}) \right)_X \\
 & + \frac{1}{L_X} \left( (U_{XY} - \omega_X \omega_Y - \dot{\omega}_Z) \delta A_{1,X} - 2 \omega_Z \delta \dot{A}_{d,14,X} + S_{d,14,Y} + M_{d,14,Y} \right) \\
 & - \frac{1}{L_X} \left( b_{d,14,Y} + n_{d,14,Y} + ([\delta MI]_{d,14} \underline{a}_{c,14})_Y + ([\delta MI]_{f,14} \underline{a}_{d,14})_Y \right) \\
 & - \frac{1}{2L_X} \left( [K2]_{f,14} (\underline{a}_{c,14} + \underline{a}_{d,14})^2 \right)_Y + \frac{1}{2L_X} \left( [K2]_{f,14} (\underline{a}_{c,14} - \underline{a}_{d,14})^2 \right)_Y \\
 & + \frac{1}{L_X} \left( ([dM]_{d,14} - [\delta MI]_{d,14})(\underline{b}_{c,14} + \underline{n}_{c,14}) \right)_Y + \frac{1}{L_X} \left( ([dM]_{f,14} - [\delta MI]_{f,14})(\underline{b}_{d,14} + \underline{n}_{d,14}) \right)_Y \\
 & + \delta \omega_X \cdot \omega_Y + \omega_X \cdot \delta \omega_Y + \delta U_{XY,TF} + \delta U_{XY,alc}
 \end{aligned}$$

In the (4.43) the term  $(\delta \omega_X \cdot \omega_Y + \omega_X \cdot \delta \omega_Y)$  denotes the difference  $\hat{\omega}_X \hat{\omega}_Y - \omega_X \omega_Y$ , and the term  $\delta U_{XY,TF}$  denotes the gradiometric error due to the coupling of the common acceleration with the differential transfer function of the accelerometer pairs  $A_2, A_5$

and  $A_1$ ,  $A_4$  and with the Gradiometer structure transfer function mismatch from the Central Stiffening to the accelerometer location:

$$\delta U_{XY,TF} = \frac{1}{L_Y} (\delta TFA_{25,X} + \delta TFS_{25,X}) \cdot a_{c,25,X} + \frac{1}{L_X} (\delta TFA_{14,Y} + \delta TFS_{14,Y}) \cdot a_{c,14,Y}$$

The term  $\delta U_{XY,alc}$  denotes the gradiometric error due to the coupling between the angular and the linear acceleration at accelerometer level:

$$\delta U_{XY,alc} = \frac{1}{L_Y} a_{d,25,cX} + \frac{1}{L_X} a_{d,14,cY}, \quad a_{d,25,cX} = \frac{\sqrt{2}}{2} C_{Ye} \cdot \dot{\omega}_Z, \quad a_{d,14,cY} = \frac{\sqrt{2}}{2} (C_{YeXe} \cdot \dot{\omega}_Z + C_{ZeXe} \cdot \dot{\omega}_X).$$

Analogous expressions can be obtained for  $\delta U_{XZ}$ ,  $\delta U_{YZ}$ :

$$\begin{aligned} \delta U_{XZ} = & \frac{1}{L_X} ((U_{XZ} - \omega_X \omega_Z + \dot{\omega}_Y) \delta A_{1,X} + 2 \omega_Y \delta \dot{A}_{d,14,X} + S_{d,14,Z} + M_{d,14,Z}) \\ & - \frac{1}{L_X} (b_{d,14,Z} + n_{d,14,Z} + ([\delta MI]_{d,14} a_{c,14})_Z + ([\delta MI]_{f,14} a_{d,14})_Z) \\ & - \frac{1}{2L_X} ([K2]_{f,14} (a_{c,14} + a_{d,14})^2)_Z + \frac{1}{2L_X} ([K2]_{f,14} (a_{c,14} - a_{d,14})^2)_Z \\ & + \frac{1}{L_X} (([dM]_{d,14} - [\delta MI]_{d,14}) (b_{c,14} + n_{c,14}))_Z + \frac{1}{L_X} (([dM]_{f,14} - [\delta MI]_{f,14}) (b_{d,14} + n_{d,14}))_Z \\ & + \frac{1}{L_Z} ((U_{XZ} - \omega_X \omega_Z - \dot{\omega}_Y) \delta A_{3,Z} - 2 \omega_Y \delta \dot{A}_{d,36,Z} + S_{d,36,X} + M_{d,36,X}) \\ & - \frac{1}{L_Z} (b_{d,36,X} + n_{d,36,X} + ([\delta MI]_{d,36} a_{c,36})_X + ([\delta MI]_{f,36} a_{d,36})_X) \\ & - \frac{1}{2L_Z} ([K2]_{f,36} (a_{c,36} + a_{d,36})^2)_X + \frac{1}{2L_Z} ([K2]_{f,36} (a_{c,36} - a_{d,36})^2)_X \\ & + \frac{1}{L_Z} (([dM]_{d,36} - [\delta MI]_{d,36}) (b_{c,36} + n_{c,36}))_X + \frac{1}{L_Z} (([dM]_{f,36} - [\delta MI]_{f,36}) (b_{d,36} + n_{d,36}))_X \\ & + \delta \omega_X \cdot \omega_Z + \omega_X \cdot \delta \omega_Z + \delta U_{XZ,TF} + \delta U_{XZ,alc} \end{aligned} \quad (4.44)$$

with

$$\begin{aligned} \delta U_{XZ,TF} = & \frac{1}{L_X} (\delta TFA_{14,Z} + \delta TFS_{14,Z}) \cdot a_{c,14,Z} + \frac{1}{L_Z} (\delta TFA_{36,X} + \delta TFS_{36,X}) \cdot a_{c,36,X} \\ \delta U_{XZ,alc} = & \frac{1}{L_X} a_{d,14,cZ} + \frac{1}{L_Z} a_{d,36,cX}, \quad a_{d,14,cZ} = \frac{\sqrt{2}}{2} C_{Ye} \cdot \dot{\omega}_Y, \quad a_{d,36,cX} = \frac{\sqrt{2}}{2} C_{Ye} \cdot \dot{\omega}_Y. \end{aligned}$$

$$\begin{aligned} \delta U_{YZ} = & \frac{1}{L_Z} ((U_{YZ} - \omega_Y \omega_Z + \dot{\omega}_X) \delta A_{3,Z} + 2 \omega_X \delta \dot{A}_{d,36,Z} + S_{d,36,Y} + M_{d,36,Y}) \\ & - \frac{1}{L_Z} (b_{d,36,Y} + n_{d,36,Y} + ([\delta MI]_{d,36} a_{c,36})_Y + ([\delta MI]_{f,36} a_{d,36})_Y) \end{aligned} \quad (4.45)$$

$$\begin{aligned}
 & -\frac{1}{2L_Z} \left( [K2]_{+,36} (a_{c,36} + a_{d,36})^2 \right)_Y + \frac{1}{2L_Z} \left( [K2]_{-,36} (a_{c,36} - a_{d,36})^2 \right)_Y \\
 & + \frac{1}{L_Z} \left( ([dM]_{d,36} - [\delta MI]_{d,36}) (b_{c,36} + n_{c,36}) \right)_Y + \frac{1}{L_Z} \left( ([dM]_{c,36} - [\delta MI]_{c,36}) (b_{d,36} + n_{d,36}) \right)_Y \\
 & + \frac{1}{L_Y} \left( (U_{YZ} - \omega_Y \omega_Z - \dot{\omega}_X) \delta A_{2,Y} - 2 \omega_X \delta \dot{A}_{d,25,Y} + S_{d,25,Z} + M_{d,25,Z} \right) \\
 & - \frac{1}{L_Y} \left( b_{d,25,Z} + n_{d,25,Z} + ([\delta MI]_{d,25} a_{c,25})_Z + ([\delta MI]_{c,25} a_{d,25})_Z \right) \\
 & - \frac{1}{2L_Y} \left( [K2]_{+,25} (a_{c,25} + a_{d,25})^2 \right)_Z + \frac{1}{2L_Z} \left( [K2]_{-,25} (a_{c,25} - a_{d,25})^2 \right)_Z \\
 & + \frac{1}{L_Y} \left( ([dM]_{d,25} - [\delta MI]_{d,25}) (b_{c,25} + n_{c,25}) \right)_Z + \frac{1}{L_Y} \left( ([dM]_{c,25} - [\delta MI]_{c,25}) (b_{d,25} + n_{d,25}) \right)_Z \\
 & + \delta \omega_Y \cdot \omega_Z + \omega_Y \cdot \delta \omega_Z + \delta U_{YZ,TF} + \delta U_{YZ,alc}
 \end{aligned}$$

with

$$\begin{aligned}
 \delta U_{YZ,TF} &= \frac{1}{L_Z} (\delta TFA_{36,Y} + \delta TFS_{36,Y}) \cdot a_{c,36,Y} + \frac{1}{L_Y} (\delta TFA_{25,Z} + \delta TFS_{25,Z}) \cdot a_{c,25,Z} \\
 \delta U_{YZ,alc} &= \frac{1}{L_Z} a_{d,36,cY} + \frac{1}{L_Y} a_{d,25,cZ}, \quad a_{d,36,cY} = \frac{\sqrt{2}}{2} (C_{YeXe} \cdot \dot{\omega}_X + C_{ZeXe} \cdot \dot{\omega}_Z), \quad a_{d,25,cZ} = \frac{\sqrt{2}}{2} (C_{YeXe} \cdot \dot{\omega}_X + C_{ZeXe} \cdot \dot{\omega}_Y).
 \end{aligned}$$

The quantities  $\delta U_{XX}$ ,  $\delta U_{YY}$ ,  $\delta U_{ZZ}$  represent the errors affecting the recovery of the GGT diagonal components in the OAGR (OAGR<sub>1</sub> for  $U_{XX}$ , OAGR<sub>2</sub> for  $U_{YY}$ , OAGR<sub>3</sub> for  $U_{ZZ}$ ). For the off-diagonal components of the GGT, obtained from the combination of differential accelerations measured by two different OAGs, the quantities  $\delta U_{XY}$ ,  $\delta U_{XZ}$ ,  $\delta U_{YZ}$  represent the error affecting their recovery in the GRF, in the assumption that the three OAGs are perfectly aligned one to another (at then to the GRF).

#### 4.1.2.7 Gravity Gradient Tensor Measurement Errors in the GRF

In order to obtain the total error on the GGT components in the GRF we have to add to  $\delta U_{XX}$ ,  $\delta U_{YY}$ ,  $\delta U_{ZZ}$ ,  $\delta U_{XY}$ ,  $\delta U_{XZ}$ ,  $\delta U_{YZ}$  expressed by the (4.40), ... (4.45), the effect of the non-orthogonality of the three OAGs (i.e. the misalignments between the OAGs and the GRF).

Let's introduce the rotation matrices defining the orientation of the OAGs in the GRF:

- $[R]_{G/OAG1}$  : rotation matrix from the OAGR<sub>1</sub> to the GRF;
- $[R]_{G/OAG2}$  : rotation matrix from the OAGR<sub>2</sub> to the GRF;
- $[R]_{G/OAG3}$  : rotation matrix from the OAGR<sub>3</sub> to the GRF =  $[1]_3$  (the GRF is defined to be coincident with the OAGR<sub>3</sub>).

The rotation matrices  $[R]_{G/OAG1}$ ,  $[R]_{G/OAG2}$ , can be expressed as:

$$[R]_{G/OAG1} \equiv [1]_3 + \begin{pmatrix} 0 & \psi_{G1} & -\theta_{G1} \\ -\psi_{G1} & 0 & \phi_{G1} \\ \theta_{G1} & -\phi_{G1} & 0 \end{pmatrix} \equiv [1]_3 + [dR]_{G/OAG1}, \dots \quad (4.46)$$

where  $\phi_{G1}$ ,  $\theta_{G1}$ ,  $\psi_{G1}$  are the (small) rotation angles about the X, Y and Z axes defining the misalignment of the GRF in the

OAGRF<sub>1</sub>, etc...

The relationship between the GGT expressed in the OAGRF<sub>1</sub> (OAGRF<sub>2</sub>, OAGRF<sub>3</sub>), denoted as [U]<sub>1</sub> ([U]<sub>2</sub>, [U]<sub>3</sub>) and the GGT expressed in the GRF, denoted as [U]<sub>G</sub> is function of the rotation matrix [R]<sub>OAG1/G</sub> ([R]<sub>G/OAG2</sub>, [R]<sub>G/OAG3</sub>) as follows:

$$\begin{aligned} [U]_G &= [R]_{G/OAG1} [U]_1 ([R]_{G/OAG1})^{-1} = [R]_{G/OAG1} [U]_1 ([R]_{G/OAG1})^T & (4.47) \\ [U]_G &= [R]_{G/OAG2} [U]_2 ([R]_{G/OAG2})^{-1} = [R]_{G/OAG2} [U]_2 ([R]_{G/OAG2})^T \\ [U]_G &= [R]_{G/OAG3} [U]_3 ([R]_{G/OAG3})^{-1} = [U]_3 \end{aligned}$$

With the approximation (4.46), the first two equations (4.47) can be expanded as follows (without further approximations):

$$\begin{aligned} [U]_G &= [U]_1 + [dR]_{G/OAG1} [U]_1 + [U]_1 ([dR]_{G/OAG1})^T + [dR]_{G/OAG1} [U]_1 ([dR]_{G/OAG1})^T & (4.48) \\ [U]_G &= [U]_2 + [dR]_{G/OAG1} [U]_2 + [U]_2 ([dR]_{G/OAG2})^T + [dR]_{G/OAG2} [U]_2 ([dR]_{G/OAG2})^T \end{aligned}$$

From the these equations we can obtain the relationship between U<sub>XX</sub>, U<sub>YY</sub> expressed respectively in the OAGRF<sub>1</sub> and OAGRF<sub>2</sub> (in which they are obtained from the differential accelerations  $\hat{a}_{d,14}$ ,  $\hat{a}_{d,25}$ ) and the same components expressed in the GRF:

$$U_{XX,G} = U_{XX,1} + \Delta U_{XX,1}, \quad \Delta U_{XX,1} = 2 \psi_{G1} U_{XY,1} - 2 \theta_{G1} U_{XZ,1} + \psi_{G1}^2 U_{YY,1} - 2 \psi_{G1} \theta_{G1} U_{YZ,1} + \theta_{G1}^2 U_{ZZ,1} \quad (4.49)$$

$$U_{YY,G} = U_{YY,2} + \Delta U_{YY,2}, \quad \Delta U_{YY,2} = 2 \varphi_{G2} U_{YZ,2} - 2 \psi_{G2} U_{XY,2} + \psi_{G2}^2 U_{XX,2} - 2 \varphi_{G2} \psi_{G2} U_{XZ,2} + \varphi_{G2}^2 U_{ZZ,2}$$

The terms  $\Delta U_{XX,1}$  and  $\Delta U_{YY,2}$ , derived from the (exact) expansion of the (4.48), can be considered as the additional errors that we make on U<sub>XX</sub>, U<sub>YY</sub> obtained from the (4.30) if we assume that they are provided by these equations directly in the GRF rather than in the respective OAGRFs. These errors arise because the three axes of the Gradiometer are not perfectly orthogonal, not only due to the limits of the integration process but also due to the variation of the Gradiometer geometry occurring during the on-ground activities (handling, tests), the launch and the on-orbit lifetime.

For the radial component we have U<sub>ZZ,G</sub> = U<sub>ZZ,3</sub>, and therefore  $\Delta U_{ZZ,3} = 0$ .

The off-diagonal components of the GGT, are obtained from the combination of two differential accelerations, measured by two different OAGs. For U<sub>XZ</sub>, obtained from  $\hat{a}_{d,14}$  (measured in the OAGRF<sub>1</sub>) and from  $\hat{a}_{d,36}$  (measured in the OAGRF<sub>3</sub> = GRF), the relationship between its expression in the OAGRF and in the GRF depends only on the rotation matrix [R]<sub>G/OAG1</sub>, and can be derived from the first equation (4.47):

$$U_{XZ,G} = U_{XZ,1} + \Delta U_{XZ,1}, \quad (4.50)$$

$$\Delta U_{XZ,1} = \theta_{G1} (U_{XX,1} - U_{ZZ,1}) - \varphi_{G1} U_{XY,1} + \psi_{G1} U_{YZ,1} + \psi_{G1} \theta_{G1} U_{XY,1} - \varphi_{G1} \psi_{G1} U_{YY,1} + \varphi_{G1} \theta_{G1} U_{YZ,1} - \theta_{G1}^2 U_{XZ,1}.$$

Similarly for U<sub>YZ</sub>, obtained from  $\hat{a}_{d,25}$  and  $\hat{a}_{d,36}$ , this relationship depends only on the rotation matrix [R]<sub>G/OAG2</sub>, and can be derived from the second equation (4.47):

$$U_{YZ,G} = U_{YZ,2} + \Delta U_{YZ,2}, \quad (4.51)$$

$$\Delta U_{YZ,2} = \varphi_{G2} (U_{ZZ,2} - U_{YY,2}) + \theta_{G2} U_{XY,2} - \psi_{G2} U_{XZ,2} - \psi_{G2} \theta_{G2} U_{XX,2} + \varphi_{G2} \psi_{G2} U_{XY,2} + \varphi_{G2} \theta_{G2} U_{XZ,2} - \varphi_{G2}^2 U_{YZ,2}.$$

For U<sub>XY</sub>, obtained from  $\hat{a}_{d,14}$  and  $\hat{a}_{d,25}$ , the relationship between its expression in the OAGRFs and in the GRF can be derived by combining the transformations of the GGT from OAGRF<sub>2</sub> to OAGRF<sub>1</sub> (to get first U<sub>XY</sub> in the frame OAGRF<sub>1</sub>) and from OAGRF<sub>1</sub> to GRF (analogously we could have transformed the GGT first from OAGRF<sub>1</sub> to OAGRF<sub>2</sub> and then from OAGRF<sub>1</sub> to GRF):

$$[U]_1 = [R]_{OAG1/OAG2} [U]_2 ([R]_{OAG1/OAG2})^T$$

$$\begin{aligned} &\cong [U]_2 + [dR]_{OAG1/OAG2} [U]_2 + [U]_2 ([dR]_{OAG1/OAG2})^T + [dR]_{OAG1/OAG2} [U]_2 ([dR]_{OAG1/OAG2})^T \\ [U]_G &= [R]_{G/OAG1} [U]_1 ([R]_{G/OAG1})^T \cong [U]_1 + [dR]_{G/OAG1} [U]_1 + [U]_1 ([dR]_{G/OAG1})^T + [dR]_{G/OAG1} [U]_1 ([dR]_{G/OAG1})^T \\ &= [U]_2 + [dR]_{OAG1/OAG2} [U]_2 + [U]_2 ([dR]_{OAG1/OAG2})^T + [dR]_{OAG1/OAG2} [U]_2 ([dR]_{OAG1/OAG2})^T \\ &\quad + [dR]_{G/OAG1} [U]_1 + [U]_1 ([dR]_{G/OAG1})^T + [dR]_{G/OAG1} [U]_1 ([dR]_{G/OAG1})^T \\ U_{XY,G} &= U_{XY,2} + \Delta U_{XY,12} + \Delta U_{XY,1} \end{aligned} \quad (4.52)$$

$$\Delta U_{XY,12} = \psi_{G12}(U_{YY,2} - U_{XX,2}) + \varphi_{G12}U_{XZ,2} - \theta_{G12}U_{YZ,2} + \psi_{G12}\theta_{G12}U_{XZ,2} + \varphi_{G12}\psi_{G12}U_{YZ,2} - \varphi_{G12}\theta_{G12}U_{ZZ,2} - \psi_{G12}^2U_{XY,2},$$

$$\Delta U_{XY,1} = \psi_{G1}(U_{YY,1} - U_{XX,1}) + \varphi_{G1}U_{XZ,1} - \theta_{G1}U_{YZ,1} + \psi_{G1}\theta_{G1}U_{XZ,1} + \varphi_{G1}\psi_{G1}U_{YZ,1} - \varphi_{G1}\theta_{G1}U_{ZZ,1} - \psi_{G1}^2U_{XY,1}.$$

The total error on the GGT components in the GRF is therefore:

$$\begin{aligned} \Delta U_{XX,G} &= \delta U_{XX} + \Delta U_{XX,1} \\ \Delta U_{YY,G} &= \delta U_{YY} + \Delta U_{YY,2} \\ \Delta U_{ZZ,G} &= \delta U_{ZZ} \\ \Delta U_{XY,G} &= \delta U_{XY} + \Delta U_{XY,12} + \Delta U_{XY,1} \\ \Delta U_{XZ,G} &= \delta U_{XZ} + \Delta U_{XZ,1} \\ \Delta U_{YZ,G} &= \delta U_{YZ} + \Delta U_{YZ,2} \end{aligned} \quad (4.53)$$

With  $\delta U_{XX}, \dots, \delta U_{YZ}$  expressed by the (4.40), ... (4.45) and  $\Delta U_{XX,1}, \dots, \Delta U_{XY,1}$  expressed by the (4.49), ... (4.52).

## 4.2 GGT MEASUREMENTS SPATIAL LOCATION

The Gradiometer measurements will be localized in space (e.g. relative to the IRF) by associating them to the satellite orbital position measured by the GPS receiver. Errors in the spatial location of the gradiometric measurements (depending also on the errors in the time tagging of the gradiometric measurements relatively to the GPS ones) are equivalent to errors in the knowledge of the GGT components. For example, the constant part of the GGT in the LORF is approximately

$$[U]_0 \approx \omega_0^2 \begin{pmatrix} -1 & 0 & 0 \\ 0 & -1 & 0 \\ 0 & 0 & 2 \end{pmatrix} \quad (4.54)$$

where  $\omega_0$  is the mean orbital angular velocity:

$$\omega_0 = \sqrt{\frac{\mu}{r^3}}$$

$\mu$  = Earth's gravitational parameters

$r$  = mean orbital radius

Thus, in this case the error on the three diagonal components due to an error ( $\delta r$ ) in the determination of the orbit radius is:

$$\Delta U_{XX} = \Delta U_{YY} = \frac{3\mu}{r^4} \delta r = 0.62 \cdot \delta r \text{ mE}, \quad \Delta U_{ZZ} = \frac{6\mu}{r^4} \delta r = 1.24 \cdot \delta r \text{ mE} \quad (\delta r \text{ in m}) \quad (4.55)$$

The resulting relative error is

$$\frac{\Delta U_{XX}}{U_{XX}} = \frac{\Delta U_{YY}}{U_{YY}} = \frac{3\delta r}{r}, \quad \frac{\Delta U_{ZZ}}{U_{ZZ}} = \frac{6\delta r}{r} \quad (4.56)$$

As a result of the precise orbit determination (Level 2 processing of the GPS receiver measurements) the satellite position will be known with a cm-level accuracy and the value of the relative errors (4.56) will be  $< 10^{-8}$ .

From this simple computation we deduce that the gradiometric error associated to the satellite location accuracy is totally negligible. Consequently it will not be considered as element of the gradiometric error breakdown and in the related requirement derivation process.

### 4.3 ANGULAR ACCELERATION MEASUREMENT ERRORS IN THE GRF

Proceeding in an analogous way as for the GGT components, it is possible to derive the expression of the error affecting the determination of the angular accelerations obtained from the transversal differential accelerations measured by the three OAGs as per equation (4.29). These angular accelerations are utilised in the data post processing for the recovery of the centrifugal accelerations to be subtracted from the measured differential accelerations in order to get the GGT components (see equations (4.30)).

Hereafter we will derive in detail the expression of the errors affecting the measurement of  $\hat{\omega}_Y$ . Analogous expressions can be derived for the errors affecting  $\hat{\omega}_X$ ,  $\hat{\omega}_Z$ .

Let's start from the expression of  $\hat{\omega}_Y$

$$\hat{\omega}_Y = -\frac{\hat{a}_{d,14,Z}}{L_X} + \frac{\hat{a}_{d,36,X}}{L_Z}$$

and develop the expressions of  $-\frac{\hat{a}_{d,14,Z}}{L_X}$  and  $\frac{\hat{a}_{d,36,X}}{L_Z}$  according to the (4.36):

$$\begin{aligned} -\frac{\hat{a}_{d,14,Z}}{L_X} &\equiv -\frac{a_{d,14,Z}}{L_X} - \frac{1}{L_X} \left( b_{d,14,Z} + n_{d,14,Z} + \left( [\delta MI]_{d,14} a_{c,14} \right)_Z + \left( [\delta MI]_{f,14} a_{d,14} \right)_Z \right) \\ &- \frac{1}{2L_X} \left( [K2]_{f,14} (a_{c,14} + a_{d,14})^2 \right)_Z + \frac{1}{2L_X} \left( [K2]_{f,14} (a_{c,14} - a_{d,14})^2 \right)_Z \\ &+ \frac{1}{L_X} \left( ([dM]_{d,14} - [\delta MI]_{d,14}) (b_{c,14} + n_{c,14}) \right)_Z + \frac{1}{L_X} \left( ([dM]_{f,14} - [\delta MI]_{f,14}) (b_{d,14} + n_{d,14}) \right)_Z \end{aligned} \quad (4.57)$$

$$\begin{aligned} \frac{\hat{a}_{d,36,X}}{L_Z} &\equiv \frac{a_{d,36,X}}{L_Z} + \frac{1}{L_Z} \left( b_{d,36,X} + n_{d,36,X} + \left( [\delta MI]_{d,36} a_{c,36} \right)_X + \left( [\delta MI]_{f,36} a_{d,36} \right)_X \right) \\ &+ \frac{1}{2L_Z} \left( [K2]_{f,36} (a_{c,36} + a_{d,36})^2 \right)_X - \frac{1}{2L_Z} \left( [K2]_{f,36} (a_{c,36} - a_{d,36})^2 \right)_X \\ &- \frac{1}{L_Z} \left( ([dM]_{d,36} - [\delta MI]_{d,36}) (b_{c,36} + n_{c,36}) \right)_X - \frac{1}{L_Z} \left( ([dM]_{f,36} - [\delta MI]_{f,36}) (b_{d,36} + n_{d,36}) \right)_X \end{aligned} \quad (4.58)$$

The expressions of  $a_{d,14,Z}$  and  $a_{d,36,X}$  appearing in the (4.57) and (4.58) are, in turn:

$$a_{d,14,Z} = -\frac{L_X}{2} (U_{XZ} - \omega_X \omega_Z + \dot{\omega}_Y) - (U_{XZ} - \omega_X \omega_Z + \dot{\omega}_Y) \delta A_{1,X} - 2 \omega_Y \delta \dot{A}_{d,14,X} - S_{d,14,Z} - M_{d,14,Z} \quad (4.59)$$

$$a_{d,36,X} = -\frac{L_Z}{2} (U_{XZ} - \omega_X \omega_Z - \dot{\omega}_Y) - (U_{XZ} - \omega_X \omega_Z - \dot{\omega}_Y) \delta A_{3,Z} + 2 \omega_Y \delta \dot{A}_{d,36,Z} - S_{d,36,X} - M_{d,36,X} \quad (4.60)$$

Thus, we can write

$$-\frac{\hat{a}_{d,14,Z}}{L_X} + \frac{\hat{a}_{d,36,X}}{L_Z} = \hat{\omega}_Y = \dot{\omega}_Y + \delta \dot{\omega}_Y$$

with:

$$\begin{aligned} \delta \dot{\omega}_Y &\cong \frac{1}{L_X} ((U_{XZ} - \omega_X \omega_Z + \dot{\omega}_Y) \delta A_{1,X} + 2 \omega_Y \delta \dot{A}_{d,14,X} + S_{d,14,Z} + M_{d,14,Z}) \\ &- \frac{1}{L_X} (b_{d,14,Z} + n_{d,14,Z}) \\ &+ \frac{1}{L_X} ([\delta \mathbf{M} \mathbf{I}]_{d,14} \cdot (([U] - [\Omega^2] - [\dot{\Omega}]) \underline{C}_1 - 2 [\Omega] \cdot \underline{\dot{C}}_1 - \underline{\ddot{C}}_1 + \underline{D}))_Z + \frac{1}{L_X} ([\delta \mathbf{M} \mathbf{I}]_{c,14} \cdot (-([U] - [\Omega^2] - [\dot{\Omega}]) \underline{A}_1)_Z \\ &- \frac{1}{2L_X} ([\mathbf{K}2]_{+,14} (a_{c,14} + a_{d,14})^2)_Z + \frac{1}{2L_X} ([\mathbf{K}2]_{-,14} (a_{c,14} - a_{d,14})^2)_Z \\ &+ \frac{1}{L_X} (([d\mathbf{M}]_{d,14} + [\delta \mathbf{M} \mathbf{I}]_{d,14}) (b_{c,14} + n_{c,14}))_Z + \frac{1}{L_X} (([d\mathbf{M}]_{c,14} + [\delta \mathbf{M} \mathbf{I}]_{c,14}) (b_{d,14} + n_{d,14}))_Z \\ &- \frac{1}{L_Z} ((U_{XZ} - \omega_X \omega_Z - \dot{\omega}_Y) \delta A_{3,Z} - 2 ([\Omega] \cdot \delta \dot{A}_{d,36})_X + S_{d,36,X} + M_{d,36,X}) \\ &+ \frac{1}{L_Z} (b_{d,36,X} + n_{d,36,X}) \\ &- \frac{1}{L_Z} ([\delta \mathbf{M} \mathbf{I}]_{d,36} \cdot (([U] - [\Omega^2] - [\dot{\Omega}]) \underline{C}_3 - 2 [\Omega] \cdot \underline{\dot{C}}_3 - \underline{\ddot{C}}_3 + \underline{D}))_X - \frac{1}{L_Z} ([\delta \mathbf{M} \mathbf{I}]_{c,36} \cdot (-([U] - [\Omega^2] - [\dot{\Omega}]) \underline{A}_3)_X \\ &+ \frac{1}{2L_Z} ([\mathbf{K}2]_{+,36} (a_{c,36} + a_{d,36})^2)_X - \frac{1}{2L_Z} ([\mathbf{K}2]_{-,36} (a_{c,36} - a_{d,36})^2)_X \\ &- \frac{1}{L_Z} (([d\mathbf{M}]_{d,36} + [\delta \mathbf{M} \mathbf{I}]_{d,36}) (b_{c,36} + n_{c,36}))_X - \frac{1}{L_Z} (([d\mathbf{M}]_{c,36} + [\delta \mathbf{M} \mathbf{I}]_{c,36}) (b_{d,36} + n_{d,36}))_X \\ &+ \delta \dot{\omega}_{Y,TF} + \delta \dot{\omega}_{Y,alc} \end{aligned} \quad (4.61)$$

with

$$\begin{aligned} \delta \dot{\omega}_{Y,TF} &= \delta U_{XZ,TF} = \frac{1}{L_X} (\delta TFA_{14,Z} + \delta TFS_{14,Z}) \cdot a_{c,14,Z} + \frac{1}{L_Z} (\delta TFA_{36,X} + \delta TFS_{36,X}) \cdot a_{c,36,X} \\ \delta \dot{\omega}_{Y,alc} &= \delta U_{XZ,alc} = \frac{1}{L_X} a_{d,14,cZ} + \frac{1}{L_Z} a_{d,36,cX}, \quad a_{d,14,cZ} = \frac{\sqrt{2}}{2} C_{Ye} \cdot \dot{\omega}_Y, \quad a_{d,36,cX} = \frac{\sqrt{2}}{2} C_{Ye} \cdot \dot{\omega}_Y \end{aligned}$$

## 5. ERROR TERMS CLASSIFICATION AND ERROR ALLOCATION

### 5.1 GRADIOMETRIC ERRORS CLASSIFICATION

The gradiometric errors can be thus be grouped in the following main categories:

- Instrument Errors (I), depending on the Gradiometer elements only (accelerometers, Gradiometer thermo-structure).
- Instrument-Satellite Coupling Errors (C), depending on the interaction of the Gradiometer with the satellite environment (Gradiometer excluded) and, in general, with the mission environment and the products of the Gradiometer in-flight calibration (accelerometer differential scale factor and misalignment coupling with the linear and angular accelerations of the satellite, with the gravity gradient itself, etc.)
- Satellite Errors (S), depending on the satellite (Gradiometer excluded) performance only (variable self-gravity field produced by the satellite masses).
- Processing Errors (P), related to the transformation of the Level 0 product to the Level 1a/1b product (essentially they consist of the errors of the estimation of the centrifugal accelerations about the Gradiometer axes).

The error terms belonging to these four categories are described in the next sections. Their mathematical expressions derive from the (4.53) and (4.61). Since the gravity gradiometry performance requirements are specified for the GGT trace, which depends on the GGT diagonal components only, the error breakdown (from which the requirements allocation is derived) is carried out just for  $U_{XX}$ ,  $U_{YY}$ ,  $U_{ZZ}$ . In addition, only the error contributors having a frequency content falling in the MBW, where the stringiest performance requirements are defined, are retained in the breakdown. For each error term which is expressed as the product of two, uncorrelated, factors ( $C = A \cdot B$ ), its spectral density (SD) in the MBW (denoted as  $\tilde{C}^W$ ) is obtained approximately as:

$$\tilde{C}^W = \sqrt{(A^0 \cdot \tilde{B}^W)^2 + (\tilde{A}^W \cdot B^0)^2} \quad (5.1)$$

where  $A^0$  ( $B^0$ ) denotes the maximum value (in modulus) of A (B) in the low frequency region outside the measurement bandwidth (from DC to 5 mHz) and  $\tilde{A}^W$  ( $\tilde{B}^W$ ) denotes the maximum value of the SD of A (B) in the MBW. Contributions of the type  $\tilde{A}^W \cdot \tilde{B}^W$ ,  $\tilde{A}^H \cdot \tilde{B}^W$ ,  $\tilde{A}^W \cdot \tilde{B}^H$ ,  $\tilde{A}^H \cdot \tilde{B}^H$ ,  $\tilde{A}^0 \cdot \tilde{B}^H$ ,  $\tilde{A}^H \cdot \tilde{B}^H$ , where  $\tilde{A}^H$  ( $\tilde{B}^H$ ) denotes the maximum value of the SD of A (B) above the MBW, are not included in the computation of  $\tilde{C}^W$  because, in general, at least one of the two factors is characterised by a SD rapidly decreasing as the frequency increases like, for instance, the GGT components (see Figure 3.3-3). An exception is constituted by the coupling of an input acceleration with itself through the accelerometer non-linear behavior. In this case the contribution of the high frequency (above the MBW) part of this input acceleration cannot be neglected, and its contribution to  $\tilde{C}^W$  must be correctly computed through a spectral density convolution technique (as described in [RD 5]).

Concerning the matrix  $\hat{M}_{ij}^W$ , it contains only constant terms (of the type  $\hat{M}_{ij}^0$ ) which are the results of the measurement of the elements of  $M_{ij}$  performed during the on-orbit calibration of the Gradiometer. Thus

$$\hat{M}_{ij}^W \cong [1]_6^W - dM_{ij}^W + \delta M_{ij}^W = -dM_{ij}^W + \delta M_{ij}^W = [0]_6 \Rightarrow \delta M_{ij}^W \cong dM_{ij}^W \quad (5.2)$$

Therefore, considering that the accelerometer bias is constant by definition, the term of the (4.40)

$$+ \frac{2}{L_X} \left( ([dM]_{d,14} - [\delta M]_{d,14}) (b_{c,14} + \underline{n}_{c,14}) \right)_X + \frac{2}{L_X} \left( ([dM]_{f,14} - [\delta M]_{f,14}) (b_{d,14} + \underline{n}_{d,14}) \right)_X$$

contributes to the Gradiometric error in MBW only for the portion containing the accelerometer noise:

$$+ \frac{2}{L_X} \left( ([dM]_{d,14} - [\delta MI]_{d,14}) \underline{l}_{c,14} \right)_X + \frac{2}{L_X} \left( ([dM]_{e,14} - [\delta MI]_{e,14}) \underline{l}_{d,14} \right)_X \quad (5.3)$$

since  $[dM]_{d,14}^W - [\delta MI]_{d,14}^W = [0]_3$  and  $([dM]_{d,14}^0 - [\delta MI]_{d,14}^0) \underline{l}_{c,14}^0$  is outside the MBW, etc...

The expressions of the various error terms reported in the following sections concerns the GGT component  $U_{XX}$ . Analogous expressions can be derived for the other components.

### 5.1.1 Instrument Errors

Instrument contributors to the measurement error spectral density of  $U_{XX}$  ( $U_{YY}$ ,  $U_{ZZ}$ ) in the MBW, denoted as  $\delta \tilde{U}_{XX,1}^W$  ( $\delta \tilde{U}_{YY,1}^W$ ,  $\delta \tilde{U}_{ZZ,1}^W$ ) include:

#### I.1 Accelerometer differential noise.

$$\delta \tilde{U}_{XX,1.1}^W = \frac{2}{L_X} \tilde{n}_{d,14,X}^W \quad (5.1.1)$$

This is the measurement noise, which is intrinsically produced by the accelerometer. This noise in turn takes contributions from the voltage reference noise, position sensor noise, contact potential difference fluctuations, drive voltage amplifier noise, parasitic forces between the proof mass and its cage (due to pressure gradients, temperature gradients, gold wire stiffness and damping, electrostatic force stiffness and damping), AD and DA converters noise.

#### I.2 Accelerometers position stability

$$\delta \tilde{U}_{XX,1.2}^W = \frac{2}{L_X} \delta \tilde{A}_{d,14,X}^W \quad (5.1.2)$$

This relative acceleration between the accelerometers is basically caused by the thermo-elastic deformations of the structure connecting the accelerometer pairs in the OAGs.

#### I.3 OAGRFs alignment errors in the GRF and alignment stability in the GRF

$$\delta \tilde{U}_{XX,1.3}^W = \left( (2\tilde{\psi}^W U_{XY}^0)^2 + (2\psi^0 \tilde{U}_{XY}^W)^2 + (2\tilde{\theta}^W U_{XZ}^0)^2 + (2\theta^0 \tilde{U}_{XZ}^W)^2 + (2\psi^0 \tilde{\psi}^W U_{YY}^0)^2 + \right. \\ \left. \left( \psi^{0^2} \tilde{U}_{YY}^W \right)^2 + (2\tilde{\psi}^W \theta^0 U_{YZ}^0)^2 + (2\psi^0 \tilde{\theta}^W U_{YZ}^0)^2 + (2\psi^0 \theta^0 \tilde{U}_{YZ}^W)^2 + (2\theta^0 \tilde{\theta}^W U_{ZZ}^0)^2 + \left( \theta^{0^2} \tilde{U}_{ZZ}^W \right)^2 \right)^{1/2} \quad (5.1.3)$$

This term includes the alignment errors and alignment stability of the OAGRFs in the GRF (section 4.1.2.7), Consequently the rotation angles  $\varphi^0$ ,  $\theta^0$ ,  $\psi^0$  include the OAGRF-GRF on-ground alignment errors and the variation of these alignment in the during the ground operations, launch, 1g-0g transition, and successive in-orbit slow changes of the gradiometer structure geometry for moisture release, ageing, thermal-elastic effects, till the end of the mission. The rotation angles spectral densities  $\tilde{\varphi}^W$ ,  $\tilde{\theta}^W$ ,  $\tilde{\psi}^W$  include the OAGRF-GRF alignment stability in the MBW essentially due to thermo-elastic effects driven by short-term temperature variations in the Gradiometer core.

I.4 Gradiometer self gravity

$$\delta\tilde{U}_{XX\_I.4}^W = \frac{2}{L_X} \tilde{S}_{d,14,X}^W \quad (5.1.4)$$

where  $\underline{S}_i$  is here intended as the gravity acceleration of the proof mass of the accelerometer  $A_i$  produced by the other masses of the Gradiometer only.

I.5 Coupling with Gradiometer magnetic field

$$\delta\tilde{U}_{XX\_I.5}^W = \frac{2}{L_X} \tilde{M}_{d,14,X}^W \quad (5.1.5)$$

where:

$$\underline{M}_{d,ij} = 0.5(\underline{M}_i - \underline{M}_j), \quad \underline{M}_i = \frac{\chi_m}{\mu_0} \frac{V}{m} \alpha_b \mathbf{B}_i \begin{pmatrix} \frac{\partial B_i}{\partial x} \\ \frac{\partial B_i}{\partial y} \\ \frac{\partial B_i}{\partial z} \end{pmatrix}, \quad \tilde{M}_{d,14,X}^W = \frac{\chi_m}{\mu_0} \frac{V}{m} \alpha_b \left( B_1 \frac{\partial B_1}{\partial x} - B_4 \frac{\partial B_4}{\partial x} \right)^W$$

and  $B_i$  is the modulus of the magnetic field at the location of the accelerometer  $A_i$  resulting from the combination of the Gradiometer equipment generated magnetic field and by the Earth magnetic field.

An approximate expression for  $\delta\tilde{U}_{XX\_I.5}^W$  has been derived in [RD 6] and reads

$$\delta\tilde{U}_{XX\_I.5}^W \approx \frac{2}{L_X} \frac{2k_i}{L_{PM}} \sqrt{\left(2B_{i,G}^0 B_{i,G}^W\right)^2 + \left(B_E^0 B_{i,G}^W\right)^2 + \left(B_E^W B_{i,G}^0\right)^2}, \quad (5.1.5a)$$

where:

- $B_{i,G}^0$  = maximum value below MBW of the modulus of the magnetic field generated by the Gradiometer at the location of the accelerometer  $A_i$ ;
- $B_{i,G}^W$  = maximum value in the MBW of the spectral density of the fluctuations of the modulus of the magnetic field generated by the Gradiometer at the location of the accelerometer  $A_i$ ;
- $B_E^0$  = maximum value below MBW of the modulus of the magnetic field generated by the Earth at the satellite location;
- $B_E^W$  = maximum value in the MBW of the spectral density of the fluctuations of the modulus of the magnetic field generated by the Earth along the GOCE orbit;
- $L_{PM}$  = proof mass size along the accelerometer ultra-sensitive axis.

I.6 Coupling of accelerometer noise with the common and differential-mode misalignments and scale factors

This error derives from the term  $-\frac{2}{L_X} \left( [dM]_{d,14} \underline{n}_{c,14} \right)_X - \frac{2}{L_X} \left( [dM]_{f,14} \underline{n}_{d,14} \right)_X$  of the (5.3).

Its contributors to the measurement error spectral density of  $U_{XX}$  in the MBW is

$$\delta\tilde{U}_{XX,1.6}^W = \frac{2}{L_X} \sqrt{\left(\left[dM\right]_{d,14}^p \tilde{n}_{c,14}^W\right)_X^2 + \left(\left[dM\right]_{c,14}^p \tilde{n}_{d,14}^W\right)_X^2} \quad (5.1.6)$$

Note that the matrices  $[dM]_c$  and  $[dM]_d$  contain the actual on-orbit values of the common/differential scale factors, misalignment and coupling of the accelerometer pairs, not the errors on their knowledge obtained during the on-orbit calibration.

### 5.1.2 Instrument-Satellite Coupling Errors

Instrument-satellite coupling contributors to the measurement error spectral density of  $U_{XX}$  ( $U_{YY}$ ,  $U_{ZZ}$ ) in the MBW (denoted as  $\delta\tilde{U}_{XX,C.}^W$ ) include:

#### C.1 Coupling with common-mode accelerations

These errors derive from the term  $\frac{2}{L_X} \left(\left[\delta MI\right]_{d,14} \underline{a}_{c,14}\right)_X$  of the (4.40) with  $\underline{a}_{c,14}$  given by the (4.13). By retaining only the first-order terms in the expansion of this expression we get:

$$\begin{aligned} \frac{2}{L_X} \left(\left[\delta MI\right]_{d,14} \underline{a}_{c,14}\right)_X &= \frac{2}{L_X} \left(\left[\delta MI\right]_{d,14} \cdot ([U] - [\Omega^2] - [\dot{\Omega}]) \underline{C}_1 + 2 [\Omega] \cdot \delta \underline{A}_{c,14} - 2 [\Omega] \cdot \dot{\underline{C}}_1 + \delta \underline{A}_{c,14} - \ddot{\underline{C}}_1 + \underline{D} - \underline{S}_{c,14} - \underline{M}_{c,14}\right)_X \\ &\cong \frac{2}{L_X} \left(\left[\delta MI\right]_{d,14} \cdot ([U] - [\Omega^2] - [\dot{\Omega}]) \underline{C}_1 - 2 [\Omega] \cdot \dot{\underline{C}}_1 - \ddot{\underline{C}}_1 + \underline{D}\right)_X \end{aligned}$$

The terms contained in the last expression can be classified as:

#### C.1.1 Coupling with non-gravitational linear acceleration of the satellite COM

$$\delta\tilde{U}_{XX,C.1.1}^W = \frac{2}{L_X} \sqrt{\left(\delta\tilde{MI}_{d,14,11}^W D_X^0\right)^2 + \left(\delta MI_{d,14,11}^0 \tilde{D}_X^W\right)^2 + \left(\delta\tilde{MI}_{d,14,12}^W D_Y^0\right)^2 + \left(\delta MI_{d,14,12}^0 \tilde{D}_Y^W\right)^2 + \left(\delta\tilde{MI}_{d,14,13}^W D_Z^0\right)^2 + \left(\delta MI_{d,14,13}^0 \tilde{D}_Z^W\right)^2} \quad (5.2.1)$$

#### C.1.2 Coupling with satellite COM location and stability in the GRF

$$\begin{aligned} \delta U_{XX,C.1.2}^W &= \frac{2}{L_X} \left( \left(\left[\delta\tilde{MI}\right]_{d,14}^W ([U]^0 - [\Omega^2]^0) \underline{C}_1^0\right)_X^2 + \left(\left[\delta MI\right]_{d,14}^0 ([U]^0 - [\Omega^2]^0) \tilde{\underline{C}}_1^W\right)_X^2 + \left(\left[\delta MI\right]_{d,14}^0 [\tilde{U}]^W \underline{C}_1^0\right)_X^2 \right. \\ &+ \left(\left[\delta MI\right]_{d,14}^0 [\tilde{\Omega}^2]^W \underline{C}_1^0\right)_X^2 + \left(\left[\delta\tilde{MI}\right]_{d,14}^W [\dot{\Omega}^0] \underline{C}_1^0\right)_X^2 + \left(\left[\delta MI\right]_{d,14}^0 [\dot{\Omega}^0] \tilde{\underline{C}}_1^W\right)_X^2 + \left(\left[\delta MI\right]_{d,14}^0 [\tilde{\Omega}^0] \underline{C}_1^0\right)_X^2 + \left(2\left[\delta\tilde{MI}\right]_{d,14}^W [\Omega^0] \underline{C}_1^0\right)_X^2 \right. \\ &\left. + \left(2\left[\delta MI\right]_{d,14}^0 [\tilde{\Omega}]^W \underline{C}_1^0\right)_X^2 + \left(2\left[\delta MI\right]_{d,14}^0 [\Omega^0] \tilde{\underline{C}}_1^W\right)_X^2 + \left(\left[\delta\tilde{MI}\right]_{d,14}^W \underline{C}_1^0\right)_X^2 + \left(\left[\delta MI\right]_{d,14}^0 \tilde{\underline{C}}_1^W\right)_X^2 \right)^{1/2} \quad (5.2.2) \end{aligned}$$

#### C.2 Coupling with differential-mode accelerations

These errors derive from the term  $\frac{2}{L_X} \left(\left[\delta MI\right]_{c,14} \underline{a}_{d,14}\right)_X$  of the (4.40) with  $\underline{a}_{d,14}$  given by the (4.14). By retaining only the first-order terms in the expansion of this expression we get:

$$\frac{2}{L_X} \left( \left[ \delta \mathbf{M} \mathbf{I} \right]_{c,14} \underline{a}_{d,14} \right)_X = \frac{2}{L_X} \left( \left[ \delta \mathbf{M} \mathbf{I} \right]_{c,14} \cdot \left( -([\mathbf{U}] - [\Omega^2] - [\dot{\Omega}]) \underline{A}_1 - ([\mathbf{U}] - [\Omega^2] - [\dot{\Omega}]) \delta \underline{A}_1 + 2 [\Omega] \cdot \delta \underline{A}_{d,14} + \delta \underline{A}_{d,14} - \underline{S}_{d,14} - \underline{M}_{d,14} \right)_X \approx \frac{2}{L_X} \left( \left[ \delta \mathbf{M} \mathbf{I} \right]_{c,14} \cdot \left( -([\mathbf{U}] - [\Omega^2] - [\dot{\Omega}]) \underline{A}_1 \right)_X \right.$$

The terms contained in the last expression can be classified as:

### C.2.1 Coupling with the angular accelerations of the satellite about its COM

$$\delta \tilde{U}_{XX.C.2.1}^W = \sqrt{\left( \delta \tilde{\mathbf{M}} \mathbf{I}_{c,14,12}^W \tilde{\omega}_Z^0 \right)^2 + \left( \delta \mathbf{M} \mathbf{I}_{c,14,12}^0 \tilde{\omega}_Z^W \right)^2 + \left( \delta \tilde{\mathbf{M}} \mathbf{I}_{c,14,13}^W \tilde{\omega}_Y^0 \right)^2 + \left( \delta \mathbf{M} \mathbf{I}_{c,14,13}^0 \tilde{\omega}_Y^W \right)^2} \quad (5.2.3)$$

### C.2.2 Coupling with the centrifugal accelerations and the Gravity Gradient Tensor

The Gravity Gradient Tensor  $[\mathbf{U}]$  and the centrifugal accelerations  $[\Omega^2]$  are considered together because, for an Earth-pointing satellite like GOCE, their constant parts  $([\mathbf{U}]^{\text{DC}}, [\Omega^2]^{\text{DC}})$ , which represent the largest contribution to  $([\mathbf{U}]^0, [\Omega^2]^0)$  have a well defined relationship:

$$[\mathbf{U}]^{\text{DC}} = \omega_0^2 \begin{pmatrix} -1 & 0 & 0 \\ 0 & -1 & 0 \\ 0 & 0 & 2 \end{pmatrix}, [\Omega^2]^{\text{DC}} = \omega_0^2 \begin{pmatrix} -1 & 0 & 0 \\ 0 & 0 & 0 \\ 0 & 0 & -1 \end{pmatrix} \Rightarrow ([\mathbf{U}]^{\text{DC}} - [\Omega^2]^{\text{DC}}) = \omega_0^2 \begin{pmatrix} 0 & 0 & 0 \\ 0 & -1 & 0 \\ 0 & 0 & 3 \end{pmatrix} \quad (5.2.4)$$

where  $\omega_0$  is the mean orbital angular velocity (which is also the mean spin rate of GOCE about its Y axis to keep the Earth-pointing attitude).

Therefore, they must be added algebraically in order to not underestimate/overestimate their contribution to the gravimetric error.

$$\delta U_{XX.C.2.2}^W = \frac{2}{L_X} \sqrt{\left( \left[ \delta \tilde{\mathbf{M}} \mathbf{I} \right]_{c,14}^W \left( [\mathbf{U}]^0 - [\Omega^2]^0 \right) \underline{A}_1 \right)_X^2 + \left( \left[ \delta \mathbf{M} \mathbf{I} \right]_{c,14}^0 \left[ \tilde{\mathbf{U}} \right]^W \underline{A}_1 \right)_X^2 + \left( \left[ \delta \mathbf{M} \mathbf{I} \right]_{c,14}^0 \left[ \tilde{\Omega}^2 \right]^W \underline{A}_1 \right)_X^2} \quad (5.2.5)$$

where  $[\tilde{\Omega}^2]^W = [\Omega]^0 [\tilde{\Omega}]^W + [\tilde{\Omega}]^W [\Omega]^0$ .

### C.3 Quadratic coupling

These errors derive from the term  $-\frac{1}{L_X} \left( \left[ \mathbf{K} \mathbf{2} \right]_{+,14} \left( \underline{a}_{c,14} + \underline{a}_{d,14} \right)^2 \right)_X + \frac{1}{L_X} \left( \left[ \mathbf{K} \mathbf{2} \right]_{-,14} \left( \underline{a}_{c,14} - \underline{a}_{d,14} \right)^2 \right)_X$  of the (4.40) with  $\underline{a}_{c,14}$  and  $\underline{a}_{d,14}$  given by the by the (4.29) and the (4.30) respectively. By retaining only the first-order terms in the expansion of this expression we get:

$$-\frac{1}{L_X} \left( \left[ \mathbf{K} \mathbf{2} \right]_{+,14} \left( \underline{a}_{c,14} + \underline{a}_{d,14} \right)^2 \right)_X + \frac{1}{L_X} \left( \left[ \mathbf{K} \mathbf{2} \right]_{-,14} \left( \underline{a}_{c,14} - \underline{a}_{d,14} \right)^2 \right)_X \approx$$

$$-\frac{1}{L_X} \left( \left[ \mathbf{K} \mathbf{2} \right]_{+,14} \left( \underline{D} - ([\mathbf{U}] - [\Omega^2] - [\dot{\Omega}]) \underline{A}_1 \right)^2 \right)_X + \frac{1}{L_X} \left( \left[ \mathbf{K} \mathbf{2} \right]_{-,14} \left( \underline{D} + ([\mathbf{U}] - [\Omega^2] - [\dot{\Omega}]) \underline{A}_1 \right)^2 \right)_X =$$

$$= -\frac{1}{L_X} \left( (K2_{c,14,X} + K2_{d,14,X}) \left( D_X - \frac{L_X}{2} (U_{XX} + \omega_Y^2 + \omega_Z^2) \right) \right)^2 + \frac{1}{L_X} \left( (K2_{c,14,X} - K2_{d,14,X}) \left( D_X + \frac{L_X}{2} (U_{XX} + \omega_Y^2 + \omega_Z^2) \right) \right)^2$$

$$= -\frac{2}{L_X} K2_{d,14,X} D_X^2 - \frac{L_X}{2} K2_{d,14,X} (U_{XX} + \omega_Y^2 + \omega_Z^2)^2 + 2 \cdot K2_{c,14,X} D_X (U_{XX} + \omega_Y^2 + \omega_Z^2)$$

Considering only the frequency contents of  $\underline{D}$ ,  $[U]$ ,  $[\Omega]$  up to the upper boundary of the MBW (the high frequency noise is considered under the error term C.7), its contribution to the measurement error spectral density of  $U_{XX}$  in the MBW is:

$$\delta \tilde{U}_{XX,C.3}^W = \left( \left( \frac{2}{L_X} \tilde{K}2_{d,14,X}^W D_X^2 \right)^2 + \left( \frac{2}{L_X} K2_{d,14,X}^0 2D_X^0 \tilde{D}_X^W \right)^2 + \left( \frac{L_X}{2} \tilde{K}2_{d,14,X}^W (U_{XX}^0 + \omega_Y^0{}^2 + \omega_Z^0{}^2) \right)^2 + \right. \\ \left. \left( \frac{L_X}{2} K2_{d,14,X}^0 2(U_{XX}^0 + \omega_Y^0{}^2 + \omega_Z^0{}^2) (\tilde{U}_{XX}^W + 2\omega_Y^0 \tilde{\omega}_Y^W + 2\omega_Z^0 \tilde{\omega}_Z^W) \right)^2 + \left( 2 \cdot \tilde{K}2_{c,14,X}^W D_X^0 (U_{XX}^0 + \omega_Y^0{}^2 + \omega_Z^0{}^2) \right)^2 \right. \\ \left. + \left( 2 \cdot K2_{c,14,X}^0 \tilde{D}_X^W (U_{XX}^0 + \omega_Y^0{}^2 + \omega_Z^0{}^2) \right)^2 + \left( 2 \cdot K2_{c,14,X}^0 D_X^0 (\tilde{U}_{XX}^W + 2\omega_Y^0 \tilde{\omega}_Y^W + 2\omega_Z^0 \tilde{\omega}_Z^W) \right)^2 \right)^{1/2} \quad (5.2.6)$$

C.4 Coupling with accelerometer misplacement from their nominal position

These errors derive from the term  $\frac{2}{L_X} (U_{XX} + \omega_Y^2 + \omega_Z^2) \delta A_{1,X}$  of the (4.40).

$$\delta \tilde{U}_{XX,C.4}^W = \frac{2}{L_X} \sqrt{\left( (U_{XX}^0 + \omega_Y^0{}^2 + \omega_Z^0{}^2) \delta \tilde{A}_{1,X}^W \right)^2 + \left( \tilde{U}_{XX}^W \delta A_{1,X}^0 \right)^2 + \left( 2\omega_Y^0 \tilde{\omega}_Y^W \delta A_{1,X}^0 \right)^2 + \left( 2\omega_Z^0 \tilde{\omega}_Z^W \delta A_{1,X}^0 \right)^2} \quad (5.2.7)$$

The error term defines the requirement on the knowledge accuracy of the value of the baseline length and on the stability of the baseline length, since:  $\delta L_X = 2\delta A_{1,X}$ ,  $\delta L_Y = 2\delta A_{2,Y}$ ,  $\delta L_Z = 2\delta A_{3,Z}$ .

C.5 Coupling with platform magnetic field

$$\delta \tilde{U}_{XX,C.6}^W = \frac{2}{L_X} \tilde{M}_{d,14,X}^W \quad (5.2.8)$$

where:

$$\underline{M}_{d,ij} = 0.5(\underline{M}_i - \underline{M}_j), \quad \underline{M}_i = \frac{\chi_m}{\mu_0} \frac{V}{m} \alpha_b \mathbf{B}_i \begin{pmatrix} \frac{\partial B_i}{\partial x} \\ \frac{\partial B_i}{\partial y} \\ \frac{\partial B_i}{\partial z} \end{pmatrix}, \quad \tilde{M}_{d,14,X}^W = \frac{\chi_m}{\mu_0} \frac{V}{m} \alpha_b \left( B_1 \frac{\partial B_1}{\partial x} - B_4 \frac{\partial B_4}{\partial x} \right)^W$$

and  $B_i$  is the modulus of the magnetic field at the location of the accelerometer  $A_i$  resulting from the combination of the Platform equipment generated magnetic field, the Gradiometer generated magnetic field and by the Earth magnetic field.

An approximate expression for  $\delta \tilde{U}_{XX,C.5}^W$  has been derived in [RD 5] and reads

$$\delta\tilde{U}_{XX\_C.5}^W \approx \frac{2}{L_X} \frac{2k_i}{L_{PM}} \sqrt{(2B_{i,P}^0 B_{i,P}^W)^2 + (B_E^0 B_{i,P}^W)^2 + (B_E^W B_{i,P}^0)^2 + (2B_{i,G}^0 B_{i,P}^W)^2 + (2B_{i,G}^W B_{i,P}^0)^2}, \quad (5.2.9)$$

where:

- $B_{i,P}^0$  maximum value below the MBW of the modulus of the magnetic field generated by the Platform at the location of the accelerometer  $A_i$ ;
- $B_{i,P}^W$  maximum value in the MBW of the spectral density of the fluctuations of the modulus of the magnetic field generated by the Platform at the location of the accelerometer  $A_i$ ;
- $B_{i,G}^0$  = maximum value below MBW of the modulus of the magnetic field generated by the Gradiometer at the location of the accelerometer  $A_i$ ;
- $B_{i,G}^W$  = maximum value in the MBW of the spectral density of the fluctuations of the modulus of the magnetic field generated by the Gradiometer at the location of the accelerometer  $A_i$ ;
- $B_E^0$  = maximum value below MBW of the modulus of the magnetic field generated by the Earth at the satellite location;
- $B_E^W$  = maximum value in the MBW of the spectral density of the fluctuations of the modulus of the magnetic field generated by the Earth along the GOCE orbit;
- $L_{PM}$  = proof mass size along the accelerometer ultra-sensitive axis.

C.6 Coupling of accelerometer noise with the common and differential-mode misalignments and scale factors knowledge uncertainty

This error derives from the term  $-\frac{2}{L_X} \left( [\delta MI]_{d,14} \underline{n}_{c,14} \right)_X - \frac{2}{L_X} \left( [\delta MI]_{c,14} \underline{n}_{d,14} \right)_X$  of the (5.3).

Its contribution to the measurement error spectral density of  $U_{XX}$  in the MBW is:

$$\delta\tilde{U}_{XX\_C.6}^W = \frac{2}{L_X} \sqrt{\left( [\delta MI]_{d,14}^p \tilde{n}_{c,14}^W \right)_X^2 + \left( [\delta MI]_{c,14}^p \tilde{n}_{d,14}^W \right)_X^2} \quad (5.2.10)$$

The difference with the error term I.6 is that here the noise is coupled with the errors in the knowledge of the elements of the inverse Calibration Matrices and not with the “by-construction” values of the elements of the Calibration Matrices.

C.7 Coupling with high frequency noise

$$\delta\tilde{U}_{XX\_C.7}^W = \frac{2}{L_X} \tilde{N}_{d,14,X}^W \quad (5.2.11)$$

where  $\underline{N}_{d,ij}$  is the differential acceleration resulting from the folding inside the MBW of high frequency (> MBW) common-mode acceleration coupled with the differential non-linearity (differential quadratic factor) of the accelerometers  $A_i$ ,  $A_j$  (for a more detailed description of this error term and on the way it is computed, see [RD 5]).

### C.8 Coupling with the transfer function difference

This is the error term  $\delta U_{XX,TF}$  in the (4.40) and arises from the coupling of a common-mode acceleration along a given axis with the differential transfer of an accelerometer pair and of the gradiometer structure along the same axis. It is described by the equation (4.39). Its contribution to the measurement error spectral density of  $U_{XX}$  in the MBW is:

$$\delta \tilde{U}_{XX,C.8}^W \equiv \delta \tilde{U}_{XX,TF}^W = \frac{2}{L_X} (\delta TFA_{14,X} + \delta TFS_{14,X}) \tilde{a}_{c,14,X}^W \quad (5.2.12)$$

where  $a_{c,14,X} \equiv (([U] - [\Omega^2] - [\dot{\Omega}])\underline{C}_1 - 2[\Omega] \cdot \underline{\dot{C}}_1 - \underline{\ddot{C}}_1 + \underline{D})_X$

### C.9 Coupling between angular and linear acceleration at accelerometer level

This is the error term  $\delta U_{XX,alc}$  in the (4.40) and arises from the coupling of the angular accelerations experienced by the accelerometer proof masses (which are equal to the angular accelerations of the satellite about its COM) with the mismatch of the electrostatic gains of the electrodes in charge of these angular acceleration control. It is described by the equation (4.39). Its contribution to the measurement error spectral density of  $U_{XX}$  in the MBW is:

$$\delta \tilde{U}_{XX,C.9}^W \equiv \delta \tilde{U}_{XX,alc}^W = \frac{\sqrt{2}}{L_X} C_{Ze} \tilde{\omega}_Y^W \quad (5.2.13)$$

## 5.1.3 Satellite Errors

Satellite contributors to the measurement error spectral density of  $U_{XX}$  ( $U_{YY}$ ,  $U_{ZZ}$ ) in the MBW (denoted as  $\delta \tilde{U}_{XX,S.}^W$ ) includes the platform self gravity only. In fact, being now the gradiometric performance requirement specified in directly in the GRF (see section 3.5), the contribution of the GRF pointing error in the LORF must not be considered any more.

### S.1 Platform self gravity

$$\delta \tilde{U}_{XX,S.1}^W = \frac{2}{L_X} \tilde{S}_{d,14,X}^W \quad (5.3.1)$$

where  $\underline{S}_j$  is here intended as the gravity acceleration of the proof mass of the accelerometer  $A_i$  produced by the other masses of the platform only.

### 5.1.4 Processing Errors

Ground processing contributors to the measurement error spectral density of  $U_{XX}$  ( $U_{YY}$ ,  $U_{ZZ}$ ) in the MBW (denoted as  $\delta \tilde{U}_{XX,P.}^W$ ) consist of the errors of the estimation of the centrifugal accelerations about the Gradiometer axes ( $\hat{\omega}_X^2$ ,  $\hat{\omega}_Y^2$ ,  $\hat{\omega}_Z^2$ ) to be subtracted from the recovered differential acceleration gradients (see (4.30)).

$$\delta \tilde{U}_{XX,P.1}^W = \sqrt{(2\omega_Y^0 \delta \hat{\omega}_Y^W)^2 + (2\tilde{\omega}_Y^W \delta \hat{\omega}_Y^0)^2 + (2\omega_Z^0 \delta \hat{\omega}_Z^W)^2 + (2\tilde{\omega}_Z^W \delta \hat{\omega}_Z^0)^2} \quad (5.4.1)$$

The spectral density in the MBW of the estimation errors of the angular rates ( $\delta\tilde{\omega}_X^W, \delta\tilde{\omega}_Y^W, \delta\tilde{\omega}_Z^W$ ) is in practice limited by the spectral density of the error affecting the angular accelerations obtained from the Gradiometer measurements by means of the (4.29). If the angular accelerations are recovered with an error spectral density  $\delta\tilde{\omega}_X^W(\nu), \delta\tilde{\omega}_Y^W(\nu), \delta\tilde{\omega}_Z^W(\nu)$  at the frequency  $\nu$ , the angular rates cannot be estimated with an error spectral density smaller than:

$$\delta\tilde{\omega}_X^W(\nu) = \frac{\delta\tilde{\omega}_X^W(\nu)}{2\pi\nu}, \quad \delta\tilde{\omega}_Y^W(\nu) = \frac{\delta\tilde{\omega}_Y^W(\nu)}{2\pi\nu}, \quad \delta\tilde{\omega}_Z^W(\nu) = \frac{\delta\tilde{\omega}_Z^W(\nu)}{2\pi\nu}$$

at the same frequency.

This because the satellite attitude quaternions measured by the Star Sensors and utilised in the estimation of the angular rates have a very small weight at the frequencies of the MBW. Here the estimation is driven by the angular acceleration measurements. The attitude quaternions are instead important for the estimation of the angular rates at very low frequencies.

## 5.2 ANGULAR ACCELERATION MEASUREMENT ERRORS

As recalled just above, the error affecting the estimated centrifugal acceleration is conditioned by the error by which the angular accelerations are recovered from the gradiometer measurements.

From the (4.61), and adopting the same procedure described in section 5.1, we can write the total SD in the MBW of the total error affecting the measurement of  $\hat{\omega}_Y$  as the quadratic sum of 14 terms:

$$\delta\tilde{\omega}_Y^W = \sqrt{\sum_{i=1}^{14} \left[ (\delta\tilde{\omega}_{Y_{14i}}^W)^2 + (\delta\tilde{\omega}_{Y_{36i}}^W)^2 \right]}$$

The expression of each of the 13 terms is provided hereafter.

$$\delta\tilde{\omega}_{Y_{14.1}}^W = \frac{1}{L_X} \sqrt{\left( (U_{XZ}^0 - \omega_X^0 \omega_Z^0) \delta\tilde{A}_{1,X}^W \right)^2 + \left( \omega_Y^0 \delta\tilde{A}_{1,X}^W \right)^2 + \left( \tilde{U}_{XZ}^W \delta A_{1,X}^0 \right)^2 + \left( \omega_X^0 \tilde{\omega}_Z^W \delta A_{1,X}^0 \right)^2 + \left( \tilde{\omega}_X^W \omega_Z^0 \delta A_{1,X}^0 \right)^2 + \left( \tilde{\omega}_Y^W \delta A_{1,X}^0 \right)^2}$$

$$\delta\tilde{\omega}_{Y_{36.1}}^W = \frac{1}{L_Z} \sqrt{\left( (U_{XZ}^0 - \omega_X^0 \omega_Z^0) \delta\tilde{A}_{3,Z}^W \right)^2 + \left( \omega_Y^0 \delta\tilde{A}_{3,Z}^W \right)^2 + \left( \tilde{U}_{XZ}^W \delta A_{3,Z}^0 \right)^2 + \left( \omega_X^0 \tilde{\omega}_Z^W \delta A_{3,Z}^0 \right)^2 + \left( \tilde{\omega}_X^W \omega_Z^0 \delta A_{3,Z}^0 \right)^2 + \left( \tilde{\omega}_Y^W \delta A_{3,Z}^0 \right)^2}$$

$$\delta\tilde{\omega}_{Y_{14.2}}^W = \frac{1}{L_X} \sqrt{\left( 2\tilde{\omega}_Y^W \delta A_{d,14,X}^0 \right)^2 + \left( 2\omega_Y^0 \delta\tilde{A}_{d,14,X}^W \right)^2}, \quad \delta\tilde{\omega}_{Y_{36.2}}^W = \frac{1}{L_Z} \sqrt{\left( 2\tilde{\omega}_Y^W \delta A_{d,36,Z}^0 \right)^2 + \left( 2\omega_Y^0 \delta\tilde{A}_{d,36,Z}^W \right)^2}$$

$$\delta\tilde{\omega}_{Y_{14.3}}^W = \frac{1}{L_X} \tilde{S}_{d,14,Z}^W, \quad \delta\tilde{\omega}_{Y_{36.3}}^W = \frac{1}{L_Z} \tilde{S}_{d,36,X}^W$$

$$\delta\tilde{\omega}_{Y_{14.4}}^W = \frac{1}{L_X} \tilde{M}_{d,14,Z}^W, \quad \delta\tilde{\omega}_{Y_{36.4}}^W = \frac{1}{L_Z} \tilde{M}_{d,36,X}^W$$

$$\delta\tilde{\omega}_{Y_{14.5}}^W = \frac{1}{L_X} \tilde{n}_{d,14,Z}^W, \quad \delta\tilde{\omega}_{Y_{36.5}}^W = \frac{1}{L_Z} \tilde{n}_{d,36,X}^W$$

$$\delta\tilde{\omega}_{Y_{14.6}}^W = \frac{1}{L_X} \left( \left( [\delta\tilde{M}I]_{d,14}^W \left( [U]^0 - [\Omega^2]^0 - [\dot{\Omega}]^0 \right) \underline{C}_1^0 \right)_Z \right)^2 + \left( [\delta MI]_{d,14}^0 \left( [\tilde{U}]^W - [\tilde{\Omega}^2]^W - [\tilde{\Omega}]^W \right) \underline{C}_1^0 \right)_Z^2$$

$$\left( [\delta MI]_{d,14}^0 \left( [U]^0 - [\Omega^2]^0 - [\dot{\Omega}]^0 \right) \underline{C}_1^W \right)_Z^2 + \left( 2[\delta\tilde{M}I]_{d,14}^W [\Omega]^0 \underline{C}_1^0 \right)_Z^2 + \left( 2[\delta MI]_{d,14}^0 [\tilde{\Omega}]^W \underline{C}_1^0 \right)_Z^2$$

$$\left( 2[\delta MI]_{d,14}^0 [\Omega]^0 \tilde{C}_1^W \right)_Z^2 + \left( [\delta \tilde{MI}]_{d,14}^W \ddot{C}_1^0 \right)_Z^2 + \left( [\delta MI]_{d,14}^0 \tilde{C}_1^W \right)_Z^2 \Big)^{1/2}$$

$$\delta \tilde{\omega}_{Y_{36.6}}^W = \frac{1}{L_Z} \left( \left( [\delta \tilde{MI}]_{d,36}^W ([U]^0 - [\Omega^2]^0 - [\dot{\Omega}]^0) \underline{C}_3 \right)_X^2 + \left( [\delta MI]_{d,36}^0 ([\tilde{U}]^W - [\tilde{\Omega}^2]^W - [\tilde{\dot{\Omega}}]^W) \underline{C}_3 \right)_X^2 \right. \\ \left. \left( [\delta MI]_{d,36}^0 ([U]^0 - [\Omega^2]^0 - [\dot{\Omega}]^0) \tilde{C}_3^W \right)_X^2 + \left( 2[\delta \tilde{MI}]_{d,36}^W [\Omega]^0 \underline{C}_3 \right)_X^2 + \left( 2[\delta MI]_{d,36}^0 [\tilde{\Omega}]^W \underline{C}_3 \right)_X^2 \right. \\ \left. \left( 2[\delta MI]_{d,36}^0 [\Omega]^0 \tilde{C}_3^W \right)_X^2 + \left( [\delta \tilde{MI}]_{d,36}^W \ddot{C}_3 \right)_X^2 + \left( [\delta MI]_{d,36}^0 \tilde{C}_3^W \right)_X^2 \right)^{1/2}$$

$$\delta \tilde{\omega}_{Y_{14.7}}^W = \frac{1}{L_X} \sqrt{\left( [\delta \tilde{MI}]_{d,14,31}^W D_X^0 \right)^2 + \left( \delta MI_{d,14,31}^0 \tilde{D}_X^W \right)^2 + \left( \delta \tilde{MI}_{d,14,32}^W D_Y^0 \right)^2 + \left( \delta MI_{d,14,32}^0 \tilde{D}_Y^W \right)^2 + \left( \delta \tilde{MI}_{d,14,33}^W D_Z^0 \right)^2 + \left( \delta MI_{d,14,33}^0 \tilde{D}_Z^W \right)^2}$$

$$\delta \tilde{\omega}_{Y_{36.7}}^W = \frac{1}{L_Z} \sqrt{\left( [\delta \tilde{MI}]_{d,36,11}^W D_X^0 \right)^2 + \left( \delta MI_{d,36,11}^0 \tilde{D}_X^W \right)^2 + \left( \delta \tilde{MI}_{d,36,12}^W D_Y^0 \right)^2 + \left( \delta MI_{d,36,12}^0 \tilde{D}_Y^W \right)^2 + \left( \delta \tilde{MI}_{d,36,13}^W D_Z^0 \right)^2 + \left( \delta MI_{d,36,13}^0 \tilde{D}_Z^W \right)^2}$$

$$\delta \tilde{\omega}_{Y_{14.8}}^W = \frac{1}{L_X} \sqrt{\left( [\delta \tilde{MI}]_{c,14}^W ([U]^0 - [\Omega^2]^0) \underline{A}_1 \right)_Z^2 + \left( [\delta MI]_{c,14}^0 [\tilde{U}]^W \underline{A}_1 \right)_Z^2 + \left( [\delta MI]_{c,14}^0 [\tilde{\Omega}^2]^W \underline{A}_1 \right)_Z^2}$$

$$\delta \tilde{\omega}_{Y_{36.8}}^W = \frac{1}{L_Z} \sqrt{\left( [\delta \tilde{MI}]_{c,36}^W ([U]^0 - [\Omega^2]^0) \underline{A}_3 \right)_X^2 + \left( [\delta MI]_{c,36}^0 [\tilde{U}]^W \underline{A}_3 \right)_X^2 + \left( [\delta MI]_{c,36}^0 [\tilde{\Omega}^2]^W \underline{A}_3 \right)_X^2}$$

$$\delta \tilde{\omega}_{Y_{14.9}}^W = \frac{1}{2} \sqrt{\left( [\delta \tilde{MI}]_{c,14,32}^W \dot{\omega}_Z^0 \right)^2 + \left( \delta MI_{c,14,32}^0 \tilde{\omega}_Z^W \right)^2 + \left( [\delta \tilde{MI}]_{c,14,33}^W \dot{\omega}_Y^0 \right)^2 + \left( \delta MI_{c,14,33}^0 \tilde{\omega}_Y^W \right)^2}$$

$$\delta \tilde{\omega}_{Y_{36.9}}^W = \frac{1}{2} \sqrt{\left( [\delta \tilde{MI}]_{c,36,11}^W \dot{\omega}_Y^0 \right)^2 + \left( \delta MI_{c,36,11}^0 \tilde{\omega}_Y^W \right)^2 + \left( [\delta \tilde{MI}]_{c,36,12}^W \dot{\omega}_X^0 \right)^2 + \left( \delta MI_{c,36,12}^0 \tilde{\omega}_X^W \right)^2}$$

$$\delta \tilde{\omega}_{Y_{14.10}}^W = \frac{1}{2} \left( \left( \frac{2}{L_X} \tilde{K} 2_{d,14,Z}^W D_Z^0 \right)^2 + \left( \frac{2}{L_X} K 2_{d,14,Z}^0 2 D_Z^0 \tilde{D}_Z^W \right)^2 + \left( \frac{L_X}{2} \tilde{K} 2_{d,14,Z}^W \left( U_{ZZ}^0 + \omega_X^0{}^2 + \omega_Y^0{}^2 \right)^2 \right)^2 + \right. \\ \left. \left( \frac{L_X}{2} K 2_{d,14,Z}^0 2 \left( U_{ZZ}^0 + \omega_X^0{}^2 + \omega_Y^0{}^2 \right) \left( \tilde{U}_{ZZ}^W + 2\omega_X^0 \tilde{\omega}_X^W + 2\omega_Y^0 \tilde{\omega}_Y^W \right) \right)^2 + \left( 2 \cdot \tilde{K} 2_{c,14,Z}^W D_Z^0 \left( U_{ZZ}^0 + \omega_X^0{}^2 + \omega_Y^0{}^2 \right) \right)^2 \right. \\ \left. + \left( 2 \cdot K 2_{c,14,Z}^0 \tilde{D}_Z^W \left( U_{ZZ}^0 + \omega_X^0{}^2 + \omega_Y^0{}^2 \right) \right)^2 + \left( 2 \cdot K 2_{c,14,Z}^0 D_Z^0 \left( \tilde{U}_{ZZ}^W + 2\omega_X^0 \tilde{\omega}_X^W + 2\omega_Y^0 \tilde{\omega}_Y^W \right) \right)^2 \right)^{1/2}$$

$$\delta \tilde{\omega}_{Y_{36.10}}^W = \frac{1}{2} \left( \left( \frac{2}{L_Z} \tilde{K} 2_{d,36,X}^W D_X^0 \right)^2 + \left( \frac{2}{L_Z} K 2_{d,36,X}^0 2 D_X^0 \tilde{D}_X^W \right)^2 + \left( \frac{L_Z}{2} \tilde{K} 2_{d,36,X}^W \left( U_{XX}^0 + \omega_Y^0{}^2 + \omega_Z^0{}^2 \right)^2 \right)^2 + \right. \\ \left. \left( \frac{L_Z}{2} K 2_{d,36,X}^0 2 \left( U_{XX}^0 + \omega_Y^0{}^2 + \omega_Z^0{}^2 \right) \left( \tilde{U}_{XX}^W + 2\omega_Y^0 \tilde{\omega}_Y^W + 2\omega_Z^0 \tilde{\omega}_Z^W \right) \right)^2 + \left( 2 \cdot \tilde{K} 2_{c,36,X}^W D_X^0 \left( U_{XX}^0 + \omega_Y^0{}^2 + \omega_Z^0{}^2 \right) \right)^2 \right. \\ \left. + \left( 2 \cdot K 2_{c,36,X}^0 \tilde{D}_X^W \left( U_{XX}^0 + \omega_Y^0{}^2 + \omega_Z^0{}^2 \right) \right)^2 + \left( 2 \cdot K 2_{c,36,X}^0 D_X^0 \left( \tilde{U}_{XX}^W + 2\omega_Y^0 \tilde{\omega}_Y^W + 2\omega_Z^0 \tilde{\omega}_Z^W \right) \right)^2 \right)^{1/2}$$

$$\delta\tilde{\omega}_{Y_{-14.11}}^W = \frac{1}{L_X} \sqrt{\left(\left[d\tilde{M}\right]_{d,14}^p \tilde{n}_{c,14}^W\right)_Z^2 + \left(\left[d\tilde{M}\right]_{f,14}^p \tilde{n}_{d,14}^W\right)_Z^2 + \left(\left[\delta\tilde{M}I\right]_{d,14}^p \tilde{n}_{c,14}^W\right)_Z^2 + \left(\left[\delta\tilde{M}I\right]_{f,14}^p \tilde{n}_{d,14}^W\right)_Z^2}$$

$$\delta\tilde{\omega}_{Y_{-36.11}}^W = \frac{1}{L_Z} \sqrt{\left(\left[d\tilde{M}\right]_{d,36}^p \tilde{n}_{c,36}^W\right)_X^2 + \left(\left[d\tilde{M}\right]_{f,36}^p \tilde{n}_{d,36}^W\right)_X^2 + \left(\left[\delta\tilde{M}I\right]_{d,36}^p \tilde{n}_{c,36}^W\right)_X^2 + \left(\left[\delta\tilde{M}I\right]_{f,36}^p \tilde{n}_{d,36}^W\right)_X^2}$$

$$\delta\tilde{\omega}_{Y_{-14.12}}^W = \frac{1}{L_X} \tilde{N}_{d,14,Z}^W, \quad \delta\tilde{\omega}_{Y_{-36.12}}^W = \frac{1}{L_Z} \tilde{N}_{d,36,X}^W$$

$$\delta\tilde{\omega}_{Y_{-14.13}}^W = \frac{1}{L_X} (\delta TFA_{14,Z} + \delta TFS_{14,Z}) \tilde{a}_{c,14,Z}^W, \quad \delta\tilde{\omega}_{Y_{-36.13}}^W = \frac{1}{L_Z} (\delta TFA_{36,X} + \delta TFS_{36,X}) \tilde{a}_{c,36,X}^W$$

$$\delta\tilde{\omega}_{Y_{-14.14}}^W = \frac{\sqrt{2}}{2L_X} C_{Ye} \tilde{\omega}_Y^W, \quad \delta\tilde{\omega}_{Y_{-36.14}}^W = \frac{\sqrt{2}}{2L_Z} C_{Ye} \tilde{\omega}_Y^W$$

The error terms  $\delta\tilde{\omega}_{Y_{-14.6}}^W, \delta\tilde{\omega}_{Y_{-14.7}}^W$  and  $\delta\tilde{\omega}_{Y_{-36.6}}^W, \delta\tilde{\omega}_{Y_{-36.7}}^W$  derive from the expansion of  $\frac{1}{L_X} \left(\left[\delta\tilde{M}I\right]_{d,14}^p \underline{a}_{c,14}\right)_Z$  and

$\frac{1}{L_Z} \left(\left[\delta\tilde{M}I\right]_{d,36}^p \underline{a}_{c,36}\right)_X$  as:

$$\frac{1}{L_X} \left(\left[\delta\tilde{M}I\right]_{d,14}^p \underline{a}_{c,14}\right)_Z \cong \frac{1}{L_X} \left(\left[\delta\tilde{M}I\right]_{d,14}^p \cdot \left(\left([U] - [\Omega^2] - [\dot{\Omega}]\right) \underline{C}_1 - 2[\Omega] \cdot \underline{\dot{C}}_1 - \underline{\ddot{C}}_1 + \underline{D}\right)\right)_Z$$

$$\frac{1}{L_Z} \left(\left[\delta\tilde{M}I\right]_{d,36}^p \underline{a}_{c,36}\right)_X \cong \frac{1}{L_Z} \left(\left[\delta\tilde{M}I\right]_{d,36}^p \cdot \left(\left([U] - [\Omega^2] - [\dot{\Omega}]\right) \underline{C}_3 - 2[\Omega] \cdot \underline{\dot{C}}_3 - \underline{\ddot{C}}_3 + \underline{D}\right)\right)_X$$

The error terms  $\delta\tilde{\omega}_{Y_{-14.8}}^W, \delta\tilde{\omega}_{Y_{-14.9}}^W$  and  $\delta\tilde{\omega}_{Y_{-36.8}}^W, \delta\tilde{\omega}_{Y_{-36.9}}^W$  derive from the expansion of  $\frac{1}{L_X} \left(\left[\delta\tilde{M}I\right]_{f,14}^p \underline{a}_{d,14}\right)_Z$  and

$\frac{1}{L_Z} \left(\left[\delta\tilde{M}I\right]_{f,36}^p \underline{a}_{d,36}\right)_X$  as:

$$\frac{1}{L_X} \left(\left[\delta\tilde{M}I\right]_{f,14}^p \underline{a}_{d,14}\right)_Z \cong \frac{1}{L_X} \left(\left[\delta\tilde{M}I\right]_{c,14}^p \cdot \left(\left([U] - [\Omega^2] - [\dot{\Omega}]\right) \underline{A}_1\right)\right)_Z$$

$$\frac{1}{L_Z} \left(\left[\delta\tilde{M}I\right]_{f,36}^p \underline{a}_{d,36}\right)_X \cong \frac{1}{L_Z} \left(\left[\delta\tilde{M}I\right]_{c,36}^p \cdot \left(\left([U] - [\Omega^2] - [\dot{\Omega}]\right) \underline{A}_3\right)\right)_X$$

The error terms  $\delta\tilde{\omega}_{Y_{-14.12}}^W, \delta\tilde{\omega}_{Y_{-36.12}}^W$  are related to the differential acceleration noise ( $N_{d,14,Z}, N_{c,14,Z}$ ) folded inside the MBW by the non-linearity of the accelerometers.

The error terms  $\delta\tilde{\omega}_{Y_{14.13}}^W$ ,  $\delta\tilde{\omega}_{Y_{36.13}}^W$  arise from the coupling of the common-mode accelerations ( $a_{c,14,Z}$ ,  $a_{c,36,X}$ ) with the differential transfer of the accelerometer pairs  $A_1$ ,  $A_4$  and  $A_3$ ,  $A_6$  ( $\delta TFA_{14,Z}$ ,  $\delta TFA_{36,X}$ ) and with the Gradiometer structure transfer function mismatch from the Central Stiffening to the accelerometer location ( $\delta TFS_{14,Z}$ ,  $\delta TFS_{36,X}$ ).

The error terms  $\delta\tilde{\omega}_{Y_{14.14}}^W$ ,  $\delta\tilde{\omega}_{Y_{36.14}}^W$  arise from the coupling between the angular and the linear acceleration at accelerometer level.

Analogous expressions can be obtained for  $\delta\tilde{\omega}_X^W$ ,  $\delta\tilde{\omega}_Z^W$ .

In addition to the previous 14 error terms we have to consider the one arising from the non-orthogonality of the Gradiometer arms, since each component of the angular acceleration is the product of the combination of differential accelerations measured by two different OAGs. The transformation of the angular acceleration vector  $\underline{\dot{\omega}}$  from a OAGRF to another one, whose misalignment in the previous frame is defined by the rotation matrix

$$[R] = \begin{pmatrix} 1 & \psi & -\theta \\ -\psi & 1 & \phi \\ \theta & -\phi & 1 \end{pmatrix}$$

is

$$\underline{\dot{\omega}}' = \begin{pmatrix} \dot{\omega}'_X \\ \dot{\omega}'_Y \\ \dot{\omega}'_Z \end{pmatrix} = \begin{pmatrix} 1 & \psi & -\theta \\ -\psi & 1 & \phi \\ \theta & -\phi & 1 \end{pmatrix} \begin{pmatrix} \dot{\omega}_X \\ \dot{\omega}_Y \\ \dot{\omega}_Z \end{pmatrix} = \begin{pmatrix} \dot{\omega}_X + \psi\dot{\omega}_Y - \theta\dot{\omega}_Z \\ \dot{\omega}_Y - \psi\dot{\omega}_X + \phi\dot{\omega}_Z \\ \dot{\omega}_Z + \theta\dot{\omega}_X - \phi\dot{\omega}_Y \end{pmatrix}$$

The corresponding spectral density in the MBW of the error on the angular acceleration components due to the misalignment and the misalignment stability between the two OAGRFs is

$$\begin{aligned} \delta\tilde{\omega}_{X,R}^W &= \sqrt{(\tilde{\psi}^W \dot{\omega}_Y^0)^2 + (\psi^0 \tilde{\omega}_Y^W)^2 + (\tilde{\theta}^W \dot{\omega}_Z^0)^2 + (\theta^0 \tilde{\omega}_Z^W)^2} \\ \delta\tilde{\omega}_{Y,R}^W &= \sqrt{(\tilde{\psi}^W \dot{\omega}_X^0)^2 + (\psi^0 \tilde{\omega}_X^W)^2 + (\tilde{\phi}^W \dot{\omega}_Z^0)^2 + (\phi^0 \tilde{\omega}_Z^W)^2} \\ \delta\tilde{\omega}_{Z,R}^W &= \sqrt{(\tilde{\theta}^W \dot{\omega}_X^0)^2 + (\theta^0 \tilde{\omega}_X^W)^2 + (\tilde{\phi}^W \dot{\omega}_Y^0)^2 + (\phi^0 \tilde{\omega}_Y^W)^2} \end{aligned}$$

Thus, the spectral densities in the MBW of the total error affecting the angular acceleration components obtained from the gradiometer measurements are:

$$\begin{aligned} \delta\tilde{\omega}_X^W &= \sqrt{\sum_{i=1}^{14} [(\delta\tilde{\omega}_{X_{25i}}^W)^2 + (\delta\tilde{\omega}_{X_{36i}}^W)^2]} + (\delta\tilde{\omega}_{X,R}^W)^2 \\ \delta\tilde{\omega}_Y^W &= \sqrt{\sum_{i=1}^{14} [(\delta\tilde{\omega}_{Y_{14i}}^W)^2 + (\delta\tilde{\omega}_{Y_{36i}}^W)^2]} + (\delta\tilde{\omega}_{Y,R}^W)^2 \\ \delta\tilde{\omega}_Z^W &= \sqrt{\sum_{i=1}^{14} [(\delta\tilde{\omega}_{Z_{14i}}^W)^2 + (\delta\tilde{\omega}_{Z_{25i}}^W)^2]} + (\delta\tilde{\omega}_{Z,R}^W)^2 \end{aligned}$$

### 5.3 ERROR TREE

The tree of the gravimetric errors including the terms identified and classified in the previous sections is provided in Figure 5.3-1.

The specified GOCE gravimetric mission goal is to provide, after Level 0 and Level 1a/1b ground processing, the diagonal components of the Earth gravity gradient tensor in the GRF with a measurement error so that the resulting error on the GGT trace does not exceed the limit shown in Figure 3.5-1:

- 100 mE/Hz<sup>1/2</sup> at 5 mHz, 18 mE/Hz<sup>1/2</sup> at 10 mHz, 11 mE/Hz<sup>1/2</sup> from 20 to 100 mHz
- increase as  $v^2$  for  $v > 100$  mHz
- increase as  $1/v$  for  $v < 1$  mHz (portion between 1 mHz and 5 mHz not constrained)

The contributors to this measurement error, as classified in the previous sections 5.1, are organised in the error tree of Figure 5.3-1.

The apportionment of the overall GGT trace error spectral density among the four top-level contributors (Instrument, Instrument-Satellite Coupling, Satellite, and Processing Errors), utilised to derive the requirements for the various lower level contributors, is provided in the plot of Figure 5.3-2.

It is based on a root-sum-square (RSS) of the error terms, which are classified under the distinct categories of the error tree. These errors can be considered uncorrelated. The accelerometer intrinsic measurement noise is not correlated with the errors arising from the coupling of the accelerometer scale factor and misalignment with the residual drag acceleration, with the errors arising from the satellite self gravity, and with the errors related to the recovery of the centrifugal accelerations.

The requirement portion pertinent to the Instrument Errors is established by the GOCE System Requirements Document [AD 1]:

- 5.8 mE/Hz<sup>1/2</sup> for each diagonal component of the GGT in the MBW → ~10 mE/Hz<sup>1/2</sup> on the GGT trace
- increase as  $v^2$  for  $v > 100$  mHz
- increase as  $1/v$  for  $v < 5$  mHz

This requirement is displayed in Figure 5.3-3.

*The detailed apportionments of the requirement on the Gravity Gradient Tensor trace error among the various contributors at 5 mHz and at 100 mHz are shown in Figure 5.3-4 and*

Figure 5.3-5: a contingency margin has been applied with respect to the SRD requirement of 100 mE/Hz<sup>1/2</sup> at 5 mHz. The measurement error in the low frequency part of the MBW is in fact affected by a large uncertainty related to the fluctuations of the drag accelerations along the uncontrolled directions (cross-track, radial) and to the amplitudes of the weakly controlled attitude motion of the satellite. These linear and angular accelerations generate gravity gradient errors through the coupling with the elements of the Inverse Calibration Matrices, which are measured in the in-flight calibration of the Gradiometer and are also affected by errors depending on the actual conditions occurring in flight (environmental perturbations, shaking profiles delivered by the propulsion system, accelerometer scale factor mismatch, misalignments, coupling factors, etc..) which are not totally predictable.

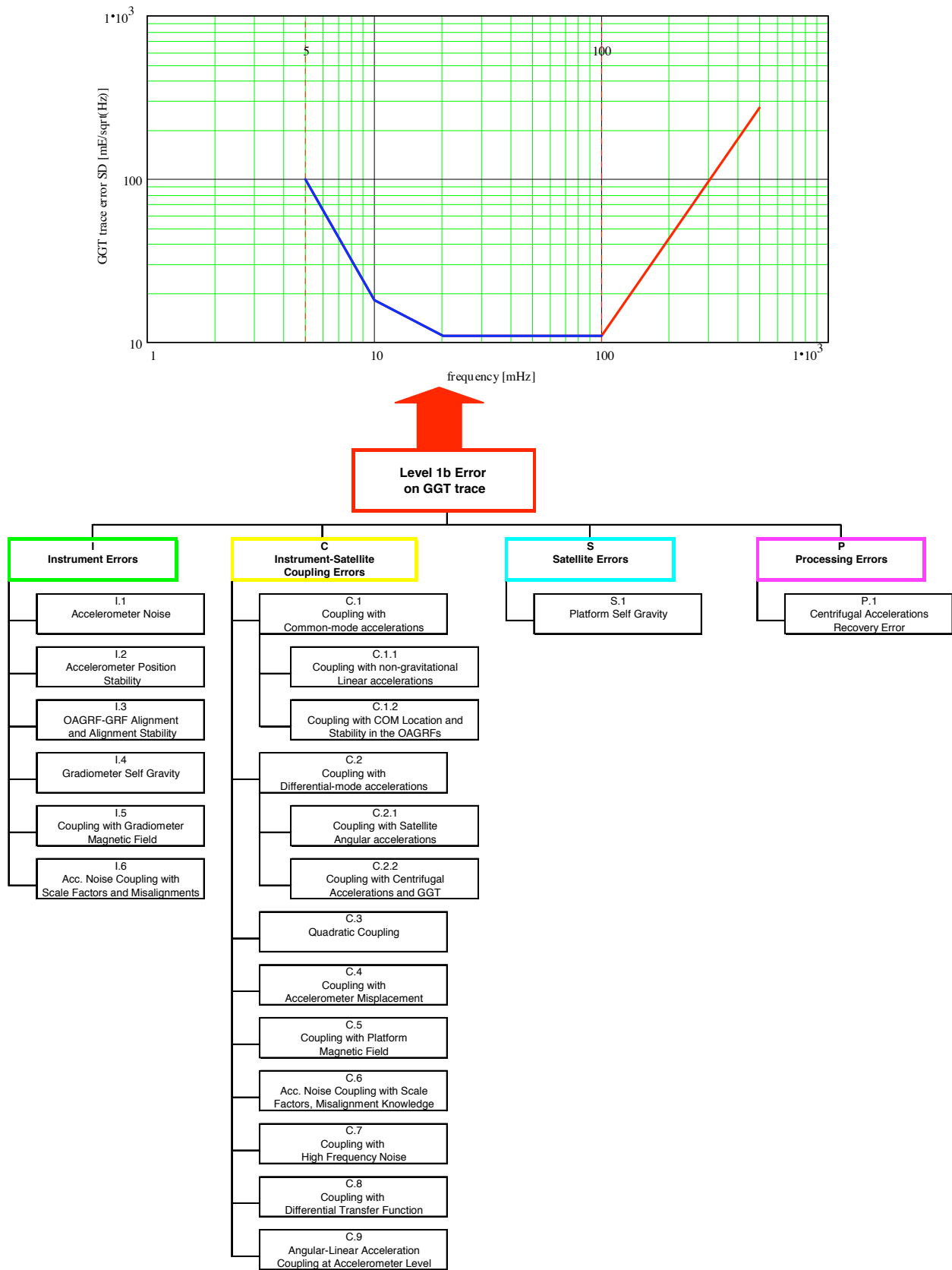


Figure 5.3-1: Gradiometric error tree

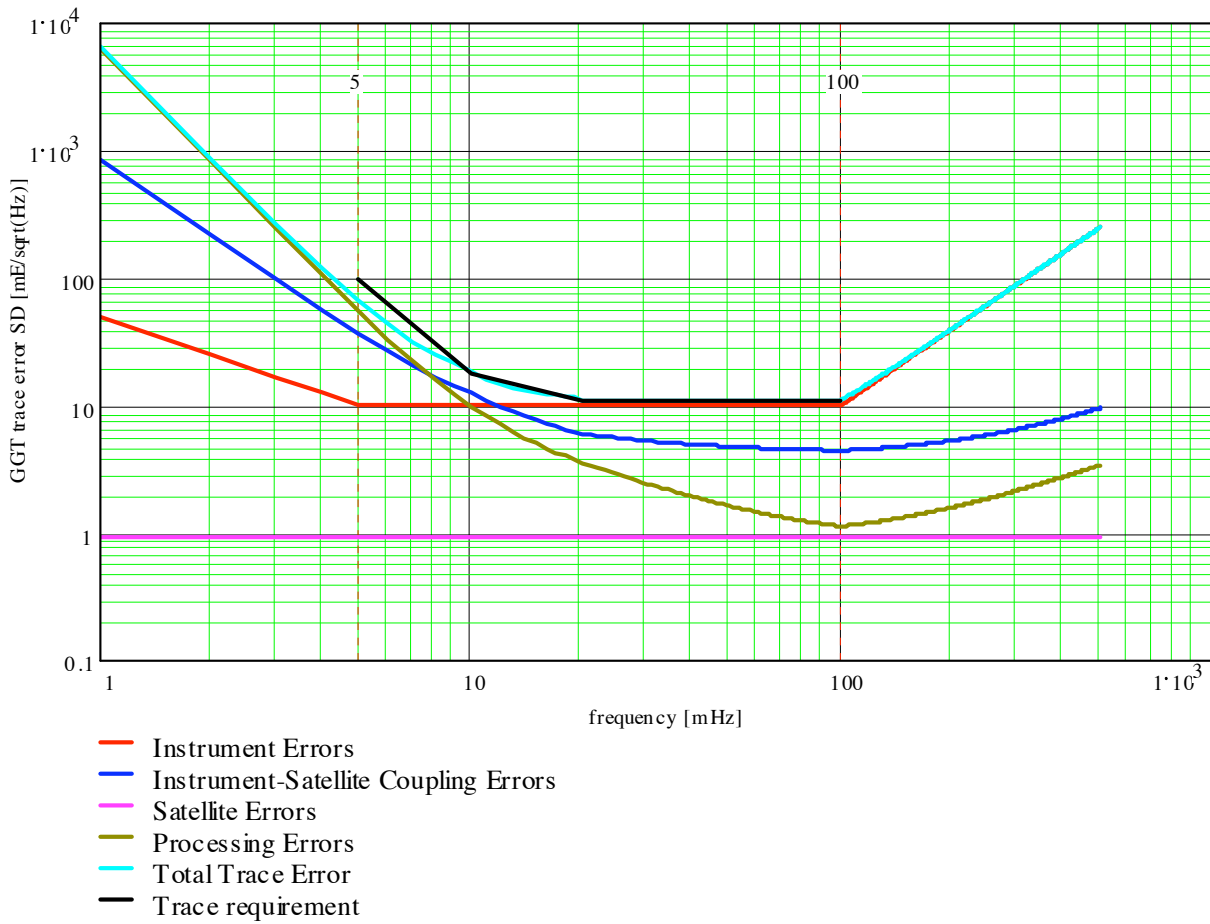


Figure 5.3-2: Apportionment of the GGT trace error spectral density in the MBW among the four top-level contributors

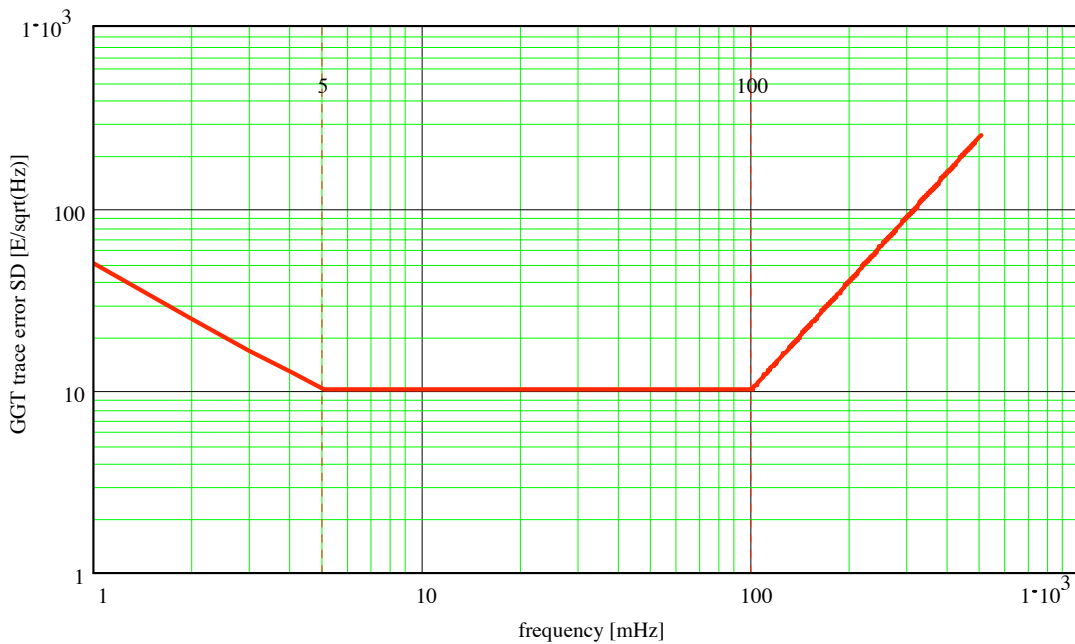


Figure 5.3-3: Instrument contributor to the GGT trace error, as per requirement defined in [AD 1]

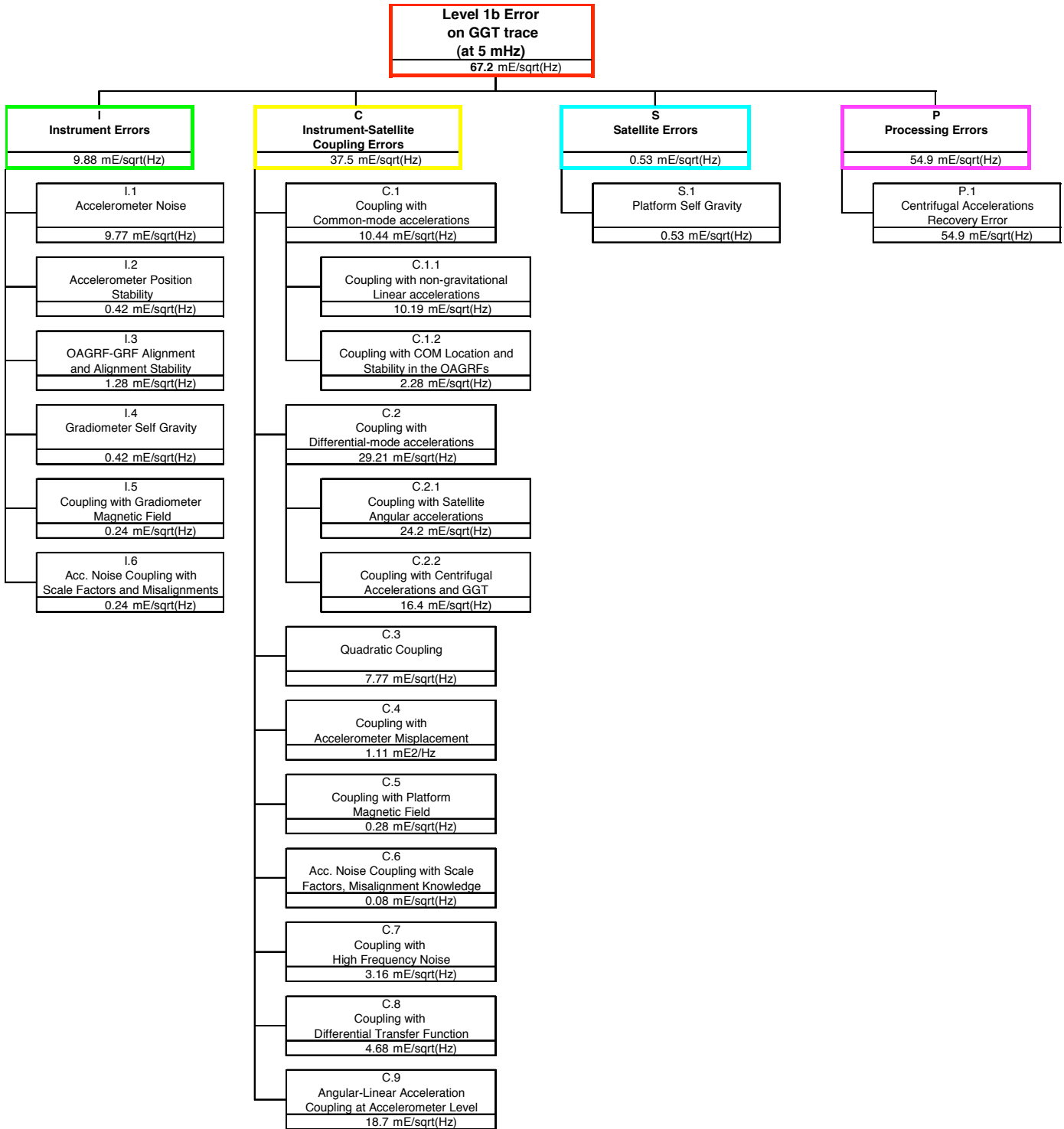


Figure 5.3-4: Apportionments of the requirement on the Gravity Gradient Tensor trace error among the various contributors at 5 mHz

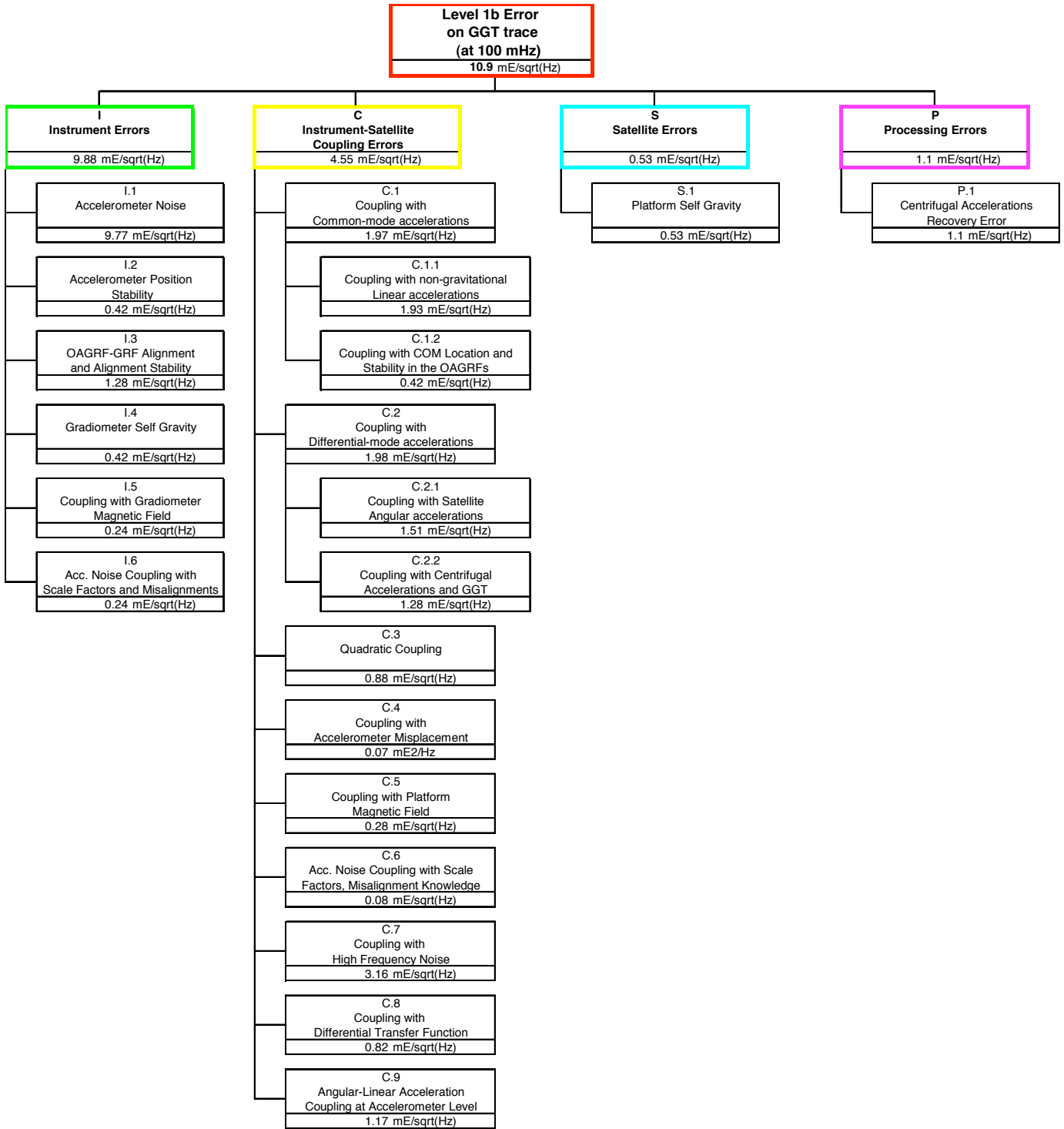


Figure 5.3-5: Apportionments of the requirement on the Gravity Gradient Tensor trace error among the various contributors at 100 mHz

## 6. SPACECRAFT PERFORMANCE REQUIREMENTS

The performance requirements for the quantities related to the GOCE platform, or defining the interaction between Gradiometer and platform, that bring a contribution to the GGT diagonal components measurement error are reported in this section. The requirements are derived from the equations establishing the relationship between these quantities and the measurement error on the GGT diagonal components (e.g equation (5.2.1) for the non-linear accelerations of the satellite COM) and the error portion allocated to the category to which the quantity belongs (e.g. Coupling with Non-gravitational Linear Accelerations). The limit value assigned to the specified quantities is such that, when plugged in the corresponding measurement equation, the resulting error on the GGT trace doesn't exceed the assigned portion. A RSS error combination is assumed in the derivation of these requirements.

None of the performance requirements has been driven by the measurement accuracy of the GGT off-diagonal components, which have not been subject to any constraint in the System Requirements Document [AD 1].

### 6.1 REQUIREMENTS RELATED TO THE INSTRUMENT-SATELLITE COUPLING ERRORS

#### 6.1.1 C.1.1: Coupling with Non-Gravitational Linear Acceleration of the Satellite COM

From the equation (5.2.1) requirements are derived for:

- the “in line” elements of the matrices  $[\delta\mathbf{MI}]_{d,14}$ ,  $[\delta\mathbf{MI}]_{d,25}$ ,  $[\delta\mathbf{MI}]_{d,36}$  ( $\cong$  differential scale factors, misalignments and couplings of the accelerometer in-line axes), i.e. the differences between the actual values of these elements during the measurement phases (between the periodic in-flight calibrations of the Gradiometer) and those measured at the Gradiometer calibrations;
- the control of the non-gravitational accelerations of the satellite COM.

##### 6.1.1.1 Differential Scale Factors, Misalignments and Couplings Knowledge and Stability Requirements

The requirements on the in-line elements of  $[\delta\mathbf{MI}]_{d,14}$ ,  $[\delta\mathbf{MI}]_{d,25}$ ,  $[\delta\mathbf{MI}]_{d,36}$  (i.e. the requirements on the knowledge accuracy of the ICM in-line, differential elements) during the measurement phases are listed in Table 6.1-1.

The values of the elements of  $\mathbf{MI}_{ij}$  are measured during an on-orbit calibration of the Gradiometer and are utilised throughout the following scientific measurement phase till the next calibration (which, if necessary, shall not occur anyway before one month from the previous one). The result of the calibration is a single value for each element: the actual mean value of this element during the calibration measurement period plus the measurement error. The maximum value achieved by the elements of  $\delta\mathbf{MI}_{ij}$  (so the maximum value of the error on the knowledge of  $\mathbf{MI}_{ij}$ ) throughout a scientific measurement phase (object of this specification) takes contributions from (see Figure 6.1-1):

- A. the maximum measurement error the elements of the matrix  $\mathbf{MI}_{ij}$  at the calibration (constant term);
- B. the maximum variation of the elements of the matrix  $\mathbf{MI}_{ij}$  (i.e. of the accelerometer scale factors misalignments and coupling factors) during the scientific measurement phase between two successive calibrations (w.r.t. to their mean values during the calibration measurement period) in the frequency range from DC (in practice from  $1/T_{mp}$  where  $T_{mp}$  = measurement phase duration) to 5 mHz (below the MBW).<sup>4</sup>

The apportionment of the overall requirement on  $\delta\mathbf{MI}_{ij}$  between the contributions A, B (measurement error at calibration and successive long-term stability) is also provided in Table 6.1-1. It is based on an algebraic sum of the two contributions.

<sup>4</sup> The variations of  $\delta\mathbf{MI}_{ij}$  over the MBW time scales are constrained by another requirement.

The in-flight stability of the calibration parameters can be predicted by analyses (e.g. thermoelastic) and verified on-orbit (indirectly) from the quality of the GGT measurements, checked in turn by means of the GGT traceless condition, or (theoretically) by repeating the measurement of these parameters at short intervals during the first in-flight gradiometer calibration phase.

The maximum value in the MBW of the SD of  $\delta MI_{ij}$  (other object of this specification) coincides with that of the SD of  $M_{ij}$  (related to the fluctuations of the accelerometer scale factors, misalignments and couplings):  $\delta MI_{ij}^W \cong dM_{ij}^W$  (see equation 5.2). In fact, since the elements of the ICMs are not measured at any time, the variation of their knowledge accuracy in time is determined just by the variation in time of the calibration matrix elements. The requirements for the maximum value of  $\delta MI_{ij}^W$  (in-line, differential elements) in the MBW are provided in Table 6.1-2. Concerning the spectral density of the in-line, differential scale factors,  $\delta \tilde{K}_{d,14,X}^W$ ,  $\delta \tilde{K}_{d,25,Y}^W$ ,  $\delta \tilde{K}_{d,36,Z}^W$  (differently to the in-line differential misalignments and couplings) the requirement is expressed not just by a constant value in the MBW, but by a limit which is a function of the frequency (with maximum in the MBW specified in Table 6.1-2), as shown in Figure 6.1-2.

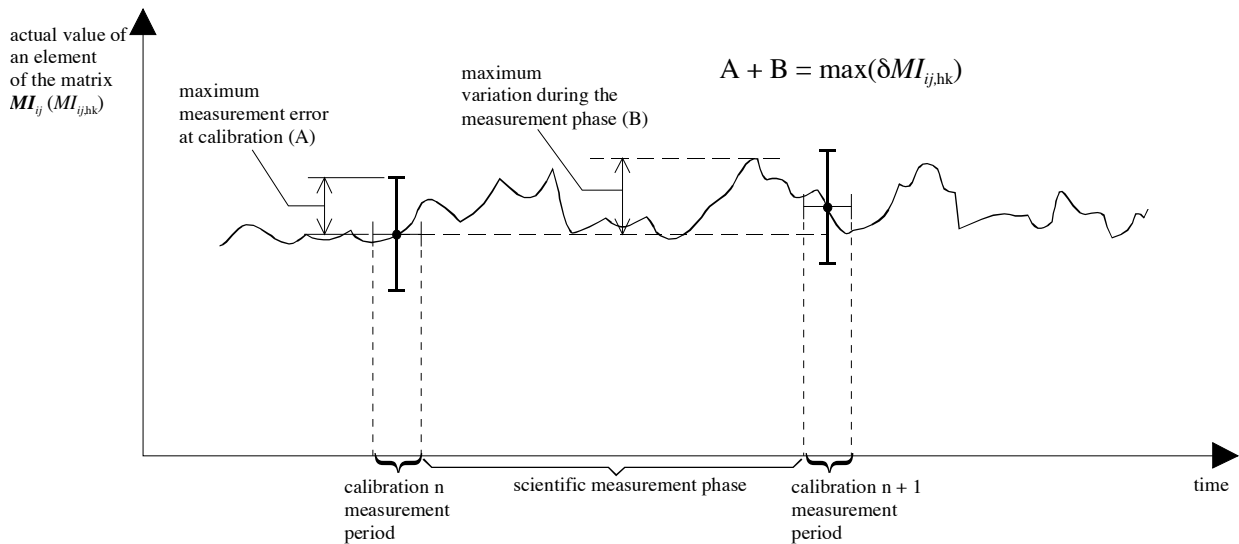


Figure 6.1-1: Contributions to the maximum value achieved by the elements of  $\delta MI_{ij}$  throughout a scientific measurement phase

| Row             | Required knowledge accuracy of the in-line, differential elements of $MI_{14}$ during the measurement phase |                                            |                                            |   |   |   |
|-----------------|-------------------------------------------------------------------------------------------------------------|--------------------------------------------|--------------------------------------------|---|---|---|
| 4 <sup>th</sup> | $\delta MI_{14,41} \leq 1.4 \cdot 10^{-5}$                                                                  | $\delta MI_{14,42} \leq 5.0 \cdot 10^{-6}$ | $\delta MI_{14,43} \leq 5.0 \cdot 10^{-6}$ | - | - | - |
| 5 <sup>th</sup> | -                                                                                                           | -                                          | -                                          | - | - | - |
| 6 <sup>th</sup> | -                                                                                                           | -                                          | -                                          | - | - | - |
| Row             | Required knowledge accuracy of the in-line, differential elements of $MI_{25}$ during the measurement phase |                                            |                                            |   |   |   |
| 4 <sup>th</sup> | -                                                                                                           | -                                          | -                                          | - | - | - |
| 5 <sup>th</sup> | $\delta MI_{25,51} \leq 5.0 \cdot 10^{-6}$                                                                  | $\delta MI_{25,52} \leq 1.4 \cdot 10^{-5}$ | $\delta MI_{25,53} \leq 5.0 \cdot 10^{-6}$ | - | - | - |
| 6 <sup>th</sup> | -                                                                                                           | -                                          | -                                          | - | - | - |
| Row             | Required knowledge accuracy of the in-line, differential elements of $MI_{36}$ during the measurement phase |                                            |                                            |   |   |   |
| 4 <sup>th</sup> | -                                                                                                           | -                                          | -                                          | - | - | - |
| 5 <sup>th</sup> | -                                                                                                           | -                                          | -                                          | - | - | - |
| 6 <sup>th</sup> | $\delta MI_{36,61} \leq 5.0 \cdot 10^{-6}$                                                                  | $\delta MI_{36,62} \leq 5.0 \cdot 10^{-6}$ | $\delta MI_{36,63} \leq 1.4 \cdot 10^{-5}$ | - | - | - |
| Row             | Maximum measurement error of the in-line, differential elements of $MI_{14}$ at calibration                 |                                            |                                            |   |   |   |
| 4 <sup>th</sup> | $\delta MI_{14,41} \leq 4.7 \cdot 10^{-6}$                                                                  | $\delta MI_{14,42} \leq 4.5 \cdot 10^{-6}$ | $\delta MI_{14,43} \leq 4.5 \cdot 10^{-6}$ | - | - | - |
| 5 <sup>th</sup> | -                                                                                                           | -                                          | -                                          | - | - | - |
| 6 <sup>th</sup> | -                                                                                                           | -                                          | -                                          | - | - | - |

| Row             | Maximum measurement error of the in-line, differential elements of $MI_{25}$ at calibration |                                            |                                            |   |   |   |
|-----------------|---------------------------------------------------------------------------------------------|--------------------------------------------|--------------------------------------------|---|---|---|
| 4 <sup>th</sup> | -                                                                                           | -                                          | -                                          | - | - | - |
| 5 <sup>th</sup> | $\delta MI_{25,51} \leq 4.5 \cdot 10^{-6}$                                                  | $\delta MI_{25,52} \leq 4.7 \cdot 10^{-6}$ | $\delta MI_{25,53} \leq 4.5 \cdot 10^{-6}$ | - | - | - |
| 6 <sup>th</sup> | -                                                                                           | -                                          | -                                          | - | - | - |
| Row             | Maximum measurement error of the in-line, differential elements of $MI_{36}$ at calibration |                                            |                                            |   |   |   |
| 4 <sup>th</sup> | -                                                                                           | -                                          | -                                          | - | - | - |
| 5 <sup>th</sup> | -                                                                                           | -                                          | -                                          | - | - | - |
| 6 <sup>th</sup> | $\delta MI_{36,61} \leq 4.5 \cdot 10^{-6}$                                                  | $\delta MI_{36,62} \leq 4.5 \cdot 10^{-6}$ | $\delta MI_{36,63} \leq 4.7 \cdot 10^{-6}$ | - | - | - |

| Row             | Maximum variation of the in-line, differential elements of $MI_{14}$ between calibration phases |                                             |                                             |   |   |   |
|-----------------|-------------------------------------------------------------------------------------------------|---------------------------------------------|---------------------------------------------|---|---|---|
| 4 <sup>th</sup> | $\delta MI_{14,41} \leq 9.05 \cdot 10^{-6}$                                                     | $\delta MI_{14,42} \leq 5.0 \cdot 10^{-7}$  | $\delta MI_{14,43} \leq 5.0 \cdot 10^{-7}$  | - | - | - |
| 5 <sup>th</sup> | -                                                                                               | -                                           | -                                           | - | - | - |
| 6 <sup>th</sup> | -                                                                                               | -                                           | -                                           | - | - | - |
| Row             | Maximum variation of the in-line, differential elements of $MI_{25}$ between calibration phases |                                             |                                             |   |   |   |
| 4 <sup>th</sup> | -                                                                                               | -                                           | -                                           | - | - | - |
| 5 <sup>th</sup> | $\delta MI_{25,51} \leq 5.0 \cdot 10^{-7}$                                                      | $\delta MI_{25,52} \leq 9.05 \cdot 10^{-6}$ | $\delta MI_{25,53} \leq 5.0 \cdot 10^{-7}$  | - | - | - |
| 6 <sup>th</sup> | -                                                                                               | -                                           | -                                           | - | - | - |
| Row             | Maximum variation of the in-line, differential elements of $MI_{36}$ between calibration phases |                                             |                                             |   |   |   |
| 4 <sup>th</sup> | -                                                                                               | -                                           | -                                           | - | - | - |
| 5 <sup>th</sup> | -                                                                                               | -                                           | -                                           | - | - | - |
| 6 <sup>th</sup> | $\delta MI_{36,61} \leq 5.0 \cdot 10^{-7}$                                                      | $\delta MI_{36,62} \leq 5.0 \cdot 10^{-7}$  | $\delta MI_{36,63} \leq 9.05 \cdot 10^{-6}$ | - | - | - |

Table 6.1-1: Knowledge accuracy requirements of the in-line elements of  $[MI]_{d,14}$ ,  $[MI]_{d,25}$ ,  $[MI]_{d,36}$  ( $\cong$  in-line differential scale factors, misalignments and couplings) during the measurement phases, and apportionement between measurement errors at calibration and stability between calibration phases.

| Row             | Maximum value in the MBW of the in-line, differential elements of $\delta MI_{14}$ SD [ $Hz^{-1/2}$ ] |                                            |                                            |   |   |   |
|-----------------|-------------------------------------------------------------------------------------------------------|--------------------------------------------|--------------------------------------------|---|---|---|
| 4 <sup>th</sup> | $\delta MI_{14,41} \leq 7.0 \cdot 10^{-7}$                                                            | $\delta MI_{14,42} \leq 1.0 \cdot 10^{-8}$ | $\delta MI_{14,43} \leq 1.0 \cdot 10^{-8}$ | - | - | - |
| 5 <sup>th</sup> | -                                                                                                     | -                                          | -                                          | - | - | - |
| 6 <sup>th</sup> | -                                                                                                     | -                                          | -                                          | - | - | - |
| Row             | Maximum value in the MBW of the in-line, differential elements of $\delta MI_{25}$ SD [ $Hz^{-1/2}$ ] |                                            |                                            |   |   |   |
| 4 <sup>th</sup> | -                                                                                                     | -                                          | -                                          | - | - | - |
| 5 <sup>th</sup> | $\delta MI_{25,51} \leq 1.0 \cdot 10^{-8}$                                                            | $\delta MI_{25,52} \leq 7.0 \cdot 10^{-7}$ | $\delta MI_{25,53} \leq 1.0 \cdot 10^{-8}$ | - | - | - |
| 6 <sup>th</sup> | -                                                                                                     | -                                          | -                                          | - | - | - |
| Row             | Maximum value in the MBW of the in-line, differential elements of $\delta MI_{36}$ SD [ $Hz^{-1/2}$ ] |                                            |                                            |   |   |   |
| 4 <sup>th</sup> | -                                                                                                     | -                                          | -                                          | - | - | - |
| 5 <sup>th</sup> | -                                                                                                     | -                                          | -                                          | - | - | - |
| 6 <sup>th</sup> | $\delta MI_{36,61} \leq 1.0 \cdot 10^{-8}$                                                            | $\delta MI_{36,62} \leq 1.0 \cdot 10^{-8}$ | $\delta MI_{36,63} \leq 7.0 \cdot 10^{-7}$ | - | - | - |

Table 6.1-2: Specification for the maximum value in the MBW of the spectral density of the in-line, elements of  $[\delta MI]_{d,14}$ ,  $[\delta MI]_{d,25}$ ,  $[\delta MI]_{d,36}$  during the measurement phases.

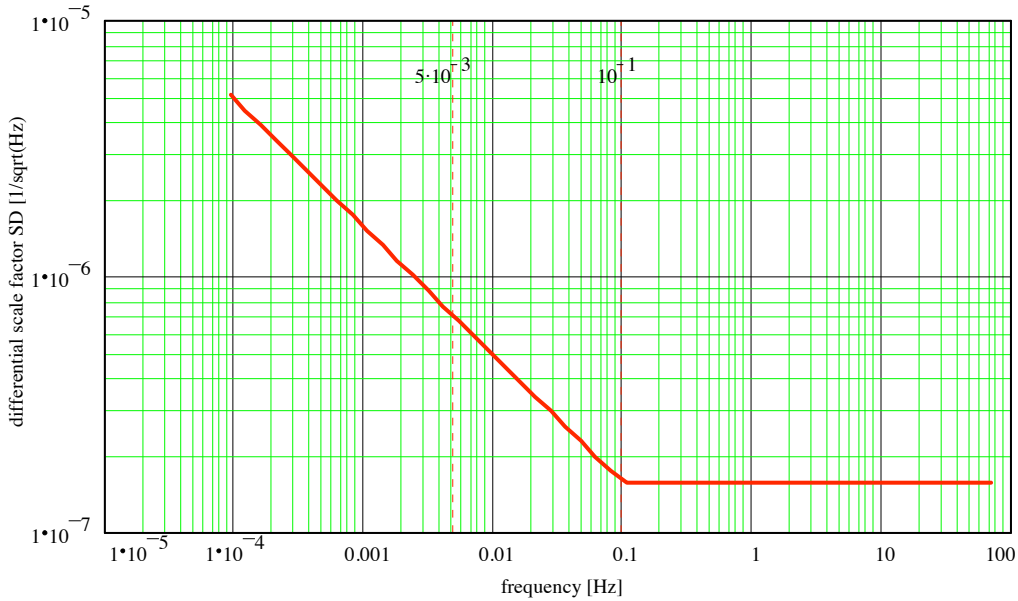


Figure 6.1-2: Spectral density upper limits for  $\delta\tilde{K}_{d,14,X}^W(v)$ ,  $\delta\tilde{K}_{d,25,Y}^W(v)$ ,  $\delta\tilde{K}_{d,36,Z}^W(v)$

6.1.1.2 Non-Gravitational Linear Acceleration Control Requirements

The requirements on the limits of the components of the non-gravitational linear accelerations of the spacecraft COM in the GRF ( $D_X, D_Y, D_Z$ ) are listed in Table 6.1-3. The plots of the spectral density limits for  $\tilde{D}_X^W(v)$ ,  $\tilde{D}_Y^W(v)$ ,  $\tilde{D}_Z^W(v)$ , are provides in Figure 6.1-3 where also the extension of these limits outside the MBW is shown.

Note that these requirements are strictly control requirements only for  $D_X$ . Since the cross-track and radial components of the drag are not controlled by the ion propulsion, the requirements for  $D_Y, D_Z$  must be intended as requirements for the environment in which the satellite will fly: is shall such that the specified limits on  $D_Y, D_Z$  (maximum value and spectral density) are not exceeded, in order to guarantee the fulfillment of the global gravimetric requirement.

| Quantity                                                                 | Requirement                                                          |
|--------------------------------------------------------------------------|----------------------------------------------------------------------|
| maximum value below the MBW (DC to 5 mHz)                                |                                                                      |
| $D_X^0, D_Y^0, D_Z^0$                                                    | $\leq 1 \cdot 10^{-6} \text{ m/s}^2$                                 |
| maximum value in the MBW ( $5 \text{ mHz} \leq v \leq 100 \text{ mHz}$ ) |                                                                      |
| $\tilde{D}_X^W(v)$                                                       | $\leq 2.5 \cdot 10^{-8} \text{ m/s}^2/\text{Hz}^{1/2}$               |
| $\tilde{D}_Y^W(v), \tilde{D}_Z^W(v)$                                     | $\leq 1 \cdot 10^{-7} \frac{0.005}{v} \text{ m/s}^2/\text{Hz}^{1/2}$ |

Table 6.1-3: Control requirements of the non-gravitational accelerations of the spacecraft COM

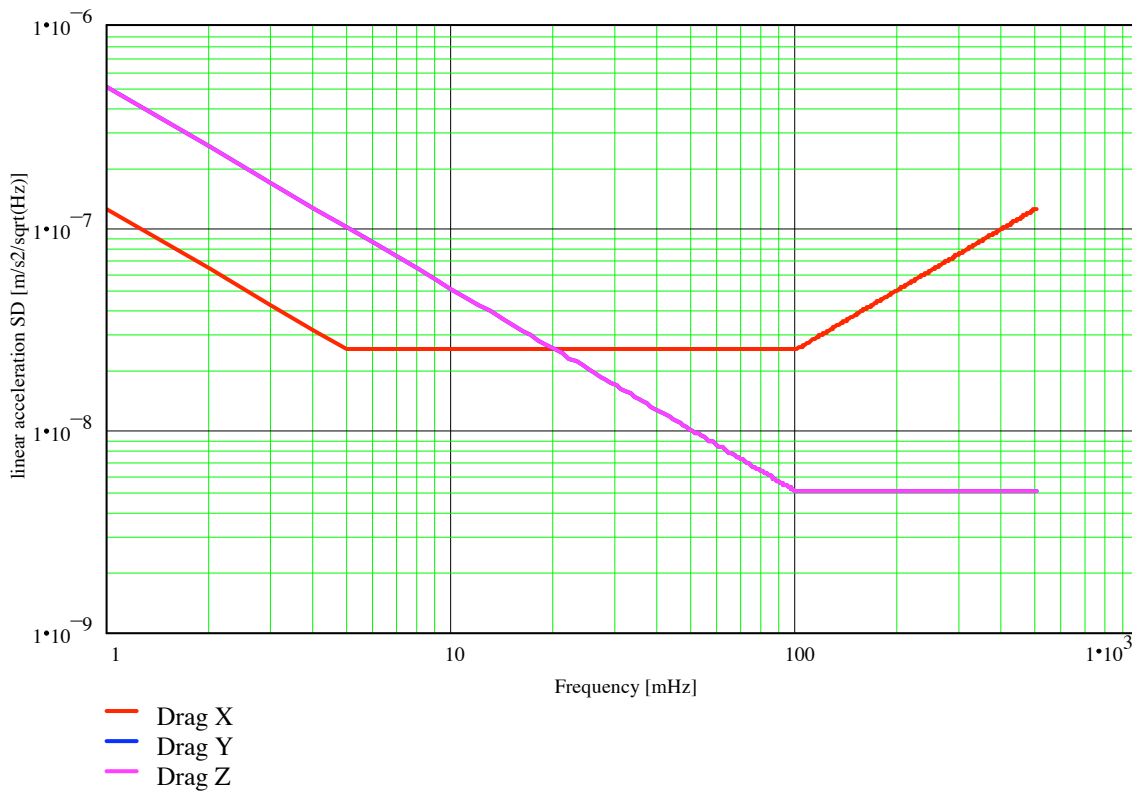


Figure 6.1-3: Spectral density upper limits for  $\tilde{D}_X^W(v)$ ,  $\tilde{D}_Y^W(v)$ ,  $\tilde{D}_Z^W(v)$

### 6.1.2 C.2.1: Coupling with the Angular Acceleration of the Satellite About its COM

From the equation (5.2.3) requirements are derived for:

- the “in line” elements of the matrices  $[\delta MI]_{c,14}$ ,  $[\delta MI]_{c,25}$ ,  $[\delta MI]_{c,36}$  related to the differences between the actual values of the common misalignments and couplings for the accelerometer in-line axes during the measurement phases (between the periodic in-flight calibrations of the Gradiometer) and those measured at the Gradiometer calibrations;
- the control of the angular accelerations about the satellite COM.

#### 6.1.2.1 Common, Misalignments and Couplings Knowledge and Stability Requirements

The requirements on the in-line elements of  $[\delta MI]_{c,14}$ ,  $[\delta MI]_{c,25}$ ,  $[\delta MI]_{c,36}$  during the measurement phases are listed in Table 6.1-4 and Table 6.1-5. The overall requirement on the maximum value below the MBW is further broken down in:

- maximum measurement error of the elements of the matrix  $MI_{ij}$  at the calibration;
- maximum variation of these elements during the scientific measurement phase between two successive calibrations.

Table 6.1-4 and Table 6.1-5 also report the elements of the ICMs specified in the previous section. The elements which are object of the current specification are highlighted in yellow.

| Row             | Required knowledge accuracy of the in-line, common elements of $MI_{14}$ (misalignment and coupling) |                                            |                                            |                                            |                                            |                                            |
|-----------------|------------------------------------------------------------------------------------------------------|--------------------------------------------|--------------------------------------------|--------------------------------------------|--------------------------------------------|--------------------------------------------|
| 4 <sup>th</sup> | $\delta MI_{14,41} \leq 1.4 \cdot 10^{-5}$                                                           | $\delta MI_{14,42} \leq 5.0 \cdot 10^{-6}$ | $\delta MI_{14,43} \leq 5.0 \cdot 10^{-6}$ | -                                          | $\delta MI_{14,45} \leq 5.1 \cdot 10^{-5}$ | $\delta MI_{14,46} \leq 5.1 \cdot 10^{-5}$ |
| 5 <sup>th</sup> | -                                                                                                    | -                                          | -                                          | -                                          | -                                          | -                                          |
| 6 <sup>th</sup> | -                                                                                                    | -                                          | -                                          | -                                          | -                                          | -                                          |
| Row             | Required knowledge accuracy of the in-line, common elements of $MI_{25}$ (misalignment and coupling) |                                            |                                            |                                            |                                            |                                            |
| 4 <sup>th</sup> | -                                                                                                    | -                                          | -                                          | -                                          | -                                          | -                                          |
| 5 <sup>th</sup> | $\delta MI_{25,51} \leq 5.0 \cdot 10^{-6}$                                                           | $\delta MI_{25,52} \leq 1.4 \cdot 10^{-5}$ | $\delta MI_{25,53} \leq 5.0 \cdot 10^{-6}$ | $\delta MI_{25,54} \leq 5.1 \cdot 10^{-5}$ | -                                          | $\delta MI_{25,56} \leq 5.1 \cdot 10^{-5}$ |
| 6 <sup>th</sup> | -                                                                                                    | -                                          | -                                          | -                                          | -                                          | -                                          |
| Row             | Required knowledge accuracy of the in-line, common elements of $MI_{36}$ (misalignment and coupling) |                                            |                                            |                                            |                                            |                                            |
| 4 <sup>th</sup> | -                                                                                                    | -                                          | -                                          | -                                          | -                                          | -                                          |
| 5 <sup>th</sup> | -                                                                                                    | -                                          | -                                          | -                                          | -                                          | -                                          |
| 6 <sup>th</sup> | $\delta MI_{36,61} \leq 5.0 \cdot 10^{-6}$                                                           | $\delta MI_{36,62} \leq 5.0 \cdot 10^{-6}$ | $\delta MI_{36,63} \leq 1.4 \cdot 10^{-5}$ | $\delta MI_{36,64} \leq 5.1 \cdot 10^{-5}$ | $\delta MI_{36,65} \leq 5.1 \cdot 10^{-5}$ | -                                          |

| Row             | Maximum measurement error of the in-line, common elements of $MI_{14}$ (misal. + coupling) at calibration |                                            |                                            |                                            |                                            |                                            |
|-----------------|-----------------------------------------------------------------------------------------------------------|--------------------------------------------|--------------------------------------------|--------------------------------------------|--------------------------------------------|--------------------------------------------|
| 4 <sup>th</sup> | $\delta MI_{14,41} \leq 4.7 \cdot 10^{-6}$                                                                | $\delta MI_{14,42} \leq 4.5 \cdot 10^{-6}$ | $\delta MI_{14,43} \leq 4.5 \cdot 10^{-6}$ | -                                          | $\delta MI_{14,45} \leq 5.0 \cdot 10^{-5}$ | $\delta MI_{14,46} \leq 5.0 \cdot 10^{-5}$ |
| 5 <sup>th</sup> | -                                                                                                         | -                                          | -                                          | -                                          | -                                          | -                                          |
| 6 <sup>th</sup> | -                                                                                                         | -                                          | -                                          | -                                          | -                                          | -                                          |
| Row             | Maximum measurement error of the in-line, common elements of $MI_{25}$ (misal. + coupling) at calibration |                                            |                                            |                                            |                                            |                                            |
| 4 <sup>th</sup> | -                                                                                                         | -                                          | -                                          | -                                          | -                                          | -                                          |
| 5 <sup>th</sup> | $\delta MI_{25,51} \leq 4.5 \cdot 10^{-6}$                                                                | $\delta MI_{25,52} \leq 4.7 \cdot 10^{-6}$ | $\delta MI_{25,53} \leq 4.5 \cdot 10^{-6}$ | $\delta MI_{25,54} \leq 5.0 \cdot 10^{-5}$ | -                                          | $\delta MI_{25,56} \leq 5.0 \cdot 10^{-5}$ |
| 6 <sup>th</sup> | -                                                                                                         | -                                          | -                                          | -                                          | -                                          | -                                          |
| Row             | Maximum measurement error of the in-line, common elements of $MI_{36}$ (misal. + coupling) at calibration |                                            |                                            |                                            |                                            |                                            |
| 4 <sup>th</sup> | -                                                                                                         | -                                          | -                                          | -                                          | -                                          | -                                          |
| 5 <sup>th</sup> | -                                                                                                         | -                                          | -                                          | -                                          | -                                          | -                                          |
| 6 <sup>th</sup> | $\delta MI_{36,61} \leq 4.5 \cdot 10^{-6}$                                                                | $\delta MI_{36,62} \leq 4.5 \cdot 10^{-6}$ | $\delta MI_{36,63} \leq 4.7 \cdot 10^{-6}$ | $\delta MI_{36,64} \leq 5.0 \cdot 10^{-5}$ | $\delta MI_{36,65} \leq 5.0 \cdot 10^{-5}$ | -                                          |

| Row             | Maximum variation of the in-line, common elements of $MI_{14}$ (misal. + coupling) between calibration phases |                                             |                                             |                                            |                                            |                                            |
|-----------------|---------------------------------------------------------------------------------------------------------------|---------------------------------------------|---------------------------------------------|--------------------------------------------|--------------------------------------------|--------------------------------------------|
| 4 <sup>th</sup> | $\delta MI_{14,41} \leq 9.05 \cdot 10^{-6}$                                                                   | $\delta MI_{14,42} \leq 5.0 \cdot 10^{-7}$  | $\delta MI_{14,43} \leq 5.0 \cdot 10^{-7}$  | -                                          | $\delta MI_{14,45} \leq 1.0 \cdot 10^{-6}$ | $\delta MI_{14,46} \leq 1.0 \cdot 10^{-6}$ |
| 5 <sup>th</sup> | -                                                                                                             | -                                           | -                                           | -                                          | -                                          | -                                          |
| 6 <sup>th</sup> | -                                                                                                             | -                                           | -                                           | -                                          | -                                          | -                                          |
| Row             | Maximum variation of the in-line, common elements of $MI_{25}$ (misal. + coupling) between calibration phases |                                             |                                             |                                            |                                            |                                            |
| 4 <sup>th</sup> | -                                                                                                             | -                                           | -                                           | -                                          | -                                          | -                                          |
| 5 <sup>th</sup> | $\delta MI_{25,51} \leq 5.0 \cdot 10^{-7}$                                                                    | $\delta MI_{25,52} \leq 9.05 \cdot 10^{-6}$ | $\delta MI_{25,53} \leq 5.0 \cdot 10^{-7}$  | $\delta MI_{25,54} \leq 1.0 \cdot 10^{-6}$ | -                                          | $\delta MI_{25,56} \leq 1.0 \cdot 10^{-6}$ |
| 6 <sup>th</sup> | -                                                                                                             | -                                           | -                                           | -                                          | -                                          | -                                          |
| Row             | Maximum variation of the in-line, common elements of $MI_{36}$ (misal. + coupling) between calibration phases |                                             |                                             |                                            |                                            |                                            |
| 4 <sup>th</sup> | -                                                                                                             | -                                           | -                                           | -                                          | -                                          | -                                          |
| 5 <sup>th</sup> | -                                                                                                             | -                                           | -                                           | -                                          | -                                          | -                                          |
| 6 <sup>th</sup> | $\delta MI_{36,61} \leq 5.0 \cdot 10^{-7}$                                                                    | $\delta MI_{36,62} \leq 5.0 \cdot 10^{-7}$  | $\delta MI_{36,63} \leq 9.05 \cdot 10^{-6}$ | $\delta MI_{36,64} \leq 1.0 \cdot 10^{-6}$ | $\delta MI_{36,65} \leq 1.0 \cdot 10^{-6}$ | -                                          |

Table 6.1-4: Knowledge accuracy requirements of the in-line elements of  $[MI]_{c,14}$ ,  $[MI]_{c,25}$ ,  $[MI]_{c,36}$  ( $\cong$  in-line common misalignments and couplings) during the measurement phases, and apportionement between measurement errors at calibration and stability between calibration phases.

| Row             | Maximum value in the MBW of the in-line, common elements of $\delta MI_{14}$ (misal. + coupling) SD [Hz <sup>-1/2</sup> ] |                                            |                                            |                                            |                                            |                                            |
|-----------------|---------------------------------------------------------------------------------------------------------------------------|--------------------------------------------|--------------------------------------------|--------------------------------------------|--------------------------------------------|--------------------------------------------|
| 4 <sup>th</sup> | $\delta MI_{14,41} \leq 7.0 \cdot 10^{-7}$                                                                                | $\delta MI_{14,42} \leq 1.0 \cdot 10^{-8}$ | $\delta MI_{14,43} \leq 1.0 \cdot 10^{-8}$ | -                                          | $\delta MI_{14,45} \leq 1.0 \cdot 10^{-8}$ | $\delta MI_{14,46} \leq 1.0 \cdot 10^{-8}$ |
| 5 <sup>th</sup> | -                                                                                                                         | -                                          | -                                          | -                                          | -                                          | -                                          |
| 6 <sup>th</sup> | -                                                                                                                         | -                                          | -                                          | -                                          | -                                          | -                                          |
| Row             | Maximum value in the MBW of the in-line, common elements of $\delta MI_{25}$ (misal. + coupling) SD [Hz <sup>-1/2</sup> ] |                                            |                                            |                                            |                                            |                                            |
| 4 <sup>th</sup> | -                                                                                                                         | -                                          | -                                          | -                                          | -                                          | -                                          |
| 5 <sup>th</sup> | $\delta MI_{25,51} \leq 1.0 \cdot 10^{-8}$                                                                                | $\delta MI_{25,52} \leq 7.0 \cdot 10^{-7}$ | $\delta MI_{25,53} \leq 1.0 \cdot 10^{-8}$ | $\delta MI_{25,54} \leq 1.0 \cdot 10^{-8}$ | -                                          | $\delta MI_{25,56} \leq 1.0 \cdot 10^{-8}$ |
| 6 <sup>th</sup> | -                                                                                                                         | -                                          | -                                          | -                                          | -                                          | -                                          |
| Row             | Maximum value in the MBW of the in-line, common elements of $\delta MI_{36}$ (misal. + coupling) SD [Hz <sup>-1/2</sup> ] |                                            |                                            |                                            |                                            |                                            |
| 4 <sup>th</sup> | -                                                                                                                         | -                                          | -                                          | -                                          | -                                          | -                                          |
| 5 <sup>th</sup> | -                                                                                                                         | -                                          | -                                          | -                                          | -                                          | -                                          |
| 6 <sup>th</sup> | $\delta MI_{36,61} \leq 1.0 \cdot 10^{-8}$                                                                                | $\delta MI_{36,62} \leq 1.0 \cdot 10^{-8}$ | $\delta MI_{36,63} \leq 7.0 \cdot 10^{-7}$ | $\delta MI_{36,64} \leq 1.0 \cdot 10^{-8}$ | $\delta MI_{36,65} \leq 1.0 \cdot 10^{-8}$ | -                                          |

Table 6.1-5: Specification for the maximum value in the MBW of the spectral density of the in-line elements of  $[\delta MI]_{c,14}$ ,  $[\delta MI]_{c,25}$ ,  $[\delta MI]_{c,36}$  ( $\approx$  in-line common misalignments and couplings) during the measurement phases.

6.1.2.2 Angular Acceleration Control Requirements

The requirements on the control of the components of the angular accelerations of the spacecraft about its COM in the GRF ( $\dot{\omega}_X, \dot{\omega}_Y, \dot{\omega}_Z$ ) are listed in Table 6.1-6. The plots of the spectral density limits for  $\tilde{\omega}_X^W(\nu)$ ,  $\tilde{\omega}_Y^W(\nu)$ ,  $\tilde{\omega}_Z^W(\nu)$ , are provides in Figure 6.1-4 where also the extension of these limits outside the MBW is shown.

| Quantity                                                 | Requirement                                                                                                                                                                                                   |
|----------------------------------------------------------|---------------------------------------------------------------------------------------------------------------------------------------------------------------------------------------------------------------|
| maximum value below the MBW (DC to 5 mHz)                |                                                                                                                                                                                                               |
| $\dot{\omega}_X^0$                                       | $\leq 2 \cdot 10^{-6} \text{ rad/s}^2$                                                                                                                                                                        |
| $\dot{\omega}_Y^0, \dot{\omega}_Z^0$                     | $\leq 1 \cdot 10^{-6} \text{ rad/s}^2$                                                                                                                                                                        |
| maximum value in the MBW (5 mHz $\leq \nu \leq$ 100 mHz) |                                                                                                                                                                                                               |
| $\tilde{\omega}_X^W(\nu)$                                | $\leq 3.2 \cdot 10^{-7} \left( \frac{0.005}{\nu} \right)^2, \nu < 0.02 \text{ Hz}; \leq 3.2 \cdot 10^{-7} \left( \frac{0.005}{0.02} \right)^2, \nu \geq 0.02 \text{ Hz} \quad \text{rad/s}^2/\text{Hz}^{1/2}$ |
| $\tilde{\omega}_Y^W(\nu), \tilde{\omega}_Z^W(\nu)$       | $\leq 7.0 \cdot 10^{-8} \left( \frac{0.005}{\nu} \right)^2, \nu < 0.02 \text{ Hz}; \leq 7.0 \cdot 10^{-8} \left( \frac{0.005}{0.02} \right)^2, \nu \geq 0.02 \text{ Hz} \quad \text{rad/s}^2/\text{Hz}^{1/2}$ |

Table 6.1-6: Control requirements of the angular accelerations of the spacecraft about its COM

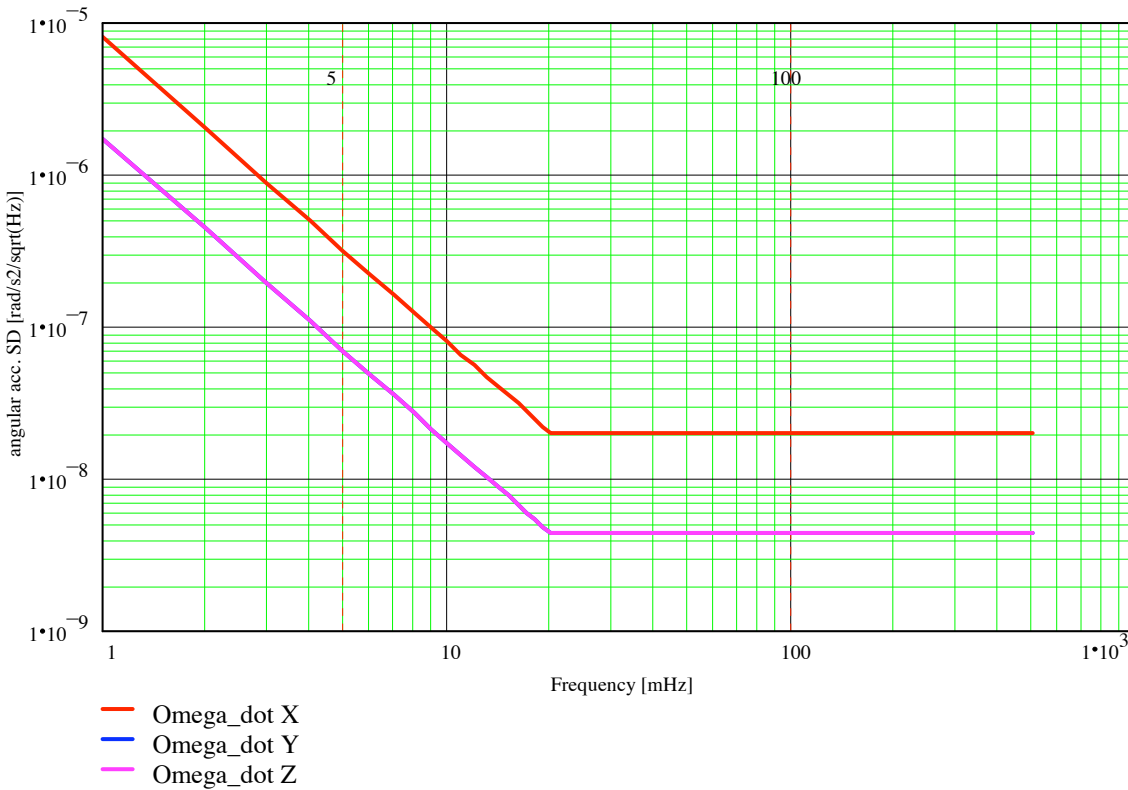


Figure 6.1-4: Spectral density upper limits for  $\tilde{\omega}_X^W(v)$ ,  $\tilde{\omega}_Y^W(v)$ ,  $\tilde{\omega}_Z^W(v)$

6.1.3 C.2.2: Coupling with the centrifugal accelerations and the GGT

From the equation (5.2.5) requirements are derived for:

- the “in-line” elements of the matrices  $[\delta MI]_{c,14}$ ,  $[\delta MI]_{c,25}$ ,  $[\delta MI]_{c,36}$  not yet constrained by the equation (5.2.3), i.e. the elements related to differences between the actual values of the common scale factors for the accelerometer in-line axes during the measurement phases (between the periodic in-flight calibrations of the Gradiometer) and those measured at the Gradiometer calibrations;
- the control of the angular velocities about the satellite COM.

6.1.3.1 Common Scale Factors Knowledge and Stability Requirements

The requirements on the common scale factors for the accelerometer in-line axes during the measurement phases are listed in and Table 6.1-8. The overall requirement on the maximum value below the MBW is further broken down in:

- maximum measurement error of the common scale factors at the calibration;
- maximum variation of these elements during the measurement phase.

and Table 6.1-8 also report the elements of the ICMs specified in the previous section. The elements which are object of the current specification are highlighted in yellow.

The spectral density requirement of the in-line, common scale factors,  $\delta\tilde{K}_{c,14,X}^W$ ,  $\delta\tilde{K}_{c,25,Y}^W$ ,  $\delta\tilde{K}_{c,36,Z}^W$  is expressed not just by a constant value in the MBW, but by a limit which is a function of the frequency (with maximum in the MBW specified in Table 6.1-8), as shown in Figure 6.1-5.

| Row             | Required knowledge accuracy of the in-line, common scale factor element of $MI_{14}$                  |                                             |                                             |                                             |                                             |                                             |
|-----------------|-------------------------------------------------------------------------------------------------------|---------------------------------------------|---------------------------------------------|---------------------------------------------|---------------------------------------------|---------------------------------------------|
| 4 <sup>th</sup> | $\delta MI_{14,41} \leq 1.4 \cdot 10^{-5}$                                                            | $\delta MI_{14,42} \leq 5.0 \cdot 10^{-6}$  | $\delta MI_{14,43} \leq 5.0 \cdot 10^{-6}$  | $\delta MI_{14,44} \leq 2.02 \cdot 10^{-3}$ | $\delta MI_{14,45} \leq 5.1 \cdot 10^{-5}$  | $\delta MI_{14,46} \leq 5.1 \cdot 10^{-5}$  |
| 5 <sup>th</sup> | -                                                                                                     | -                                           | -                                           | -                                           | -                                           | -                                           |
| 6 <sup>th</sup> | -                                                                                                     | -                                           | -                                           | -                                           | -                                           | -                                           |
| Row             | Required knowledge accuracy of the in-line, common scale factor element of $MI_{25}$                  |                                             |                                             |                                             |                                             |                                             |
| 4 <sup>th</sup> | -                                                                                                     | -                                           | -                                           | -                                           | -                                           | -                                           |
| 5 <sup>th</sup> | $\delta MI_{25,51} \leq 5.0 \cdot 10^{-6}$                                                            | $\delta MI_{25,52} \leq 1.4 \cdot 10^{-5}$  | $\delta MI_{25,53} \leq 5.0 \cdot 10^{-6}$  | $\delta MI_{25,54} \leq 5.1 \cdot 10^{-5}$  | $\delta MI_{25,55} \leq 2.02 \cdot 10^{-3}$ | $\delta MI_{25,56} \leq 5.1 \cdot 10^{-5}$  |
| 6 <sup>th</sup> | -                                                                                                     | -                                           | -                                           | -                                           | -                                           | -                                           |
| Row             | Required knowledge accuracy of the in-line, common scale factor element of $MI_{36}$                  |                                             |                                             |                                             |                                             |                                             |
| 4 <sup>th</sup> | -                                                                                                     | -                                           | -                                           | -                                           | -                                           | -                                           |
| 5 <sup>th</sup> | -                                                                                                     | -                                           | -                                           | -                                           | -                                           | -                                           |
| 6 <sup>th</sup> | $\delta MI_{36,61} \leq 5.0 \cdot 10^{-6}$                                                            | $\delta MI_{36,62} \leq 5.0 \cdot 10^{-6}$  | $\delta MI_{36,63} \leq 1.4 \cdot 10^{-5}$  | $\delta MI_{36,64} \leq 5.1 \cdot 10^{-5}$  | $\delta MI_{36,65} \leq 5.1 \cdot 10^{-5}$  | $\delta MI_{36,66} \leq 2.02 \cdot 10^{-3}$ |
| Row             | Maximum measurement error of the in-line, common scale factor element of $MI_{14}$ at calibration     |                                             |                                             |                                             |                                             |                                             |
| 4 <sup>th</sup> | $\delta MI_{14,41} \leq 4.7 \cdot 10^{-6}$                                                            | $\delta MI_{14,42} \leq 4.5 \cdot 10^{-6}$  | $\delta MI_{14,43} \leq 4.5 \cdot 10^{-6}$  | $\delta MI_{14,44} \leq 2.0 \cdot 10^{-3}$  | $\delta MI_{14,45} \leq 5.0 \cdot 10^{-5}$  | $\delta MI_{14,46} \leq 5.0 \cdot 10^{-5}$  |
| 5 <sup>th</sup> | -                                                                                                     | -                                           | -                                           | -                                           | -                                           | -                                           |
| 6 <sup>th</sup> | -                                                                                                     | -                                           | -                                           | -                                           | -                                           | -                                           |
| Row             | Maximum measurement error of the in-line, common scale factor element of $MI_{25}$ at calibration     |                                             |                                             |                                             |                                             |                                             |
| 4 <sup>th</sup> | -                                                                                                     | -                                           | -                                           | -                                           | -                                           | -                                           |
| 5 <sup>th</sup> | $\delta MI_{25,51} \leq 4.5 \cdot 10^{-6}$                                                            | $\delta MI_{25,52} \leq 4.7 \cdot 10^{-6}$  | $\delta MI_{25,53} \leq 4.5 \cdot 10^{-6}$  | $\delta MI_{25,54} \leq 5.0 \cdot 10^{-5}$  | $\delta MI_{25,55} \leq 2.0 \cdot 10^{-3}$  | $\delta MI_{25,56} \leq 5.0 \cdot 10^{-5}$  |
| 6 <sup>th</sup> | -                                                                                                     | -                                           | -                                           | -                                           | -                                           | -                                           |
| Row             | Maximum measurement error of the in-line, common scale factor element of $MI_{36}$ at calibration     |                                             |                                             |                                             |                                             |                                             |
| 4 <sup>th</sup> | -                                                                                                     | -                                           | -                                           | -                                           | -                                           | -                                           |
| 5 <sup>th</sup> | -                                                                                                     | -                                           | -                                           | -                                           | -                                           | -                                           |
| 6 <sup>th</sup> | $\delta MI_{36,61} \leq 4.5 \cdot 10^{-6}$                                                            | $\delta MI_{36,62} \leq 4.5 \cdot 10^{-6}$  | $\delta MI_{36,63} \leq 4.7 \cdot 10^{-6}$  | $\delta MI_{36,64} \leq 5.0 \cdot 10^{-5}$  | $\delta MI_{36,65} \leq 5.0 \cdot 10^{-5}$  | $\delta MI_{36,66} \leq 2.0 \cdot 10^{-3}$  |
| Row             | Maximum variation of the in-line, common scale factor element of $MI_{14}$ between calibration phases |                                             |                                             |                                             |                                             |                                             |
| 4 <sup>th</sup> | $\delta MI_{14,41} \leq 9.05 \cdot 10^{-6}$                                                           | $\delta MI_{14,42} \leq 5.0 \cdot 10^{-7}$  | $\delta MI_{14,43} \leq 5.0 \cdot 10^{-7}$  | $\delta MI_{14,44} \leq 2.0 \cdot 10^{-5}$  | $\delta MI_{14,45} \leq 1.0 \cdot 10^{-6}$  | $\delta MI_{14,46} \leq 1.0 \cdot 10^{-6}$  |
| 5 <sup>th</sup> | -                                                                                                     | -                                           | -                                           | -                                           | -                                           | -                                           |
| 6 <sup>th</sup> | -                                                                                                     | -                                           | -                                           | -                                           | -                                           | -                                           |
| Row             | Maximum variation of the in-line, common scale factor element of $MI_{25}$ between calibration phases |                                             |                                             |                                             |                                             |                                             |
| 4 <sup>th</sup> | -                                                                                                     | -                                           | -                                           | -                                           | -                                           | -                                           |
| 5 <sup>th</sup> | $\delta MI_{25,51} \leq 5.0 \cdot 10^{-7}$                                                            | $\delta MI_{25,52} \leq 9.05 \cdot 10^{-6}$ | $\delta MI_{25,53} \leq 5.0 \cdot 10^{-7}$  | $\delta MI_{25,54} \leq 1.0 \cdot 10^{-6}$  | $\delta MI_{25,55} \leq 2.0 \cdot 10^{-5}$  | $\delta MI_{25,56} \leq 1.0 \cdot 10^{-6}$  |
| 6 <sup>th</sup> | -                                                                                                     | -                                           | -                                           | -                                           | -                                           | -                                           |
| Row             | Maximum variation of the in-line, common scale factor element of $MI_{36}$ between calibration phases |                                             |                                             |                                             |                                             |                                             |
| 4 <sup>th</sup> | -                                                                                                     | -                                           | -                                           | -                                           | -                                           | -                                           |
| 5 <sup>th</sup> | -                                                                                                     | -                                           | -                                           | -                                           | -                                           | -                                           |
| 6 <sup>th</sup> | $\delta MI_{36,61} \leq 5.0 \cdot 10^{-7}$                                                            | $\delta MI_{36,62} \leq 5.0 \cdot 10^{-7}$  | $\delta MI_{36,63} \leq 9.05 \cdot 10^{-6}$ | $\delta MI_{36,64} \leq 1.0 \cdot 10^{-6}$  | $\delta MI_{36,65} \leq 1.0 \cdot 10^{-6}$  | $\delta MI_{36,66} \leq 2.0 \cdot 10^{-5}$  |

Table 6.1-7: Knowledge accuracy requirements of the in-line common scale factor element of  $[MI]_{c,14}$ ,  $[MI]_{c,25}$ ,  $[MI]_{c,36}$  during the measurement phases, and apportionment between measurement errors at calibration and stability between calibration phases.

| Row             | Maximum value in the MBW of the in-line, common scale factor element of $\delta MI_{14}$ SD [Hz <sup>-1/2</sup> ] |                                            |                                            |                                            |                                            |                                            |
|-----------------|-------------------------------------------------------------------------------------------------------------------|--------------------------------------------|--------------------------------------------|--------------------------------------------|--------------------------------------------|--------------------------------------------|
| 4 <sup>th</sup> | $\delta MI_{14,41} \leq 7.0 \cdot 10^{-7}$                                                                        | $\delta MI_{14,42} \leq 1.0 \cdot 10^{-8}$ | $\delta MI_{14,43} \leq 1.0 \cdot 10^{-8}$ | $\delta MI_{14,44} \leq 9.0 \cdot 10^{-7}$ | $\delta MI_{14,45} \leq 1.0 \cdot 10^{-8}$ | $\delta MI_{14,46} \leq 1.0 \cdot 10^{-8}$ |
| 5 <sup>th</sup> | -                                                                                                                 | -                                          | -                                          | -                                          | -                                          | -                                          |
| 6 <sup>th</sup> | -                                                                                                                 | -                                          | -                                          | -                                          | -                                          | -                                          |
| Row             | Maximum value in the MBW of the in-line, common scale factor element $\delta MI_{25}$ SD [Hz <sup>-1/2</sup> ]    |                                            |                                            |                                            |                                            |                                            |
| 4 <sup>th</sup> | -                                                                                                                 | -                                          | -                                          | -                                          | -                                          | -                                          |
| 5 <sup>th</sup> | $\delta MI_{25,51} \leq 1.0 \cdot 10^{-8}$                                                                        | $\delta MI_{25,52} \leq 7.0 \cdot 10^{-7}$ | $\delta MI_{25,53} \leq 1.0 \cdot 10^{-8}$ | $\delta MI_{25,54} \leq 1.0 \cdot 10^{-8}$ | $\delta MI_{25,55} \leq 9.0 \cdot 10^{-7}$ | $\delta MI_{25,56} \leq 1.0 \cdot 10^{-8}$ |
| 6 <sup>th</sup> | -                                                                                                                 | -                                          | -                                          | -                                          | -                                          | -                                          |
| Row             | Maximum value in the MBW of the in-line, common scale factor element of $\delta MI_{36}$ SD [Hz <sup>-1/2</sup> ] |                                            |                                            |                                            |                                            |                                            |
| 4 <sup>th</sup> | -                                                                                                                 | -                                          | -                                          | -                                          | -                                          | -                                          |
| 5 <sup>th</sup> | -                                                                                                                 | -                                          | -                                          | -                                          | -                                          | -                                          |
| 6 <sup>th</sup> | $\delta MI_{36,61} \leq 1.0 \cdot 10^{-8}$                                                                        | $\delta MI_{36,62} \leq 1.0 \cdot 10^{-8}$ | $\delta MI_{36,63} \leq 7.0 \cdot 10^{-7}$ | $\delta MI_{36,64} \leq 1.0 \cdot 10^{-8}$ | $\delta MI_{36,65} \leq 1.0 \cdot 10^{-8}$ | $\delta MI_{36,66} \leq 9.0 \cdot 10^{-7}$ |

Table 6.1-8: Specification for the maximum value in the MBW of the spectral density of the in-line common scale factor element of  $[\delta MI]_{c,14}$ ,  $[\delta MI]_{c,25}$ ,  $[\delta MI]_{c,36}$  during the measurement phases.

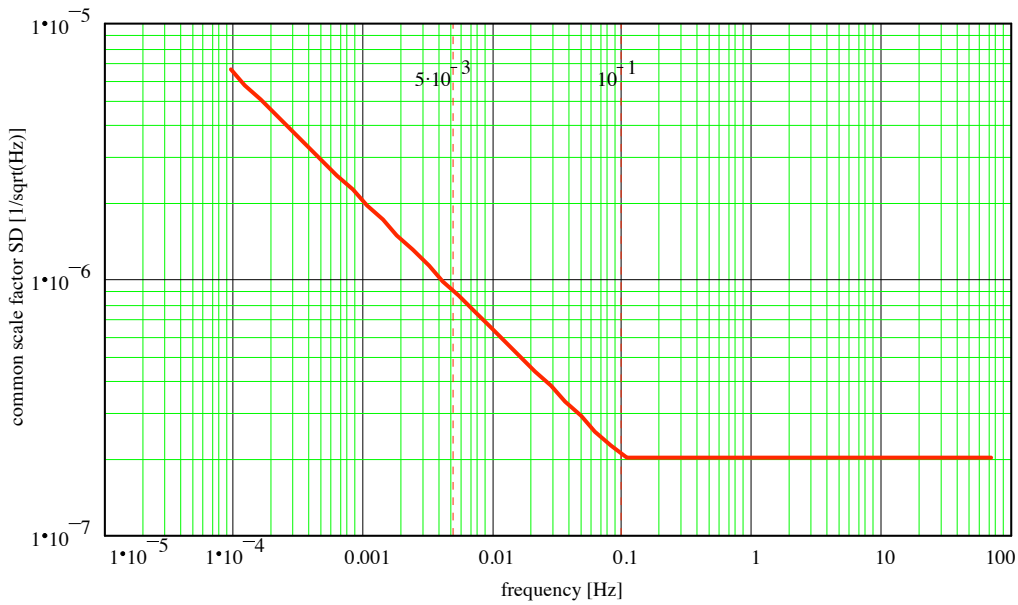


Figure 6.1-5: Spectral density upper limits for  $\delta \tilde{K}_{c,14,X}^W(v)$ ,  $\delta \tilde{K}_{c,25,Y}^W(v)$ ,  $\delta \tilde{K}_{c,36,Z}^W(v)$

### 6.1.3.2 Angular Rates Control Requirements

The requirements on the control of the components of the angular velocities of the spacecraft about its COM in the GRF ( $\omega_X$ ,  $\omega_Y$ ,  $\omega_Z$ ) are listed in Table 6.1-9. The plots of the spectral density limits for  $\tilde{\omega}_X^W(v)$ ,  $\tilde{\omega}_Y^W(v)$ ,  $\tilde{\omega}_Z^W(v)$ , are provides in Figure 6.1-6 where also the extension of these limits outside the MBW is shown.

| Quantity                                                 | Requirement                                                                                                                                                                    |
|----------------------------------------------------------|--------------------------------------------------------------------------------------------------------------------------------------------------------------------------------|
| maximum value below the MBW (DC to 5 mHz)                |                                                                                                                                                                                |
| $\omega_X^0, \omega_Z^0$                                 | $\leq 2 \cdot 10^{-4}$ rad/s                                                                                                                                                   |
| $\omega_Y^0$                                             | $\leq 1.2 \cdot 10^{-3}$ rad/s (*)                                                                                                                                             |
| maximum value in the MBW (5 mHz $\leq \nu \leq$ 100 mHz) |                                                                                                                                                                                |
| $\tilde{\omega}_X^W(\nu)$                                | $\leq 1.0 \cdot 10^{-5} \left(\frac{0.005}{\nu}\right)^2, \nu < 0.02$ Hz; $\leq 1.0 \cdot 10^{-5} \left(\frac{0.005}{0.02}\right)^2, \nu \geq 0.02$ Hz rad/s/Hz <sup>1/2</sup> |
| $\tilde{\omega}_Y^W(\nu)$                                | $\leq 5.0 \cdot 10^{-7} \left(\frac{0.005}{\nu}\right)^2, \nu < 0.02$ Hz; $\leq 5.0 \cdot 10^{-7} \left(\frac{0.005}{0.02}\right)^2, \nu \geq 0.02$ Hz rad/s/Hz <sup>1/2</sup> |
| $\tilde{\omega}_Z^W(\nu)$                                | $\leq 1.0 \cdot 10^{-6} \left(\frac{0.005}{\nu}\right)^2, \nu < 0.02$ Hz; $\leq 1.0 \cdot 10^{-6} \left(\frac{0.005}{0.02}\right)^2, \nu \geq 0.02$ Hz rad/s/Hz <sup>1/2</sup> |

(\*) the mean spin rate of the satellite about the Y axis is  $\sim 1.17 \cdot 10^{-3}$  rad/s

Table 6.1-9: Control requirements of the angular rates of the spacecraft about its COM

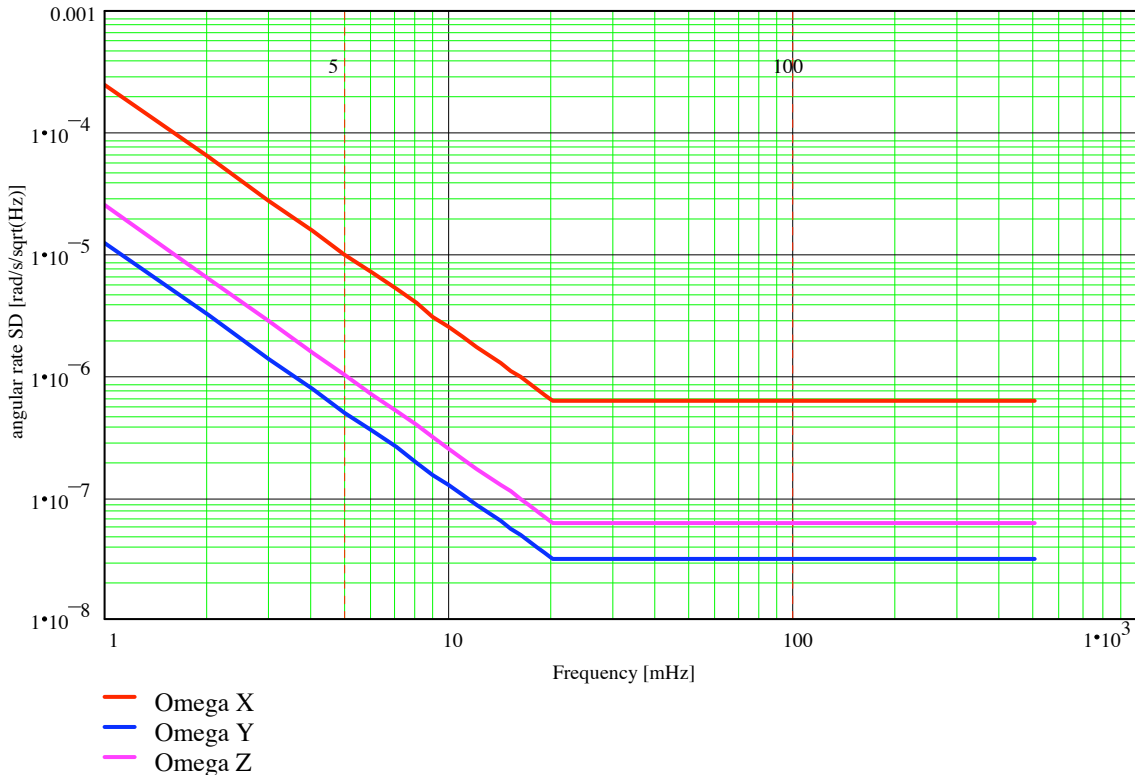


Figure 6.1-6: Spectral density upper limits for  $\tilde{\omega}_X^W(\nu)$ ,  $\tilde{\omega}_Y^W(\nu)$ ,  $\tilde{\omega}_Z^W(\nu)$

6.1.4 C.1.2: Couplings with COM Location and Stability in the OAGRF

From the equation (5.2.2) requirements are derived for the components of the position vector of the spacecraft COM in the OAGRF ( $C_X, C_Y, C_Z$ ), their variation rate ( $\dot{C}_X, \dot{C}_Y, \dot{C}_Z$ ) and their variation acceleration ( $\ddot{C}_X, \ddot{C}_Y, \ddot{C}_Z$ ).

| Quantity                                                           | Requirement                                                |
|--------------------------------------------------------------------|------------------------------------------------------------|
| maximum value below the MBW (DC to 5 mHz)                          |                                                            |
| $C_X^0$                                                            | $\leq 0.15$ m                                              |
| $C_Y^0$                                                            | $\leq 0.05$ m                                              |
| $C_Z^0$                                                            | $\leq 0.05$ m                                              |
| $\dot{C}_X^0, \dot{C}_Y^0, \dot{C}_Z^0$                            | $\leq 1 \cdot 10^{-4}$ m/s                                 |
| $\ddot{C}_X^0, \ddot{C}_Y^0, \ddot{C}_Z^0$                         | $\leq 1 \cdot 10^{-7}$ m/s <sup>2</sup>                    |
| maximum value in the MBW (5 mHz to 100 mHz)                        |                                                            |
| $\tilde{C}_X^W, \tilde{C}_Y^W, \tilde{C}_Z^W$                      | $\leq 1 \cdot 10^{-6}$ m/Hz <sup>1/2</sup>                 |
| $\tilde{\dot{C}}_X^W, \tilde{\dot{C}}_Y^W, \tilde{\dot{C}}_Z^W$    | $\leq 1 \cdot 10^{-6}$ m/s/Hz <sup>1/2</sup>               |
| $\tilde{\ddot{C}}_X^W, \tilde{\ddot{C}}_Y^W, \tilde{\ddot{C}}_Z^W$ | $\leq 1 \cdot 10^{-9}$ m/s <sup>2</sup> /Hz <sup>1/2</sup> |

Table 6.1-10: Requirements on spacecraft COM location and stability in the OAGRF

6.1.5 C.3: Quadratic Couplings

From the equation (5.2.6) requirements are derived for the values of the in-line common and differential quadratic factors ( $K2_{c,14,X}, K2_{d,14,X}, K2_{c,25,Y}, K2_{d,25,Y}, K2_{c,36,Z}, K2_{d,36,Z}$ ) during the measurement phases (between the periodic in-flight calibrations of the Gradiometer).

The common and differential scale factors are measured and physically adjusted, if needed, at each on-orbit calibration of the Gradiometer. The maximum variation below the MBW achieved by these elements depends on:

- A. the limits under which they have been reduced during the calibration
- B. their maximum variation during the scientific measurement phase (w.r.t. the calibration limits) in the frequency range from DC to 5 mHz.

The apportionment of the overall requirement on the elements of  $K2_{ij}$  between the contributions A, B is provided in Table 6.1-11. The required limit of the quadratic factors SD in the MBW is provided in the same table.

| Quantity                                                                                                                                                                                                                                                                 | Requirement                                      |
|--------------------------------------------------------------------------------------------------------------------------------------------------------------------------------------------------------------------------------------------------------------------------|--------------------------------------------------|
| maximum value below the MBW (DC to 5 mHz)                                                                                                                                                                                                                                |                                                  |
| $K2_{c,14,X} \leq 10 \text{ s}^2/\text{m}$ , $K2_{d,14,X} \leq 4 \text{ s}^2/\text{m}$<br>$K2_{c,25,Y} \leq 7 \text{ s}^2/\text{m}$ , $K2_{d,25,Y} \leq 4 \text{ s}^2/\text{m}$<br>$K2_{c,36,Z} \leq 7 \text{ s}^2/\text{m}$ , $K2_{d,36,Z} \leq 4 \text{ s}^2/\text{m}$ |                                                  |
| upper limit under which the above quantities have to be reduced at Gradiometer calibration                                                                                                                                                                               |                                                  |
| $K2_{c,14,X} \leq 9 \text{ s}^2/\text{m}$ , $K2_{d,14,X} \leq 3 \text{ s}^2/\text{m}$<br>$K2_{c,25,Y} \leq 6 \text{ s}^2/\text{m}$ , $K2_{d,25,Y} \leq 3 \text{ s}^2/\text{m}$<br>$K2_{c,36,Z} \leq 6 \text{ s}^2/\text{m}$ , $K2_{d,36,Z} \leq 3 \text{ s}^2/\text{m}$  |                                                  |
| maximum variation below the MBW of the above quantities during the measurement phase                                                                                                                                                                                     | $\leq 1 \text{ s}^2/\text{m}$                    |
| maximum value in the MBW (5 mHz to 100 mHz)                                                                                                                                                                                                                              |                                                  |
| $\tilde{K}2_{c,14,X}^W, \tilde{K}2_{d,14,X}^W$                                                                                                                                                                                                                           | $\leq 0.01 \text{ s}^2/\text{m}/\text{Hz}^{1/2}$ |
| $\tilde{K}2_{c,25,Y}^W, \tilde{K}2_{d,25,Y}^W$                                                                                                                                                                                                                           | $\leq 0.01 \text{ s}^2/\text{m}/\text{Hz}^{1/2}$ |
| $\tilde{K}2_{c,36,Z}^W, \tilde{K}2_{d,36,Z}^W$                                                                                                                                                                                                                           | $\leq 0.01 \text{ s}^2/\text{m}/\text{Hz}^{1/2}$ |

Table 6.1-11: Requirements on the values of the in-line common and differential quadratic factors and their stability

6.1.6 C.4: Coupling with Accelerometer Misplacement from their Nominal Position in the OAGRF

From the equation (5.2.7) requirements are derived for the displacements of the accelerometers from their nominal position in the OAGRF ( $\delta A_{1,X}$ ,  $\delta A_{2,Y}$ ,  $\delta A_{3,Z}$ ). They are equivalent to requirements on the knowledge accuracy of the value of the baseline length and on the stability of the baseline length, since:  $\delta L_X = 2\delta A_{1,X}$ ,  $\delta L_Y = 2\delta A_{2,Y}$ ,  $\delta L_Z = 2\delta A_{3,Z}$ .

| Quantity                                                                                                                                                     | Requirement                                      |
|--------------------------------------------------------------------------------------------------------------------------------------------------------------|--------------------------------------------------|
| maximum value below the MBW (DC to 5 mHz)                                                                                                                    |                                                  |
| $\delta L_X^0 = 2\delta A_{1,X}^0$ , $\delta L_Y^0 = 2\delta A_{2,Y}^0$ , $\delta L_Z^0 = 2\delta A_{3,Z}^0$                                                 | $\leq 50 \cdot 10^{-6} \text{ m}$                |
| maximum value in the MBW (5 mHz to 100 mHz)                                                                                                                  |                                                  |
| $\delta \tilde{L}_X^W = 2\delta \tilde{A}_{1,X}^W$ , $\delta \tilde{L}_Y^W = 2\delta \tilde{A}_{2,Y}^W$ , $\delta \tilde{L}_Z^W = 2\delta \tilde{A}_{3,Z}^W$ | $\leq 1 \cdot 10^{-9} \text{ m}/\text{Hz}^{1/2}$ |

Table 6.1-12: Requirements on displacements of the accelerometers in the OAGRF (= requirements on OAG baseline length knowledge accuracy and stability)

6.1.7 C.5: Coupling with the Platform Magnetic Field

From the equation (5.2.9) requirements are derived for the modulus of the magnetic field generated by the Platform at the location of the accelerometer  $A_i$  ( $B_{i,P}$ ), and constraints are derived for the modulus of the magnetic field generated by the Gradiometer at the location of the accelerometer  $A_i$  ( $B_{i,G}$ ). About the latter, they must be considered upper limits to  $B_{i,G}$ . These requirements and constraints have been computed by considering the following values for the Earth magnetic field modulus along the GOCE orbit (see [RD 6] for more details):

$$B_E^0 = 5.5 \cdot 10^{-5} \text{ Tesla}, B_E^W = 2 \cdot 10^{-6} \text{ Tesla}/\text{Hz}^{1/2}.$$

| Quantity                                    | Requirement/Constraint                                       |
|---------------------------------------------|--------------------------------------------------------------|
| maximum value below the MBW (DC to 5 mHz)   |                                                              |
| $B_{i,P}^0$                                 | $\leq 2 \cdot 10^{-6}$ Tesla (requirement)                   |
| $B_{i,G}^0$                                 | $\leq 4 \cdot 10^{-6}$ Tesla (constraint)                    |
| maximum value in the MBW (5 mHz to 100 mHz) |                                                              |
| $B_{i,P}^W$                                 | $\leq 5 \cdot 10^{-7}$ Tesla/Hz <sup>1/2</sup> (requirement) |
| $B_{i,G}^W$                                 | $\leq 1 \cdot 10^{-7}$ Tesla/Hz <sup>1/2</sup> (constraint)  |

Table 6.1-10: Requirements on Platform magnetic field and constraints on Gradiometer magnetic field

### 6.1.8 C.7: Coupling with the High Frequency Noise

From the folding inside the MBW of high frequency noise (> MBW) produced by the non linearity of the accelerometer (the expression of which is provided in [RD 5]), the following requirements are derived for the spectral density of the linear acceleration ( $\tilde{a}(v)$ ) along the in-line axis of each accelerometer:

- for 0.1 Hz < v ≤ 5 Hz:  $\tilde{a}(v) = 2 \cdot 10^{-7} \text{ m s}^{-2} \text{ Hz}^{-1/2}$
- above 5 Hz, up to 20 Hz:  $\tilde{a}(v) = 5 \cdot 10^{-8} \text{ m s}^{-2} \text{ Hz}^{-1/2}$
- above 20 Hz:  $\tilde{a}(v) = 5 \cdot 10^{-8} \frac{v}{20 \text{ Hz}} \text{ m s}^{-2} \text{ Hz}^{-1/2}$

### 6.1.9 C.8: Coupling with the Transfer Function Difference

From the equation (5.2.12), considering for the spectral density of the linear accelerations in the MBW the value specified in Table 6.1-3 and Figure 6.1-3, the following requirements are derived:

- Accelerometer TF contribution to CMRR:  $\delta TFA_{14,X} \leq 4 \cdot 10^{-6}$ ,  $\delta TFA_{25,Y} \leq 4 \cdot 10^{-6}$ ,  $\delta TFA_{36,Z} \leq 4 \cdot 10^{-6}$
- Gradiometer structure TF contribution to CMRR:  $\delta TFS_{14,X} \leq 4 \cdot 10^{-6}$ ,  $\delta TFS_{25,Y} \leq 4 \cdot 10^{-6}$ ,  $\delta TFS_{36,Z} \leq 4 \cdot 10^{-6}$

Since the accelerometer TF is estimated and utilised in the post processing for the recovery of the actual accelerations from the measured ones, the above requirements on  $\delta TFA_{14,X}$ , etc..., refer to the residual contribution of the accelerometer TF to the CMRR (or differential scale factor) after it has been post-processed.

The requirements on  $\delta TFS_{14,X}$ , etc..., are instead real constraints to the maximum difference (in stiffness and damping) between the two “halves” of the gradiometer arms.

In general, the accelerometer and structure TF contribution to the CMRR is variable as function of the frequency. It is sufficient that the above specified values of CMRR are not exceeded in the MBW.

#### 6.1.10 C.9: Angular-Linear Acceleration Coupling at Accelerometer Level

From the equation (5.2.13), considering for the spectral density of the angular accelerations in the MBW the value specified in Table 6.1-6 and

Figure 6.1-4, the following requirement is derived for the angular-linear acceleration coupling factor for accelerometer in-line US axes.

$$C_{Zc} \leq 5.5 \cdot 10^{-5}$$

The value of the angular-linear acceleration coupling factor can be reduced during the raw measurements post processing, by exploiting the on-ground characterisation of the accelerometer parameters (in particular, the measured value of the gap between the proof mass and the electrodes, from which the value of the electrostatic gains is obtained). The above requirement thus refers to the residual angular-linear acceleration coupling left by its estimation and recovery method in the data post-processing.

6.2 REQUIREMENTS RELATED TO THE SATELLITE ERRORS

6.2.1 S.1: Platform Self Gravity

From the equation (5.3.1) requirements are derived for the differential self-gravity acceleration in the MBW produced by the satellite masses (Gradiometer excluded) on the accelerometer proof masses.

| Quantity                                                           | Requirement                                              |
|--------------------------------------------------------------------|----------------------------------------------------------|
| maximum value in the MBW (5 mHz to 100 mHz)                        |                                                          |
| $\tilde{S}_{d,14,X}^W, \tilde{S}_{d,25,Y}^W, \tilde{S}_{d,36,Z}^W$ | $\leq 1.37 \cdot 10^{-13} \text{ m/s}^2/\text{Hz}^{1/2}$ |

Table 6.2-1: Requirements on platform generated differential self-gravity acceleration on the proof masses

6.3 REQUIREMENTS RELATED TO PROCESSING ERRORS

6.3.1 P.1: Centrifugal Accelerations Recovery Error

From the equation (5.4.1) requirements are derived for the accuracy by which the angular velocities recovered in the Level 1 data processing ( $\hat{\omega}_X, \hat{\omega}_Y, \hat{\omega}_Z$ ) must be known.

The plots of the spectral density limits for  $\delta\hat{\omega}_X^W(\nu), \delta\hat{\omega}_Y^W(\nu), \delta\hat{\omega}_Z^W(\nu)$  in the MBW are provided in Figure 6.3-1 (with maximum in the MBW specified in Table 6.3-1) where also the extension of these limits outside the MBW is shown.

| Quantity                                                                   | Requirement                                     |
|----------------------------------------------------------------------------|-------------------------------------------------|
| maximum value below the MBW (DC to 5 mHz)                                  |                                                 |
| $\delta\hat{\omega}_X^0$                                                   | $\leq 5 \cdot 10^{-7} \text{ rad/s}$            |
| $\delta\hat{\omega}_Y^0$                                                   | $\leq 5 \cdot 10^{-7} \text{ rad/s}$            |
| $\delta\hat{\omega}_Z^0$                                                   | $\leq 5 \cdot 10^{-7} \text{ rad/s}$            |
| maximum value in the MBW ( $5 \text{ mHz} \leq \nu \leq 100 \text{ mHz}$ ) |                                                 |
| $\delta\hat{\omega}_X^W(\nu)$                                              | $\leq 8.5 \cdot 10^{-8} \text{ rad/s/Hz}^{1/2}$ |
| $\delta\hat{\omega}_Y^W(\nu)$                                              | $\leq 4.1 \cdot 10^{-9} \text{ rad/s/Hz}^{1/2}$ |
| $\delta\hat{\omega}_Z^W(\nu)$                                              | $\leq 3.2 \cdot 10^{-8} \text{ rad/s/Hz}^{1/2}$ |

Table 6.3-1: Requirements on angular rates recovery accuracy

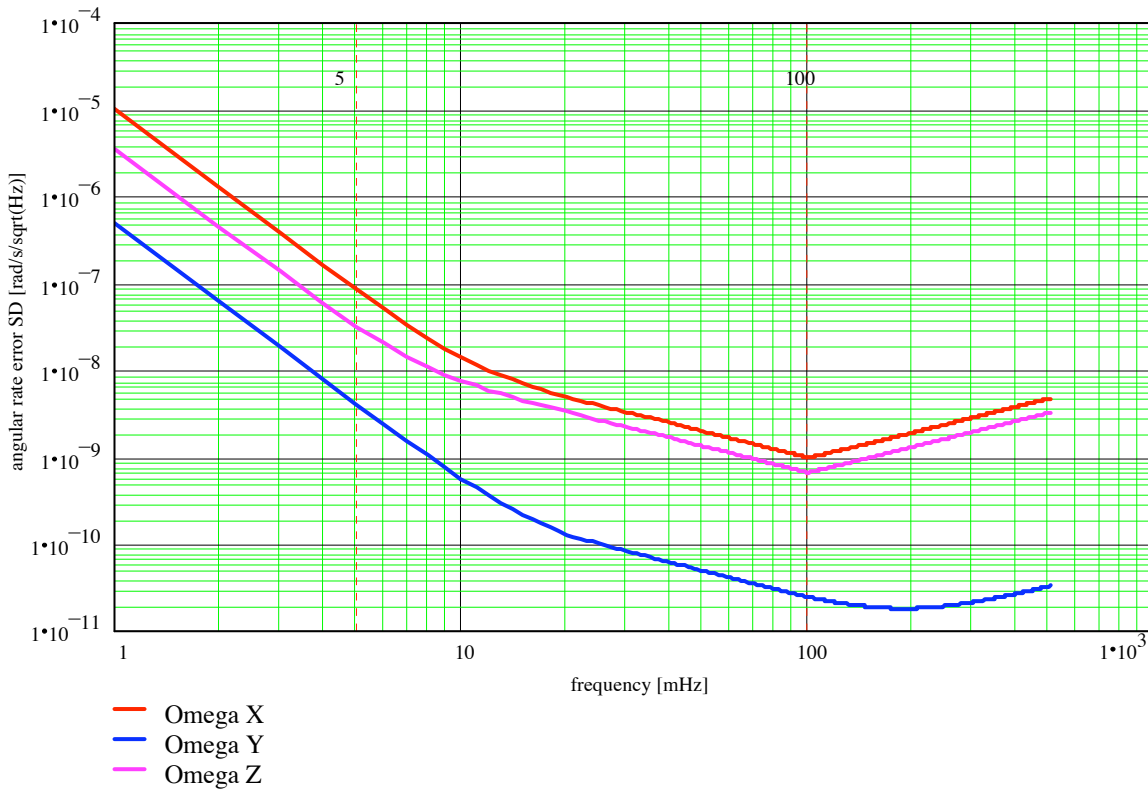


Figure 6.3-1: Spectral density upper limits for  $\delta\hat{\omega}_X^W(\nu)$ ,  $\delta\hat{\omega}_Y^W(\nu)$ ,  $\delta\hat{\omega}_Z^W(\nu)$

6.3.2 Derived Requirements: Angular Acceleration Recovery Error

The relationship between the SD of the angular acceleration and of the angular rate at a given frequency  $\nu$ , is:

$$\tilde{\omega}(\nu) = 2\pi\nu \tilde{\omega}(\nu)$$

Thus, the previous requirements on the angular velocities recovery accuracy in the MBW induce in turn requirements on the accuracy by which the angular acceleration must be recovered in the Level 1 data processing (in particular on the SD of the error affecting the estimated angular accelerations  $\hat{\omega}_X, \hat{\omega}_Y, \hat{\omega}_Z$ ). The plots of the spectral density limits for  $\delta\hat{\omega}_X^W(\nu)$ ,  $\delta\hat{\omega}_Y^W(\nu)$ ,  $\delta\hat{\omega}_Z^W(\nu)$  in the MBW are provided in Figure 6.3-2 (with maximum in the MBW specified in Table 6.3-2) where also the extension of these limits outside the MBW is shown.

| Quantity                                                                   | Requirement                                               |
|----------------------------------------------------------------------------|-----------------------------------------------------------|
| maximum value in the MBW ( $5 \text{ mHz} \leq \nu \leq 100 \text{ mHz}$ ) |                                                           |
| $\delta\hat{\omega}_X^W(\nu)$                                              | $\leq 2.7 \cdot 10^{-9} \text{ rad/s}^2/\text{Hz}^{1/2}$  |
| $\delta\hat{\omega}_Y^W(\nu)$                                              | $\leq 1.3 \cdot 10^{-10} \text{ rad/s}^2/\text{Hz}^{1/2}$ |
| $\delta\hat{\omega}_Z^W(\nu)$                                              | $\leq 1.0 \cdot 10^{-9} \text{ rad/s}^2/\text{Hz}^{1/2}$  |

Table 6.3-2: Requirements on angular acceleration recovery accuracy

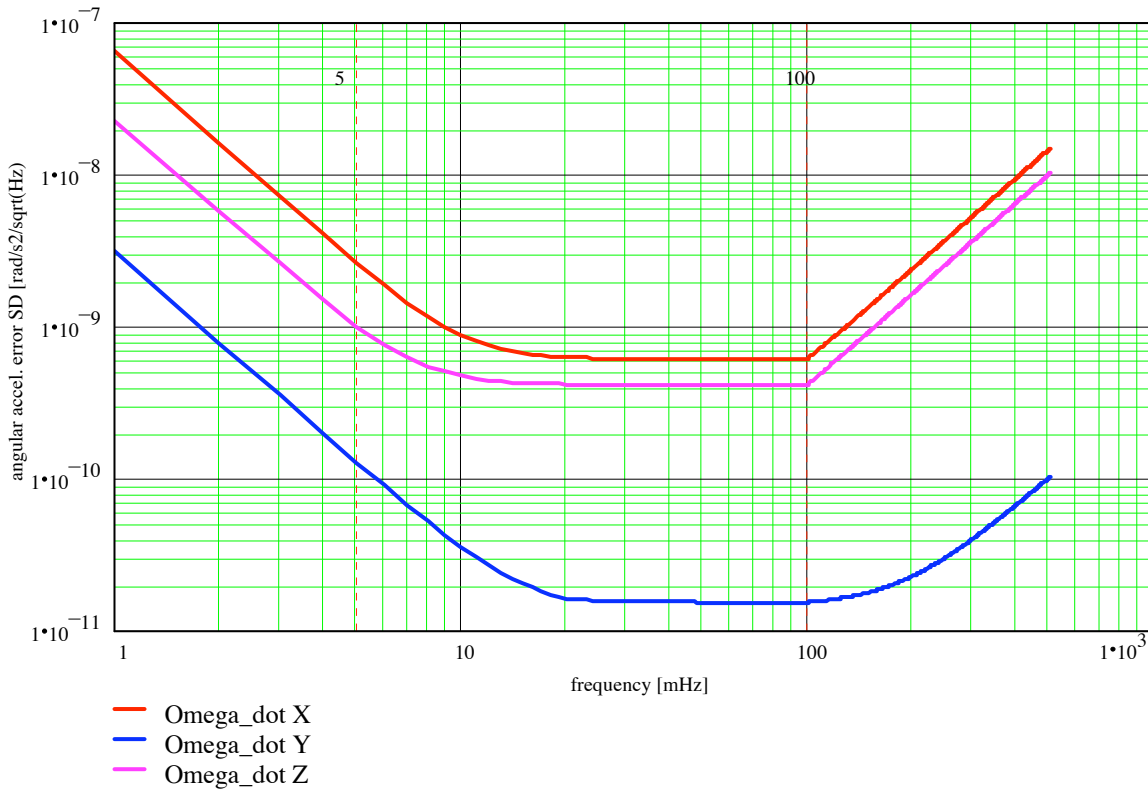


Figure 6.3-2: Spectral density upper limits for  $\hat{\delta\omega}_X^W(\nu)$ ,  $\hat{\delta\omega}_Y^W(\nu)$ ,  $\hat{\delta\omega}_Z^W(\nu)$

According to the error breakdown for the angular acceleration (see section 5.2), the specified measurement error for  $\hat{\delta\omega}_X^W(\nu)$ ,  $\hat{\delta\omega}_Y^W(\nu)$ ,  $\hat{\delta\omega}_Z^W(\nu)$  can be achieved if the additional requirements provided in Table 6.3-3, Table 6.3-4, Table 6.3-5, Table 6.3-6, Table 6.3-7, Table 6.3-8, Table 6.3-9, Table 6.3-10, Table 6.3-11, Table 6.3-12 (beside those already reported in section 6.1) are fulfilled.

Only the accelerometer noise requirement along the less sensitive axis is provided in Table 6.3-3. For the other ultra-sensitive transversal axes involved in the computation of the angular accelerations, the same accelerometer noise requirement along the in-line axis derived within the Instrument Error allocation are applied here. The plot with the accelerometer noise spectral density limit for the less sensitive axis, showing also the the extension of these limits outside the MBW, is provided in Figure 6.3-3.

The requirement on the spectral density of common and differential scale factors about the transversal axes of the OAGs (both ultra sensitive and less sensitive) is actually a function of the frequency, with maximum in the MBW specified in Table 6.3-8. The plot of this function is provided in Figure 6.1-2 (differential scale factors) and Figure 6.1-5 (common scale factors).

| Quantity                                                                                | Requirement                                           |
|-----------------------------------------------------------------------------------------|-------------------------------------------------------|
| maximum value in the MBW ( $5 \text{ mHz} \leq \nu \leq 100 \text{ mHz}$ )              |                                                       |
| $\tilde{n}_{c,14,Y}^W(\nu)$ , $\tilde{n}_{c,25,Z}^W(\nu)$ , $\tilde{n}_{c,36,Y}^W(\nu)$ | $\leq 3 \cdot 10^{-10} \text{ m/s}^2/\text{Hz}^{1/2}$ |
| $\tilde{n}_{d,14,Y}^W(\nu)$ , $\tilde{n}_{d,25,Z}^W(\nu)$ , $\tilde{n}_{d,36,Y}^W(\nu)$ | $\leq 3 \cdot 10^{-10} \text{ m/s}^2/\text{Hz}^{1/2}$ |

Table 6.3-3: Requirements on the common and differential noise of the accelerometer along the less sensitive axis

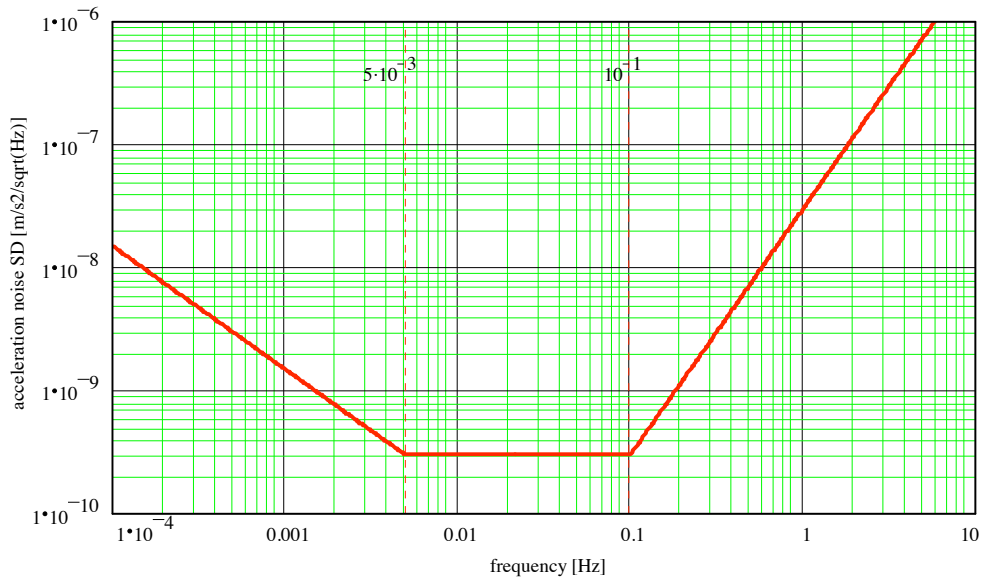


Figure 6.3-3: Spectral density upper limits for the accelerometer noise along the less sensitive axis

| Quantity                                                                             | Requirement                                  |
|--------------------------------------------------------------------------------------|----------------------------------------------|
| maximum value below the MBW (DC to 5 mHz)                                            |                                              |
| $\delta\dot{A}_{d,14,X}^0, \delta\dot{A}_{d,25,Y}^0, \delta\dot{A}_{d,36,Z}^0$       | $\leq 1 \cdot 10^{-7} \text{ m/s}$           |
| maximum value in the MBW (5 mHz to 100 mHz)                                          |                                              |
| $\delta\tilde{A}_{d,14,X}^W, \delta\tilde{A}_{d,25,Y}^W, \delta\tilde{A}_{d,36,Z}^W$ | $\leq 1 \cdot 10^{-10} \text{ m/s/Hz}^{1/2}$ |

Table 6.3-4: Requirements on the on the variation rates of the accelerometer differential displacements in the OAGRF

| Quantity                                                                                 | Requirement                                           |
|------------------------------------------------------------------------------------------|-------------------------------------------------------|
| maximum value in the MBW (5 mHz to 100 mHz)                                              |                                                       |
| $\tilde{S}_{d,14,Z}^W, \tilde{S}_{d,36,X}^W$                                             | $\leq 1 \cdot 10^{-12} \text{ m/s}^2/\text{Hz}^{1/2}$ |
| $\tilde{S}_{d,14,Y}^W, \tilde{S}_{d,25,X}^W, \tilde{S}_{d,25,Z}^W, \tilde{S}_{d,36,Y}^W$ | $\leq 1 \cdot 10^{-11} \text{ m/s}^2/\text{Hz}^{1/2}$ |

Table 6.3-5: Requirements on the transversal components of the differential acceleration between the accelerometers belonging to the same OAG generated by the overall satellite self-gravity

| Quantity                                                                                 | Requirement                                           |
|------------------------------------------------------------------------------------------|-------------------------------------------------------|
| maximum value in the MBW (5 mHz to 100 mHz)                                              |                                                       |
| $\tilde{M}_{d,14,Z}^W, \tilde{M}_{d,36,X}^W$                                             | $\leq 1 \cdot 10^{-12} \text{ m/s}^2/\text{Hz}^{1/2}$ |
| $\tilde{M}_{d,14,Y}^W, \tilde{M}_{d,25,X}^W, \tilde{M}_{d,25,Z}^W, \tilde{M}_{d,36,Y}^W$ | $\leq 1 \cdot 10^{-11} \text{ m/s}^2/\text{Hz}^{1/2}$ |

Table 6.3-6: Requirements on the transversal components of the differential acceleration between the accelerometers belonging to the same OAG generated by the coupling with spacecraft and Earth magnetic fields

| Row             | Required knowledge accuracy of the transversal common and differential elements of $MI_{14}$ |                                            |                                            |                                             |                                             |                                             |
|-----------------|----------------------------------------------------------------------------------------------|--------------------------------------------|--------------------------------------------|---------------------------------------------|---------------------------------------------|---------------------------------------------|
| 4 <sup>th</sup> | $\delta MI_{14,41} \leq 1.4 \cdot 10^{-5}$                                                   | $\delta MI_{14,42} \leq 5.0 \cdot 10^{-6}$ | $\delta MI_{14,43} \leq 5.0 \cdot 10^{-6}$ | $\delta MI_{14,44} \leq 2.02 \cdot 10^{-3}$ | $\delta MI_{14,45} \leq 5.1 \cdot 10^{-5}$  | $\delta MI_{14,46} \leq 5.1 \cdot 10^{-5}$  |
| 5 <sup>th</sup> | $\delta MI_{14,51} \leq 1.5 \cdot 10^{-4}$                                                   | $\delta MI_{14,52} \leq 5.5 \cdot 10^{-4}$ | $\delta MI_{14,53} \leq 1.5 \cdot 10^{-4}$ | $\delta MI_{14,54} \leq 1.5 \cdot 10^{-4}$  | $\delta MI_{14,55} \leq 1.01 \cdot 10^{-2}$ | $\delta MI_{14,56} \leq 1.5 \cdot 10^{-4}$  |
| 6 <sup>th</sup> | $\delta MI_{14,61} \leq 5.0 \cdot 10^{-5}$                                                   | $\delta MI_{14,62} \leq 5.0 \cdot 10^{-5}$ | $\delta MI_{14,63} \leq 5.8 \cdot 10^{-5}$ | $\delta MI_{14,64} \leq 1.5 \cdot 10^{-4}$  | $\delta MI_{14,65} \leq 1.5 \cdot 10^{-4}$  | $\delta MI_{14,66} \leq 2.02 \cdot 10^{-3}$ |
| Row             | Required knowledge accuracy of the transversal common and differential elements of $MI_{25}$ |                                            |                                            |                                             |                                             |                                             |
| 4 <sup>th</sup> | $\delta MI_{25,41} \leq 1.5 \cdot 10^{-4}$                                                   | $\delta MI_{25,42} \leq 1.5 \cdot 10^{-4}$ | $\delta MI_{25,43} \leq 1.5 \cdot 10^{-4}$ | $\delta MI_{25,44} \leq 2.1 \cdot 10^{-3}$  | $\delta MI_{25,45} \leq 1.5 \cdot 10^{-4}$  | $\delta MI_{25,46} \leq 1.5 \cdot 10^{-4}$  |
| 5 <sup>th</sup> | $\delta MI_{25,51} \leq 5.0 \cdot 10^{-6}$                                                   | $\delta MI_{25,52} \leq 1.4 \cdot 10^{-5}$ | $\delta MI_{25,53} \leq 5.0 \cdot 10^{-6}$ | $\delta MI_{25,54} \leq 5.1 \cdot 10^{-5}$  | $\delta MI_{25,55} \leq 2.02 \cdot 10^{-3}$ | $\delta MI_{25,56} \leq 5.1 \cdot 10^{-5}$  |
| 6 <sup>th</sup> | $\delta MI_{25,61} \leq 1.5 \cdot 10^{-4}$                                                   | $\delta MI_{25,62} \leq 1.5 \cdot 10^{-4}$ | $\delta MI_{25,63} \leq 5.5 \cdot 10^{-4}$ | $\delta MI_{25,64} \leq 1.5 \cdot 10^{-4}$  | $\delta MI_{25,65} \leq 1.5 \cdot 10^{-4}$  | $\delta MI_{25,66} \leq 1.01 \cdot 10^{-2}$ |
| Row             | Required knowledge accuracy of the transversal common and differential elements of $MI_{36}$ |                                            |                                            |                                             |                                             |                                             |
| 4 <sup>th</sup> | $\delta MI_{36,41} \leq 5.8 \cdot 10^{-5}$                                                   | $\delta MI_{36,42} \leq 5.0 \cdot 10^{-5}$ | $\delta MI_{36,43} \leq 5.0 \cdot 10^{-5}$ | $\delta MI_{36,44} \leq 2.02 \cdot 10^{-3}$ | $\delta MI_{36,45} \leq 1.5 \cdot 10^{-4}$  | $\delta MI_{36,46} \leq 1.5 \cdot 10^{-4}$  |
| 5 <sup>th</sup> | $\delta MI_{36,51} \leq 1.5 \cdot 10^{-4}$                                                   | $\delta MI_{36,52} \leq 5.5 \cdot 10^{-4}$ | $\delta MI_{36,53} \leq 1.5 \cdot 10^{-4}$ | $\delta MI_{36,54} \leq 1.5 \cdot 10^{-4}$  | $\delta MI_{36,55} \leq 1.01 \cdot 10^{-2}$ | $\delta MI_{36,56} \leq 1.5 \cdot 10^{-4}$  |
| 6 <sup>th</sup> | $\delta MI_{36,61} \leq 5.0 \cdot 10^{-6}$                                                   | $\delta MI_{36,62} \leq 5.0 \cdot 10^{-6}$ | $\delta MI_{36,63} \leq 1.4 \cdot 10^{-5}$ | $\delta MI_{36,64} \leq 5.1 \cdot 10^{-5}$  | $\delta MI_{36,65} \leq 5.1 \cdot 10^{-5}$  | $\delta MI_{36,66} \leq 2.02 \cdot 10^{-3}$ |

| Row             | Maximum measurement error of the transversal common and differential elements of $MI_{14}$ at calibration |                                            |                                             |                                            |                                            |                                            |
|-----------------|-----------------------------------------------------------------------------------------------------------|--------------------------------------------|---------------------------------------------|--------------------------------------------|--------------------------------------------|--------------------------------------------|
| 4 <sup>th</sup> | $\delta MI_{14,41} \leq 4.7 \cdot 10^{-6}$                                                                | $\delta MI_{14,42} \leq 4.5 \cdot 10^{-6}$ | $\delta MI_{14,43} \leq 4.5 \cdot 10^{-6}$  | $\delta MI_{14,44} \leq 2.0 \cdot 10^{-3}$ | $\delta MI_{14,45} \leq 5.0 \cdot 10^{-5}$ | $\delta MI_{14,46} \leq 5.0 \cdot 10^{-5}$ |
| 5 <sup>th</sup> | $\delta MI_{14,51} \leq 1.0 \cdot 10^{-4}$                                                                | $\delta MI_{14,52} \leq 5.0 \cdot 10^{-4}$ | $\delta MI_{14,53} \leq 1.0 \cdot 10^{-4}$  | $\delta MI_{14,54} \leq 5.0 \cdot 10^{-5}$ | $\delta MI_{14,55} \leq 1.0 \cdot 10^{-2}$ | $\delta MI_{14,56} \leq 5.0 \cdot 10^{-5}$ |
| 6 <sup>th</sup> | $\delta MI_{14,61} \leq 4.5 \cdot 10^{-5}$                                                                | $\delta MI_{14,62} \leq 4.5 \cdot 10^{-5}$ | $\delta MI_{14,63} \leq 4.87 \cdot 10^{-5}$ | $\delta MI_{14,64} \leq 5.0 \cdot 10^{-5}$ | $\delta MI_{14,65} \leq 5.0 \cdot 10^{-5}$ | $\delta MI_{14,66} \leq 2.0 \cdot 10^{-3}$ |
| Row             | Maximum measurement error of the transversal common and differential elements of $MI_{25}$ at calibration |                                            |                                             |                                            |                                            |                                            |
| 4 <sup>th</sup> | $\delta MI_{25,41} \leq 1.0 \cdot 10^{-4}$                                                                | $\delta MI_{25,42} \leq 1.0 \cdot 10^{-4}$ | $\delta MI_{25,43} \leq 1.0 \cdot 10^{-4}$  | $\delta MI_{25,44} \leq 2.0 \cdot 10^{-3}$ | $\delta MI_{25,45} \leq 5.0 \cdot 10^{-5}$ | $\delta MI_{25,46} \leq 5.0 \cdot 10^{-5}$ |
| 5 <sup>th</sup> | $\delta MI_{25,51} \leq 4.5 \cdot 10^{-6}$                                                                | $\delta MI_{25,52} \leq 4.7 \cdot 10^{-6}$ | $\delta MI_{25,53} \leq 4.5 \cdot 10^{-6}$  | $\delta MI_{25,54} \leq 5.0 \cdot 10^{-5}$ | $\delta MI_{25,55} \leq 2.0 \cdot 10^{-3}$ | $\delta MI_{25,56} \leq 5.0 \cdot 10^{-5}$ |
| 6 <sup>th</sup> | $\delta MI_{25,61} \leq 1.0 \cdot 10^{-4}$                                                                | $\delta MI_{25,62} \leq 1.0 \cdot 10^{-4}$ | $\delta MI_{25,63} \leq 5.0 \cdot 10^{-4}$  | $\delta MI_{25,64} \leq 5.0 \cdot 10^{-5}$ | $\delta MI_{25,65} \leq 5.0 \cdot 10^{-5}$ | $\delta MI_{25,66} \leq 1.0 \cdot 10^{-2}$ |
| Row             | Maximum measurement error of the transversal common and differential elements of $MI_{36}$ at calibration |                                            |                                             |                                            |                                            |                                            |
| 4 <sup>th</sup> | $\delta MI_{36,41} \leq 4.87 \cdot 10^{-5}$                                                               | $\delta MI_{36,42} \leq 4.5 \cdot 10^{-5}$ | $\delta MI_{36,43} \leq 4.5 \cdot 10^{-5}$  | $\delta MI_{36,44} \leq 2.0 \cdot 10^{-3}$ | $\delta MI_{36,45} \leq 5.0 \cdot 10^{-5}$ | $\delta MI_{36,46} \leq 5.0 \cdot 10^{-5}$ |
| 5 <sup>th</sup> | $\delta MI_{36,51} \leq 1.0 \cdot 10^{-4}$                                                                | $\delta MI_{36,52} \leq 5.0 \cdot 10^{-4}$ | $\delta MI_{36,53} \leq 1.0 \cdot 10^{-4}$  | $\delta MI_{36,54} \leq 5.0 \cdot 10^{-5}$ | $\delta MI_{36,55} \leq 1.0 \cdot 10^{-2}$ | $\delta MI_{36,56} \leq 5.0 \cdot 10^{-5}$ |
| 6 <sup>th</sup> | $\delta MI_{36,61} \leq 4.5 \cdot 10^{-6}$                                                                | $\delta MI_{36,62} \leq 4.5 \cdot 10^{-6}$ | $\delta MI_{36,63} \leq 4.7 \cdot 10^{-6}$  | $\delta MI_{36,64} \leq 5.0 \cdot 10^{-5}$ | $\delta MI_{36,65} \leq 5.0 \cdot 10^{-5}$ | $\delta MI_{36,66} \leq 2.0 \cdot 10^{-3}$ |

| Row             | Maximum variation of the transversal common and differential elements of $MI_{14}$ between calibration phases |                                             |                                             |                                            |                                            |                                            |
|-----------------|---------------------------------------------------------------------------------------------------------------|---------------------------------------------|---------------------------------------------|--------------------------------------------|--------------------------------------------|--------------------------------------------|
| 4 <sup>th</sup> | $\delta MI_{14,41} \leq 9.05 \cdot 10^{-6}$                                                                   | $\delta MI_{14,42} \leq 5.0 \cdot 10^{-7}$  | $\delta MI_{14,43} \leq 5.0 \cdot 10^{-7}$  | $\delta MI_{14,44} \leq 2.0 \cdot 10^{-5}$ | $\delta MI_{14,45} \leq 1.0 \cdot 10^{-6}$ | $\delta MI_{14,46} \leq 1.0 \cdot 10^{-6}$ |
| 5 <sup>th</sup> | $\delta MI_{14,51} \leq 5.0 \cdot 10^{-5}$                                                                    | $\delta MI_{14,52} \leq 5.0 \cdot 10^{-5}$  | $\delta MI_{14,53} \leq 5.0 \cdot 10^{-5}$  | $\delta MI_{14,54} \leq 1.0 \cdot 10^{-4}$ | $\delta MI_{14,55} \leq 1.0 \cdot 10^{-4}$ | $\delta MI_{14,56} \leq 1.0 \cdot 10^{-4}$ |
| 6 <sup>th</sup> | $\delta MI_{14,61} \leq 5.0 \cdot 10^{-6}$                                                                    | $\delta MI_{14,62} \leq 5.0 \cdot 10^{-6}$  | $\delta MI_{14,63} \leq 9.05 \cdot 10^{-6}$ | $\delta MI_{14,64} \leq 1.0 \cdot 10^{-4}$ | $\delta MI_{14,65} \leq 1.0 \cdot 10^{-4}$ | $\delta MI_{14,66} \leq 2.0 \cdot 10^{-5}$ |
| Row             | Maximum variation of the transversal common and differential elements of $MI_{25}$ between calibration phases |                                             |                                             |                                            |                                            |                                            |
| 4 <sup>th</sup> | $\delta MI_{25,41} \leq 5.0 \cdot 10^{-5}$                                                                    | $\delta MI_{25,42} \leq 5.0 \cdot 10^{-5}$  | $\delta MI_{25,43} \leq 5.0 \cdot 10^{-5}$  | $\delta MI_{25,44} \leq 1.0 \cdot 10^{-4}$ | $\delta MI_{25,45} \leq 1.0 \cdot 10^{-4}$ | $\delta MI_{25,46} \leq 1.0 \cdot 10^{-4}$ |
| 5 <sup>th</sup> | $\delta MI_{25,51} \leq 5.0 \cdot 10^{-7}$                                                                    | $\delta MI_{25,52} \leq 9.05 \cdot 10^{-6}$ | $\delta MI_{25,53} \leq 5.0 \cdot 10^{-7}$  | $\delta MI_{25,54} \leq 1.0 \cdot 10^{-6}$ | $\delta MI_{25,55} \leq 2.0 \cdot 10^{-5}$ | $\delta MI_{25,56} \leq 1.0 \cdot 10^{-6}$ |
| 6 <sup>th</sup> | $\delta MI_{25,61} \leq 5.0 \cdot 10^{-5}$                                                                    | $\delta MI_{25,62} \leq 5.0 \cdot 10^{-5}$  | $\delta MI_{25,63} \leq 5.0 \cdot 10^{-5}$  | $\delta MI_{25,64} \leq 1.0 \cdot 10^{-4}$ | $\delta MI_{25,65} \leq 1.0 \cdot 10^{-4}$ | $\delta MI_{25,66} \leq 1.0 \cdot 10^{-4}$ |
| Row             | Maximum variation of the transversal common and differential elements of $MI_{36}$ between calibration phases |                                             |                                             |                                            |                                            |                                            |
| 4 <sup>th</sup> | $\delta MI_{36,41} \leq 9.05 \cdot 10^{-6}$                                                                   | $\delta MI_{36,42} \leq 5.0 \cdot 10^{-6}$  | $\delta MI_{36,43} \leq 5.0 \cdot 10^{-6}$  | $\delta MI_{36,44} \leq 2.0 \cdot 10^{-5}$ | $\delta MI_{36,45} \leq 1.0 \cdot 10^{-4}$ | $\delta MI_{36,46} \leq 1.0 \cdot 10^{-4}$ |
| 5 <sup>th</sup> | $\delta MI_{36,51} \leq 5.0 \cdot 10^{-5}$                                                                    | $\delta MI_{36,52} \leq 5.0 \cdot 10^{-5}$  | $\delta MI_{36,53} \leq 5.0 \cdot 10^{-5}$  | $\delta MI_{36,54} \leq 1.0 \cdot 10^{-4}$ | $\delta MI_{36,55} \leq 1.0 \cdot 10^{-4}$ | $\delta MI_{36,56} \leq 1.0 \cdot 10^{-4}$ |
| 6 <sup>th</sup> | $\delta MI_{36,61} \leq 5.0 \cdot 10^{-7}$                                                                    | $\delta MI_{36,62} \leq 5.0 \cdot 10^{-7}$  | $\delta MI_{36,63} \leq 9.05 \cdot 10^{-6}$ | $\delta MI_{36,64} \leq 1.0 \cdot 10^{-6}$ | $\delta MI_{36,65} \leq 1.0 \cdot 10^{-6}$ | $\delta MI_{36,66} \leq 2.0 \cdot 10^{-5}$ |

Table 6.3-7: Knowledge accuracy requirements of the transversal elements of  $[MI]_{d,14}$ ,  $[MI]_{d,25}$ ,  $[MI]_{d,36}$  and  $[MI]_{c,14}$ ,  $[MI]_{c,25}$ ,  $[MI]_{c,36}$ , during the measurement phases, and apportionement between measurement errors at calibration and stability between calibration phases.

|                 |                                                                                                                           |                                            |                                            |                                            |                                            |                                            |
|-----------------|---------------------------------------------------------------------------------------------------------------------------|--------------------------------------------|--------------------------------------------|--------------------------------------------|--------------------------------------------|--------------------------------------------|
| Row             | Maximum value in the MBW of the transversal common and differential elements of $\delta MI_{14}$ SD [Hz <sup>-1/2</sup> ] |                                            |                                            |                                            |                                            |                                            |
| 4 <sup>th</sup> | $\delta MI_{14,41} \leq 7.0 \cdot 10^{-7}$                                                                                | $\delta MI_{14,42} \leq 1.0 \cdot 10^{-8}$ | $\delta MI_{14,43} \leq 1.0 \cdot 10^{-8}$ | $\delta MI_{14,44} \leq 9.0 \cdot 10^{-7}$ | $\delta MI_{14,45} \leq 1.0 \cdot 10^{-8}$ | $\delta MI_{14,46} \leq 1.0 \cdot 10^{-8}$ |
| 5 <sup>th</sup> | $\delta MI_{14,42} \leq 1.0 \cdot 10^{-8}$                                                                                | $\delta MI_{14,41} \leq 7.0 \cdot 10^{-7}$ | $\delta MI_{14,42} \leq 1.0 \cdot 10^{-8}$ | $\delta MI_{14,42} \leq 1.0 \cdot 10^{-8}$ | $\delta MI_{14,44} \leq 9.0 \cdot 10^{-7}$ | $\delta MI_{14,42} \leq 1.0 \cdot 10^{-8}$ |
| 6 <sup>th</sup> | $\delta MI_{14,42} \leq 1.0 \cdot 10^{-8}$                                                                                | $\delta MI_{14,42} \leq 1.0 \cdot 10^{-8}$ | $\delta MI_{14,41} \leq 7.0 \cdot 10^{-7}$ | $\delta MI_{14,42} \leq 1.0 \cdot 10^{-8}$ | $\delta MI_{14,42} \leq 1.0 \cdot 10^{-8}$ | $\delta MI_{14,44} \leq 9.0 \cdot 10^{-7}$ |
| Row             | Maximum value in the MBW of the transversal common and differential elements of $\delta MI_{25}$ SD [Hz <sup>-1/2</sup> ] |                                            |                                            |                                            |                                            |                                            |
| 4 <sup>th</sup> | $\delta MI_{25,52} \leq 7.0 \cdot 10^{-7}$                                                                                | $\delta MI_{14,42} \leq 1.0 \cdot 10^{-8}$ | $\delta MI_{14,42} \leq 1.0 \cdot 10^{-8}$ | $\delta MI_{25,55} \leq 9.0 \cdot 10^{-7}$ | $\delta MI_{14,42} \leq 1.0 \cdot 10^{-8}$ | $\delta MI_{14,42} \leq 1.0 \cdot 10^{-8}$ |
| 5 <sup>th</sup> | $\delta MI_{25,51} \leq 1.0 \cdot 10^{-8}$                                                                                | $\delta MI_{25,52} \leq 7.0 \cdot 10^{-7}$ | $\delta MI_{25,53} \leq 1.0 \cdot 10^{-8}$ | $\delta MI_{25,54} \leq 1.0 \cdot 10^{-8}$ | $\delta MI_{25,55} \leq 9.0 \cdot 10^{-7}$ | $\delta MI_{25,56} \leq 1.0 \cdot 10^{-8}$ |
| 6 <sup>th</sup> | $\delta MI_{14,42} \leq 1.0 \cdot 10^{-8}$                                                                                | $\delta MI_{14,42} \leq 1.0 \cdot 10^{-8}$ | $\delta MI_{25,52} \leq 7.0 \cdot 10^{-7}$ | $\delta MI_{14,42} \leq 1.0 \cdot 10^{-8}$ | $\delta MI_{14,42} \leq 1.0 \cdot 10^{-8}$ | $\delta MI_{25,55} \leq 9.0 \cdot 10^{-7}$ |
| Row             | Maximum value in the MBW of the transversal common and differential elements of $\delta MI_{36}$ SD [Hz <sup>-1/2</sup> ] |                                            |                                            |                                            |                                            |                                            |
| 4 <sup>th</sup> | $\delta MI_{36,63} \leq 7.0 \cdot 10^{-7}$                                                                                | $\delta MI_{14,42} \leq 1.0 \cdot 10^{-8}$ | $\delta MI_{14,42} \leq 1.0 \cdot 10^{-8}$ | $\delta MI_{36,66} \leq 9.0 \cdot 10^{-7}$ | $\delta MI_{14,42} \leq 1.0 \cdot 10^{-8}$ | $\delta MI_{14,42} \leq 1.0 \cdot 10^{-8}$ |
| 5 <sup>th</sup> | $\delta MI_{14,42} \leq 1.0 \cdot 10^{-8}$                                                                                | $\delta MI_{36,63} \leq 7.0 \cdot 10^{-7}$ | $\delta MI_{14,42} \leq 1.0 \cdot 10^{-8}$ | $\delta MI_{14,42} \leq 1.0 \cdot 10^{-8}$ | $\delta MI_{36,66} \leq 9.0 \cdot 10^{-7}$ | $\delta MI_{14,42} \leq 1.0 \cdot 10^{-8}$ |
| 6 <sup>th</sup> | $\delta MI_{36,61} \leq 1.0 \cdot 10^{-8}$                                                                                | $\delta MI_{36,62} \leq 1.0 \cdot 10^{-8}$ | $\delta MI_{36,63} \leq 7.0 \cdot 10^{-7}$ | $\delta MI_{36,64} \leq 1.0 \cdot 10^{-8}$ | $\delta MI_{36,65} \leq 1.0 \cdot 10^{-8}$ | $\delta MI_{36,66} \leq 9.0 \cdot 10^{-7}$ |

Table 6.3-8: Specification for the maximum value in the MBW of the spectral density of the transversal element of  $[MI]_{d,14}$ ,  $[MI]_{d,25}$ ,  $[MI]_{d,36}$  and  $[MI]_{c,14}$ ,  $[MI]_{c,25}$ ,  $[MI]_{c,}$ , during the measurement phases.

| Quantity                                                                                                                                                                                                                                                                                         | Requirement                                      |
|--------------------------------------------------------------------------------------------------------------------------------------------------------------------------------------------------------------------------------------------------------------------------------------------------|--------------------------------------------------|
| maximum value below the MBW (DC to 5 mHz)                                                                                                                                                                                                                                                        |                                                  |
| $K 2_{c,14,Z}^0, K 2_{d,14,Z}^0, K 2_{c,25,X}^0, K 2_{d,25,X}^0, K 2_{c,36,X}^0, K 2_{d,36,X}^0$                                                                                                                                                                                                 | $\leq 10 \text{ s}^2/\text{m}$                   |
| upper limit under which the above quantities have to be reduced at Gradiometer calibration                                                                                                                                                                                                       | $\leq 9 \text{ s}^2/\text{m}$                    |
| maximum variation below the MBW of the above quantities during the measurement phase                                                                                                                                                                                                             | $\leq 1 \text{ s}^2/\text{m}$                    |
| $K 2_{c,14,Y}^0, K 2_{d,14,Y}^0, K 2_{c,25,Z}^0, K 2_{d,25,Z}^0, K 2_{c,36,Y}^0, K 2_{d,36,Y}^0$                                                                                                                                                                                                 | $\leq 2 \text{ s}^2/\text{m}$                    |
| upper limit under which the above quantities have to be reduced at Gradiometer calibration                                                                                                                                                                                                       | $\leq 1 \text{ s}^2/\text{m}$                    |
| maximum variation below the MBW of the above quantities during the measurement phase                                                                                                                                                                                                             | $\leq 1 \text{ s}^2/\text{m}$                    |
| maximum value in the MBW (5 mHz to 100 mHz)                                                                                                                                                                                                                                                      |                                                  |
| $\tilde{K} 2_{c,14,Z}^W, \tilde{K} 2_{d,14,Z}^W, \tilde{K} 2_{c,36,X}^W, \tilde{K} 2_{d,36,X}^W, \tilde{K} 2_{c,14,Y}^W, \tilde{K} 2_{d,14,Y}^W, \tilde{K} 2_{c,25,X}^W, \tilde{K} 2_{d,25,X}^W, \tilde{K} 2_{c,25,Z}^W, \tilde{K} 2_{d,25,Z}^W, \tilde{K} 2_{c,36,Y}^W, \tilde{K} 2_{d,36,Y}^W$ | $\leq 0.01 \text{ s}^2/\text{m}/\text{Hz}^{1/2}$ |

Table 6.3-9: Requirements on the values of the transversal common and differential quadratic factors and their stability

| Quantity                                              | Requirement                                        |
|-------------------------------------------------------|----------------------------------------------------|
| maximum value below the MBW (DC to 5 mHz)             |                                                    |
| $\varphi^0, \theta^0, \psi^0$                         | $\leq 2 \cdot 10^{-4} \text{ rad}$                 |
| maximum value in the MBW (5 mHz to 100 mHz)           |                                                    |
| $\tilde{\varphi}^W, \tilde{\theta}^W, \tilde{\psi}^W$ | $\leq 1 \cdot 10^{-6} \text{ rad}/\text{Hz}^{1/2}$ |

Table 6.3-10: Requirements on the mutual alignment of the three OAGRFs ( $\varphi, \theta, \psi =$  rotation angles defining the relative orientation between any pair of OAGRFs)

| Quantity                                                                                             | Requirement              |
|------------------------------------------------------------------------------------------------------|--------------------------|
| $\delta TFA_{14,Z}, \delta TFA_{25,X}, \delta TFA_{36,X}$                                            | $\leq 4 \cdot 10^{-6}$   |
| $\delta TFA_{14,Y}, \delta TFA_{25,Z}, \delta TFA_{36,Y}$                                            | $\leq 1.5 \cdot 10^{-5}$ |
| $TFS_{14,Y}, TFS_{14,Z}, \delta TFS_{25,X}, \delta TFS_{25,Z}, \delta TFS_{36,X}, \delta TFS_{36,Y}$ | $\leq 4 \cdot 10^{-6}$   |

Table 6.3-11: Requirements on the contribution to CMRR along the OAG transversal axes of the accelerometer TF and of the Gradiometer structure TF

| Quantity             | Requirement              |
|----------------------|--------------------------|
| $C_{Ye}$             | $\leq 1.1 \cdot 10^{-4}$ |
| $C_{YeXe}, C_{ZeXe}$ | $\leq 9.2 \cdot 10^{-4}$ |

Table 6.3-12: Requirements on the angular-linear acceleration coupling factors at accelerometer level

Beside the above requirements, the angular acceleration measurement imposes also constraints on the limit values assumed all along the mission by the common and differential scale factors, misalignments and couplings of the accelerometer pairs about the OAGs transversal axes (i.e. the axes perpendicular to the OAG baseline). The limits for these elements already provided in Table 4.1-2 are compatible with the angular acceleration measurement requirements (Figure 6.3-2).

## 7. IN-FLIGHT PERFORMANCE PREDICTION FOR THE GRADIOMETRIC MISSION

### 7.1 PROCEDURE AND REFERENCE DATA FOR THE PERFORMANCE PREDICTION COMPUTATION

The error budget for the Gravimetric mission provided in the following section has been obtained by evaluating the value assumed during the mission measurement phase by each parameter (accelerometer noise, residual drag acceleration, self-gravity etc..) identified in the error breakdown and by composing their contributions according to the equations of the sections 5.1 and 5.2. As for the overall error apportionement for the requirements derivation, the error terms which are classified under the distinct categories of the error tree are added quadratically (RSS).

The prediction of the in-flight value of each parameter contributing to the error budget is based on analytical and/or numerical models correlated with the results of the tests performed on the models of the satellite, gradiometer, equipments, components implemented so far. The reference sources, the method and the assumptions which are at the basis of the parameter value prediction are provided in the sub-sections of this chapter.

The error budget for the GGT tensor components and for the GGT trace in the GRF is provided as function of the frequency, with extension also outside the MBW. This implies the prediction not just of a single value of the parameters contributing to the error budget, but of their spectral density as function of the frequency. This has been done for the major contributors. For the minor ones, a simplified but conservative approach has been adopted of assuming a flat spectral density with a level corresponding to the maximum estimated value in the MBW.

#### 7.1.1 Instrument Errors Contributors

The Instrument Error budget computation and results are detailed in [RD 2], [RD 14]. The Accelerometer Noise is by far dominating over the other contributors.

##### 7.1.1.1 Accelerometer Noise (I.1)

The accelerometer intrinsic measurement noise spectral density  $\tilde{n}_{d,ij,k}(v)$  has been computed by ONERA, including the contributions of the noise of the electronics components (position sensor, voltage reference, AD and DA converters, drive voltage amplifier), the contact potential difference fluctuations, the parasitic forces between the proof mass and its cage (due to the radiometer effect, radiation pressure, Lorentz force, gold wire stiffness and damping, electrostatic force stiffness and damping).

The accelerometer noise prediction is based on a worst-case analysis, correlated with the results of the tests performed on the FEEU development models. These tests provide measurements of the noise contributions of the various electronics components which, combined in a model of the accelerometer measurement chain, allow to estimate the resulting measurement noise. The tests performed on the accelerometer do allow quantifying directly the contribution of the contact potential difference fluctuations (for which an upper limit has been indirectly derived from the experimental data) and of the parasitic forces. These are estimated by means of analytical models depending on physical parameters (pressure, temperature and temperature gradient inside the ASH, stiffness and damping of the gold wire, etc..) whose value is either derived from measurements (like the pressure inside the ASH) or from numerical simulations (like the in-flight operating temperature of the ASH), or extrapolated from experimental data (like the damping of the gold wire).

The predicted acceleration measurement noise spectral density along the ultra sensitive and less sensitive axes of the six accelerometers is shown in Figure 7.1-1 and Figure 7.1-2. The predicted noise is representative of the last Gradiometer configuration, after the replacement of the ASH PFM with the ASH SM01 [RD 15].

In case the accelerometer quadratic factor along the US axes is as large as its predicted maximum value ( $\pm 1206 \text{ s}^2/\text{m}$ ) and this quadratic factor is compensated in flight by displacement of the proof mass (current approach, [RD 7]), this operation produces an increase of the accelerometer noise along the US axes as shown in Figure 7.1-3.

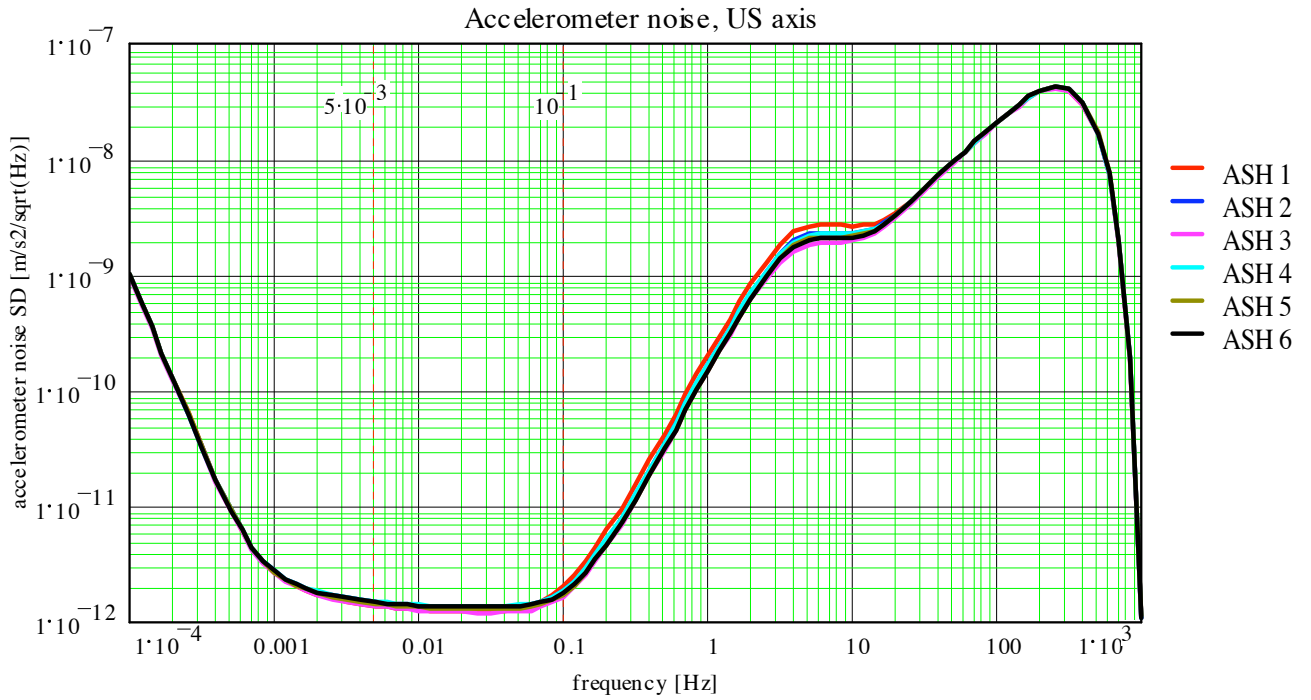


Figure 7.1-1: Predicted spectral density of the accelerometer noise along the ultra sensitive axes

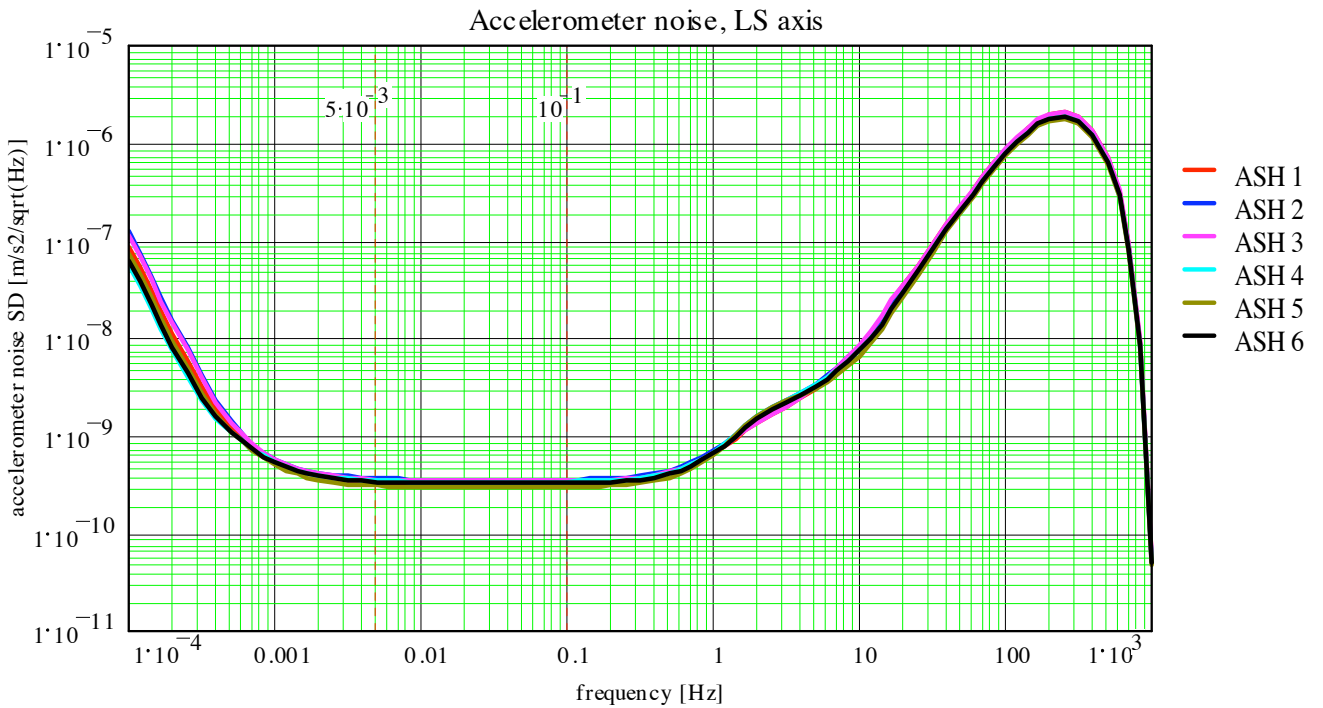


Figure 7.1-2: Predicted spectral density of the accelerometer noise along the less sensitive axes

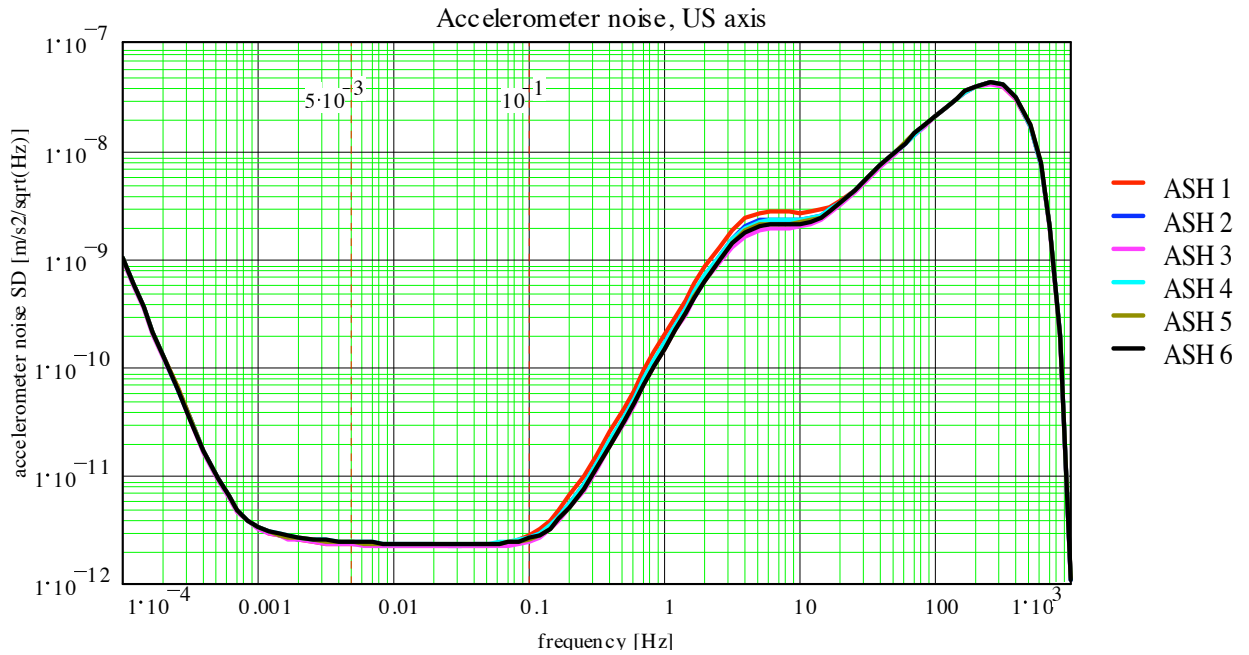


Figure 7.1-3: Predicted spectral density of the accelerometer noise along the ultra sensitive axes after the compensation of a quadratic factor of 1206 s<sup>2</sup>/m by displacement of the proof mass.

7.1.1.2 Accelerometer Position Stability (I.2)

This error term, deriving from the deformations of the gradiometer baselines, has been evaluated by Alcatel by means of a thermo-elastic analysis. Its contribution to the gradiometric error is:

$$\delta\tilde{U}_{XX,1,2}^W \cong 0, \delta\tilde{U}_{YY,1,2}^W \cong 0, \delta\tilde{U}_{ZZ,1,3}^W \cong (1.8)^{1/2} = 1.34 \text{ mE/Hz}^{1/2}$$

7.1.1.3 OAGRFs alignment errors in the GRF and alignment stability in the GRF (I.3)

This error term has been evaluated by Alcatel by means of an analysis of the integration errors and of the successive variations of the initial alignment of the OAGs. Its contribution to the gradiometric error in the MBW is:

$$\delta\tilde{U}_{XX,1,3}^W = (0.27)^{1/2} = 0.52 \text{ mE/Hz}^{1/2}, \delta\tilde{U}_{YY,1,3}^W = (0.42)^{1/2} = 0.65 \text{ mE/Hz}^{1/2}, \delta\tilde{U}_{ZZ,1,3}^W = (0.01)^{1/2} = 0.1 \text{ mE/Hz}^{1/2}$$

7.1.1.4 Gradiometer Self Gravity (I.4)

This error term has been evaluated by Alcatel by means of a self-gravity model of the Gradiometer (based on a point-like model of the mass distribution) and taking into account the results of the thermoelastic analysis. The estimated contribution of the Gradiometer self-gravity to the gradiometric error in the MBW is negligible (<0.01 mE/Hz<sup>1/2</sup>).

### 7.1.1.5 Coupling with Gradiometer Magnetic Field (I.5)

The contribution of this term to the gradiometric error has been evaluated by Alcatel, taking into account the specified attenuation of the magnetic shield surrounding the accelerometer (the measured attenuation is actually better). Its contribution to the gradiometric error is:

$$\delta\tilde{U}_{XX,1.5}^W = 0.05 \text{ mE/Hz}^{1/2}, \delta\tilde{U}_{YY,1.5}^W = 0.055 \text{ mE/Hz}^{1/2}, \delta\tilde{U}_{ZZ,1.5}^W = 0.033 \text{ mE/Hz}^{1/2}$$

### 7.1.1.6 Accelerometer Noise Coupling with Common/Differential Misalignments and Scale Factors (I.6)

This error term has been computed from equation (5.1.6) using the following inputs.

- accelerometer noise spectral density about the ultra-sensitive and less-sensitive axes as per section 7.1.1.1;
- the expected on-orbit upper limits for the values of the Calibration Matrices as per table 4.1-2:

The contribution of this term to the gradiometric error at 5 mHz is:

$$\delta\tilde{U}_{XX,1.6}^W = 0.177 \text{ mE/Hz}^{1/2}, \delta\tilde{U}_{YY,1.6}^W = 0.178 \text{ mE/Hz}^{1/2}, \delta\tilde{U}_{ZZ,1.6}^W = 0.182 \text{ mE/Hz}^{1/2}$$

## 7.1.2 Instrument-Satellite Coupling Errors

### 7.1.2.1 Coupling with Common-Mode Accelerations (C.1)

#### 7.1.2.1.1 Coupling with Non-Gravitational Linear Accelerations of the Satellite COM (C.1.1)

This error term has been computed from equation (5.2.1) using the following inputs.

- Maximum error on the in-flight knowledge of the elements of the differential-mode part of the Inverse Calibration Matrices derived from the results of the numerical simulations performed to verify the validity of the calibration method (ref. [RD 7]), with the addition of the monthly drifts of the ICM elements as per their specification provided in Table 6.3-7 (the specified limits have been confirmed by the corresponding budgets – [RD 14]):

$$\delta MI_{ij,hk} = \delta MI_{ij,hk\_calibration} \text{ (from calibration simulation results)} + \delta MI_{ij,hk\_drift} \text{ (from Table 6.3-7)}$$

In particular, the values of  $\delta MI_{ij,hk\_calibration}$  have been obtained from the statistics of the 20 test cases of the “simulations set 1”, with the accelerometer proof mass rotation about the X axis of the AESRF controlled by 4 ultra-sensitive electrode pairs:

$$\delta MI_{ij,hk\_calibration} = (\delta MI_{ij,hk} \text{ calibration specification from Table 6.3-7}) \times [\max(\Gamma_{ijkl})]$$

where  $\Gamma_{ijkl}$  is the ratio between the determination error of the elements of the ICMs (result of the calibration simulation) and their required accuracy (Table 6.3-7) and the maximum value of each element of  $(\Gamma_{ijkl})$  has been computed over the 20 simulation cases. The results are summarized in the following table (where also the common-mode part of the ICM is provided)

| Row             | Maximum measurement error of the common and differential elements of $MI_{14}$ at calibration |                                            |                                            |                                            |                                            |                                            |
|-----------------|-----------------------------------------------------------------------------------------------|--------------------------------------------|--------------------------------------------|--------------------------------------------|--------------------------------------------|--------------------------------------------|
| 4 <sup>th</sup> | $\delta MI_{14,41} \leq 7.0 \cdot 10^{-6}$                                                    | $\delta MI_{14,42} \leq 7.7 \cdot 10^{-7}$ | $\delta MI_{14,43} \leq 5.1 \cdot 10^{-6}$ | $\delta MI_{14,44} \leq 3.4 \cdot 10^{-3}$ | $\delta MI_{14,45} \leq 3.6 \cdot 10^{-6}$ | $\delta MI_{14,46} \leq 7.7 \cdot 10^{-5}$ |
| 5 <sup>th</sup> | $\delta MI_{14,51} \leq 2.5 \cdot 10^{-5}$                                                    | $\delta MI_{14,52} \leq 7.6 \cdot 10^{-4}$ | $\delta MI_{14,53} \leq 1.1 \cdot 10^{-4}$ | $\delta MI_{14,54} \leq 2.4 \cdot 10^{-5}$ | $\delta MI_{14,55} \leq 3.6 \cdot 10^{-3}$ | $\delta MI_{14,56} \leq 1.2 \cdot 10^{-5}$ |
| 6 <sup>th</sup> | $\delta MI_{14,61} \leq 2.6 \cdot 10^{-5}$                                                    | $\delta MI_{14,62} \leq 1.1 \cdot 10^{-4}$ | $\delta MI_{14,63} \leq 3.5 \cdot 10^{-5}$ | $\delta MI_{14,64} \leq 1.0 \cdot 10^{-4}$ | $\delta MI_{14,65} \leq 9.9 \cdot 10^{-6}$ | $\delta MI_{14,66} \leq 3.5 \cdot 10^{-3}$ |
| Row             | Maximum measurement error of the common and differential elements of $MI_{25}$ at calibration |                                            |                                            |                                            |                                            |                                            |
| 4 <sup>th</sup> | $\delta MI_{25,41} \leq 3.6 \cdot 10^{-5}$                                                    | $\delta MI_{25,42} \leq 2.7 \cdot 10^{-5}$ | $\delta MI_{25,43} \leq 1.1 \cdot 10^{-4}$ | $\delta MI_{25,44} \leq 3.5 \cdot 10^{-3}$ | $\delta MI_{25,45} \leq 1.4 \cdot 10^{-4}$ | $\delta MI_{25,46} \leq 7.6 \cdot 10^{-6}$ |
| 5 <sup>th</sup> | $\delta MI_{25,51} \leq 4.7 \cdot 10^{-6}$                                                    | $\delta MI_{25,52} \leq 1.1 \cdot 10^{-5}$ | $\delta MI_{25,53} \leq 5.1 \cdot 10^{-7}$ | $\delta MI_{25,54} \leq 1.4 \cdot 10^{-4}$ | $\delta MI_{25,55} \leq 4.0 \cdot 10^{-3}$ | $\delta MI_{25,56} \leq 3.8 \cdot 10^{-6}$ |
| 6 <sup>th</sup> | $\delta MI_{25,61} \leq 9.8 \cdot 10^{-4}$                                                    | $\delta MI_{25,62} \leq 2.6 \cdot 10^{-5}$ | $\delta MI_{25,63} \leq 7.8 \cdot 10^{-4}$ | $\delta MI_{25,64} \leq 7.5 \cdot 10^{-6}$ | $\delta MI_{25,65} \leq 2.3 \cdot 10^{-5}$ | $\delta MI_{25,66} \leq 2.0 \cdot 10^{-3}$ |
| Row             | Maximum measurement error of the common and differential elements of $MI_{36}$ at calibration |                                            |                                            |                                            |                                            |                                            |
| 4 <sup>th</sup> | $\delta MI_{36,41} \leq 2.3 \cdot 10^{-5}$                                                    | $\delta MI_{36,42} \leq 1.0 \cdot 10^{-4}$ | $\delta MI_{36,43} \leq 2.8 \cdot 10^{-5}$ | $\delta MI_{36,44} \leq 3.4 \cdot 10^{-3}$ | $\delta MI_{36,45} \leq 8.0 \cdot 10^{-6}$ | $\delta MI_{36,46} \leq 8.9 \cdot 10^{-5}$ |
| 5 <sup>th</sup> | $\delta MI_{36,51} \leq 9.9 \cdot 10^{-5}$                                                    | $\delta MI_{36,52} \leq 8.4 \cdot 10^{-4}$ | $\delta MI_{36,53} \leq 2.7 \cdot 10^{-5}$ | $\delta MI_{36,54} \leq 7.0 \cdot 10^{-6}$ | $\delta MI_{36,55} \leq 2.6 \cdot 10^{-3}$ | $\delta MI_{36,56} \leq 2.2 \cdot 10^{-5}$ |
| 6 <sup>th</sup> | $\delta MI_{36,61} \leq 4.4 \cdot 10^{-6}$                                                    | $\delta MI_{36,62} \leq 4.5 \cdot 10^{-7}$ | $\delta MI_{36,63} \leq 1.7 \cdot 10^{-5}$ | $\delta MI_{36,64} \leq 8.2 \cdot 10^{-5}$ | $\delta MI_{36,65} \leq 4.6 \cdot 10^{-6}$ | $\delta MI_{36,66} \leq 3.4 \cdot 10^{-3}$ |

Table 7.1-1: Errors on the determination of the of  $[MI]_{d,14}$ ,  $[MI]_{d,25}$ ,  $[MI]_{d,36}$  and  $[MI]_{c,14}$ ,  $[MI]_{c,25}$ ,  $[MI]_{c,36}$ , resulting from the in-flight calibration

- Spectral density in the MBW of the on-orbit variation of the elements of the differential-mode part of the Inverse Calibration Matrices taken equal to the specification (table 6.3.8) for the off-diagonal terms (the specified limits have been confirmed by the corresponding budgets – [RD 14]), and taken from the budget computed by ONERA for the diagonal terms (differential scale factors):

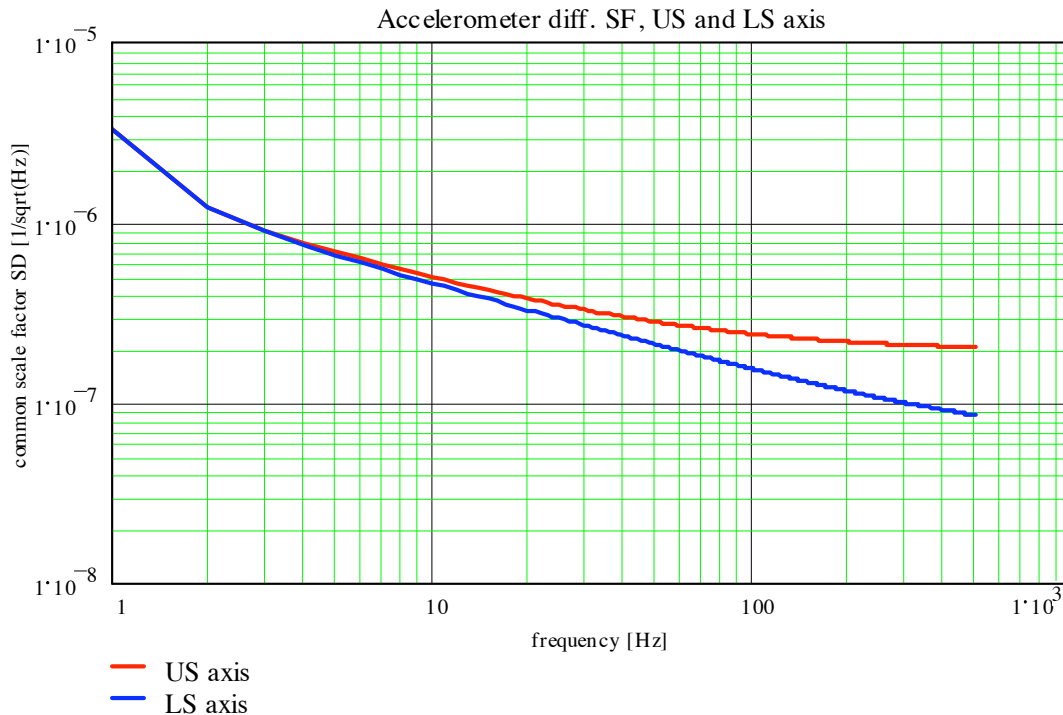


Figure 7.1-4: Differential scale factor spectral densities for ultra sensitive ( $\delta MI_{14,41}$ ,  $\delta MI_{14,63}$ ,  $\delta MI_{25,41}$ ,  $\delta MI_{25,52}$ ,  $\delta MI_{36,41}$ ,  $\delta MI_{36,63}$ ) and less sensitive axes ( $\delta MI_{14,52}$ ,  $\delta MI_{25,63}$ ,  $\delta MI_{36,52}$ )

- Non-gravitational linear accelerations ( $D_x$ ,  $D_y$ ,  $D_z$ ) of the spacecraft COM in the GRF (maximum value below the MBW and spectral density in the MBW) computed from a numerical simulation performed with the GOCE End-to-End System Simulator, including models payload, satellite configuration and equipment, DFACS algorithms for the drag-free mode

updated at the current status of the project. Concerning the satellite parameters that mainly affect the environmental perturbations on the satellite (mass properties, residual magnetic dipole moment, ion thruster force vector misalignment, magnetic torquer quantization level) the values provided in [RD 8] have been used.

The maximum values of the spectral densities of the non-gravitational accelerations have been computed from time histories covering 60 days of the GOCE mission, after having removed the initial transient. Since the cross-track and radial drag forces are not controlled, the value of the non-gravitational accelerations along these axes depends on the environmental conditions experienced by the satellite. To assess the sensitivity of the gravimetric performances to these conditions, a mission scenario representative of the first Mission Operational Phase (MOP-1) has been simulated, characterized by the following parameters:

- *Orbit type:* Sun-synchronous, Dawn-Dusk
- *Solar activity parameters:*  $F10.7 = 144.4$ ,  $A_p = 17.9$  (95% probability forecast)
- *Mean spherical altitude:* 268.6 km
- *Mean/max air density:*  $4.5 \cdot 10^{-11}$  kg/m<sup>3</sup> /  $8.1 \cdot 10^{-11}$  kg/m<sup>3</sup>
- *Mean/max ion thruster force for drag compensation:* 5.7 mN / 10.8 mN

#### 7.1.2.1.2 Coupling with Satellite COM Location and Stability in the GRF (C.1.2)

This error term has been computed from equation (5.2.2) using for the OAGRF-COM position vector ( $C_X, C_Y, C_Z$ ), its time derivatives ( $\dot{C}_X^0, \dot{C}_Y^0, \dot{C}_Z^0, \ddot{C}_X^0, \ddot{C}_Y^0, \ddot{C}_Z^0$ ) and its stability spectral densities the specified values (Table 6.1-10), but for the components that were found exceeding these limits from the system-level thermo-elastic distortion analysis (ref. [RD 9]):

- $\ddot{C}_Y^0 = 1.4 \cdot 10^{-7}$  m/s<sup>2</sup>,  $\ddot{C}_Z^0 = 1.1 \cdot 10^{-7}$  m/s<sup>2</sup>,
- $\tilde{C}_X^W = 1.5 \cdot 10^{-6}$  m/Hz<sup>1/2</sup>,  $\tilde{C}_Z^W = 1.2 \cdot 10^{-6}$  m/Hz<sup>1/2</sup>,
- $\tilde{C}_Y^W = 1.5 \cdot 10^{-9}$  m/s<sup>2</sup>/Hz<sup>1/2</sup>,  $\tilde{C}_Z^W = 1.2 \cdot 10^{-9}$  m/s<sup>2</sup>/Hz<sup>1/2</sup>.

In addition, the values of  $[\delta \mathbf{M} \mathbf{I}]_{d,ij}^0$ ,  $[\delta \tilde{\mathbf{M}} \mathbf{I}]_{d,ij}^W$  provided by the calibration performance analysis (section 7.1.2.1.1), and the values of  $\dot{\omega}_X^0, \dot{\omega}_Y^0, \dot{\omega}_Z^0, \tilde{\omega}_X^W, \tilde{\omega}_Y^W, \tilde{\omega}_Z^W, \dot{\omega}_X^0, \dot{\omega}_Y^0, \dot{\omega}_Z^0, \tilde{\omega}_X^W, \tilde{\omega}_Y^W, \tilde{\omega}_Z^W$  provided GOCE End-to-End System Simulator for the three mission scenario described in section 7.1.2.1.1 have been utilised to compute this error term.

#### 7.1.2.2 Coupling with Differential-Mode Accelerations (C.2)

##### 7.1.2.2.1 Coupling with the Angular Acceleration of the Satellite about its COM (C.2.1)

This error term has been computed from equation (5.2.3) using the following inputs.

- Maximum value and spectral density of the angular accelerations of the spacecraft about its COM in the GRF ( $\dot{\omega}_X^0, \dot{\omega}_Y^0, \dot{\omega}_Z^0, \tilde{\omega}_X^W, \tilde{\omega}_Y^W, \tilde{\omega}_Z^W$ ) provided GOCE End-to-End System Simulator for the mission scenario described in section 7.1.2.1.1.
- Maximum error on the in-flight knowledge of the elements of the common-mode part of the Inverse Calibration Matrices derived from the calibration performance analysis and from the specified drift in the inter-calibration period (as described in section 7.1.2.1.1).
- Spectral density in the MBW of the on-orbit variation of the elements of the common-mode part of the Inverse Calibration Matrices taken equal to the specification (Table 6.3-8) for the off-diagonal terms (the specified limits are fulfilled by the corresponding budgets – [RD 2]), and taken from the budget computed by ONERA for the diagonal terms (common scale factors):

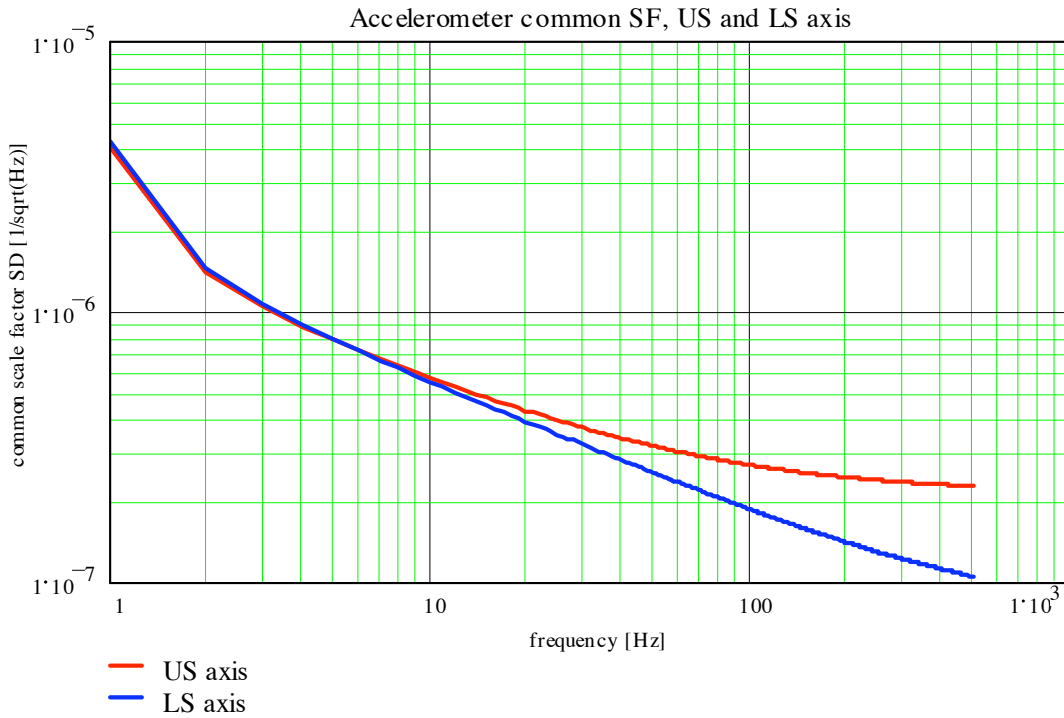


Figure 7.1-5: Common scale factor spectral densities for ultra sensitive ( $\delta MI_{14,44}$ ,  $\delta MI_{14,66}$ ,  $\delta MI_{25,44}$ ,  $\delta MI_{25,55}$ ,  $\delta MI_{36,44}$ ,  $\delta MI_{36,66}$ ) and less sensitive axes ( $\delta MI_{14,55}$ ,  $\delta MI_{25,66}$ ,  $\delta MI_{36,56}$ )

7.1.2.2.2 Coupling with the Centrifugal Accelerations and the Gravity Gradient Tensor (C.2.2)

This error term has been computed from equation (5.2.5) using the following inputs.

- Maximum value and spectral density of the angular velocities of the spacecraft about its COM in the GRF ( $\omega_X^0, \omega_Y^0, \omega_Z^0, \tilde{\omega}_X^W, \tilde{\omega}_Y^W, \tilde{\omega}_Z^W$ ) provided GOCE End-to-End System Simulator for the mission scenario described in section 7.1.2.1.1.
- the GGT values in the GRF provided in section 3.4.2 (for  $U_{ij}^0$  and  $\tilde{U}_{ij}^W$ ).
- values of  $[\delta MI]_{d,ij}^0, [\delta \tilde{MI}]_{d,ij}^W$  provided by the calibration performance analysis (section 7.1.2.1.1).

7.1.2.3 Quadratic Coupling (C.3)

This error term has been computed from equation (5.2.6) using the following inputs.

- Maximum values of the quadratic factors and of their spectral density in the MBW during the measurement phase, after on-orbit calibration, as specified in Table 6.1-11 and Table 6.3-9:

| Sensor Pair                     | Quadratic factors maximum value below the MBW                                      | Quadratic factors spectral density maximum value in the MBW                                |
|---------------------------------|------------------------------------------------------------------------------------|--------------------------------------------------------------------------------------------|
| A <sub>1</sub> , A <sub>4</sub> | $K2_{c,14,X} = 10 \text{ s}^2/\text{m}, K2_{d,14,X} = 4 \text{ s}^2/\text{m}$      | $\tilde{K}2_{c,14,X}^W, \tilde{K}2_{d,14,X}^W = 0.01 \text{ s}^2/\text{m}/\text{Hz}^{1/2}$ |
|                                 | $K2_{c,14,Y}, K2_{d,14,Y} = 10 \text{ s}^2/\text{m}$                               | $\tilde{K}2_{c,14,Y}^W, \tilde{K}2_{d,14,Y}^W = 0.01 \text{ s}^2/\text{m}/\text{Hz}^{1/2}$ |
|                                 | $K2_{c,14,Z}, K2_{d,14,Z} = 10 \text{ s}^2/\text{m}$                               | $\tilde{K}2_{c,14,Z}^W, \tilde{K}2_{d,14,Z}^W = 0.01 \text{ s}^2/\text{m}/\text{Hz}^{1/2}$ |
| A <sub>2</sub> , A <sub>5</sub> | $K2_{c,25,X}, K2_{d,25,X} = 10 \text{ s}^2/\text{m}$                               | $\tilde{K}2_{c,25,X}^W, \tilde{K}2_{d,25,X}^W = 0.01 \text{ s}^2/\text{m}/\text{Hz}^{1/2}$ |
|                                 | $K2_{c,25,Y} \leq 7 \text{ s}^2/\text{m}, K2_{d,25,Y} \leq 4 \text{ s}^2/\text{m}$ | $\tilde{K}2_{c,25,Y}^W, \tilde{K}2_{d,25,Y}^W = 0.01 \text{ s}^2/\text{m}/\text{Hz}^{1/2}$ |
|                                 | $K2_{c,25,Z}, K2_{d,25,Z} = 10 \text{ s}^2/\text{m}$                               | $\tilde{K}2_{c,25,Z}^W, \tilde{K}2_{d,25,Z}^W = 0.01 \text{ s}^2/\text{m}/\text{Hz}^{1/2}$ |
| A <sub>3</sub> , A <sub>6</sub> | $K2_{c,36,X}, K2_{d,36,X} = 10 \text{ s}^2/\text{m}$                               | $\tilde{K}2_{c,36,X}^W, \tilde{K}2_{d,36,X}^W = 0.01 \text{ s}^2/\text{m}/\text{Hz}^{1/2}$ |
|                                 | $K2_{c,36,Y}, K2_{d,36,Y} = 10 \text{ s}^2/\text{m}$                               | $\tilde{K}2_{c,36,Y}^W, \tilde{K}2_{d,36,Y}^W = 0.01 \text{ s}^2/\text{m}/\text{Hz}^{1/2}$ |
|                                 | $K2_{c,36,Z} \leq 7 \text{ s}^2/\text{m}, K2_{d,36,Z} \leq 4 \text{ s}^2/\text{m}$ | $\tilde{K}2_{c,36,Z}^W, \tilde{K}2_{d,36,Z}^W = 0.01 \text{ s}^2/\text{m}/\text{Hz}^{1/2}$ |

Table 7.1-2: Values of the quadratic factors considered for the gradiometric error budget computation

The possibility of measuring and adjusting in flight the quadratic factors within the specified limits has been demonstrated in [RD 7].  
 The specified limits for the inter-calibration drifts (1 s<sup>2</sup>/m) and for the spectral densities of the quadratic factors in the MBW are fulfilled by the corresponding budgets (ref. [RD 14]).

7.1.3 Coupling with Accelerometer Misplacement from their Nominal Position (C.4)

This error term has been computed from equation (5.2.7) using the following inputs.

- Maximum value below the MBW and maximum value in the MBW of the spectral density of the accelerometer displacements from its nominal position in the OAGRf ( $\delta A_{1,X}^0, \delta A_{2,Y}^0, \delta A_{3,Z}^0, \delta \tilde{A}_{1,X}^W, \delta \tilde{A}_{2,Y}^W, \delta \tilde{A}_{3,Z}^W$ ) as specified in Table 6.1-12. The specified limits are fulfilled by the corresponding budgets (ref. [RD 14]).
- Values of  $\omega_X^0, \omega_Y^0, \omega_Z^0, \tilde{\omega}_X^W, \tilde{\omega}_Y^W, \tilde{\omega}_Z^W, \dot{\omega}_X^0, \dot{\omega}_Y^0, \dot{\omega}_Z^0, \tilde{\omega}_X^W, \tilde{\omega}_Y^W, \tilde{\omega}_Z^W$  provided GOCE End-to-End System Simulator for the mission scenario described in section 7.1.2.1.1.

7.1.3.1 Coupling with Platform Magnetic Field (C.5)

This error term has been computed from equation (5.2.9) using the following inputs.

- maximum value below the MBW of the modulus of the magnetic field generated by the Platform at the location of each proof mass:  $B_{i,p}^0 = 3.1 \cdot 10^{-6}$  Tesla (produced by the magnetic torquers during the Gradiometer calibration by satellite shaking, when the magnetic torquers activity is higher);

- maximum value in the MBW of the spectral density of the fluctuations of the modulus of the magnetic field generated by the Platform at the location of each proof mass, computed from the magnetic torquers activity during the Gradiometer calibration by satellite shaking:

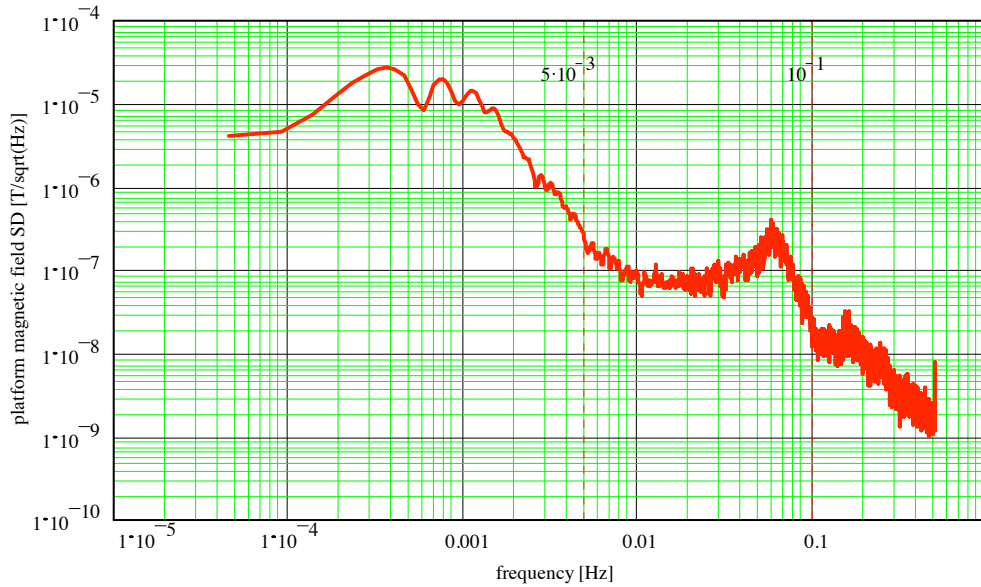


Figure 7.1-6: Spectral density of the platform magnetic field at the accelerometer location ( $B_{i,P}^W$ ) considered for the gradiometric error budget computation

- maximum value below MBW of the modulus of the magnetic field generated by the Gradiometer at the location of each proof mass equal to the specified constraint in table 6.1-10:  $B_{i,G}^0 = 4 \cdot 10^{-6}$  Tesla;
- maximum value in the MBW of the spectral density of the fluctuations of the modulus of the magnetic field generated by the Gradiometer at the location of each proof mass equal to the specified constraint in Table 6.1-10:  $B_{i,G}^W = 1 \cdot 10^{-7}$  Tesla/Hz<sup>1/2</sup>;
- maximum value below MBW of the modulus of the magnetic field generated by the Earth at the satellite location:  $B_E^0 = 5.5 \cdot 10^{-5}$  Tesla (derived from the available models of the Earth magnetic field [RD 6]);
- maximum value in the MBW of the spectral density of the fluctuations of the modulus of the magnetic field generated by the Earth along the GOCE orbit:  $B_E^W = 2 \cdot 10^{-6}$  Tesla/Hz<sup>1/2</sup> (derived from the available models of the Earth magnetic field [RD 6]);
- volume of the accelerometer proof mass  $V = 1.6 \cdot 10^{-5}$  m<sup>3</sup>;
- mass of the accelerometer proof mass  $m = 0.32$  kg;
- magnetic susceptibility of the accelerometer proof mass  $\chi_m = 3 \cdot 10^{-4}$ ;
- proof mass size along the accelerometer ultra-sensitive axis  $L_{PM} = 4 \cdot 10^{-2}$  m;
- magnetic field attenuation factor due to the shielding effect of the accelerometer Invar housing  $\alpha_b = 0.02$ .
- magnetic field attenuation due to the 0.63 mm thick mumetal sheet placed around the accelerometers: 12 dB

7.1.3.2 Coupling of Accelerometer Noise with Common and Differential-Mode Misalignments and Scale Factors Knowledge Uncertainty (C.6)

This error term has been computed from equation (5.2.10) using the accelerometer noise spectral density provided in section 7.1.1.1 (and assuming  $\tilde{n}_{c,ij,k}^W = \tilde{n}_{d,ij,k}^W$ ) and the values of  $[\delta MI]_{d,ij}^0$ ,  $[\delta MI]_{c,ij}^0$  provided by the calibration performance analysis (section 7.1.2.1.1).

7.1.3.3 Coupling with High Frequency Noise (C.7)

This error term has been evaluated by numerical simulations, by computing the amount of differential acceleration produced in the MBW by the coupling of an high frequency common-mode acceleration with the shape provided in Figure 7.1-7 (which envelopes the requirement for the residual non-gravitational linear acceleration in the region from 0.1 to 1 Hz, giving the largest contribution the aliasing) with a differential quadratic factor = 1 s<sup>2</sup>/m. The “aliasing factor” so computed is  $\sim 0.4 \cdot 10^{-12}$  m/s<sup>2</sup>/Hz<sup>1/2</sup> ( $\sim 0.8$  mE/Hz<sup>1/2</sup>) for each 1 s<sup>2</sup>/m of differential quadratic factor. A cubic aliasing term of 0.53 mE/Hz<sup>1/2</sup> has been also considered, according to [RD 5].

This aliasing factor is then multiplied by the quadratic factor values of Table 7.1.3 to obtain the corresponding gradiometric error.

The acceleration noise envelope of Figure 7.1-7 applies to the X-axis of the satellite only, i.e. the axis aligned to the orbital velocity direction, along which the drag force is compensated by the ion thruster. Along the transversal axes Y, Z the linear acceleration noise (due to the lateral components of the drag only) above the MBW is negligible. Thus, no aliasing effect due to the high frequency noise coupling with the accelerometer non linearities has been considered for these axes.

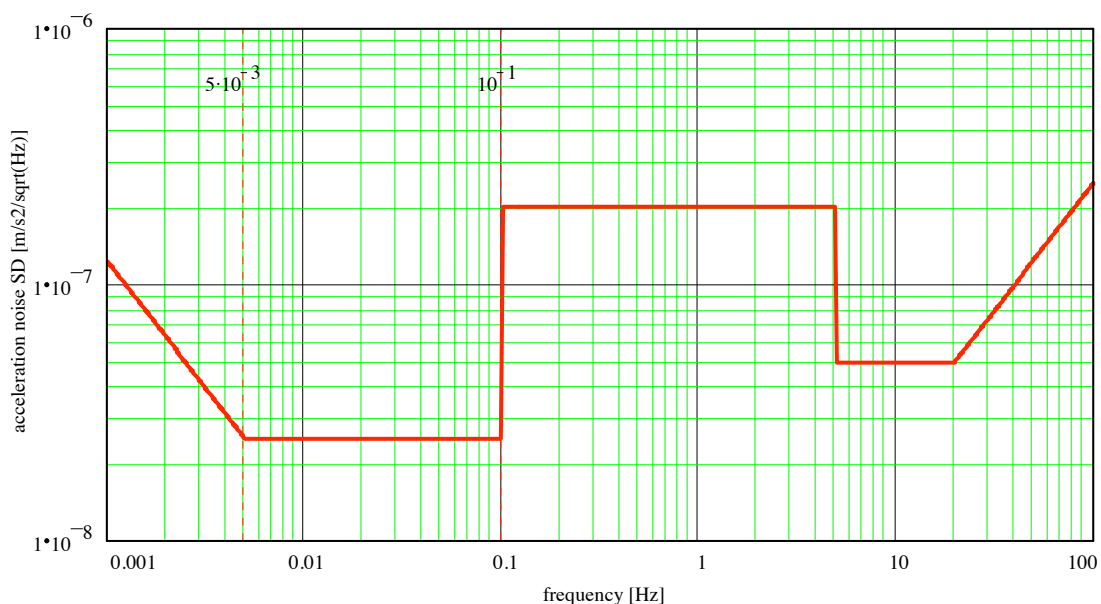


Figure 7.1-7: Spectral density of the high-frequency common-mode acceleration assumed for the computation of the aliasing by coupling with the accelerometer quadratic factor.

### 7.1.3.4 Coupling with the Transfer Function Difference (C.8)

The contribution of this error term to the gradiometric error has been computed from equations (5.2.12) and (4.39) using the following inputs.

- Difference in the accelerometer transfer functions  $\delta TFA_{ij,k} = 22 \cdot 10^{-6}$  for the US axis and  $\delta TFA_{ij,k} = 380 \cdot 10^{-6}$  for the LS axis at 100 mHz (decreasing proportionally with the frequency from 100 to 5 mHz). This difference derives from the phase mismatch of the transfer functions of the accelerometer readout anti-aliasing analogue filter and of the DVA2. The precise physical matching between the transfer functions has been achieved at component level only for the anti-aliasing analogue filter of the accelerometer readout only. For the DVA2, the transfer function will be determined on ground through the (indirect) measurements of the value of the DVA2 resistors and capacitors. Then the knowledge of the TF will be exploited in the post processing to recover the phase delay introduced by the DVA2. The possibility of achieving a knowledge of the DVA2 TF accurate enough to get  $\delta TFA_{ij,k} \leq 22 \cdot 10^{-6}$  has been demonstrated by simulation.
- Difference in the Gradiometer baseline structure transfer functions  $\delta TFS_{ij,k} = 4 \cdot 10^{-6}$  in the MBW (actually it increases with the frequency; thus assuming a constant value in the whole MBW is conservative). This difference, computed from a FEM analysis turns out to be much smaller than this value (ref. [RD 11]). An approximate computation made using the expression:

$$\delta TFS_{ij,k} \cong 2 \frac{\zeta_0}{f_0} \left| \frac{\Delta f_{ij,k} - \Delta \zeta_{ij,k}}{1 + \Delta f_{ij,k}} \right| \nu$$

with  $f_0 = 1000$  Hz (lowest resonant frequency of the first traction-compression mode of the gradiometer baselines (ref. [RD 11]),  $\zeta_0 = 0.1$ ,  $\Delta f_{ij,k} = 25\%$ ,  $\Delta \zeta_{ij,k} = 0.4\%$ , gives  $\delta TFS_{ij,k} \cong 4 \cdot 10^{-6}$  at 0.1 Hz (linearly decreasing at lower frequencies).

- Spectral density of the common-mode acceleration  $\underline{a}_{c,ij} \cong ([U] - [\Omega^2] - [\dot{\Omega}])\underline{C}_i - 2[\Omega] \cdot \dot{\underline{C}}_i - \ddot{\underline{C}}_i + \underline{D}$  obtained from the results of the GOCE End-to-End System Simulator for the mission scenario described in section 7.1.2.1.1, and from the values of  $\underline{C}_i$ ,  $\dot{\underline{C}}_i$ ,  $\ddot{\underline{C}}_i$  utilised in section 7.1.2.1.2.

### 7.1.3.5 Coupling Between Angular and Linear Acceleration at Accelerometer Level (C.9)

The contribution of this error term to the gradiometric error has been computed from equation (5.2.13) and (4.39) using the following inputs.

- Angular-linear acceleration coupling factors at accelerometer level:
  - $C_{Ye} = 1.1 \cdot 10^{-4}$  (transversal ultra-sensitive axis)
  - $C_{Ze} = 1.1 \cdot 10^{-4}$  (in-line ultra-sensitive axis)
  - $C_{YeXe} = 9.2 \cdot 10^{-4}$  (less sensitive axis)
  - $C_{ZeXe} = 9.2 \cdot 10^{-4}$  (less sensitive axis)

These are almost equal to the coupling factors “by construction”, for a control of the proof mass rotations performed by means of all the electrode pairs (ref. [RD 12]). A further reduction of these values can be achieved by exploiting in the post processing the knowledge of the electrostatic gains measured on ground. The ground processing algorithms are in fact written so to exploit this knowledge (ref. [RD 4]).

- Spectral density of the angular accelerations of the spacecraft about its COM in the GRF ( $\tilde{\omega}_X^W$ ,  $\tilde{\omega}_Y^W$ ,  $\tilde{\omega}_Z^W$ ) provided GOCE End-to-End System Simulator for the mission scenario described in section 7.1.2.1.1.

## 7.1.4 Satellite Errors

### 7.1.4.1 Platform Self Gravity (S.1)

This error term has been computed from equation (5.3.1), using for the differential self-gravity acceleration between the accelerometer pairs the specified values (Table 6.2-1). The results of the system-level thermo-elastic distortion analysis (ref. [RD 9]) are substantially smaller than these limits.

## 7.1.5 Processing Errors

### 7.1.5.1 Centrifugal Accelerations Recovery Error (P.1)

This error term has been computed from equation (5.4.1) using the following inputs.

- Maximum value below the MBW of the error on the angular velocities recovered in the Level 1b ground data processing ( $\hat{\omega}_X, \hat{\omega}_Y, \hat{\omega}_Z$ ) from numerical simulations results:

$$\delta\hat{\omega}_X^0 = 1.2 \cdot 10^{-6} \text{ rad/s}, \delta\hat{\omega}_Y^0 = 1.2 \cdot 10^{-6} \text{ rad/s}, \delta\hat{\omega}_Z^0 = 1.2 \cdot 10^{-6} \text{ rad/s}$$

The performance analysis of the ground processing algorithms for the estimation of the angular velocities shows that these specifications are fulfilled (ref. [RD 13]).

- Maximum value in the MBW of the spectral density of the recovery error of  $\hat{\omega}_X, \hat{\omega}_Y, \hat{\omega}_Z$  ( $\delta\hat{\omega}_X^W, \delta\hat{\omega}_Y^W, \delta\hat{\omega}_Z^W$ ) computed from the spectral density in the MBW of the error on the angular acceleration recovered at Level 1b from the Gradiometer measurements:

$$\delta\hat{\omega}_X^W(v) = \frac{\delta\hat{\omega}_X^W(v)}{2\pi v}, \delta\hat{\omega}_Y^W(v) = \frac{\delta\hat{\omega}_Y^W(v)}{2\pi v}, \delta\hat{\omega}_Z^W(v) = \frac{\delta\hat{\omega}_Z^W(v)}{2\pi v}$$

The values of  $\delta\hat{\omega}_X^W, \delta\hat{\omega}_Y^W, \delta\hat{\omega}_Z^W$  have been obtained in turn from the angular acceleration measurement error budget computed using the equations provided in section 5.2, feed by the following inputs:

- accelerometer noise spectral density provided in section 7.1.1.1;
- measurement error on the ICM elements provided in section 7.1.2.1.1 and 7.1.2.2.1;
- quadratic factors provided in section 7.1.2.3;
- values of  $D_X^0, D_Y^0, D_Z^0, \tilde{D}_X^W, \tilde{D}_Y^W, \tilde{D}_Z^W, \omega_X^0, \omega_Y^0, \omega_Z^0, \tilde{\omega}_X^W, \tilde{\omega}_Y^W, \tilde{\omega}_Z^W, \dot{\omega}_X^0, \dot{\omega}_Y^0, \dot{\omega}_Z^0, \tilde{\omega}_X^W, \tilde{\omega}_Y^W, \tilde{\omega}_Z^W$  provided GOCE End-to-End System Simulator for the mission scenario described in section 7.1.2.1.1;
- differential accelerations generated by self-gravity and coupling with magnetic field equal to the specified values (Table 6.3-5 and Table 6.3-6);
- coupling factors with high frequency noise provided in section 7.1.3.3;
- coupling factors with the accelerometer and structure transfer function difference equal to the specified limits (Table 6.3-11);
- coupling factors between angular and linear accelerations at accelerometer level equal to the specified limits (Table 6.3-12);
- mutual alignment and alignment stabilities of the three OAGRFs equal to the specified values (Table 6.3-10); this specified limits are fulfilled by the corresponding budgets (ref. [RD 14]).

The performance analysis of the ground processing algorithms for the estimation of the angular velocities confirms the budget of  $\delta\hat{\omega}_X^W, \delta\hat{\omega}_Y^W, \delta\hat{\omega}_Z^W$  obtained with this approach and shows that the specifications provided in Table 6.3-1 are fulfilled (ref. [RD 13]).

## 7.2 PERFORMANCE BUDGET FOR THE GGT DIAGONAL COMPONENTS AND FOR THE GGT TRACE

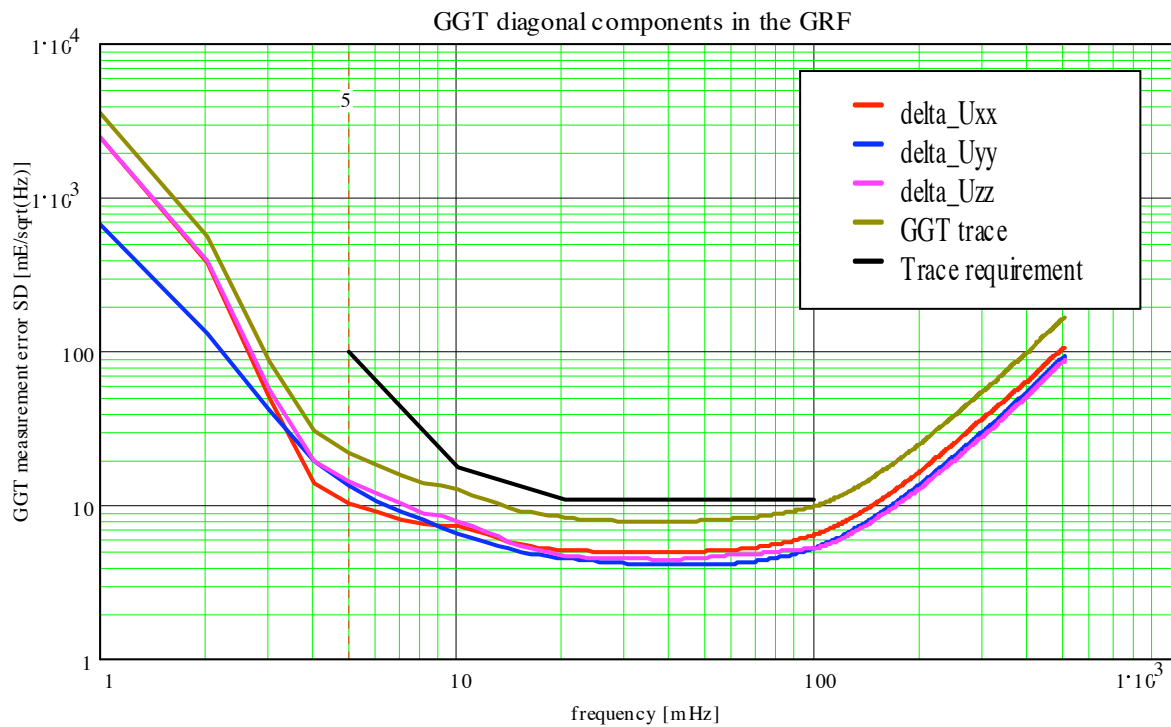
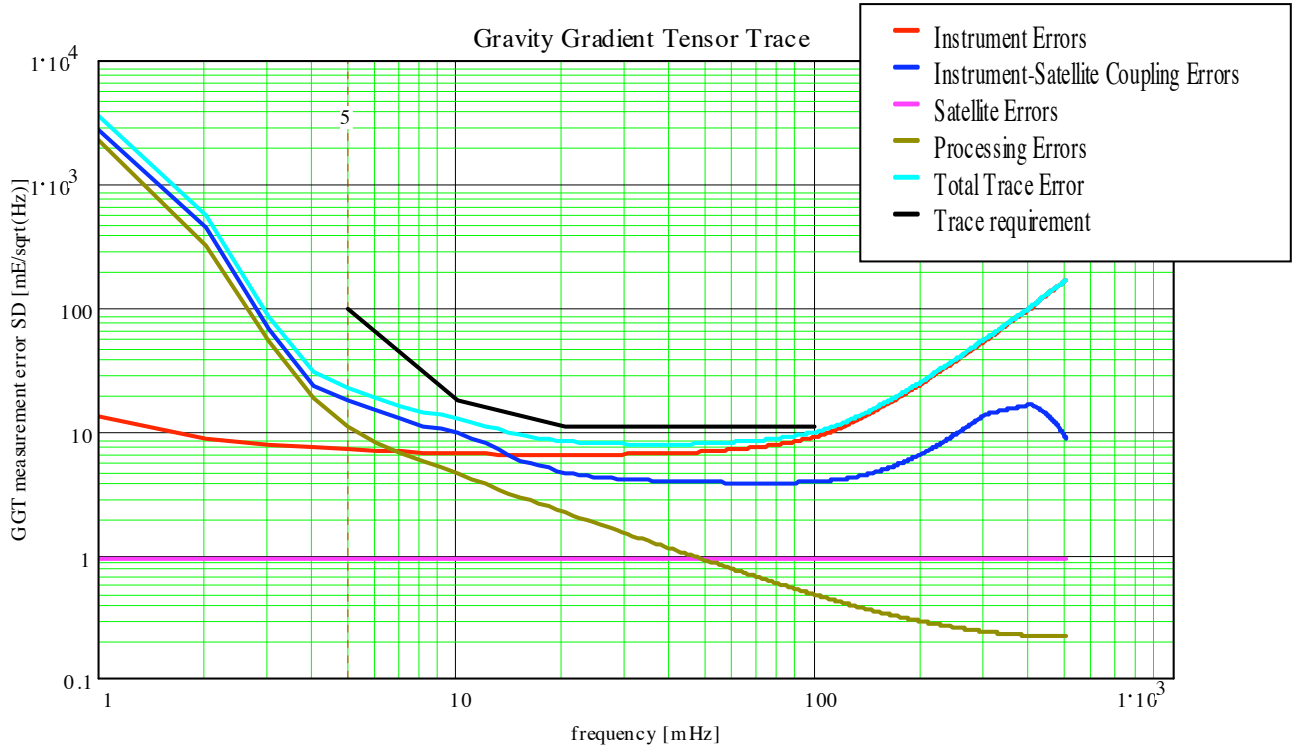
The error budgets for the GGT diagonal components in the GRF and for the corresponding GGT trace are provided in Figure 7.2-1 for the mission scenario described in section 7.1.2.1.1 and representative of the MOP-1. Here it is assumed that the in-flight compensation of the accelerometer quadratic factor (the so-called K2) through the proof mass displacement is not affecting the accelerometer noise itself.

The following results are provided:

- Plot with the spectral density inside and outside the MBW of the total error on the GGT trace built with the three diagonal components measured in the GRF; in the same plot, the breakdown of the total error among the four error categories (Instrument, Instrument-Satellite Coupling, Satellite, Processing) and the specification for the GGT trace maximum error in the MBW are shown.
- Plot with the spectral density inside and outside the MBW of the total error on the three diagonal components of the GGT in the GRF; in the same plot, the resulting error on the GGT trace and the specification for the GGT trace maximum error in the MBW are shown.
- Table with the error spectral density of the three diagonal components of the GGT in the GRF and of GGT trace at the frequencies 5, 10, 20, 100 mHz and with the requirement on the GGT trace.

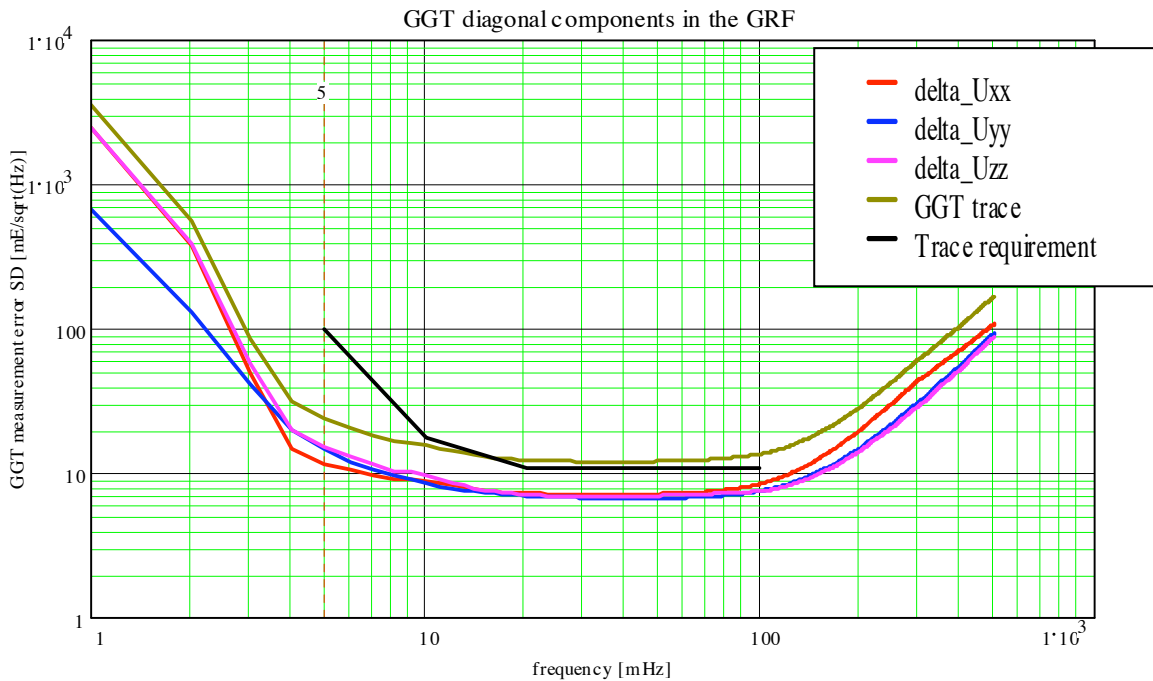
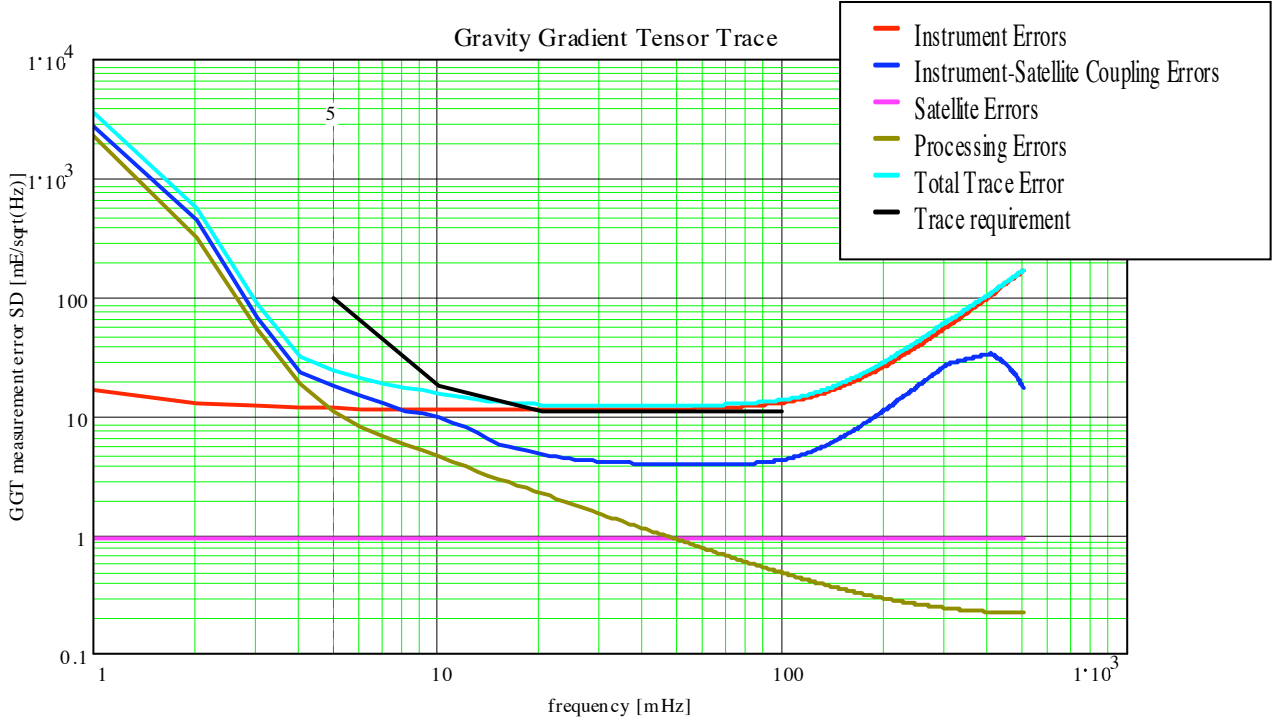
The error budget on the GGT trace so computed is compliant with the specified requirements.

The error budget computed for the same mission scenario, but for the situation in which the in-flight compensation of the accelerometer quadratic factors produces the maximum expected effect on the accelerometer noise (Figure 7.1-3) is presented in Figure 7.2-2. The compensation of a  $K2 = 1206 \text{ s}^2/\text{m}$  has also the effect of increasing the difference in the accelerometer transfer functions ( $\delta TFA_{ij,k}$ ) by  $25 \cdot 10^{-6}$  for the US axis. This is taken into account in the error budget too. In this case, the error budget on the GGT trace is slightly exceeding the requirement from 20 to 100 mHz.



|         | error SD mE/sqrt(Hz) |      |      |       | req. |
|---------|----------------------|------|------|-------|------|
|         | Uxx                  | Uyy  | Uzz  | Trace |      |
| 5 mHz   | 10.3                 | 14.3 | 14.9 | 23.1  | 100  |
| 10 mHz  | 7.3                  | 6.5  | 8    | 12.6  | 18   |
| 20 mHz  | 5.1                  | 4.5  | 4.7  | 8.3   | 11   |
| 100 mHz | 6.5                  | 5.3  | 5.3  | 9.9   | 11   |

Figure 7.2-1: Gradiometric error budget for the MOP-1 mission scenario (no effect on the noise from K2 compensation)



|         | error SD mE/sqrt(Hz) |      |      |       |      |
|---------|----------------------|------|------|-------|------|
|         | Uxx                  | Uyy  | Uzz  | Trace | req. |
| 5 mHz   | 11.5                 | 15.3 | 15.9 | 24.9  | 100  |
| 10 mHz  | 9                    | 8.5  | 9.6  | 15.6  | 18   |
| 20 mHz  | 7.3                  | 7    | 7.1  | 12.4  | 11   |
| 100 mHz | 8.5                  | 7.6  | 7.6  | 13.7  | 11   |

Figure 7.2-2: Gradiometric error budget for the MOP-1 mission scenario (maximum effect on the noise from K2 compensation)

### 7.3 PERFORMANCE BUDGET FOR THE OFF-DIAGONAL COMPONENTS OF THE GGT

By comparing the expressions (4.30) of the GGT off-diagonal components and those (4.29) of the angular accelerations recovered from the accelerometer measurements, it turns out that we can write the SD in the MBW of total error affecting the measurement of the GGT off-diagonal components as:

$$\begin{aligned}\delta\tilde{U}_{XY}^W &= \sqrt{(\delta\tilde{U}_{XY\_O}^W)^2 + (\delta\tilde{U}_{XY\_I.3}^W)^2 + (\delta\tilde{U}_{XY\_P}^W)^2} \\ \delta\tilde{U}_{XZ}^W &= \sqrt{(\delta\tilde{U}_{XZ\_O}^W)^2 + (\delta\tilde{U}_{XZ\_I.3}^W)^2 + (\delta\tilde{U}_{XZ\_P}^W)^2} \\ \delta\tilde{U}_{YZ}^W &= \sqrt{(\delta\tilde{U}_{YZ\_O}^W)^2 + (\delta\tilde{U}_{YZ\_I.3}^W)^2 + (\delta\tilde{U}_{YZ\_P}^W)^2}\end{aligned}\tag{7.3.1}$$

where the terms

$$\begin{aligned}\delta\tilde{U}_{XY\_O}^W &= \sqrt{\sum_{i=1}^{14} \left[ (\delta\tilde{\omega}_{Z\_14i}^W)^2 + (\delta\tilde{\omega}_{Z\_25i}^W)^2 \right]}, \\ \delta\tilde{U}_{XZ\_O}^W &= \sqrt{\sum_{i=1}^{14} \left[ (\delta\tilde{\omega}_{Y\_14i}^W)^2 + (\delta\tilde{\omega}_{Y\_36i}^W)^2 \right]}, \\ \delta\tilde{U}_{YZ\_O}^W &= \sqrt{\sum_{i=1}^{14} \left[ (\delta\tilde{\omega}_{X\_25i}^W)^2 + (\delta\tilde{\omega}_{X\_36i}^W)^2 \right]}\end{aligned}$$

are those defined in section 5.2 for the angular accelerations.

The terms  $\delta\tilde{U}_{XY\_I.3}^W$ ,  $\delta\tilde{U}_{XZ\_I.3}^W$ ,  $\delta\tilde{U}_{YZ\_I.3}^W$  are the instrument errors related to the OAGRFs alignment errors and alignment stability in the GRF. Their expression is derived from the (4.50,51,52):

$$\begin{aligned}\delta\tilde{U}_{XY\_I.3}^W &= \left( (\tilde{\psi}^W (U_{YY}^0 - U_{XX}^0))^2 + (\psi^0 \tilde{U}_{YY}^W)^2 + (\psi^0 \tilde{U}_{XX}^W)^2 + (\tilde{\varphi}^W U_{XZ}^0)^2 + (\varphi^0 \tilde{U}_{XZ}^W)^2 + (\tilde{\theta}^W U_{YZ}^0)^2 + (\theta^0 \tilde{U}_{YZ}^W)^2 + \right. \\ &+ (\psi^0 \tilde{\theta}^W U_{XZ}^0)^2 + (\tilde{\psi}^W \theta^0 U_{XZ}^0)^2 + (\psi^0 \theta^0 \tilde{U}_{XZ}^W)^2 + (\tilde{\varphi}^W \psi^0 U_{YZ}^0)^2 + (\varphi^0 \tilde{\psi}^W U_{YZ}^0)^2 + (\varphi^0 \psi^0 \tilde{U}_{YZ}^W)^2 \\ &\left. + (\varphi^0 \tilde{\theta}^W U_{ZZ}^0)^2 + (\tilde{\varphi}^W \theta^0 U_{ZZ}^0)^2 + (\varphi^0 \theta^0 \tilde{U}_{ZZ}^W)^2 + (2\psi^0 \tilde{\psi}^W U_{XY}^0)^2 + (\psi^0 \tilde{U}_{XY}^W)^2 \right)^{1/2} \\ \delta\tilde{U}_{XZ\_I.3}^W &= \left( (\tilde{\theta}^W (U_{XX}^0 - U_{ZZ}^0))^2 + (\theta^0 \tilde{U}_{XX}^W)^2 + (\theta^0 \tilde{U}_{ZZ}^W)^2 + (\tilde{\varphi}^W U_{XY}^0)^2 + (\varphi^0 \tilde{U}_{XY}^W)^2 + (\tilde{\psi}^W U_{YZ}^0)^2 + (\psi^0 \tilde{U}_{YZ}^W)^2 + \right. \\ &+ (\psi^0 \tilde{\theta}^W U_{XY}^0)^2 + (\tilde{\psi}^W \theta^0 U_{XY}^0)^2 + (\psi^0 \theta^0 \tilde{U}_{XY}^W)^2 + (\tilde{\varphi}^W \psi^0 U_{YY}^0)^2 + (\varphi^0 \tilde{\psi}^W U_{YY}^0)^2 + (\varphi^0 \psi^0 \tilde{U}_{YY}^W)^2 \\ &\left. + (\varphi^0 \tilde{\theta}^W U_{YZ}^0)^2 + (\tilde{\varphi}^W \theta^0 U_{YZ}^0)^2 + (\varphi^0 \theta^0 \tilde{U}_{YZ}^W)^2 + (2\theta^0 \tilde{\theta}^W U_{XZ}^0)^2 + (\theta^0 \tilde{U}_{XZ}^W)^2 \right)^{1/2}\end{aligned}\tag{7.3.2}$$

$$\begin{aligned} \delta \tilde{U}_{YZ,1,3}^W = & \left( \tilde{\varphi}^W (U_{ZZ}^0 - U_{YY}^0) \right)^2 + \left( \varphi^0 \tilde{U}_{ZZ}^W \right)^2 + \left( \varphi^0 \tilde{U}_{YY}^W \right)^2 + \left( \tilde{\theta}^W U_{XY}^0 \right)^2 + \left( \theta^0 \tilde{U}_{XY}^W \right)^2 + \left( \tilde{\psi}^W U_{XZ}^0 \right)^2 + \left( \psi^0 \tilde{U}_{XZ}^W \right)^2 + \\ & + \left( \psi^0 \tilde{\theta}^W U_{XX}^0 \right)^2 + \left( \tilde{\psi}^W \theta^0 U_{XX}^0 \right)^2 + \left( \psi^0 \theta^0 \tilde{U}_{XX}^W \right)^2 + \left( \tilde{\varphi}^W \psi^0 U_{XY}^0 \right)^2 + \left( \varphi^0 \tilde{\psi}^W U_{XY}^0 \right)^2 + \left( \varphi^0 \psi^0 \tilde{U}_{XY}^W \right)^2 \\ & + \left( \varphi^0 \tilde{\theta}^W U_{XZ}^0 \right)^2 + \left( \tilde{\varphi}^W \theta^0 U_{XZ}^0 \right)^2 + \left( \varphi^0 \theta^0 \tilde{U}_{XZ}^W \right)^2 + \left( 2\varphi^0 \tilde{\varphi}^W U_{YZ}^0 \right)^2 + \left( \varphi^{0^2} \tilde{U}_{YZ}^W \right)^2 \end{aligned} \quad (7.3.2)$$

The rotation angles  $\varphi^0, \theta^0, \psi^0$  include the OAGRF-GRF alignment errors at integration and the successive variations (due to launch effects, in-flight long-term modifications of the structure); the rotation angles spectral densities  $\tilde{\varphi}^W, \tilde{\theta}^W, \tilde{\psi}^W$  include the OAGRF-GRF alignment stability in the MBW. In particular

- for  $U_{XY}$ :  $\varphi^0 (\theta^0, \psi^0) = \sqrt{(\varphi_{G12}^0)^2 + (\varphi_{G1}^0)^2}$ ,  $\tilde{\varphi}^W (\tilde{\theta}^W, \tilde{\psi}^W) = \sqrt{(\tilde{\varphi}_{G12}^W)^2 + (\tilde{\varphi}_{G1}^W)^2}$
- for  $U_{XZ}$ :  $\varphi^0 (\theta^0, \psi^0) = \varphi_{G1}^0$ ,  $\tilde{\varphi}^W (\tilde{\theta}^W, \tilde{\psi}^W) = \tilde{\varphi}_{G1}^W$
- for  $U_{YZ}$ :  $\varphi^0 (\theta^0, \psi^0) = \varphi_{G2}^0$ ,  $\tilde{\varphi}^W (\tilde{\theta}^W, \tilde{\psi}^W) = \tilde{\varphi}_{G2}^W$

where

- $\varphi_{G1}, \theta_{G1}, \psi_{G1}$  are the rotation angles about the X, Y and Z axes defining the misalignment of the OAGRF<sub>1</sub> in the GRF;
- $\varphi_{G2}, \theta_{G2}, \psi_{G2}$  are the rotation angles about the X, Y and Z axes defining the misalignment of the OAGRF<sub>2</sub> in the GRF;
- $\varphi_{G12}, \theta_{G12}, \psi_{G12}$  are the rotation angles about the X, Y and Z axes defining the misalignment of the OAGRF<sub>2</sub> in the OAGRF<sub>1</sub>;

The terms  $\delta \tilde{U}_{XY,P}^W, \delta \tilde{U}_{XZ,P}^W, \delta \tilde{U}_{YZ,P}^W$  are the processing errors related to the estimation of the centrifugal accelerations  $\hat{\omega}_X \hat{\omega}_Y, \hat{\omega}_X \hat{\omega}_Z, \hat{\omega}_Y \hat{\omega}_Z$  to be subtracted from the recovered differential acceleration gradients to get the GGT off-diagonal components (see 4.30):

$$\begin{aligned} \delta \tilde{U}_{XY,P}^W &= \sqrt{(\omega_X^0 \delta \hat{\omega}_Y^W)^2 + (\tilde{\omega}_X^W \delta \hat{\omega}_Y^0)^2 + (\delta \hat{\omega}_X^W \omega_Y^0)^2 + (\delta \hat{\omega}_X^0 \tilde{\omega}_Y^W)^2} \\ \delta \tilde{U}_{XZ,P}^W &= \sqrt{(\omega_X^0 \delta \hat{\omega}_Z^W)^2 + (\tilde{\omega}_X^W \delta \hat{\omega}_Z^0)^2 + (\delta \hat{\omega}_X^W \omega_Z^0)^2 + (\delta \hat{\omega}_X^0 \tilde{\omega}_Z^W)^2} \\ \delta \tilde{U}_{YZ,P}^W &= \sqrt{(\omega_Y^0 \delta \hat{\omega}_Z^W)^2 + (\tilde{\omega}_Y^W \delta \hat{\omega}_Z^0)^2 + (\delta \hat{\omega}_Y^W \omega_Z^0)^2 + (\delta \hat{\omega}_Y^0 \tilde{\omega}_Z^W)^2} \end{aligned} \quad (7.3.3)$$

The error budgets for the off-diagonal components of the GGT have been computed using the same inputs utilised for the diagonal ones. The plots with the spectral density inside and outside the MBW of the total error on the three off-diagonal components of the GGT in the GRF are provided in Figure 7.3-1, Figure 7.3-2 for the mission scenario described in section 7.1.2.1.1 and for the two cases:

- No effect on the accelerometer noise from quadratic factor compensation by proof mass displacement.
- Maximum expected accelerometer noise increase from quadratic factor compensation by proof mass displacement.

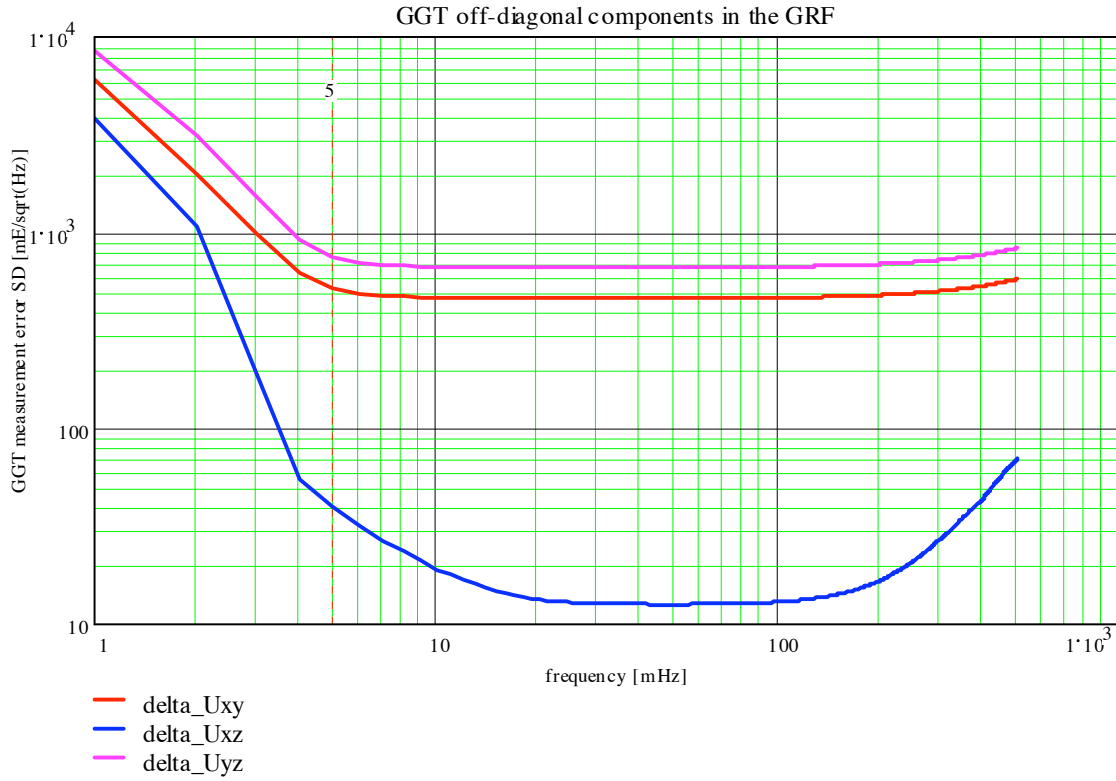


Figure 7.3-1: Error budget for the off-diagonal GGT components for the MOP-1 mission scenario (no effect on the noise from K2 compensation)

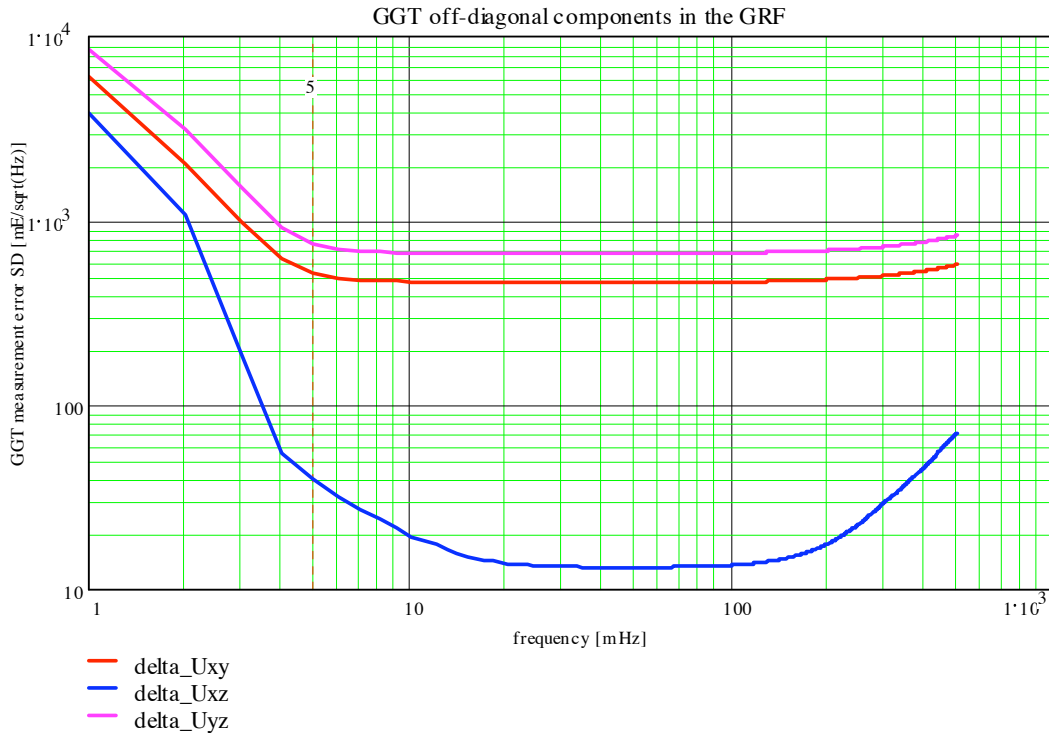


Figure 7.3-2: Error budget for the off-diagonal GGT components for the MOP-1 mission scenario (maximum effect on the noise from K2 compensation)

#### 7.4 PERFORMANCE BUDGET TREE

The expected performance budget for each of the error terms composing the error tree has been computed at the two corner frequencies of the MBW, with the assumption of the MOP-1 mission scenario. The case in which the in-flight compensation of the accelerometer quadratic factor is not affecting the acceleration measurement noise is considered here.

- The comparison of the error budget at 5 mHz (Figure 7.4-1) and 100 mHz (Figure 7.4-2) with the corresponding requirement allocations (Figure 5.3-4, Figure 5.3-5) shows that these allocations are substantially fulfilled.

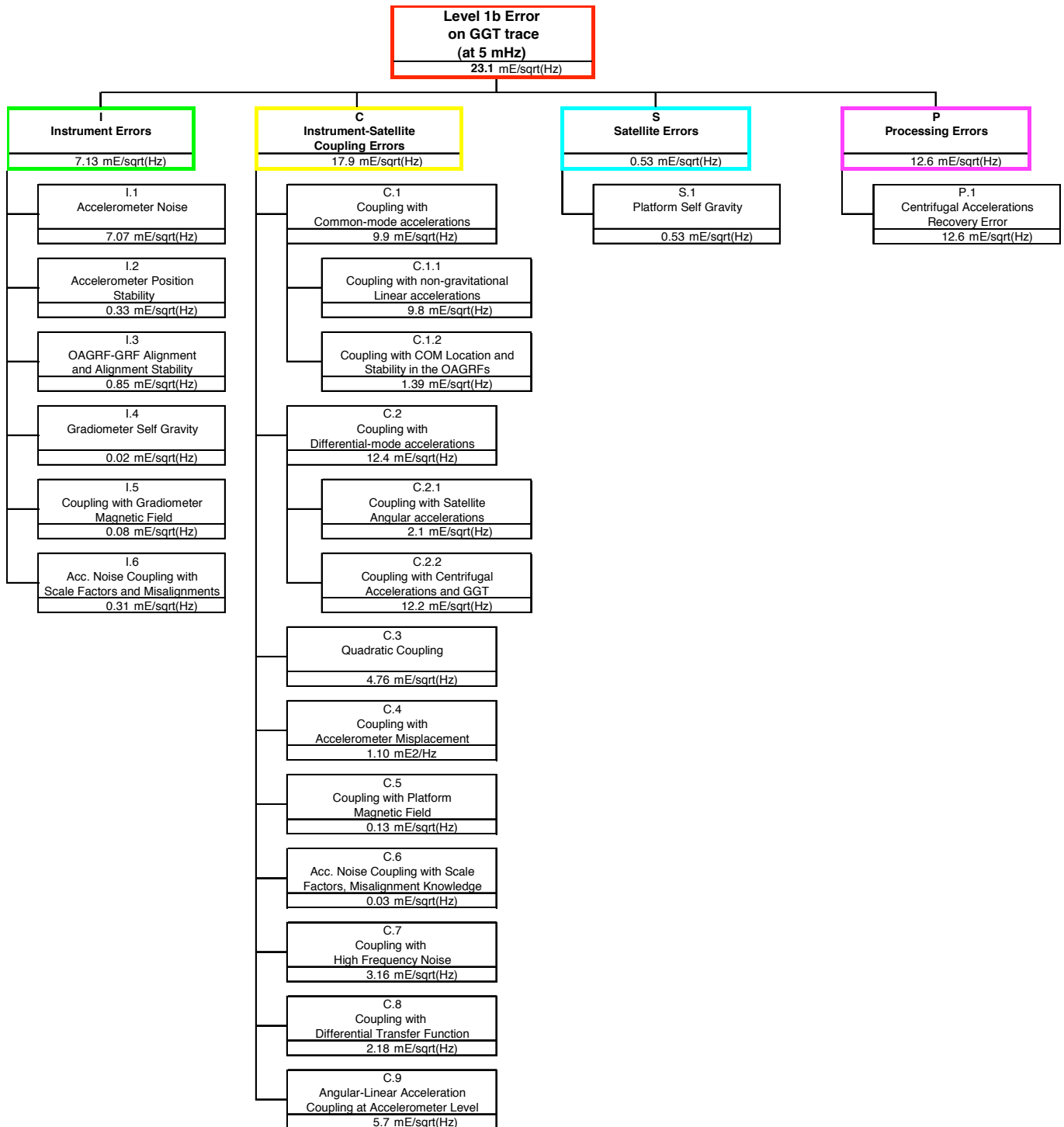


Figure 7.4-1: Performance budget for Gravity Gradient Tensor trace at 5 mHz.

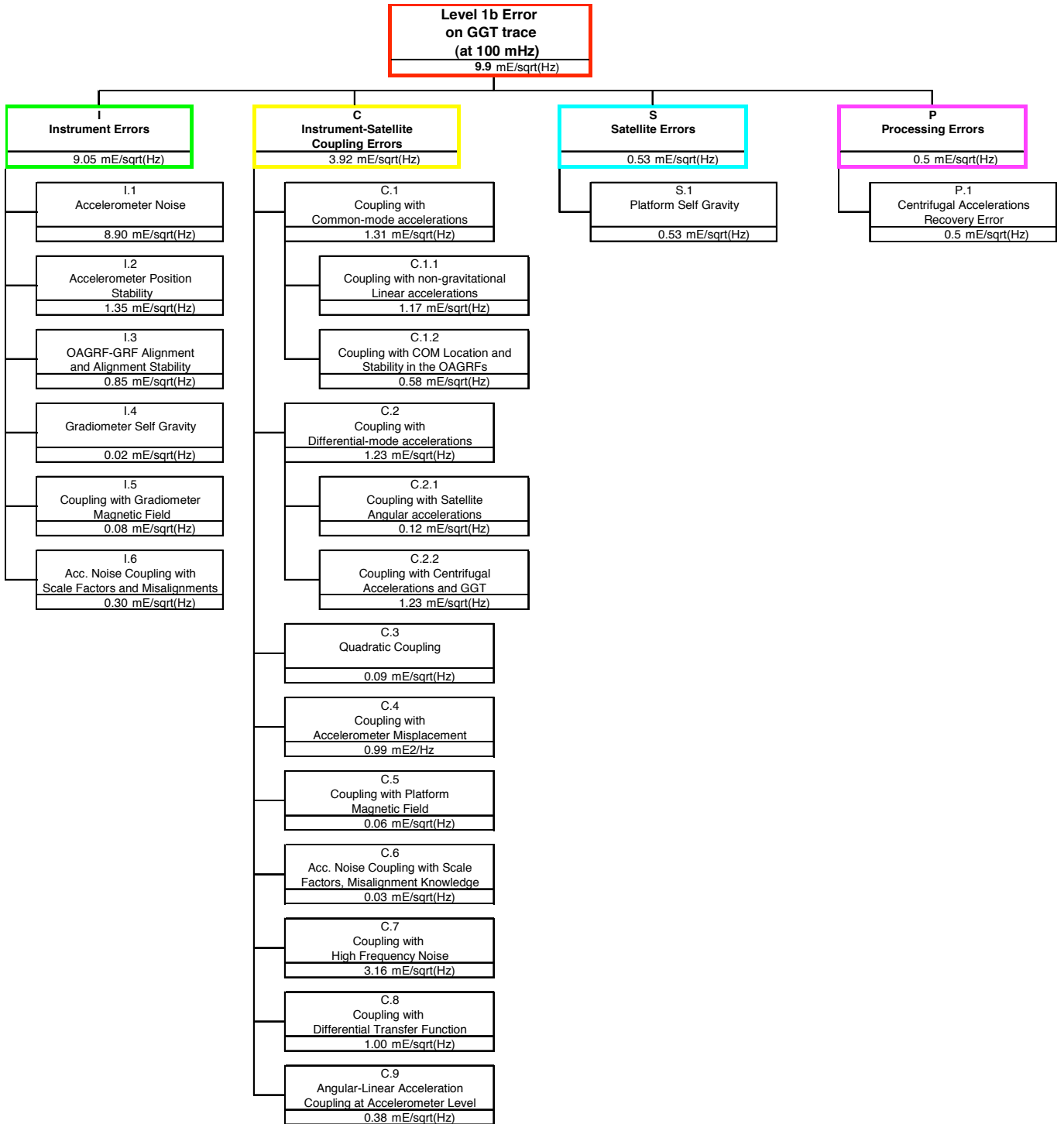


Figure 7.4-2: Performance budget for Gravity Gradient Tensor trace at 100 mHz.

7.4.1 Payloads Performance Prediction vs Specified Requirements

According to Figure 7.4-3, the predicted accelerometer noise along the ultra-sensitive axis (main contributor of the Instrument Errors) is within the specified requirement. This applies to the case in which the in-flight compensation of the accelerometer quadratic factor is not affecting the acceleration measurement noise. The situation in this case, assuming a compensation of the maximum value expected for the quadratic factor ( $\pm 1206 \text{ s}^2/\text{m}$ ) is shown in Figure 7.4-4.

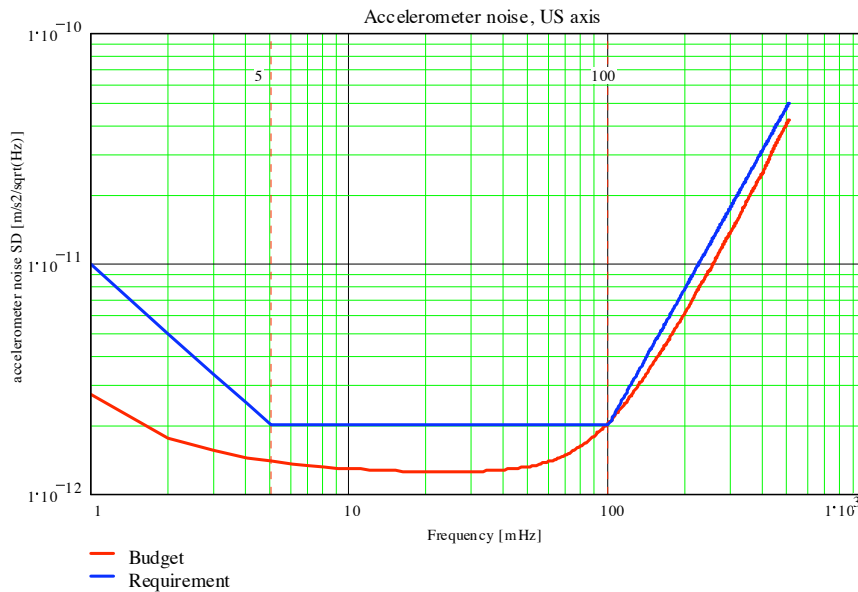


Figure 7.4-3: Accelerometer noise error budget vs requirements (no effect on the noise from the in-flight compensation of the quadratic factor)

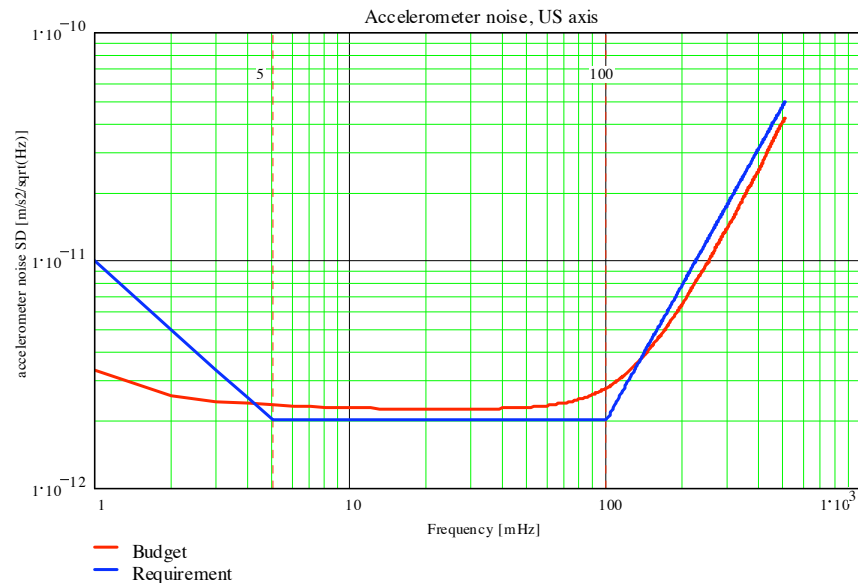


Figure 7.4-4: Accelerometer noise error budget vs requirements (maximum effect on the noise from the in-flight compensation of the quadratic factor)

Figure 7.4-5 shows that the residual linear acceleration along the X-axis of the satellite (the only one which is controlled by the ion thruster) is below the specified requirement. The linear acceleration along the Y and Z axes are not controlled, so there are strictly links to the environment experienced by the satellite. For the MOP-1 mission scenario these acceleration components are within the specified limits too.

The three components of the satellite angular accelerations (see Figure 7.4-6), controlled by magneto-torquers, are all within the specified requirements (especially  $\dot{\omega}_Y$ , for which there is the full controllability from the magnetic torquers).

The three components of the satellite angular rate, controlled by magneto-torquers, substantially match the specified requirements at low frequency (see Figure 7.4-7).

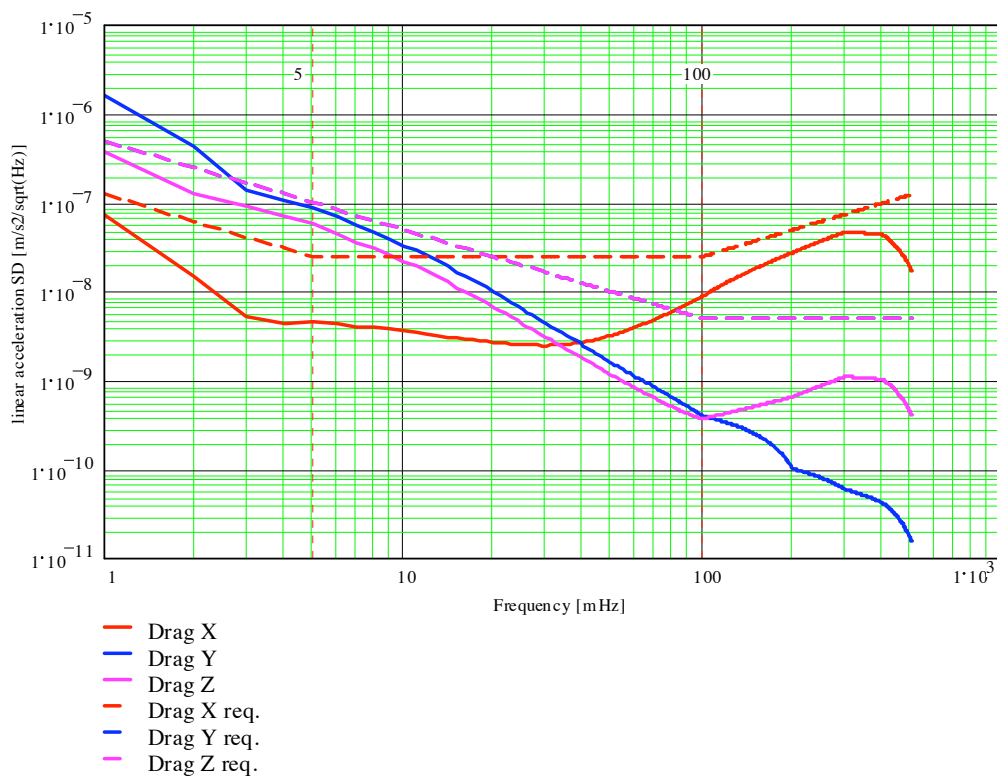


Figure 7.4-5: Satellite linear acceleration control performance vs requirements

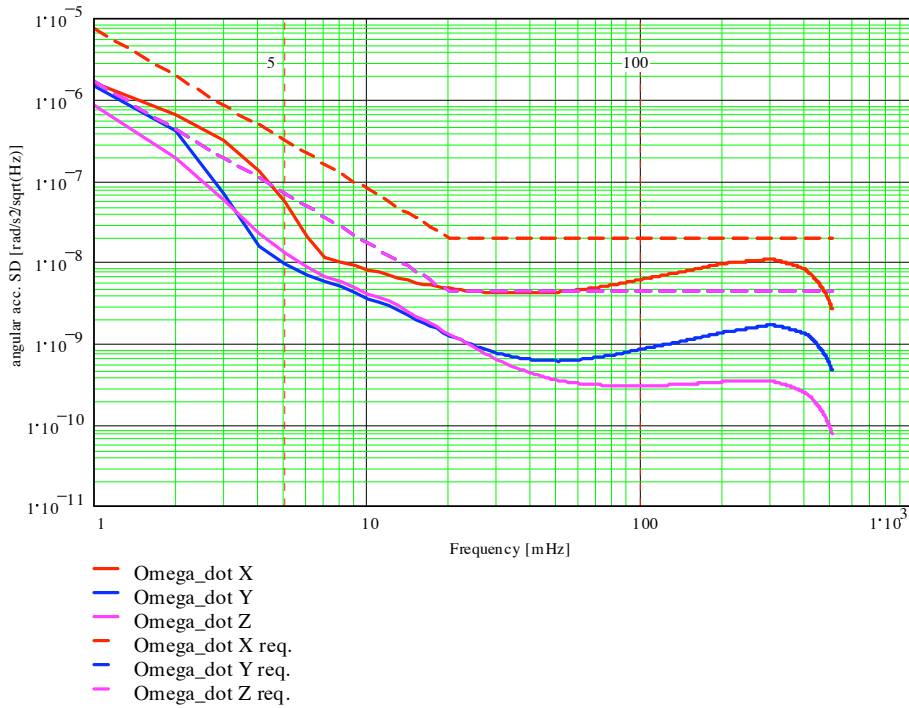


Figure 7.4-6: Satellite angular acceleration control performance vs requirements

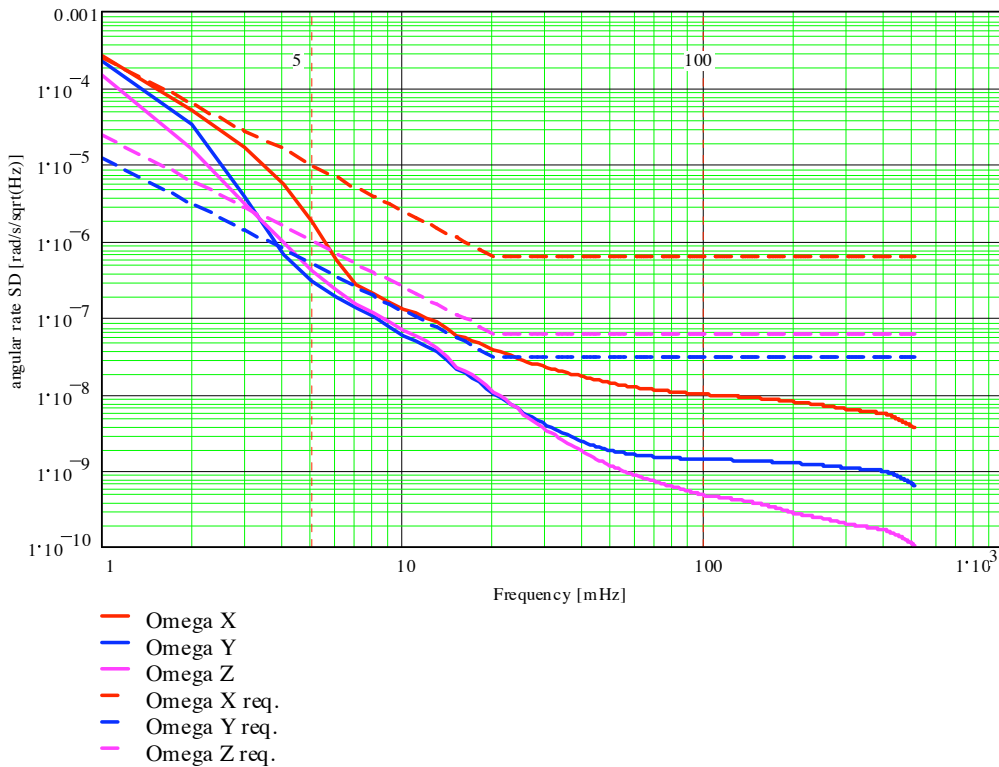


Figure 7.4-7: Satellite angular rate control performance vs requirements

7.4.2 Comparison of the analytical error budget with the numerical simulation results

An E2E simulator run has been performed in the same environmental conditions of the MOP-1 in order to check the validity of the analytical error prediction (modelling of the various error terms and error summation rule). The raw measurements produced by the E2E simulator have been post processed using Inverse Calibration Matrices affected by the same error utilised for the analytical error budget (see previous section). The gradiometric error terms taken into account in the E2E simulator are the main ones: accelerometer noise, coupling with common-mode and differential mode accelerations, quadratic coupling, coupling with platform magnetic field, with high-frequency noise, with differential transfer function (DVA), linear-angular acceleration coupling at ASH level, centrifugal acceration recovery error (they are mapped on the error tree provided in Figure 7.4-8). The simulated case assumes a “nominal” accelerometer noise, not affected by the in-flight compensation of the accelerometer quadratic factor.

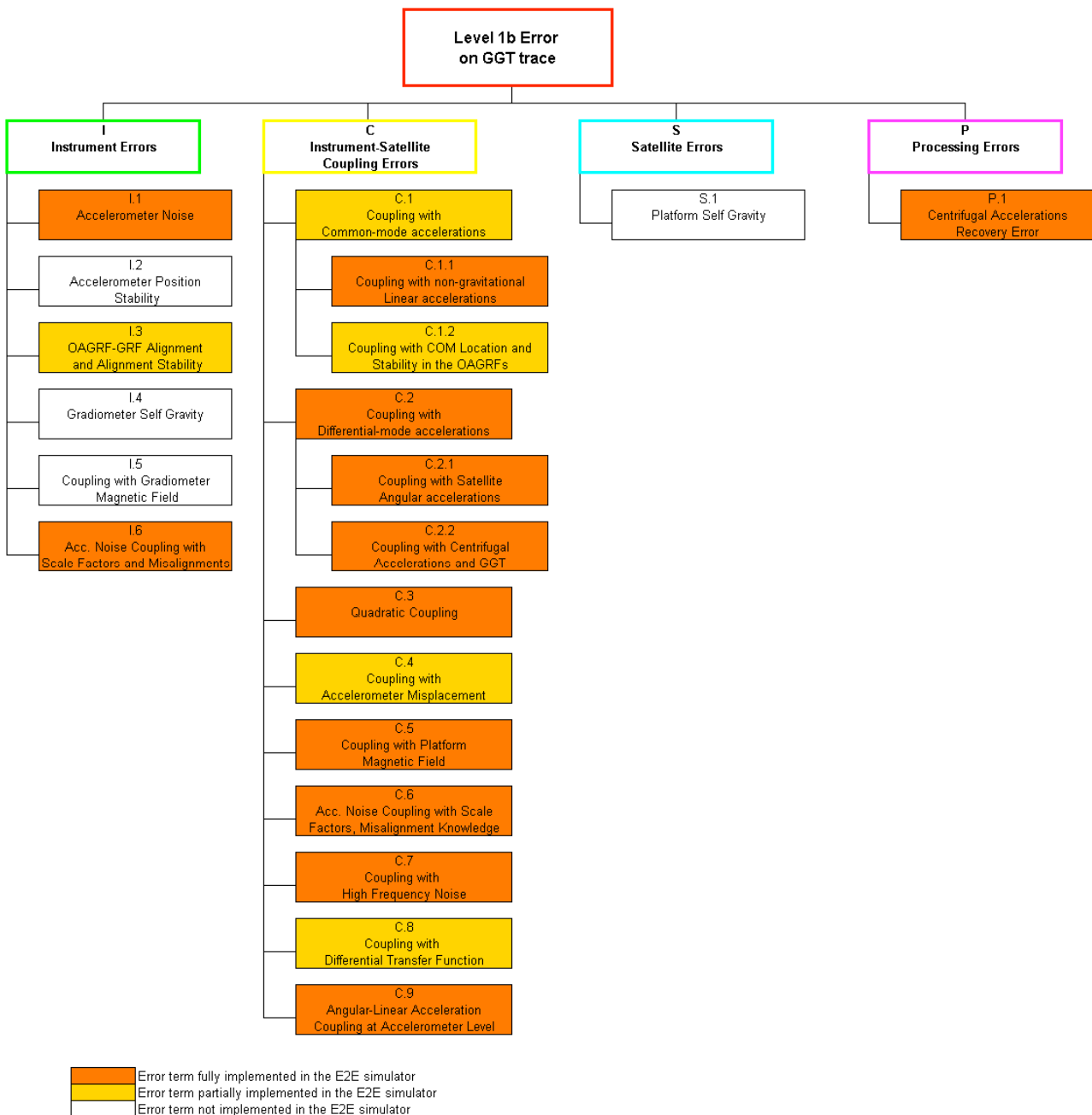


Figure 7.4-8: Status of the implementation of the error tree within the E2E simulator

The time history of the error affecting the measurement of the GGT components has been computed by subtracting the “true” GGT (i.e. the one utilised as input to the simulation) from the components obtained in the post processing of the raw measurements. The sum of the three GGT diagonal components provided the time history of the trace. The Power Spectral Density has been computed for each of these time histories in order to provide the error spectral density. From the comparison of Figure 7.4-9 with Figure 7.2-1 and of Figure 7.4-10 with Figure 7.3-1, it turns out that there is a good agreement between the numerical and the analytical error budget.

The trace of the GGT obtained from the measurements of the un-calibrated gradiometer (i.e. using in the data processing Inverse Calibration Matrices affected by the by-construction knowledge of the various terms) is also shown in Figure 7.4-9, in order to highlight the effectiveness and the importance of the in-flight calibration for the performance achievement.

Among the off-diagonal GGT terms, the  $U_{XZ}$  one it that retrieved with a quality level compared to the diagonal components. In fact, it is derived from measurements of the accelerometer ultra-sensitive axes only. The noise on other two diagonal components is dominated by the less sensitive axis of the accelerometer (one LS axes for  $U_{XY}$  and two LS axes for  $U_{YZ}$ ).

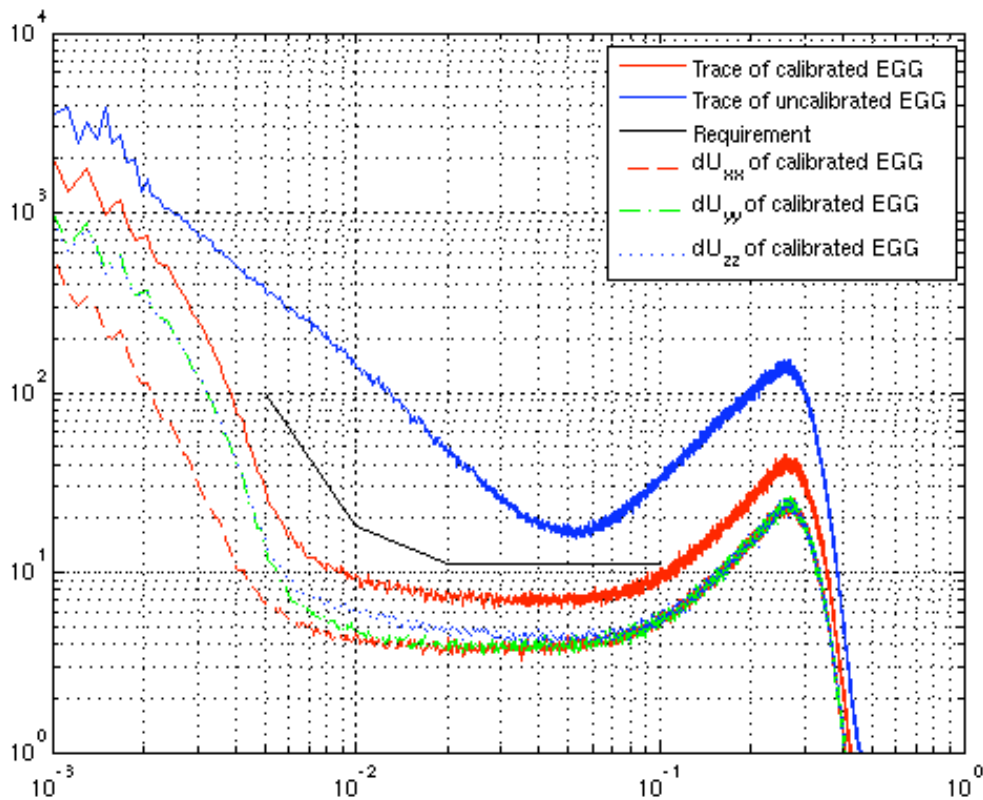


Figure 7.4-9: PSD of the diagonal GGT components  $[mE/Hz^{1/2}]$  and trace from the E2E LIB Product

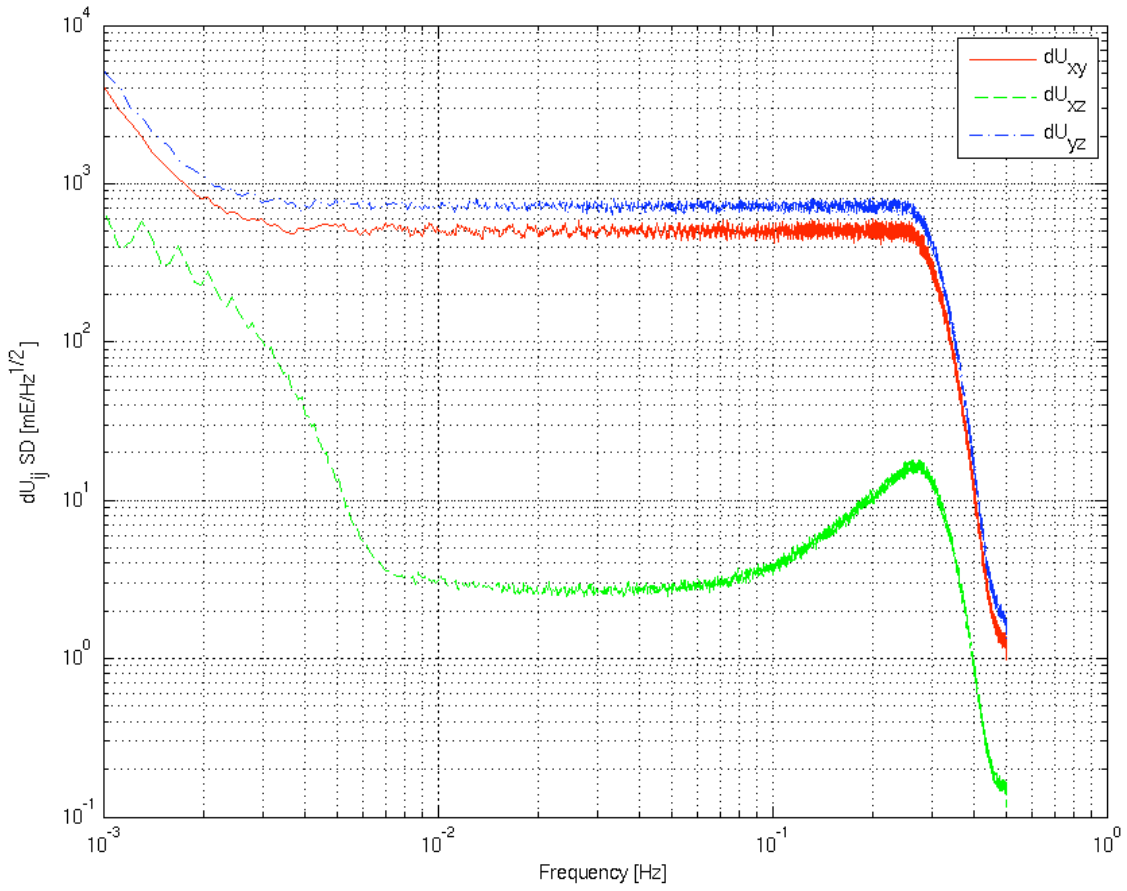


Figure 7.4-10: PSD of the off-diagonal GGT components from the E2E LIB Product

## 8. ACRONYMS AND ABBREVIATIONS

|                   |                                                                                          |
|-------------------|------------------------------------------------------------------------------------------|
| AARF              | Accelerometer Alignment Reference Frame                                                  |
| AT-CF             | Attitude Control Frame                                                                   |
| AERF              | Accelerometer External Reference Frame                                                   |
| AESRF             | Accelerometer Electrode System Reference Frame                                           |
| ARF               | Accelerometer Reference Frame                                                            |
| CMRR              | Common-Mode Rejection Ratio                                                              |
| COM               | Centre Of Mass                                                                           |
| DFACS             | Drag Free and Attitude Control Subsystem                                                 |
| DOF               | Degree Of Freedom                                                                        |
| E                 | Eötvös (acceleration gradient measurement unit; $1 E = 10^{-9} \text{ m/s}^2/\text{m}$ ) |
| EGG               | Electrostatic Gravity Gradiometer                                                        |
| FM                | Flight Model (of the Gradiometer)                                                        |
| Gal               | acceleration measurement unit; $1 \text{ Gal} = 10^{-2} \text{ m/s}^2$                   |
| GASRF             | Gradiometer Assembly Reference Frame                                                     |
| GARF              | Gradiometer Alignment Reference Frame                                                    |
| GGT               | Gravity Gradient Tensor                                                                  |
| GOCE              | Gravity field and steady-state Ocean Circulation Explorer                                |
| GPS               | Global Positioning System                                                                |
| GRF               | Gradiometer Reference Frame                                                              |
| ICM               | Inverse Calibration Matrix                                                               |
| IRF               | Inertial Reference Frame                                                                 |
| JERF              | J2000 Equatorial Reference Frame                                                         |
| LORF              | Local Orbital Reference Frame                                                            |
| LTOAN             | Local Time Of Ascending Node                                                             |
| MBW               | Measurement Bandwidth [5 mHz to 100 mHz]                                                 |
| OAG               | One-Axis Gradiometer                                                                     |
| OAGRF             | One-Axis Gradiometer Reference Frame                                                     |
| POD               | Precise Orbit Determination                                                              |
| PSD               | Power Spectral Density                                                                   |
| rms               | root-meas-square                                                                         |
| RSS               | root-sum-square                                                                          |
| SARF              | Satellite Alignment Reference Frame                                                      |
| SD                | spectral density                                                                         |
| SGG               | satellite gravity gradiometry                                                            |
| SSARF             | Star Sensor Alignment Reference Frame                                                    |
| SSRF              | Star Sensor Reference Frame                                                              |
| SST               | satellite-to-satellite tracking                                                          |
| TAG               | Three-Axis Gradiometer (= Gradiometer)                                                   |
| TBC               | To Be Confirmed                                                                          |
| TBD               | To Be Defined                                                                            |
| TBV               | To Be Verified                                                                           |
| TF                | Transfer Function                                                                        |
| ULE <sup>TM</sup> | Ultra-Low Expansion glass                                                                |

**END OF DOCUMENT**